IMPACT OF PASSENGER COMFORT LEVEL ON DESIGN OF SHORT SPAN COMPOSITE STEEL I-GIRDER HIGH SPEED RAILROAD BRIDGES

A THESIS SUBMITTED TO
THE GRADUATE SCHOOL OF NATURAL AND APPLIED SCIENCES
OF
MIDDLE EAST TECHNICAL UNIVERSITY

BY

TOLGA ŞENTÜRK

IN PARTIAL FULFILLMENT OF THE REQUIREMENTS
FOR
THE DEGREE OF MASTER OF SCIENCE
IN
CIVIL ENGINEERING

DECEMBER 2009

Approval of the thesis:

IMPACT OF PASSENGER COMFORT LEVEL ON DESIGN OF SHORT SPAN COMPOSITE STEEL I-GIRDER HIGH SPEED RAILROAD BRIDGES

submitted by **TOLGA ŞENTÜRK** in partial fulfillment of the requirements for the degree of **Master of Science in Civil Engineering Department, Middle East Technical University** by,

Prof. Dr. Canan Özgen _____
Dean, Graduate School of **Natural and Applied Sciences**

Prof. Dr. Güney Özcebe _____
Head of Department, **Civil Engineering**

Asst. Prof. Dr. Alp Caner _____
Supervisor, **Civil Engineering Dept., METU**

Examining Committee Members:

Prof. Dr. Çetin Yılmaz _____
Civil Engineering Dept., METU

Asst. Prof. Dr. Alp Caner _____
Civil Engineering Dept., METU

Assoc. Prof. Dr. Uğurhan Akyüz _____
Civil Engineering Dept., METU

Assoc. Prof. Dr. Ahmet Türer _____
Civil Engineering Dept., METU

Altuğ Aksaray, MSc. _____
General Manager, SPM Engineering Inc.

Date: 08.12.2009

I hereby declare that all information in this document has been obtained and presented in accordance with academic rules and ethical conduct. I also declare that, as required by these rules and conduct, I have fully cited and referenced all material and results that are not original to this work.

Name, Last name : TOLGA ŞENTÜRK

Signature :

ABSTRACT

IMPACT OF PASSENGER COMFORT LEVEL ON DESIGN OF SHORT-SPAN COMPOSITE STEEL I-GIRDER HIGH SPEED RAILROAD BRIDGES

Şentürk, Tolga

M.Sc. Department of Civil Engineering

Supervisor: Asst. Prof Dr. Alp Caner

December 2009, 205 pages

In globalizing world, increase in demand for high speed rail travel requires comfortable ride over bridges while maintaining an economical design. These bridges either have composite steel I-girders, prestressed precast I or box girder superstructures. The span lengths can reach up to 40 meters. If frequency of wheel load pass at a point on bridge matches with one the critical frequencies of the structure, excessive vibration can developed both at the train and the bridge even if the structure is structurally safe. Excessive vibration can discomfort the passengers. Focus of this study is given to identify certain thresholds for the rigidity of span to minimize the passenger discomfort at short-span composite steel I-girder high speed railroad bridges. In this context, various span lengths with different girder configurations have been analyzed under various train design speeds and ballast stiffness. Eigenvalue analyses are performed to determine critical frequencies of bridges. Moving force models are used to determine structural vibrations

as recommended by high speed railroad bridge design specifications. It is well-known that stiffer structures can have significantly less vibration amplitudes than lighter ones providing a comfortable ride for high speed train passes.

Keywords: Bridge, High-Speed Train, Train-Bridge Interaction, Vibration Effects, Passenger Comfort.

ÖZ

HIZLI TRENLER İÇİN KISA AÇIKLI KOMPOZİT I-KİRİŞLİ ÇELİK KÖPRÜLERİN TASARIMINA YOLCU KONFOR DÜZEYİNİN ETKİSİ

Şentürk, Tolga
Yüksek Lisans, İnşaat Mühendisliği Bölümü
Tez Yöneticisi: Y. Doç. Dr. Alp Caner

Aralık 2009, 205 sayfa

Küreselleşen dünyada yüksek hızlı demiryolu ulaşımına duyulan talep artışı, ekonomik tasarımın yanısıra demiryolu köprüleründen konforlu geçişi de gerektirmiştir. Bu demiryolu köprülerinin, kompozit çelik I kirişli veya ön germeli prekast I veya kutu kirişli üst yapıları vardır. Açıklık uzunlukları 40 metreye kadar ulaşabilir. Yapı, yapısal olarak güvenli olsa dahi eğer bir noktadan geçen tekerlek yükü frekansı yapı kritik frekansı ile örtüşürse, köprüde ve trende aşırı titeşim oluşabilir. Aşırı titreşim, yolcuları rahatsız edebilir. Bu çalışmanın odağı, kısa açıklı kompozit çelik I-kirişli yüksek hızlı demiryolu köprülerinde yolcu rahatsızlıklarını azaltmak için mutlak asgari açıklık rijitlikleri belirlemektir. Bu çalışmada, değişken açıklıklar, farklı kiriş konfigürasyonları ile çeşitli tren tasarım hızları ve balast rijitlikleri için analiz edilmiştir. Köprülerin kritik frekansları özdeğer analizleri ile belirlenmiştir. Yapısal titreşimlerin belirlenmesi için ise yüksek hızlı tren köprüleri tasarım şartnamelerinde de tavsiye edildiği üzere muharrik güç modelleri kullanılmıştır. Bilindiği üzere rijit yapılar, daha az rijit yapılara nazaran mühim derecede

az titreşim derinliğine sahiptirler ki bu yüksek hızlı tren geçişinde konforlu geçişi sağlar.

Anahtar Kelimeler: Köprü, Yüksek Hızlı Tren, Tren-Köprü Etkileşimi, Vibrasyon Etkisi, Yolcu Konforu.

To my family

ACKNOWLEDGEMENTS

It is a great pleasure for me to complete my master thesis and have the opportunity to thank all who were always nearby me during the whole studies.

First of all, I would like to thank my advisor Asst. Prof. Dr. Alp Caner, who directed me to the area of bridges and high-speed trains, for his expert guidance. Working with him has been a rewarding experience.

I would especially like to thank my family for helping me throughout the years to finally become an engineer. Also, I would like to thank my colleagues, Eser and Mutlu, for all of the support that they have given me.

TABLE OF CONTENTS

ABSTRACT..... iv

ÖZ..... vi

ACKNOWLEDGEMENTS..... ix

TABLE OF CONTENTS..... x

LIST OF TABLES..... xiv

LIST OF FIGURES..... xviii

LIST OF SYMBOLS AND ABBREVIATIONS..... xxxiii

CHAPTERS

1. INTRODUCTION..... 1

    1.1. History..... 1

    1.2. Objectives and Scope of the Study..... 4

2. LITERATURE REVIEW..... 10

3. DESIGN CRITERIA & ANALYSIS PROCEDURE..... 18

    3.1. Analysis Guidelines..... 18

    3.2. Dynamic Analysis Parameters..... 25

        3.2.1. Structural Damping Ratio..... 25

        3.2.2. Train Analysis Speed..... 28

        3.2.3. Train Loading..... 31

3.3 Passenger Comfort Criteria..... 35
3.3.1. Eurocode Passenger Comfort Criteria..... 35
3.3.2. A.R.E.M.A Passenger Comfort Criteria..... 37
3.4. Computational Analysis Methods..... 38
3.4.1. Non-Linear Force-Time Analysis..... 38
3.4.2. Eigenvalue Analysis..... 40
4. CASE STUDY AND COMPUTER MODELING..... 41
4.1. Description of the Bridge..... 41
4.2. Computer Modeling..... 48
4.2.1. Static Load Model Multiplied By Dynamic Factors..... 53
4.2.2. Moving Force Model..... 61
4.2.3. Moving Mass Model..... 63
4.3. Dynamic Analysis Parameters..... 67
4.3.1. Structural Damping Ratio..... 67
4.3.2. Train Analysis Speed..... 69
4.3.3. Train Loading..... 71
5. ANALYSIS RESULTS..... 73
5.1. Introduction..... 73
5.2. Mid-Span Joint Acceleration Results..... 76
5.3. Mid-Span Joint Displacement Results..... 86
5.4. Mid-Span Deck Twist Results..... 94
5.5. Mid-Span Composite Section Stress Results..... 103

5.6. Eigenvalue Analysis Results..... 105

6. SUMMARY & CONCLUSION..... 106

6.1. Summary..... 106

6.2. Discussion on Results..... 106

6.2.1. Discussion on Results of Acceleration..... 107

6.2.2. Discussion on Results of Displacement..... 121

6.2.3. Discussion on Results of Deck Twist..... 121

6.2.4. Discussion on Results of Stresses..... 122

6.3. Conclusion..... 122

REFERENCES..... 124

APPENDICES

A. SELECTED ANALYSIS RESULTS..... 128

A.1. Eigenvalue Analysis Joint Mode Shapes..... 128

A.2. Moving Force Model Joint Acceleration Graphs..... 136

B.COMPOSITE SECTION SELECTED CALCULATIONS & CHECKS..... 185

B.1. Calculations for Bridge Having 8.75 m Span Length,

0.75 m Girder Height and 350 MPa Ballast Stiffness..... 185

B.2. Calculations for Bridge Having 24.5 m Span Length,

0.75 m Girder Height and 350 MPa Ballast Stiffness..... 189

C.CORRELATION OF PASSENGER COMFORT PARAMETERS & COMPOSITE SPAN FLEXURAL RIGITY FOR CONSTANT VEHICLE SPEEDS..... 194

C.1. Joint Acceleration vs. Span Flexural Rigidity Graphs..... 194

C.2. Joint Displacement vs. Span Flexural Rigidity Graphs..... 196

C.3. Deck Twist vs. Span Flexural Rigidity Graphs..... 198

D. MODAL DISPLACEMENT COMPARISONS..... 201

D.1. Vertical Modal Displacements for Selected Frequencies..... 201

LIST OF TABLES

TABLES

Table 1.1.	Large Scaled Train Accidents in Turkey Since 2000.....	7
Table 1.2.	Comparison of Railroad Bridge Specifications	8
Table 1.3.	Load Cases of Specifications.....	9
Table 3.1	Maximum value of $(v/n_0)_{lim}$ for a simply supported beam or slab and a maximum permitted acceleration of $a_{max} < 3.50$ m/s^2	20
Table 3.2	Values of damping to be assumed for design purposes...	25
Table 3.3	Application of HSLM-A and HSLM-B.....	32
Table 3.4	HSLM-A Train Types Properties.....	34
Table 3.5	Indicative Levels of Comfort.....	36
Table 3.6	Limiting Values of Deck Twist.....	37
Table 4.1	Geometrical and Material Properties of Superstructure....	47
Table 4.2	Flexural Rigidity of Analyzed Composite Spans.....	51
Table 4.3	Properties of Investigated Bridge Models.....	52
Table 4.4	Classification of ballast material based on particle size....	59
Table 4.5	Effective Stiffness of Ballast Material at Different Combinations of Density and Saturation.	60
Table 4.6	Properties of German ICE, Japanese SKS, and French TGV High Speed Railway Trains.	64
Table 4.7	Rayleigh damping coefficients and natural frequencies....	68
Table 4.8	Estimated Train Speeds Cause Resonance of Bridge.....	69
Table 4.9	Train Speeds Selected For Analysis.....	70
Table 4.10	Data of critical HSLM-A Train Determination Procedure...	72
Table 5.1	Selected Vehicle Speeds, V_{select} (m/s) for Flexural Rigidities..	74

Table 5.2 Mid-Span Joint Accelerations (m/s^2) of Bridge Having 8.75m Span Length for Flexural Rigidities and Ballast Stiffness's with varying Vehicle Speeds..... 78

Table 5.3 Mid-Span Joint Accelerations (m/s^2) of Bridge Having 24.5m Span Length for Flexural Rigidities and Ballast Stiffness's with varying Vehicle Speeds..... 78

Table 5.4 Maximum Mid-Span Joint Accelerations (m/s^2) of Bridge Having 8.75m Span Length for Flexural Rigidities and Ballast Stiffness's..... 79

Table 5.5 Maximum Mid-Span Joint Accelerations (m/s^2) of Bridge Having 24.5m Span Length for Flexural Rigidities and Ballast Stiffness's..... 79

Table 5.6 Mid-Span Joint Displacements (mm) of Bridge Having 8.75m Span Length for Flexural Rigidities and Ballast Stiffness's with varying Vehicle Speeds..... 87

Table 5.7 Mid-Span Joint Displacements (mm) of Bridge Having 24.5m Span Length for Flexural Rigidities and Ballast Stiffness's with varying Vehicle Speeds..... 88

Table 5.8 Maximum Mid-Span Joint Displacements (mm) of Bridge Having 8.75m Span Length for Flexural Rigidities and Ballast Stiffness's..... 88

Table 5.9 Maximum Mid-Span Joint Displacements (mm) of Bridge Having 24.5m Span Length for Flexural Rigidities and Ballast Stiffness's..... 89

Table 5.10 Mid-Span Deck Twist (mm/3m) of Bridge Having 8.75m Span Length for Flexural Rigidities and Ballast Stiffness's with varying Vehicle Speeds..... 96

Table 5.11 Mid-Span Deck Twist (mm/3m) of Bridge Having 24.5m Span Length for Flexural Rigidities and Ballast Stiffness's with varying Vehicle Speeds..... 96

Table 5.12 Maximum Mid-Span Deck Twist (mm/3m) of Bridge Having 8.75m Span Length for Flexural Rigidities and Ballast Stiffness's..... 97

Table 5.13 Maximum Mid-Span Deck Twist (mm/3m) of Bridge Having 24.5m Span Length for Flexural Rigidities and Ballast Stiffness's..... 97

Table 5.14 Composite Section Top Flange Compression Stress (MPa) of Bridge Having 8.75m Span Length for Flexural Rigidities and Ballast Stiffness's with varying Vehicle Speeds..... 103

Table 5.15 Composite Section Bottom Flange Tension Stress (MPa) of Bridge Having 8.75m Span Length for Flexural Rigidities and Ballast Stiffness with varying Vehicle Speeds..... 103

Table 5.16 Composite Section Top Flange Compression Stress (MPa) of Bridge Having 24.5m Span Length for Flexural Rigidities and Ballast Stiffness's with varying Vehicle Speeds..... 104

Table 5.17 Composite Section Bottom Flange Tension Stress (MPa) of Bridge Having 24.5m Span Length for Flexural Rigidities and Ballast Stiffness's with varying Vehicle Speeds..... 104

Table 5.18 First and Second Natural Frequencies (Hz) and Periods (s) of Bridge Having 8.75m Span Length for Flexural Rigidities..... 105

Table 5.19 First and Second Natural Frequencies (Hz) and Periods (s) of Bridge Having 24.5m Span Length for Flexural Rigidities..... 105

Table 6.1 Ratio of Modal Displacements of Selected Frequency and Frequency Caused Peak Modal Displacement in the Design Frequency Range 109

Table 6.2 Ratios of Modal Displacements of the Closet Natural Frequency and Frequency Caused Peak Modal Displacement in the Design Frequency Range for Minimum Design Speed, 40 m/s and 13.33 Hz Frequency..... 112

Table 6.3 Frequencies Ratio and Modal Displacements of Non-Resonance Speeds..... 118

Table 6.4 Required Flexural Stiffness for Passenger Comfort Levels..... 119

Table D.1 Vertical Modal Displacements of Selected Frequencies and Frequencies cause Peak Modal Displacement in Range of Design Speed Frequencies for Bridge having 8.75 m Span Length and 40 m/s Design Speed..... 201

Table D.2 Vertical Modal Displacements for Selected Frequencies and Frequencies cause Peak Modal Displacement in Range of Design Speed Frequencies for Bridge having 8.75 m Span Length and 44.13 m/s Design Speed..... 202

Table D.3 Vertical Modal Displacements for Selected Frequencies and Frequencies cause Peak Modal Displacement in Range of Design Speed Frequencies for Bridge having 8.75 m Span Length and 68.75 m/s Design Speed..... 202

Table D.4 Vertical Modal Displacements for Selected Frequencies and Frequencies cause Peak Modal Displacement in Range of Design Speed Frequencies for Bridge having 8.75 m Span Length and 83.3 m/s Design Speed..... 203

Table D.5 Vertical Modal Displacements of Selected Frequencies and Frequencies cause Peak Modal Displacement in Range of Design Speed Frequencies for Bridge having 24.5 m Span Length and 40 m/s Design Speed..... 203

Table D.6 Vertical Modal Displacements for Selected Frequencies and Frequencies cause Peak Modal Displacement in Range of Design Speed Frequencies for Bridge having 24.5 m Span Length and 54.27 m/s Design Speed..... 204

Table D.7 Vertical Modal Displacements for Selected Frequencies and Frequencies cause Peak Modal Displacement in Range of Design Speed Frequencies for Bridge having 24.5 m Span Length and 76.07 m/s Design Speed..... 204

Table D.8 Vertical Modal Displacements for Selected Frequencies and Frequencies cause Peak Modal Displacement in Range of Design Speed Frequencies for Bridge having 24.5 m Span Length and 83.3 m/s Design Speed..... 205

LIST OF FIGURES

FIGURES

Figure 1.1	Pamukova Train Accident.....	5
Figure 1.2	Hasanbeyli Train Accident.....	5
Figure 1.3	Hasanbeyli Train Accident.....	6
Figure 3.1	Flow chart for determining whether a dynamic analysis is required.....	19
Figure 3.2	Limits of bridge natural frequency n_0 (Hz) as a function of L (m).....	22
Figure 3.3	Additional damping $\Delta\zeta$ (%) as a function of span length L (m).....	26
Figure 3.4	Vertical Modal Displacements vs. Natural Frequency Graph.....	30
Figure 3.5	HSLM-B Type High Speed Train Model.....	32
Figure 3.6	HSLM-A Type High Speed Train Model.....	33
Figure 3.7	Parameters defining critical Universal Train in HSLM-A as a function of critical wavelength of excitation λ_C (m).....	34
Figure 3.8	HSLM-B Train Type Properties.....	35
Figure 3.9	Maximum permissible vertical deflection, δ for railway bridges with 3 or more successive simply supported spans corresponding to a permissible vertical acceleration of b_v = 1 m/s² in a coach for speed V (km/h)	36
Figure 3.10	Definition of Deck Twist.....	37
Figure 4.1	Formation of Non-Existing Composite Steel I-Girder Railway Bridge.....	42
Figure 4.2	General View of Steel I-Girder Suburban Railway Bridge.....	43
Figure 4.3	Views of Steel I-Girder Suburban Railway Bridge Members.....	43

Figure 4.4	General View of Precast Concrete I-Girder High Speed Train Bridge.....	44
Figure 4.5	Views of Precast Concrete I-Girder High Speed Train Bridge Members and Rail Curvature.....	45
Figure 4.6	General Layout of Analyzed Composite Bridges.....	48
Figure 4.7	General View of 3-D Frame and Shell Analysis Bridge Model.....	49
Figure 4.8	Example of a model of a track/structure system.....	54
Figure 4.9	Basic Structure and Function of Railway Tracks.....	57
Figure 4.10	Distribution of Cycling Load in Ballast.....	57
Figure 4.11	Variation of longitudinal shear force per unit length with longitudinal track displacement for one track.....	58
Figure 4.12	Single Moving Force for an Axle Load F Moving at Velocity V.....	62
Figure 4.13	Nodal Moving Force Definition for an Axle Load F Moving at Velocity V.....	63
Figure 4.14	Bernoulli beam with simplified vehicle–bridge interaction model.....	66
Figure 4.15	HSLM-A Type High Speed Train Model.....	71
Figure 5.1	Longitudinal Cross-Section of Model for 8.75 m Span Length.....	74
Figure 5.2	Longitudinal Cross-section of Model for 24.5 m Span Length.....	74
Figure 5.3	Structural Members of Model for 8.75 m Span Length.	75
Figure 5.4	Vertical Cross-section of Bridge Model for 8.75 m Span Length.....	75
Figure 5.5	Vertical Cross-section of Bridge Model for 24.5 m Span Length.....	76
Figure 5.6	Joint Acceleration vs. Time graph of the bridge having 8.75 m span length, 0.75 m girder height for 44.13 m/s vehicle speed.....	77
Figure 5.7	Joint Acceleration vs. Time graph of the bridge having 24.5 m span length, 0.75 m girder height for 40 m/s vehicle speed.....	77

Figure 5.8 Correlations of Max. Joint Acceleration with Span Flexural Rigidity for Bridge Having 8.75 m Span Length..... 80
Figure 5.9 Correlations of Max. Joint Acceleration in Limits with Span Flexural Rigidity for Bridge Having 8.75 m Span Length..... 80
Figure 5.10 Correlations of Max. Joint Acceleration with Vehicle Speed for Bridge Having 8.75 m Span Length & 350 MPa Ballast Stiffness..... 81
Figure 5.11 Correlations of Max. Joint Acceleration with Vehicle Speed for Bridge Having 8.75 m Span Length & 700 MPa Ballast Stiffness..... 81
Figure 5.12 Correlations of Max. Joint Acceleration with Span Flexural Rigidity for Bridge Having 24.5 m Span Length..... 82
Figure 5.13 Correlations of Max. Joint Acceleration in Limits with Span Flexural Rigidity for Bridge Having 24.5 m Span Length..... 82
Figure 5.14 Correlations of Max. Joint Acceleration with Vehicle Speed for Bridge Having 24.5 m Span Length & 350 MPa Ballast Stiffness..... 83
Figure 5.15 Correlations of Max. Joint Acceleration with Vehicle Speed for Bridge Having 24.5 m Span Length & 700 MPa Ballast Stiffness..... 83
Figure 5.16 Correlations of Max. Joint Acceleration with Span Flexural Rigidity for 40m/s Constant Design Speed and Bridge Having 8.75 m Span Length..... 84
Figure 5.17 Correlations of Max. Joint Acceleration with Span Flexural Rigidity for 83.3m/s Constant Design Speed and Bridge Having 8.75 m Span Length..... 84
Figure 5.18 Correlations of Max. Joint Acceleration with Span Flexural Rigidity for 40m/s Constant Design Speed and Bridge Having 24.5 m Span Length..... 85
Figure 5.19 Correlations of Max. Joint Acceleration with Span Flexural Rigidity for 83.3m/s Constant Design Speed and Bridge Having 24.5 m Span Length..... 85
Figure 5.20 Joint Displacement vs. Time graph of the bridge having 8.75 m span length, 0.75 m girder height for 44.13 m/s vehicle speed..... 86

Figure 5.21 Joint Displacement vs. Time graph of the bridge having 24.5 m span length, 0.75 m girder height for 40 m/s vehicle speed..... 87
Figure 5.22 Correlations of Max. Joint Displacement with Span Flexural Rigidity for Bridge Having 8.75 m Span Length..... 89
Figure 5.23 Correlations of Max. Joint Displacement with Vehicle Speed for Bridge Having 8.75 m Span Length & 350 MPa Ballast Stiffness..... 90
Figure 5.24 Correlations of Max. Joint Displacement with Vehicle Speed for Bridge Having 8.75 m Span Length & 700 MPa Ballast Stiffness..... 90
Figure 5.25 Correlations of Max. Joint Displacement with Span Flexural Rigidity for Bridge Having 24.5 m Span Length..... 91
Figure 5.26 Correlations of Max. Joint Displacement with Vehicle Speed for Bridge Having 24.5 m Span Length & 350 MPa Ballast Stiffness..... 91
Figure 5.27 Correlations of Max. Joint Displacement with Vehicle Speed for Bridge Having 24.5 m Span Length & 700 MPa Ballast Stiffness..... 92
Figure 5.28 Correlations of Max. Joint Displacement with Span Flexural Rigidity for 40m/s Constant Design Speed and Bridge Having 8.75 m Span Length..... 92
Figure 5.29 Correlations of Max. Joint Displacement with Span Flexural Rigidity for 83.3m/s Constant Design Speed and Bridge Having 8.75 m Span Length..... 93
Figure 5.30 Correlations of Max. Joint Displacement with Span Flexural Rigidity for 40m/s Constant Design Speed and Bridge Having 24.5 m Span Length..... 93
Figure 5.31 Correlations of Max. Joint Displacement with Span Flexural Rigidity for 83.3m/s Constant Design Speed and Bridge Having 24.5 m Span Length..... 94
Figure 5.32 Deck Twist vs. Time graph of the bridge having 8.75 m span length, 0.75 m girder height for 44.13 m/s vehicle speed..... 95
Figure 5.33 Deck Twist vs. Time graph of the bridge having 24.5 m span length, 0.75 m girder height for 40 m/s vehicle speed..... 95

Figure 5.34 Correlations of Max. Deck Twist with Span Flexural Rigidity for Bridge Having 8.75 m Span Length..... 98

Figure 5.35 Correlations of Max. Deck Twist with Vehicle Speed for Bridge Having 8.75 m Span Length & 350 MPa Ballast Stiffness..... 98

Figure 5.36 Correlations of Max. Deck Twist with Vehicle Speed for Bridge Having 8.75 m Span Length & 700 MPa Ballast Stiffness..... 99

Figure 5.37 Correlations of Max. Deck Twist with Span Flexural Rigidity for Bridge Having 24.5 m Span Length..... 99

Figure 5.38 Correlations of Max. Deck Twist with Vehicle Speed for Bridge Having 24.5 m Span Length & 350 MPa Ballast Stiffness..... 100

Figure 5.39 Correlations of Max. Deck Twist with Vehicle Speed for Bridge Having 24.5 m Span Length & 700 MPa Ballast Stiffness..... 100

Figure 5.40 Correlations of Max. Deck Twist with Span Flexural Rigidity for 40m/s Constant Design Speed and Bridge Having 8.75 m Span Length..... 101

Figure 5.41 Correlations of Max. Deck Twist with Span Flexural Rigidity for 83.3m/s Constant Design Speed and Bridge Having 8.75 m Span Length..... 101

Figure 5.42 Correlations of Max. Deck Twist with Span Flexural Rigidity for 40m/s Constant Design Speed and Bridge Having 24.5 m Span Length..... 102

Figure 5.43 Correlations of Max. Deck Twist with Span Flexural Rigidity for 83.3m/s Constant Design Speed and Bridge Having 24.5 m Span Length..... 102

Figure 6.1 Correlations of Max. Joint Acceleration with Span Flexural Rigidity per Span Length of Railway Bridge..... 108

Figure 6.2 Correlations of Joint Acceleration with Span Flexural Stiffness for minimum Analysis Speed, 40 m/s..... 111

Figure 6.3 Correlations of Joint Acceleration with Span Flexural Stiffness for maximum Analysis Speed, 83.3 m/s..... 111

Figure 6.4 Joint Modal Displacement vs. Mode Shape Frequency graph of bridge having 713,689 $kN.m^2/m$ Span Flexural Stiffness..... 113

Figure 6.5 Joint Modal Displacement vs. Mode Shape Frequency graph of bridge having 969,425 kN.m^2/m Span Flexural Stiffness..... 113

Figure 6.6 Joint Modal Displacement vs. Mode Shape Frequency graph of bridge having 1,058,281 kN.m^2/m Span Flexural Stiffness..... 114

Figure 6.7 Steady state responses of damped systems for three values of the frequency ratio..... 116

Figure 6.8 Frequency-Acceleration Response Curve of damped systems..... 117

Figure 6.9 Threshold values of Span Flexural Stiffness for Acceleration Limits of Passenger Comfort Levels..... 120

Figure A.1 Joint Modal Shape vs. Mode Shape graph of the bridge having 8.75 m span length, 4.421.563 kN.m^2 Span Flexural Rigidity..... 128

Figure A.2 Joint Modal Shape vs. Mode Shape graph of the bridge having 8.75 m span length, 6.244.779 kN.m^2 Span Flexural Rigidity..... 129

Figure A.3 Joint Modal Shape vs. Mode Shape graph of the bridge having 8.75 m span length, 9.259.963 kN.m^2 Span Flexural Rigidity..... 129

Figure A.4 Joint Modal Shape vs. Mode Shape graph of the bridge having 8.75 m span length, 12.981.221 kN.m^2 Span Flexural Rigidity..... 130

Figure A.5 Joint Modal Shape vs. Mode Shape graph of the bridge having 8.75 m span length, 23.750.916 kN.m^2 Span Flexural Rigidity..... 130

Figure A.6 Joint Modal Shape vs. Mode Shape graph of the bridge having 8.75 m span length, 195.898.160 kN.m^2 Span Flexural Rigidity..... 131

Figure A.7 Joint Modal Shape vs. Mode Shape graph of the bridge having 8.75 m span length, 768.263.855 kN.m^2 Span Flexural Rigidity..... 131

Figure A.8 Joint Modal Shape vs. Mode Shape graph of the bridge having 8.75 m span length, 1.912.920.565 kN.m^2 Span Flexural Rigidity..... 132

Figure A.9 Joint Modal Shape vs. Mode Shape graph of the bridge having 24.5 m span length, 4.421.563 kN.m^2 Span Flexural Rigidity..... 132

Figure A.10 Joint Modal Shape vs. Mode Shape graph of the bridge having 24.5 m span length, 6.244.779 kN.m^2 Span Flexural Rigidity..... 133

Figure A.11 Joint Modal Shape vs. Mode Shape graph of the bridge having 24.5 m span length, 9.259.963 kN.m^2 Span Flexural Rigidity..... 133

Figure A.12 Joint Modal Shape vs. Mode Shape graph of the bridge having 24.5 m span length, 12.981.221 kN.m^2 Span Flexural Rigidity..... 134

Figure A.13 Joint Modal Shape vs. Mode Shape graph of the bridge having 24.5 m span length, 23.750.916 kN.m^2 Span Flexural Rigidity..... 134

Figure A.14 Joint Modal Shape vs. Mode Shape graph of the bridge having 24.5 m span length, 195.898.160 kN.m^2 Span Flexural Rigidity..... 135

Figure A.15 Joint Modal Shape vs. Mode Shape graph of the bridge having 24.5 m span length, 768.263.855 kN.m^2 Span Flexural Rigidity..... 135

Figure A.16 Joint Modal Shape vs. Mode Shape graph of the bridge having 24.5 m span length, 1.912.920.565 kN.m^2 Span Flexural Rigidity..... 136

Figure A.17 Joint Acceleration vs. Time graphic of the bridge having 8.75 m span length, 0.75 m girder height, 300 MPa ballast stiffness for 44.13 m/s vehicle speed..... 136

Figure A.18 Joint Acceleration vs. Time graphic of the bridge having 8.75 m span length, 0.75 m girder height, 300 MPa ballast stiffness for 83 m/s vehicle speed..... 137

Figure A.19 Joint Acceleration vs. Time graphic of the bridge having 8.75 m span length, 0.90 m girder height, 300 MPa ballast stiffness for 44.13 m/s vehicle speed..... 137

Figure A.20 Joint Acceleration vs. Time graphic of the bridge having 8.75 m span length, 0.90 m girder height, 300 MPa ballast stiffness for 83 m/s vehicle speed..... 138

Figure A.21 Joint Acceleration vs. Time graphic of the bridge having 8.75 m span length, 1.10 m girder height, 300 MPa ballast stiffness for 44.13 m/s vehicle speed..... 138

Figure A.22 Joint Acceleration vs. Time graphic of the bridge having 8.75 m span length, 1.10 m girder height, 300 MPa ballast stiffness for 83 m/s vehicle speed..... 139
Figure A.23 Joint Acceleration vs. Time graphic of the bridge having 8.75 m span length, 1.30 m girder height, 300 MPa ballast stiffness for 44.13 m/s vehicle speed..... 139
Figure A.24 Joint Acceleration vs. Time graphic of the bridge having 8.75 m span length, 1.30 m girder height, 300 MPa ballast stiffness for 83 m/s vehicle speed..... 140
Figure A.25 Joint Acceleration vs. Time graphic of the bridge having 8.75 m span length, 0.75 m girder height, 700 MPa ballast stiffness for 44.13 m/s vehicle speed..... 140
Figure A.26 Joint Acceleration vs. Time graphic of the bridge having 8.75 m span length, 0.75 m girder height, 700 MPa ballast stiffness for 83 m/s vehicle speed..... 141
Figure A.27 Joint Acceleration vs. Time graphic of the bridge having 8.75 m span length, 0.90 m girder height, 700 MPa ballast stiffness for 44.13 m/s vehicle speed..... 141
Figure A.28 Joint Acceleration vs. Time graphic of the bridge having 8.75 m span length, 0.90 m girder height, 700 MPa ballast stiffness for 83 m/s vehicle speed..... 142
Figure A.29 Joint Acceleration vs. Time graphic of the bridge having 8.75 m span length, 1.10 m girder height, 700 MPa ballast stiffness for 44.13 m/s vehicle speed..... 142
Figure A.30 Joint Acceleration vs. Time graphic of the bridge having 8.75 m span length, 1.10 m girder height, 700 MPa ballast stiffness for 83 m/s vehicle speed..... 143
Figure A.31 Joint Acceleration vs. Time graphic of the bridge having 8.75 m span length, 1.30 m girder height, 700 MPa ballast stiffness for 44.13 m/s vehicle speed..... 143
Figure A.32 Joint Acceleration vs. Time graphic of the bridge having 8.75 m span length, 1.30 m girder height, 700 MPa ballast stiffness for 83 m/s vehicle speed..... 144
Figure A.33 Joint Acceleration vs. Time graphic of the bridge having 24.5 m span length, 0.75 m girder height, 300 MPa ballast stiffness for 40 m/s vehicle speed..... 144
Figure A.34 Joint Acceleration vs. Time graphic of the bridge having 24.5 m span length, 0.75 m girder height, 300 MPa ballast stiffness for 76.08 m/s vehicle speed..... 145

Figure A.35 Joint Acceleration vs. Time graphic of the bridge having 24.5 m span length, 0.90 m girder height, 300 MPa ballast stiffness for 40 m/s vehicle speed..... 145
Figure A.36 Joint Acceleration vs. Time graphic of the bridge having 24.5 m span length, 0.90 m girder height, 300 MPa ballast stiffness for 76.08 m/s vehicle speed..... 146
Figure A.37 Joint Acceleration vs. Time graphic of the bridge having 24.5 m span length, 1.10 m girder height, 300 MPa ballast stiffness for 40 m/s vehicle speed..... 146
Figure A.38 Joint Acceleration vs. Time graphic of the bridge having 24.5 m span length, 1.10 m girder height, 300 MPa ballast stiffness for 76.08 m/s vehicle speed..... 147
Figure A.39 Joint Acceleration vs. Time graphic of the bridge having 24.5 m span length, 1.30 m girder height, 300 MPa ballast stiffness for 40 m/s vehicle speed..... 147
Figure A.40 Joint Acceleration vs. Time graphic of the bridge having 24.5 m span length, 1.30 m girder height, 300 MPa ballast stiffness for 76.08 m/s vehicle speed..... 148
Figure A.41 Joint Acceleration vs. Time graphic of the bridge having 24.5 m span length, 0.75 m girder height, 700 MPa ballast stiffness for 40 m/s vehicle speed..... 148
Figure A.42 Joint Acceleration vs. Time graphic of the bridge having 24.5 m span length, 0.75 m girder height, 700 MPa ballast stiffness for 76.08 m/s vehicle speed..... 149
Figure A.43 Joint Acceleration vs. Time graphic of the bridge having 24.5 m span length, 0.90 m girder height, 700 MPa ballast stiffness for 40 m/s vehicle speed..... 149
Figure A.44 Joint Acceleration vs. Time graphic of the bridge having 24.5 m span length, 0.90 m girder height, 700 MPa ballast stiffness for 76.08 m/s vehicle speed..... 150
Figure A.45 Joint Acceleration vs. Time graphic of the bridge having 24.5 m span length, 1.10 m girder height, 700 MPa ballast stiffness for 40 m/s vehicle speed..... 150
Figure A.46 Joint Acceleration vs. Time graphic of the bridge having 24.5 m span length, 1.10 m girder height, 700 MPa ballast stiffness for 76.08 m/s vehicle speed..... 151
Figure A.47 Joint Acceleration vs. Time graphic of the bridge having 24.5 m span length, 1.30 m girder height, 700 MPa ballast stiffness for 40 m/s vehicle speed..... 151

Figure A.48 Joint Acceleration vs. Time graphic of the bridge having 24.5 m span length, 1.30 m girder height, 700 MPa ballast stiffness for 76.08 m/s vehicle speed..... 152
Figure A.49 Joint Displacement vs. Time graphic of the bridge having 8.75 m span length, 0.75 m girder height, 300 MPa ballast stiffness for 44.13 m/s vehicle speed..... 152
Figure A.50 Joint Displacement vs. Time graphic of the bridge having 8.75 m span length, 0.75 m girder height, 300 MPa ballast stiffness for 83 m/s vehicle speed..... 153
Figure A.51 Joint Displacement vs. Time graphic of the bridge having 8.75 m span length, 0.90 m girder height, 300 MPa ballast stiffness for 44.13 m/s vehicle speed..... 153
Figure A.52 Joint Displacement vs. Time graphic of the bridge having 8.75 m span length, 0.90 m girder height, 300 MPa ballast stiffness for 83 m/s vehicle speed..... 154
Figure A.53 Joint Displacement vs. Time graphic of the bridge having 8.75 m span length, 1.10 m girder height, 300 MPa ballast stiffness for 44.13 m/s vehicle speed..... 154
Figure A.54 Joint Displacement vs. Time graphic of the bridge having 8.75 m span length, 1.10 m girder height, 300 MPa ballast stiffness for 83 m/s vehicle speed..... 155
Figure A.55 Joint Displacement vs. Time graphic of the bridge having 8.75 m span length, 1.30 m girder height, 300 MPa ballast stiffness for 44.13 m/s vehicle speed..... 155
Figure A.56 Joint Displacement vs. Time graphic of the bridge having 8.75 m span length, 1.30 m girder height, 300 MPa ballast stiffness for 83 m/s vehicle speed..... 156
Figure A.57 Joint Displacement vs. Time graphic of the bridge having 8.75 m span length, 0.75 m girder height, 700 MPa ballast stiffness for 44.13 m/s vehicle speed..... 156
Figure A.58 Joint Displacement vs. Time graphic of the bridge having 8.75 m span length, 0.75 m girder height, 700 MPa ballast stiffness for 83 m/s vehicle speed..... 157
Figure A.59 Joint Displacement vs. Time graphic of the bridge having 8.75 m span length, 0.90 m girder height, 700 MPa ballast stiffness for 44.13 m/s vehicle speed..... 157
Figure A.60 Joint Displacement vs. Time graphic of the bridge having 8.75 m span length, 0.90 m girder height, 700 MPa ballast stiffness for 83 m/s vehicle speed..... 158

Figure A.61 Joint Displacement vs. Time graphic of the bridge having 8.75 m span length, 1.10 m girder height, 700 MPa ballast stiffness for 44.13 m/s vehicle speed..... 158
Figure A.62 Joint Displacement vs. Time graphic of the bridge having 8.75 m span length, 1.10 m girder height, 700 MPa ballast stiffness for 83 m/s vehicle speed..... 159
Figure A.63 Joint Displacement vs. Time graphic of the bridge having 8.75 m span length, 1.30 m girder height, 700 MPa ballast stiffness for 44.13 m/s vehicle speed..... 159
Figure A.64 Joint Displacement vs. Time graphic of the bridge having 8.75 m span length, 1.30 m girder height, 700 MPa ballast stiffness for 83 m/s vehicle speed..... 160
Figure A.65 Joint Displacement vs. Time graphic of the bridge having 24.5 m span length, 0.75 m girder height, 300 MPa ballast stiffness for 40 m/s vehicle speed..... 160
Figure A.66 Joint Displacement vs. Time graphic of the bridge having 24.5 m span length, 0.75 m girder height, 300 MPa ballast stiffness for 76.08 m/s vehicle speed..... 161
Figure A.67 Joint Displacement vs. Time graphic of the bridge having 24.5 m span length, 0.90 m girder height, 300 MPa ballast stiffness for 40 m/s vehicle speed..... 161
Figure A.68 Joint Displacement vs. Time graphic of the bridge having 24.5 m span length, 0.90 m girder height, 300 MPa ballast stiffness for 76.08 m/s vehicle speed..... 162
Figure A.69 Joint Displacement vs. Time graphic of the bridge having 24.5 m span length, 1.10 m girder height, 300 MPa ballast stiffness for 40 m/s vehicle speed..... 162
Figure A.70 Joint Displacement vs. Time graphic of the bridge having 24.5 m span length, 1.10 m girder height, 300 MPa ballast stiffness for 76.08 m/s vehicle speed..... 163
Figure A.71 Joint Displacement vs. Time graphic of the bridge having 24.5 m span length, 1.30 m girder height, 300 MPa ballast stiffness for 40 m/s vehicle speed..... 163
Figure A.72 Joint Displacement vs. Time graphic of the bridge having 24.5 m span length, 1.30 m girder height, 300 MPa ballast stiffness for 76.08 m/s vehicle speed..... 164
Figure A.73 Joint Displacement vs. Time graphic of the bridge having 24.5 m span length, 0.75 m girder height, 700 MPa ballast stiffness for 40 m/s vehicle speed..... 164

Figure A.74 Joint Displacement vs. Time graphic of the bridge having 24.5 m span length, 0.75 m girder height, 700 MPa ballast stiffness for 76.08 m/s vehicle speed..... 165
Figure A.75 Joint Displacement vs. Time graphic of the bridge having 24.5 m span length, 0.90 m girder height, 700 MPa ballast stiffness for 40 m/s vehicle speed..... 165
Figure A.76 Joint Displacement vs. Time graphic of the bridge having 24.5 m span length, 0.90 m girder height, 700 MPa ballast stiffness for 76.08 m/s vehicle speed..... 166
Figure A.77 Joint Displacement vs. Time graphic of the bridge having 24.5 m span length, 1.10 m girder height, 700 MPa ballast stiffness for 40 m/s vehicle speed..... 166
Figure A.78 Joint Displacement vs. Time graphic of the bridge having 24.5 m span length, 1.10 m girder height, 700 MPa ballast stiffness for 76.08 m/s vehicle speed..... 167
Figure A.79 Joint Displacement vs. Time graphic of the bridge having 24.5 m span length, 1.30 m girder height, 700 MPa ballast stiffness for 40 m/s vehicle speed..... 167
Figure A.80 Joint Displacement vs. Time graphic of the bridge having 24.5 m span length, 1.30 m girder height, 700 MPa ballast stiffness for 76.08 m/s vehicle speed..... 168
Figure A.81 Deck Twist vs. Time graphic of the bridge having 8.75 m span length, 0.75 m girder height, 300 MPa ballast stiffness for 44.13 m/s vehicle speed..... 168
Figure A.82 Deck Twist vs. Time graphic of the bridge having 8.75 m span length, 0.75 m girder height, 300 MPa ballast stiffness for 83 m/s vehicle speed..... 169
Figure A.83 Deck Twist vs. Time graphic of the bridge having 8.75 m span length, 0.90 m girder height, 300 MPa ballast stiffness for 44.13 m/s vehicle speed..... 169
Figure A.84 Deck Twist vs. Time graphic of the bridge having 8.75 m span length, 0.90 m girder height, 300 MPa ballast stiffness for 83 m/s vehicle speed..... 170
Figure A.85 Deck Twist vs. Time graphic of the bridge having 8.75 m span length, 1.10 m girder height, 300 MPa ballast stiffness for 44.13 m/s vehicle speed..... 170
Figure A.86 Deck Twist vs. Time graphic of the bridge having 8.75 m span length, 1.10 m girder height, 300 MPa ballast stiffness for 83 m/s vehicle speed..... 171

Figure A.87 Deck Twist vs. Time graphic of the bridge having 8.75 m span length, 1.30 m girder height, 300 MPa ballast stiffness for 44.13 m/s vehicle speed..... 171
Figure A.88 Deck Twist vs. Time graphic of the bridge having 8.75 m span length, 1.30 m girder height, 300 MPa ballast stiffness for 83 m/s vehicle speed..... 172
Figure A.89 Deck Twist vs. Time graphic of the bridge having 8.75 m span length, 0.75 m girder height, 700 MPa ballast stiffness for 44.13 m/s vehicle speed..... 172
Figure A.90 Deck Twist vs. Time graphic of the bridge having 8.75 m span length, 0.75 m girder height, 700 MPa ballast stiffness for 83 m/s vehicle speed..... 173
Figure A.91 Deck Twist vs. Time graphic of the bridge having 8.75 m span length, 0.90 m girder height, 700 MPa ballast stiffness for 44.13 m/s vehicle speed..... 173
Figure A.92 Deck Twist vs. Time graphic of the bridge having 8.75 m span length, 0.90 m girder height, 700 MPa ballast stiffness for 83 m/s vehicle speed..... 174
Figure A.93 Deck Twist vs. Time graphic of the bridge having 8.75 m span length, 1.10 m girder height, 700 MPa ballast stiffness for 44.13 m/s vehicle speed..... 174
Figure A.94 Deck Twist vs. Time graphic of the bridge having 8.75 m span length, 1.10 m girder height, 700 MPa ballast stiffness for 83 m/s vehicle speed..... 175
Figure A.95 Deck Twist vs. Time graphic of the bridge having 8.75 m span length, 1.30 m girder height, 700 MPa ballast stiffness for 44.13 m/s vehicle speed..... 175
Figure A.96 Deck Twist vs. Time graphic of the bridge having 8.75 m span length, 1.30 m girder height, 700 MPa ballast stiffness for 83 m/s vehicle speed..... 176
Figure A.97 Deck Twist vs. Time graphic of the bridge having 24.5 m span length, 0.75 m girder height, 300 MPa ballast stiffness for 40 m/s vehicle speed..... 176
Figure A.98 Deck Twist vs. Time graphic of the bridge having 24.5 m span length, 0.75 m girder height, 300 MPa ballast stiffness for 76.08 m/s vehicle speed..... 177
Figure A.99 Deck Twist vs. Time graphic of the bridge having 24.5 m span length, 0.90 m girder height, 300 MPa ballast stiffness for 40 m/s vehicle speed..... 177

Figure A.100 Deck Twist vs. Time graphic of the bridge having 24.5 m span length, 0.90 m girder height, 300 MPa ballast stiffness for 76.08 m/s vehicle speed..... 178
Figure A.101 Deck Twist vs. Time graphic of the bridge having 24.5 m span length, 1.10 m girder height, 300 MPa ballast stiffness for 40 m/s vehicle speed..... 178
Figure A.102 Deck Twist vs. Time graphic of the bridge having 24.5 m span length, 1.10 m girder height, 300 MPa ballast stiffness for 76.08 m/s vehicle speed..... 179
Figure A.103 Deck Twist vs. Time graphic of the bridge having 24.5 m span length, 1.30 m girder height, 300 MPa ballast stiffness for 40 m/s vehicle speed..... 179
Figure A.104 Deck Twist vs. Time graphic of the bridge having 24.5 m span length, 1.30 m girder height, 300 MPa ballast stiffness for 76.08 m/s vehicle speed..... 180
Figure A.105 Deck Twist vs. Time graphic of the bridge having 24.5 m span length, 0.75 m girder height, 700 MPa ballast stiffness for 40 m/s vehicle speed..... 180
Figure A.106 Deck Twist vs. Time graphic of the bridge having 24.5 m span length, 0.75 m girder height, 700 MPa ballast stiffness for 76.08 m/s vehicle speed..... 181
Figure A.107 Deck Twist vs. Time graphic of the bridge having 24.5 m span length, 0.90 m girder height, 700 MPa ballast stiffness for 40 m/s vehicle speed..... 181
Figure A.108 Deck Twist vs. Time graphic of the bridge having 24.5 m span length, 0.90 m girder height, 700 MPa ballast stiffness for 76.08 m/s vehicle speed..... 182
Figure A.109 Deck Twist vs. Time graphic of the bridge having 24.5 m span length, 1.10 m girder height, 700 MPa ballast stiffness for 40 m/s vehicle speed..... 182
Figure A.110 Deck Twist vs. Time graphic of the bridge having 24.5 m span length, 1.10 m girder height, 700 MPa ballast stiffness for 76.08 m/s vehicle speed..... 183
Figure A.111 Deck Twist vs. Time graphic of the bridge having 24.5 m span length, 1.30 m girder height, 700 MPa ballast stiffness for 40 m/s vehicle speed..... 183
Figure A.112 Deck Twist vs. Time graphic of the bridge having 24.5 m span length, 1.30 m girder height, 700 MPa ballast stiffness for 76.08 m/s vehicle speed..... 184

Figure C.1 Joint Acceleration vs. Span Flexural Rigidity graph of the bridge having 8.75 m span length for 44.13 m/s vehicle speed..... 194
Figure C.2 Joint Acceleration vs. Span Flexural Rigidity graph of the bridge having 8.75 m span length for 68.75 m/s vehicle speed..... 195
Figure C.3 Joint Acceleration vs. Span Flexural Rigidity graph of the bridge having 24.5 m span length for 54.27 m/s vehicle speed..... 195
Figure C.4 Joint Acceleration vs. Span Flexural Rigidity graph of the bridge having 24.5 m span length for 76.08 m/s vehicle speed..... 196
Figure C.5 Joint Displacement vs. Span Flexural Rigidity graph of the bridge having 8.75 m span length for 44.13 m/s vehicle speed..... 196
Figure C.6 Joint Displacement vs. Span Flexural Rigidity graph of the bridge having 8.75 m span length for 68.75 m/s vehicle speed..... 197
Figure C.7 Joint Displacement vs. Span Flexural Rigidity graph of the bridge having 24.5 m span length for 54.27 m/s vehicle speed..... 197
Figure C.8 Joint Displacement vs. Span Flexural Rigidity graph of the bridge having 24.5 m span length for 76.08 m/s vehicle speed..... 198
Figure C.9 Deck Twist vs. Span Flexural Rigidity graph of the bridge having 8.75 m span length for 44.13 m/s vehicle speed..... 198
Figure C.10 Deck Twist vs. Span Flexural Rigidity graph of the bridge having 8.75 m span length for 68.75 m/s vehicle speed..... 199
Figure C.11 Deck Twist vs. Span Flexural Rigidity graph of the bridge having 24.5 m span length for 54.27 m/s vehicle speed..... 199
Figure C.12 Deck Twist vs. Span Flexural Rigidity graph of the bridge having 24.5 m span length for 76.08 m/s vehicle speed..... 200

LIST OF SYMBOLS AND ABBREVIATIONS

TGV	:	Train a Grande Vitesse
TCDD	:	Turkish State Railways
EN	:	Eurocode
AREMA	:	American Railway Engineering and Maintenance of Way Association
METU	:	Middle East Technical University
GHz	:	Gigahertz
Hz	:	Hertz
v	:	velocity
m_{vk}	:	Half mass of the k^{th} train car
c_{vk}	:	Damping coefficient of vertical bolster spring of the k^{th} train car
k_{vk}	:	Stiffness coefficient of vertical bolster spring of the k^{th} train car
m_b	:	Mass of the bogie
I_b	:	Moment of inertia of bogie
c_b	:	Damping coefficient of axle springs
k_b	:	Stiffness coefficient of axle springs
m_w	:	Mass of wheel set
l_w	:	Half distance of wheel base
d	:	Regular spacing of group of axles
e_v	:	Eccentricity of the train loading
L	:	Span Length
LM	:	Load Model
HSLM	:	High Speed Load Model

Φ_3	:	Dynamic factor for railway Load Model 71
φ', φ''	:	Dynamic enhancement of static loading for real trains
φ'_{dyn}	:	Dynamic enhancement of static loading for real train determined from a dynamic analysis
L_φ	:	Determinant length
Y_{dyn}, y_{stat}	:	Maximum dynamic response and maximum corresponding static response at any particular point
Max	:	Maximum
a	:	Distance between rail supports, distributed loads length
n_0	:	First natural bending frequency of the bridge loaded by permanent actions (Hz)
n_t	:	First natural torsional frequency of the structure
ζ	:	Lower limit of percentage of critical damping (%), or damping ratio
$\Delta\zeta$	:	Additional damping (%)
ζ_{Total}	:	Total damping (%)
w_i, w_j	:	Natural frequencies (rad/s)
a_0	:	Mass proportional coefficient of Rayleigh Damping
a_1	:	Stiffness proportional coefficient of Rayleigh Damping
v_i	:	Resonant Speed
λ_i	:	Principal wavelength of frequency of excitation
E	:	Elastic Modulus
I	:	Moment of Inertia
EI	:	Flexural Rigidity
EI/L	:	Flexural Stiffness
u	:	Vertical Modal Displacement

CHAPTER 1

INTRODUCTION

1.1. History

In the 19th and early 20th Centuries, railway trains played a vital role in passenger and freight transport. In the latter half of the 20th Century, the automobiles and the aircraft have eroded the importance of railway passenger transportation. Over the last couple of decades, high speed rail transport have been started to become popular compared to highway and airway transportation since it is cost competitive. Especially, high speed freight has come into prominence. Transportation of large amount of freight in short-time period with less fuel consumption makes high-speed freight trains essential in freight transportation.

Travel speed, in exceedence of 200 km/h is called as high-speed rail travel. High-speed rail trains are typically electrically driven via catenaries except in some countries like Germany where diesel locomotives are used. Magnetic levitation (MAGLEV) trains fall under the category of high-speed rail trains due to their association with track oriented vehicles; however their inability to operate on conventional railroads often leads to their classification in a separate category [1].

In 1964, the first high-speed train, called Tōkaidō Shinkansen built by Kawasaki Heavy Industries, was operated in Japan. The first high-speed train achieved speeds of 200 km/h on the Tokyo–Nagoya–Kyoto–Osaka route. In

Europe, high-speed rail travel started during the International Munich traffic exposition when DB Class 103 hauled a total of 347 demonstration trains at 200 km/h between Munich and Augsburg. The first regular service at speeds of 200 km/h was the TEE "Le Capitole" route between Paris and Toulouse with SNCF Class BB 9200 locomotives adapted to high speed travel [1].

The most popular examples of high-speed trains are the TGV of France and the APT of The United Kingdom. The name "Train à Grande Vitesse" translated into English means high speed train. The TGV project started in the 1960's when SNCF realized that if it would have to compete against the growing highway and air transport, it had to offer seriously better speeds cutting down the duration of transport. The very first electric TGV launched in 1981. In commercial use, it travels at speeds up to 270 km/h. It broke a speed world record of 370km/h in 1981.

The Advanced Passenger Train (APT) project was developed around the late 70's and early 80's. Railways in the UK typically have more curves than the ones in Europe. Curved alignment is a disadvantage in terms of passenger comfort is considered. The trains have a floating centre of gravity of its own when going round corners, to minimize undesired effects of turning. In the late 1970's three prototypes were built by this cutting edge technology.

The regular-service with full size trains started on the London-Glasgow line for a period, until the service was shut-down due to frequent operational and mechanical problems. The problems were sorted out after a while but people had lost interest in the project because of financial problems.

The new world speed record by the French TGV is 515 km/h. However these high speeds are not really viable commercially at the moment for a number

of reasons. There are problems encountered with pantographs contact and wear and tear to equipment is too high. There are also safety issues which prevent civilians travelling at such high speeds. Travel speeds are generally in around 300 km/h in Europe, while the UK travel speeds are likely to remain stable. In the future travel speeds are planned to be around 360 km/h for commercial use which can be quite feasible, for the next generation of TGV but not for the Inter City Experimental (ICE) which is high speed train of Germany. The ICE which was firstly operated in 1985, was capable of 330 km/h in 1999 although speeds were limited to 300 km/h in revenue service [2].

In Turkey, high-speed rail project has started in 2003 by the coordination of The Turkish State Railways. The first line, which has a length of 533 km from Istanbul via Eskişehir to Ankara is under construction and will reduce the travelling time from 6–7 hours to 3 hours 10 minutes. Trials began on April 23, 2007 but revenue earning service has yet to commence. The completion of the first line is scheduled to be achieved in 2009. The second line, began in 2006 is Ankara - Konya line whose length is 300 km. The commercial high speed trains are expected to reach top speeds of 250-300 km/h in Turkey. The first ten TCDD HT65000 high-speed train sets were purchased from CAF of Spain, and have a maximum speed of 250 km/h [3].

1.2. Objectives and Scope of the Study

Multiple simple span precast prestressed concrete superstructure is a very common type selected by railroad agencies in Turkey. Composite steel I-girder railroad bridges are known to be used in other countries such as France, USA and Germany.

Number of standard railroad passenger train services cannot meet increasing demand in transportation. A need rose to improve vehicle speeds, which would result in increase in number of train services. Increasing vehicle speed without an improvement of the line including bridge superstructures can result in discomfort of passengers and can also result in derailment. In year 2004, 80 of 230 passengers injured and 41 passengers died due to an accelerated service on a standard railroad line. Train named Yakup Kadri Karaosmanoğlu derailed at Pamukova Region in Ankara-İstanbul accelerated service as seen Figure 1.1. According to accident technical report, train passed the horizontal curve which has 345 m radius with a speed of 132 km/hr. However, the upper speed limit in a horizontal curve is 80 km/hr. Improper railroad line, inadequate signalization system and rough line surface were shown as reason of accelerated train service accident [33]. Another derailment accident occurred in Eskişehir in November, 2009. 91003 service numbered high speed train derailed at Hasanbeyli Region which is 10 km away from Eskişehir as seen Figure 1.2 and Figure 1.3. Train derailed at turnout point where high speed rail line connects to conventional line. Train passed to conventional line at this turnout due to maintenance and repair of high speed rail line. Train speed was 105 km/hr at turnout where the speed limit was stated as 30 km/hr. Fortunately, no people died in Hasanbeyli accident. In Turkey, 10 large scaled train accidents have occurred since 2000. Four accidents caused by derailment as shown in Table 1.1.

Bir şov uğruna öldüler

Uzmanlar, "Raydan çıkma olabilir. Seferi durdurun" dedi. Kimse dinlemedi. Ve facia dün geldi

TCDD, gece boyunca trenin hızını açıklayamadı. Yolculara göre 136 kilometre hızla gidiyordu

Hatam varsa istifa ederim

TCDD yetkililerine göre trenin kaza sırasında 80 kilometreydi. Ancak yolculardan Muhittin Arık, "Dijital göstergeyi gördüm. Raydan çıkmadan 5 dakika önce hız 136 kilometreydi" dedi. TCDD Genel Müdürü Süleyman Karaman "Konuyu halletse, hatam varsa yüz kere istifa ederim" dedi.

Fotoğraf: ERCAN ARSLAN

Bir skandal da ölü sayısında

Haydarpaşa'dan dün saat 18.00'de hareket eden Yakup Kadri Karaosmanoğlu Ekspresi'nin yemekli dahil beş vagonu Pamukova'da raydan çıktı. Sağlık Bakanlığı'na göre 234 yolcudan, 130'u hayatını kaybetti. Bu rakam daha sonra değiştirildi, 36'ya indirildi. Çelişki, yabancı ajanslar tarafından da tüm dünyaya duyuruldu.

Figure 1.1 Pamukova Train Accident [33]

Figure 1.2 Hasanbeyli Train Accident [33]

Figure 1.3 Hasanbeyli Train Accident [33]

Dynamic train-bridge interactions can intensify vibration amplitudes dramatically with the increase of train speeds. Track radius, curves, use of continuous welded rail segments can impose restrictions to train speed. Passenger discomfort can be one of the important factors on limiting train speed rather than derailment. Flexural rigidity and ballast stiffness can also impose critical effects on the comfort of passengers.

The aim of this research is to identify superstructure rigidity thresholds to minimize passenger discomfort.

Some of the design parameters of widely used railroad bridge specifications are presented in Tables 1.2 and 1.3. Most of the steel railroad bridge design is governed by the service conditions such as deflection, passenger comfort, fatigue criteria, but not by the load resistance factor design.

Table 1.1. Large Scaled Train Accidents in Turkey Since 2000 [1]

Date	Region	Accident
April 16, 2004	Temelli, Ankara	İzmir to Ankara express hits a truck in Temelli, near Ankara, as it crossed a level-crossing. 7 to 10 children die and 2 to 5 more injured.
July 23, 2004	Pamukova, Sakarya	An Istanbul-Ankara express with 230 people on board, and carriages overturned with derailed at Pamukova, Sakarya Province, according to Turkish government official confirmed, killing at least 41, injuring another 80.
August 4, 2004	Tavşancıl, Kocaeli	6 die and 85 injured when a train driver falls asleep at the controls, goes through a red light and hits a stationary train head-on.
November 10, 2004	Ankara	37 die when an express train hits a truck on a crossing near Ankara and derailed.
November 14, 2004	Ankara	15 die and 45 injured as another express train derails near Ankara.
November 23, 2005	Mersin	At 6.30 am a train hit a truck on a level crossing between Tarsus and Mersin. 9 died and 18 were injured.
January 4, 2007	Hatay	A freight train smashes into a truck carrying farm workers at a railroad crossing in Hatay Province, killing 7 and injuring 19.
January 27, 2008	Pamukkale, Denizli	A Pamukkale Express bound for Denizli, with 436 passengers on board derailed after two cars rolled over at Kutahya due to ice on the tracks in western Turkey, killing nine, and injuring another 50.
June 23, 2008	Nurdağı, Gaziantep	A freight train rammed into a minibus at a level crossing in Nurdagi, Gaziantep, killing 11 bus passengers.
November 14, 2009	Hasanbeyli, Eskişehir	An Ankara-Eskişehir express with 245 passengers overturned with derailed at Hasanbeyli, Eskişehir Province.

In scope, a dynamic and a static bridge model have been developed to understand the effect of dynamic responses of a train passing over a bridge. The effect of passenger comfort on design is investigated.

In many railroad bridge specifications, static load representative of train load is magnified by a dynamic factor to account for the dynamic effects induced by the train passage. This dynamic factor covers the dynamic effects associated to a single moving load but does not include the possibility of resonant effects due to the periodicity of the moving loads. In this thesis, resonant effects due to train passes were investigated through force-time analyses and comparison of dynamic factor approach and force-time approach was done.

Table 1.2. Comparison of Railroad Bridge Specifications

Specification / **Subject**	**A.R.E.M.A.**	**EUROCODE**
Design Method	Allowable Stress Design	Allowable Stress Design & Load Factor Design
Design Speed Limit	110 km/hr to 145 km/hr	144 km/hr to 300 km/hr
Deflection Limit	Vertical: ℓ / 640 Lateral : 10 mm/19m	Vertical : ℓ / 600 Twist : 1.5 mm/3m
Vibration Limit	---	Ballasted Deck : 3.5 m/s^2 Open Deck : 5.0 m/s^2
F_y-Min. Yield Point	244 MPa	235 MPa
F_u-Ultimate Strength	380 MPa	420 MPa
Allowable Tensile Stress	0.55 F_y	---

Table 1.3. Load Cases of Specifications

Load Case & Explanation	A.R.E.M.A.	EUROCODE
Dead Load		
Steel	7850 kg/m^3	7850 kg/m^3
Concrete	2400 kg/m^3	2400 kg/m^3
Ballast	1920 kg/m^3	1720 kg/m^3
Live Load		
Dynamic Train Load	Cooper E 80	HSLM
Static Train Load	Live Load on 4 axles	LM 71
Impact Load (live load)		
Percentage of Live load Open deck: L < 24.4 m	$(40-\frac{3(L*3.28)^2}{1600})\%$	$\frac{\alpha}{100}\left[56e^{-\left(\frac{L_\phi}{10}\right)^2}+50\left(\frac{L_\phi n_0}{80}-1\right)e^{-\left(\frac{L_\phi}{20}\right)^2}\right]$
L ≥ 24.4 m	$(16+\frac{600}{(L*3.28)-30})\%$	
Ballasted deck: Percentage of open deck	90 %	
Impact Load (rocking effect)		
Percentage of Wheel load	20 %	---
Longitudinal Force		
Braking Force	(200 + 17.5 L) kN	(20 L) kN
Traction Force	$200\sqrt{L}$	(33 L) kN

CHAPTER 2

LITERATURE REVIEW

Zhai and Cai [4] described a numerical simulation technique that was used to investigate the dynamic train-bridge interaction. Two dynamic analysis models were developed to simulate the structural dynamic responses due to train passes over a bridge with ballasted track and non-ballasted slab track. Effect of the wheel and track-structure interaction on the system dynamics was considered in the models. Influence of track random irregularities on train-bridge dynamic interactions was also investigated. The proposed simulation technique was utilized at the Chinese first special railway line for passenger service. In this study, the structural design of three extraordinary large bridges with non-ballasted tracks was evaluated through a detailed simulation in the design stage and results showed that these bridges were able to satisfy the demand of dynamic performance for the high-speed transport.

In Song's, Nohb's and Choi's study [5], a new finite element model for three-dimensional analysis of high-speed train–bridge interaction was developed, in which various improved finite elements were used for modeling the structural members of a railway bridge. Specifically, the deck of a railway bridge was modeled by nonconforming flat shell (NFS) elements with 6 DOFs, which showed high performance in the numerical examples of previous researches of Song's. The track structures were idealized using beam finite elements with the offset of beam nodes and assumed to be beams on a two-parameter elastic foundation. Also, the vehicle model devised for a high-

speed train was employed, which had a combined bogie system. Using Lagrange's equation, the equations of motion of the vehicle–bridge system can be formulated. By deriving the equations of the forces acting on the bridge considering the vehicle–bridge interaction forces, the complete system matrices of the total vehicle–bridge system can be constructed. As numerical examples of this study, a simply supported steel–concrete composite railroad bridge and a two-span PC box-girder railroad bridge were analyzed and results were compared with those of previous research and experimental results.

In the study of Frỳba [6] an elementary theoretical model of a railroad bridge was investigated using the integral transformation method which provides an estimation of the amplitudes of the free vibration and also the critical speeds at which the resonance vibration may occur were given. As a result of this study, simple expressions similar to dynamic impact factor which was defined as the difference between the maximum dynamic response and the maximum static deflection, bending moment and acceleration of the bridge deck values which enable to assess the railway bridges for high speed trains were taken. These theoretical values were satisfactorily compared with the experimental data.

A paper of Geier and Osterreicher [7] presents a combined assessment method that can be applied to evaluate railway bridges subject to dynamic stress in accordance with Eurocode 1. The objective of the method described in the paper was to assess the adherence to permissible structural acceleration by taking into account dynamic magnification factors based on a computer model. As a conclusion, the effects of boundary beams, ballast and rails had a major influence on the dynamic properties of the structure as far as short to medium span railway bridges were concerned.

Museros, Romero, Poy and Alarcon [8] made a study to eliminate the difference between the results of a moving load model and more sophisticated model analysis on short bridges. They concluded that the maximum accelerations of the deck are not significantly affected from the load distribution through the sleepers and ballast layer and train-bridge interaction causes reductions of considerable importance in the maximum displacements and accelerations of short bridges.

By idealizing the train as a sequence of identical vehicles moving at constant speed, Biondi, Muscolino and Sofi [9] investigated the dynamic interaction between a running train, the track structure and the supporting bridge by using substructure technique. The rails and the bridge were modeled as Bernoulli-Euler beams and the ballast was characterized as viscoelastic foundation. Consequently, an accurate and efficient model was developed.

De Roeck, Maeck and Teughels [10] studied vibration issue to validate the previously developed numerical models at a high speed train bridge in Antoing. A dynamic displacement of 2 mm for a span of 50 m and a bridge acceleration of 1 m/sec^2 was measured which were very small values when compared with usual values of other bridge measurements. This situation was associated with the stiffness of the bridge.

Xia and Zhang [11] studied dynamic interaction between high speed train and railroad bridge by theoretical analysis and field experiment. Each vehicle was composed of a body, two bogies and four wheel-sets and the spring-dashpot suspensions between three components. Each of the bodies, bogies and wheels respectively has five, five and three degrees of freedom systems. Consequently vehicles were modeled by twenty seven degrees of freedom and the bridge was modeled by modal superposition technique. The whole

recorded histories of the China-Star high speed train on the Qin-Shen Special Passenger Railway in China were applied on the computational analysis model and the calculated results were compared with the measured data. Consequently, a well match was achieved between the calculated and the measured data.

Cheung, Au, Zheng and Cheng [12] also had similar study as Xia and Zhang. Based on the Lagrangian approach, the vibration of a multi-span non-uniform bridge subjected to a moving vehicle was analyzed by using modified beam vibration functions as the assumed modes in their study. The vehicle was modeled as a two-degree-of-freedom system. The method was extended to the action of a moving train by modeling it as a series of two-degree-of-freedom systems. All the derived formulas were expressed in matrix form. The total number of unknowns for this method was very small compared with that of the finite element method. Convergence was very quick and in almost all cases twelve to sixteen terms were sufficient to give satisfactory results.

Heiden, Bokan, Simoes da Silva, Greiner, Pirchere and Pircher [13] discussed the organization of part 2 of Eurocode 1 and the annex A2 of Eurocode 0, with special emphasis on the design checks associated with dynamic effects and train-bridge interaction. Additional rules recently imposed in the German regulations and the application of these rules to a composite railway bridge which was currently being designed for the German rail network were handled in details. It was found that the type of bridge that presented at the study complies with both of the requirements.

Dynamic experiments on the Antoing Bridge were executed and reported by Xia, De Roeck, Zhang and Maeck. [14] In the experiments, dynamic

responses of the bridge like deflections, accelerations and strains were gauged by a laser velocity displacement transducer accelerometers and strain gauges.

Analysis modeling methodologies were studied by Delgado and dos Santos. [15] The railway traffic on bridges was performed by two different methodologies. The first model contained a set of moving masses which the effects of the moving forces and masses implied. In the second model both the structural behavior of the train and the interaction with the bridge were involved. The main aim of the study was to evidence the importance of different parameters such as stiffness and mass of the bridge, stiffness of the train; in order to investigate the structural behavior of the bridge and the passenger comfort. Various parameters were studied with a railroad bridge, such as stiffness and length of the railroad bridge, existence of ballast, structural damping and irregularities in the track. In parametric study, stiffness and irregularities were investigated as the most important parameters inducing the response.

Goicolea, Dominguez, Navarro and Gabaldon [16] proposed a general revision of available methods for dynamic calculation, as well as a description of the provisions in the new Spanish Code IAPF and Eurocode 1 for actions on bridges. They also proposed a simplified method for dynamic analysis of portal frames. In this study, several simplified or sophisticated analysis models were described for the purpose of design of high speed railroad bridges which requires consideration of dynamic vibration under moving loads because of the real possibility of resonance.

Ju and Lin [17] investigated resonant characteristics of three-dimensional bridges under high-speed train loadings. Multi-span bridges with high piers

and simply supported beams were used in the dynamic finite element analysis. It was concluded that to avoid resonance, the dominated train frequencies and the bridge natural frequencies should be as different as possible, especially for the first dominated train frequency and the first bridge natural frequency in each direction. This study also indicated that a suitable axial stiffness between two simple beams can reduce vibrations at a near-resonance condition.

Yang, Yau and Hsu [18] developed a train model to investigate the vibration of simple beams subjected to the passage of high speed trains as a composition of two subsystems of wheel loads of constant intervals, with one consisting of all the front wheel front wheel assemblies and the other rear assemblies. By an analytical approach, the key parameters that govern the dynamic responses of the beams were identified, using the moving load assumption. As a result, several design parameters were obtained to avoid resonance situation.

Lin, Wan and Chen [19] researched applicability of multiple tuned mass dampers to suppress train-induced vibration on railway bridges. A railway bridge was modeled as an Euler-Bernoulli beam and a train was simulated as a series of moving forces, moving masses, or moving suspension masses. An MTMD system and single PTMD system were designed to alter the bridge dynamic characteristics to avoid excessive vibrations. The MTMD vibration control effectiveness for the simply supported bridges were proposed in the original THSR design proposal subjected to the German ICE, French TGV, and Japanese SKS train loads. As a result, simply supported bridges of the Taiwan High-Speed Railway under real trains show that the proposed MTMD is more effective and reliable than a single TMD in reducing dynamic responses during resonant speeds, as the train axle arrangement is regular.

It was observed that since each PTMD moves independently, the MTMD system thus contains multiple adjustable natural frequencies. This makes the MTMD system own a wider frequency range than a single PTMD and be more reliable to cover the vibration frequency of the primary structure through proper design of the MTMD parameters. As a result of comparison of a single PTMD and a MTMD, it was shown that the MTMDs were more effective in reducing the dynamic bridge responses in the existence of detuning effect. Meanwhile, the resonant responses excited by the TGV train were more apparent than those by other trains. This was due to the fact that the axle arrangement of the TGV train is more regular than those of other trains. The MTMD was more effective in reducing the maximal dynamic responses excited by the TGV train. The reductions are about 36% and 57% for maximal displacement and acceleration, respectively. The results of this study show that TMD systems are effective to reduce vibrations in range of 10% to 45%. The most inefficient results which were 10% reduction in vertical acceleration and 5% reduction in vertical displacement at mid-span were taken for a single PTMD system for ICE train type passage. The most efficient results which were 45% reduction in vertical acceleration and 25% reduction in vertical displacement at mid-span were taken for a MTMD system for TGV train type passage.

Theyse and Transportek [20] studied to illustrate the effect of the level of compaction and the degree of saturation on stiffness, strength, and plastic deformation of ballast layers. The behavior of ballast material and modeling methods were investigated.

Guerrero and Vallejo [21] presented the results of two discrete element method simulations intended to study the effect of crushing on the behavior of a simulated track ballast material forming part of a simulated track section. The

simulated track sections were subjected to a cyclic load, and the values of permanent deformation as a function of number of cycles were recorded. The obtained results showed that the induced permanent deformation strongly increased when considering particle crushing even though only a few particles were broken.

Caner, Erdem and Bozalioğlu [34] studied types of superstructures of high speed railroad bridges. Prestressed precast I-girder and post-tensioned box girder superstructures in terms of passenger comfort and vibration, traction and braking forces, thermal effects and earthquake effects were compared. The obtained results showed that vertical accelerations of post-tensioned box girder were smaller than vertical accelerations prestressed precast I-girder and also it was observed that maximum vertical accelerations occurred in resonance speed. As a conclusion, it was stated that box girder superstructure was more efficient than prestressed I-girder superstructure in aspects of train security, passenger comfort level, earthquake performance and maintenance cost.

In this context, modeling of the vehicle-bridge interaction system is in great importance, since the main scope is to determine the relation between the bridge span length, ballast stiffness, flexural rigidity and passenger comfort. Moving Force Models and Static Models with dynamic factors have been used by combining the train and bridge parameters of Eurocode 1991-2 [22] and A.R.E.M.A. [23].

CHAPTER 3

DESIGN CRITERIA & ANALYSIS PROCEDURE

3.1. Analysis Guidelines

Railway bridge specifications classify the design of high speed railway bridges into two main groups. In one, it is required to check when bridge is in service and in other one it is required to check the rail tension and superstructure displacement. Dynamic effects due to train, traffic safety and passenger comfort can be checked per requirements of A.R.E.M.A., 2006 and Eurocode 1991-2:2003. The rail tension and superstructure displacement can be checked for bridge-rail live load interaction. The aim of this study is to evaluate impact of high speed travel on bridges designed for conventional speeds per A.R.E.M.A. [23] in whose scope high speed trains are not included under high speed train loads of Eurocode 1991-2. Checks for track system; rail, sleepers and ballast are not in scope of this thesis.

The requirement of whether a static or a dynamic analysis is determined using the flow chart in EN 1991-2 as shown in Figure 3.1. The flow chart depends on limit design speed of vehicle, simplicity of bridge, span length, and first natural torsional and bending frequencies of bridge.

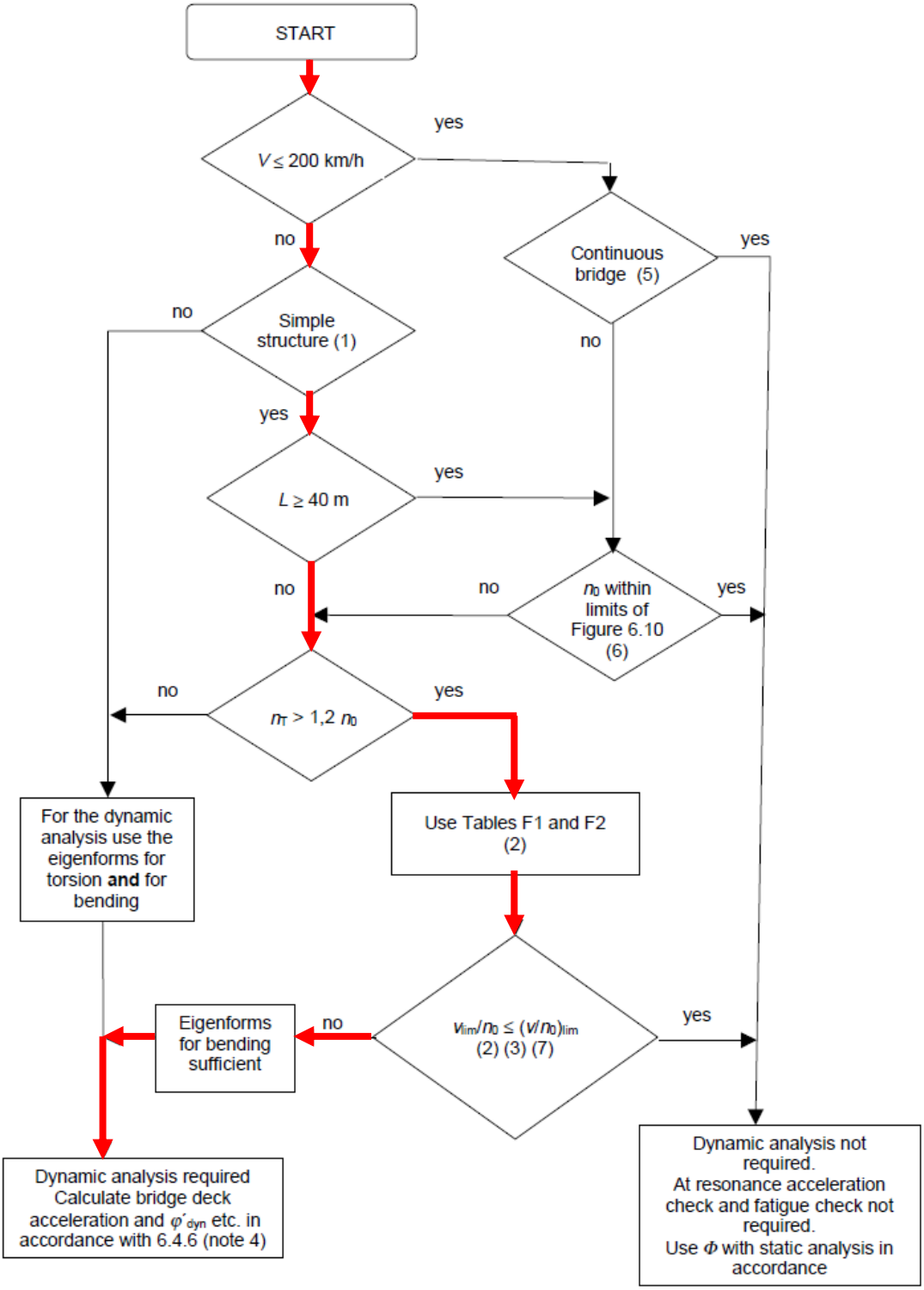

Figure 3.1 Flow chart for determining whether a dynamic analysis is required [22]

Table 3.1 Maximum Value of $(v/n_o)_{lim}$ for a simply supported beam or slab and a maximum permitted acceleration of $a_{max} < 3.50$ m/s^2 [22]

Mass m 10^3 kg/m		≥ 5.0 <7.0	≥ 7.0 <9.0	≥ 9.0 <10.0	≥ 10.0 <13.0	≥ 13.0 <15.0	≥ 15.0 <18.0	≥ 18.0 <20.0	≥ 20.0 <25.0	≥ 25.0 <30.0	≥ 30.0 <40.0	≥ 40.0 <50.0	≥ 50.0 -
Span $L \in$ m	ζ %	v/n_0 m	v/n_0 m	v/n_0 m	v/n_0 m	v/n_0 m	v/n_0 m	v/n_0 m	v/n_0 m	v/n_0 m	v/n_0 m	v/n_0 m	v/n_0 m
[5.00,7.50)	2	1.71	1.78	1.88	1.88	1.93	1.93	2.13	2.13	3.08	3.08	3.54	3.59
	4	1.71	1.83	1.93	1.93	2.13	2.24	3.03	3.08	3.38	3.54	4.31	4.31
[7.50,10.0)	2	1.94	2.08	2.64	2.64	2.77	2.77	3.06	5.00	5.14	5.20	5.35	5.42
	4	2.15	2.64	2.77	2.98	4.93	5.00	5.14	5.21	5.35	5.62	6.39	6.53
[10.0,12.5)	1	2,40	2.50	2.50	2.50	2.71	6.15	6.25	6.36	6.36	6.45	6.45	6.57
	2	2.50	2.71	2.71	5.83	6.15	6.25	6.36	6.36	6.45	6.45	7.19	7.29
[12.5,15.0)	1	2.50	2.50	3.58	3.58	5.24	5.24	5.36	5.36	7.86	9.14	9.14	9.14
	2	3.45	5.12	5.24	5.24	5.36	5.36	7.86	8.22	9.53	9.76	10.36	10.48
[15.0,17.5)	1	3.00	5.33	5.33	5.33	6.33	6.33	6.50	6.50	6.50	7.80	7.80	7.80
	2	5.33	5.33	6.33	6.33	6.50	6.50	10.17	10.33	10.33	10.50	10.67	12.40
[17.5,20.0)	1	3,50	6.33	6.33	6.33	6.50	6.50	7.17	7.17	10.67	12.80	12.80	12.80
[20.0,25.0)	1	5.21	5.21	5.42	7.08	7.50	7.50	13.54	13.54	13.96	14.17	14.38	14.38
[25.0,30.0)	1	6.25	6.46	6.46	10.21	10.21	10.21	10.63	10.63	12.75	12.75	12.75	12.75
[30.0,40.0)	1				10.56	18.33	18.33	18.61	18.61	18.89	19.17	19.17	19.17
≥ 40.0,	1				14.73	15.00	15.56	15.56	15.83	18.33	18.33	18.33	18.33

In Figure 3.1;

V is the maximum line speed equal to 300 km/h

L is the span length

n_0 is the first natural bending frequency of the bridge loaded by permanent actions (Hz)

n_T is the first natural torsional frequency of the bridge loaded by permanent actions (Hz)

$(v/n_0)_{lim}$ is given as a function of v_{lim}/n_0 in EN 1991-2 Annex F Table F1 given in Table 3.1.

In Table 3.1;

L is the span length

m is the mass of bridge

ζ is the percentage of critical damping equal to 0.5 %,

v is the Maximum Nominal Speed and is generally the Maximum Line Speed at the site equal to 83.3 m/s,

n_0 is the first natural frequency of the span (Hz).

Additionally, dynamic analysis requisite was checked according to the bridge first natural frequency by using EN 1991-2 Figure 6.10 shown in Figure 3.2.

As per EN 1991-2 Section 6.4.4;

The upper limit denoted as line (1) in Figure 3.2 ;

$$n_0 = 94.76\ L^{-0.748} \quad \text{..... (3.1)}$$

The lower limit denoted as line (2) in Figure 3.2;

$$n_0 = 80/L \quad \text{for } 4m \leq L \leq 20m \quad \text{..... (3.2)}$$

$$n_0 = 23.58\ L^{-0.592} \quad \text{for } 20m < L \leq 100m \quad \text{..... (3.3)}$$

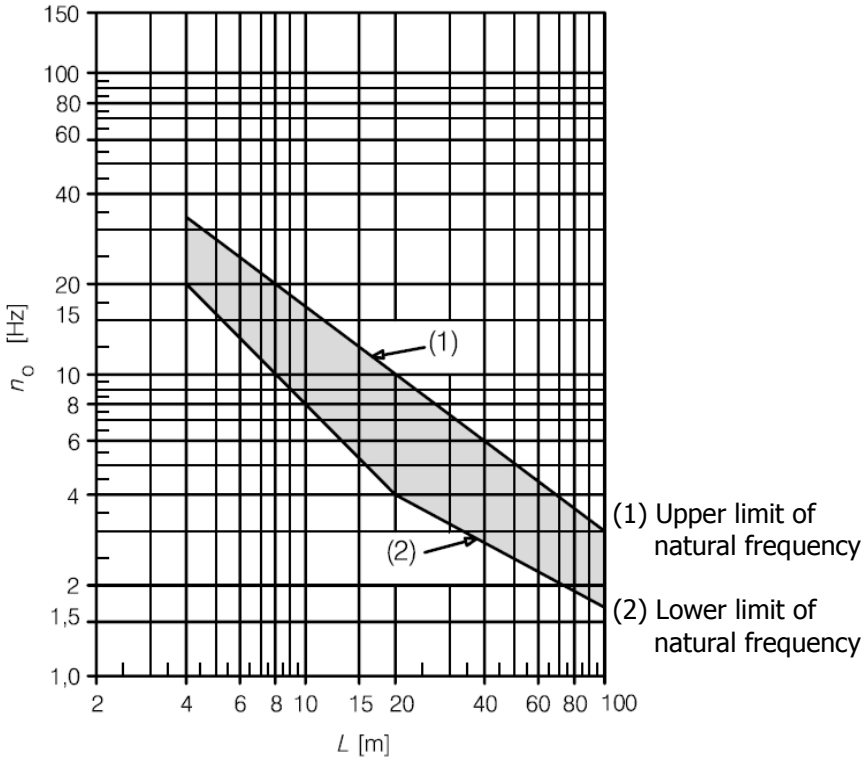

Figure 3.2 Limits of bridge natural frequency n_0 (Hz) as a function of L (m) [22]

The upper limit of n_0 is governed by dynamic increments due to track irregularities which are not in scope of this study and the lower limit of n_0 is governed by dynamic impact criteria. If first natural frequency of bridge exceeds the upper limit, a dynamic analysis is required [22].

The natural frequency of simply supported bridge subjected to bending only can be approximately calculated by equation given below as stated in Eurocode 1991-2 Section 6.4.4

$$n_0 = \frac{17.75}{\sqrt{\delta_0}} \text{ (Hz)} \quad \text{..... (3.4)}$$

δ_0 is mid-span deflection in millimeters under permanent actions.

Dynamic impact effects of trains were calculated according to A.R.E.M.A., 2006 Chapter 15 Section 1.3.5 and Eurocode 1991-2:2003 Section 6.4.6.

Statically modeled axle load for track with standard track maintenance in Eurocode 1991-2 is,

HSLM x $(1 + \varphi'_{dyn} + \varphi'')$ ..... (3.5)

Dynamic increment as per section 6.4.6.5;

$$\varphi'_{dyn} = \max\left|y_{dyn}/y_{stat}\right| - 1 \quad \text{..... (3.6)}$$

where;

- y_{dyn} is the maximum dynamic response at any particular point in the structural element due to load model HSLM
- y_{stat} is the maximum static response at any particular point in the structural element due to load model HSLM

The increase resulting from track defects and vehicle imperfections in accordance with EN 1991-2 Annex C;

$$\varphi'' = \frac{\alpha}{100}\left[56e^{-\left(\frac{L_\Phi}{10}\right)^2} + 50\left(\frac{L_\Phi n_0}{80} - 1\right)e^{-\left(\frac{L_\Phi}{20}\right)^2}\right] \quad \text{..... (3.7)}$$

$\varphi'' \geq 0$

where;

- v is the Maximum Permitted Vehicle Speed, m/s
- n_o is the first natural bending frequency of the bridge loaded by permanent actions

L_Φ is the determinant length in accordance with Table 6.2 Section 6.4.5.3, m

α is a coefficient for speed

$\alpha = \frac{v}{22}$ if v ≤ 22 m/s

$\alpha = 1$ if v > 22 m/s ..... (3.8)

The determinant length allows dynamic factors to be used for structural members with different support conditions rather than simply supported girders.

Eurocode high speed trains were used in dynamic analysis in accordance with A.R.E.M.A. As a result, dynamic effect for statically modeled axle load in A.R.E.M.A. is,

HSLM x (1 + φ + $\varphi_{rocking}$) ..... (3.9)

Dynamic factor for rolling equipment without hammer as per chapter 15 section 1.3.5;

$\varphi = 40 - \frac{3(Lx3.28)^2}{1600}\%$ for L < 24.4 m

$\varphi = 16 + \frac{600}{(Lx3.28) - 30}\%$ for L ≥ 24.4 m ..... (3.10)

A.R.E.M.A states that 90 % percentage of dynamic effect should be considered for ballasted deck.

Rocking effect factor can be taken as,

$\varphi_{rocking}$= 20 % ..... (3.11)

3.2. Dynamic Analysis Parameters

3.2.1. Structural Damping Ratio

Damping is an effect that tends to reduce the amplitude of response and the damping ratio is a measure describing how vibrations in a system decay after a disturbance.

In dynamic analysis damping ratio values according to EN 1991-2 Section 6.4.6.3 were used.

Table 3.2 Values of damping to be assumed for design purposes [22]

Bridge Type	**ζ (%) Lower Limit Percentage of Critical Damping**	
	Span L < 20 m	**Span L ≥ 20 m**
Steel and Composite	$\zeta = 0.5 + 0.125\ (20 - L)$	$\zeta = 0.5$
Prestressed Concrete	$\zeta = 1.0 + 0.07\ (20 - L)$	$\zeta = 1.0$
Filler Beam and Reinforced Concrete	$\zeta = 1.5 + 0.07\ (20 - L)$	$\zeta = 1.5$

Bridge-vehicle mass interaction has reduction effect on peak response at resonance for spans less than 30m. This was taken account as stated in EN 1991-2 section 6.4.6.4;

$$\Delta\zeta = \frac{0.0187L - 0.00064L^2}{1 - 0.0441L - 0.0044L^2 + 0.000255L^3} \quad \text{..... (3.12)}$$

$$\zeta_{TOTAL} = \zeta + \Delta\zeta \quad \text{..... (3.13)}$$

Total damping ratio is summation of critical damping and additional damping caused by vehicle-bridge mass interaction.

Lower limit percentage of critical damping was calculated according to the Table 3.2 which depends on bridge type and span length.

Additional damping value can be calculated by either Equation 3.12 or Figure 3.3 which only depend span length of bridge.

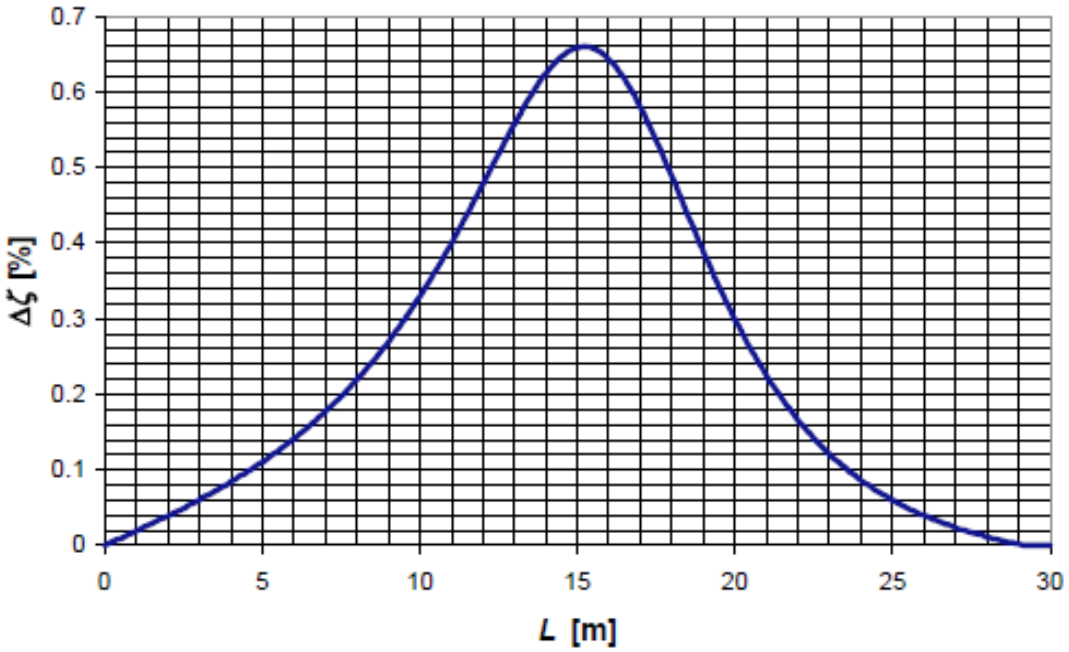

Figure 3.3 Additional damping $\Delta\zeta$ (%) as a function of span length L (m) [22]

In the transient dynamic analysis, it is necessary to apply Rayleigh damping. Rayleigh damping coefficients are required to define structural damping ratio to used structural analysis software in order to obtain results for numerically sensitive structural systems.

Rayleigh damping is a procedure to idealize the classical damping if similar damping mechanisms are distributed through the structure. The major advantage gained in converting the damping matrix into an equivalent Rayleigh damping lies in the fact that using orthogonal transformation a structure having n degrees of freedom can be reduced to n-number of uncoupled equations.

Rayleigh damping procedure consists mass-proportional damping and stiffness proportional damping [32].

$c = a_0 \mathbf{m} + a_1 \mathbf{k}$ ..... (3.14)

The damping ratio of system for n^{th} mode is [32],

$$\zeta_n = \frac{a_0}{2}\frac{1}{\omega_n} + \frac{a_1}{2}\omega_n \quad \text{..... (3.15)}$$

It is apparent that modal damping can be specified exactly at only two natural frequencies in order to solve for a_0 and a_1 in the Equation 3.15. Modal frequency analyses were performed to calculate the natural frequencies. Damping coefficients can be decomposed by solving equation 3.15 for two modes. [32]

$$a_0 = \zeta \frac{2\omega_i \omega_j}{\omega_i + \omega_j} \quad \text{..... (3.16)}$$

$$a_1 = \zeta \frac{2}{\omega_i + \omega_j} \quad \text{..... (3.17)}$$

3.2.2. Train Analysis Speed

Train model as moving forces was passed over bridge in various speeds. Design speed is limited to 145 km/hr for passenger trains in A.R.E.M.A which does not include high speed trains as stated before while Eurocode permits up to 350 km/hr. Eurocode limits the analysis of train speeds which may cause resonance. Train speeds in range of 40 m/s to maximum design speed should be analyzed as stated in equation 6.10 of EN 1991-2. The maximum design speed is 1.2 times of line speed. In this study, the effects of line speeds were analyzed. The analysis of line speed is more realistic when the technical limitations and security precautions of countries are considered. Consequently, train speeds in rage of 40 m/s to 83.3 m/s (~350 km/hr / 1.2) were investigated.

The high-speed train passage over simply supported bridges causes vertical vibrations. Bridges can exhibit a highly peaked response due to resonance effects. The resonance in the vertical direction occurs when the train-dominated frequencies approach or match the vertical natural frequencies of railway bridge. The vertical vibrations, thus vertical accelerations, become critical in resonance situation. Accordingly, speeds used in analysis were chosen as speeds cause resonance of structure. The structural natural frequencies can be determined through modal analysis. Structural frequencies with peak model displacements can be investigated in vibration analysis.

Speeds cause resonance can be estimated by two methods, one analytical peak frequencies estimation and other first natural frequency and principle wavelength of frequency estimation. First natural frequency and principle wavelength of frequency estimation method was provided by Eurocode. According to Eurocode, resonance speeds can be estimated from principle

wavelength of frequency as the multiplier of first natural frequency for simply supported bridges as formulated in EN 1991-2 section 6.4.6.2.

$$v_i = n_0 \lambda_i \quad \text{..... (3.18)}$$

where;

v_i is the Resonant Speed (m/sec),

n_0 is the first natural frequency of the unloaded structure (Hz),

λ_i is the principal wavelength of frequency of excitation,

$$\lambda_i = \frac{d}{i} \quad \text{..... (3.19)}$$

d is the regular spacing of groups of axles (m),

i is series of 1, 2, 3 or 4.

In analytical peak frequencies estimation method, resonance speeds can be estimated as back calculations of frequencies cause peak modal displacement of bridge according to regular axle distance of vehicle. Modal analysis of bridge should firstly be executed to determine the frequencies and modal displacements for each frequency. Since vertical acceleration is the parameter of passenger comfort, vertical vibration amplitude; that is vertical modal displacement, should be investigated. The critical frequency which causes the largest vertical modal displacement in range of design frequency limits should be determined. There may be a number of peak vertical modal displacements of structure for a number of frequencies as shown in Figure 3.4. The critical frequency has to be in range of design frequency limits which can be determined from the design speed limits and regular axle distance of vehicle as given in Equation 3.20.

$$n_{limit} = \frac{v_{design}}{d} \quad \text{.....(3.20)}$$

where;

v_{design} is the Design Speed Limits (m/sec),

n_{limit} is the limit natural frequency of the structure (Hz),

d is the regular axle distance (m),

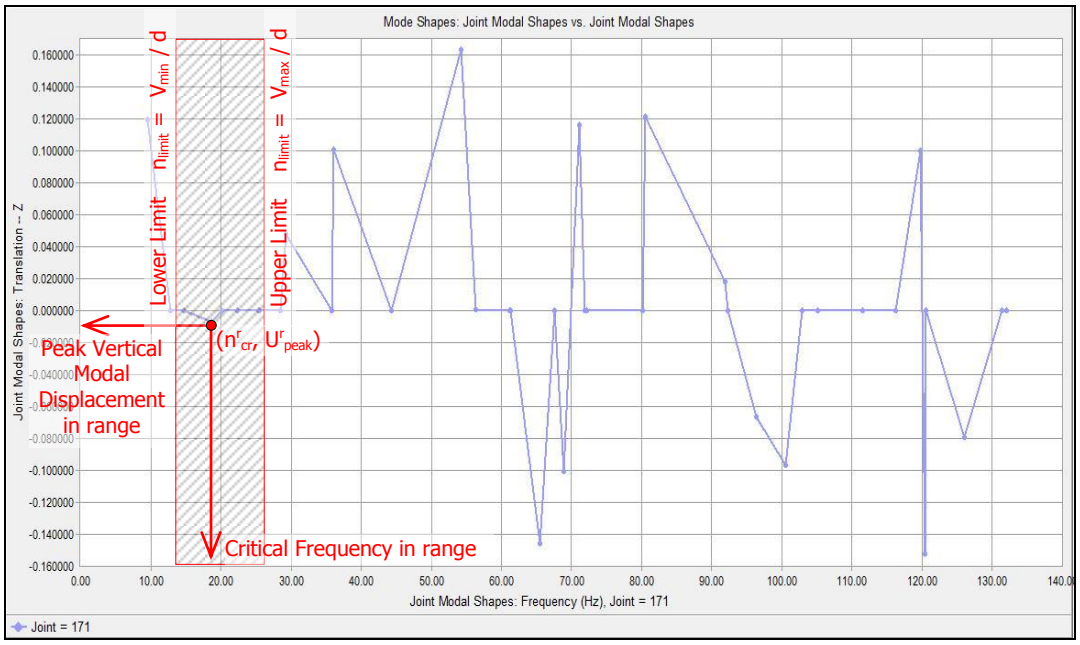

Figure 3.4 Vertical Modal Displacements vs. Natural Frequency Graph

Vertical modal displacement versus natural frequency graph shown in Figure 3.4 is an illustrative example of analytical peak frequency estimation method. This graph is taken from modal analaysis results of a case study analysis model explained in Chapter 4 and graphs for all other case studies are provided in Appendix A. In Figure 3.4, selected vertical modal displacement is not the largest vetical modal displacement of structure, however it is the peak vertical modal displacement in range of design frequency limits. Impact

load regularly applied in critical frequency determined from vertical modal displacement can cause resonance of structure. Resonance speed can be computed by back calculation; that is the multiplication of critical frequency and regular axle distance as given in Equation 3.21.

$$v_{resonance} = n_{critical} \times d \quad \text{.....(3.21)}$$

where;

$v_{resonance}$ is the Estimated Resonance Speed (m/sec),

$n_{critical}$ is the critical natural frequency of the structure (Hz),

d is the regular axle distance (m).

3.2.3. Train Loading

Eurocode defines two different type universal high speed train models, such as HSLM-A and HSLM-B. These two HSLM model differ from each other in coach length. HSLM-A and HSLM-B represent the dynamic load effects of single axle, articulated and conventional high speed passenger trains in accordance with the requirements for the European Technical Specification [22]. In accordance with the requirements of EN 1991-2 Table 6.4, shown as Table 3.3; type of HSLM model was selected since Eurocode recommends HSLM Load Model for bridges designed for international lines where European high speed interoperability criteria are applicable. Table 3.3 which depends on the structural configuration and span length of structure is only valid for bridges with longitudinal line beam or simple plate behavior with negligible skew effects on rigid supports [22].

Table 3.3 Application of HSLM-A and HSLM-B [22]

Structural configuration	Span	
	$L < 7$m	$L \geq 7$m
Simply supported span[a]	HSLM-B[b]	HSLM-A[c]
Continuous structure[a] or Complex structure[e]	HSLM-A Trains A1 to A10 inclusive[d]	HSLM-A Trains A1 to A10 inclusive[d]

[a] Valid for bridges with only longitudinal line beam or simple plate behaviour with negligible skew effects on rigid supports.
[b] For simply supported spans with a span of up to 7 m a single critical Universal Train from HSLM-B may be used for the analysis in accordance with 6.4.6.1.1(5).
[c] For simply supported spans with a span of 7 m or greater a single critical Universal Train from HSLM-A may be used for the dynamic analysis in accordance with annex E (Alternatively Universal trains A1 to A10 inclusive may be used).
[d] All Trains A1 to A10 inclusive should be used in the design.
[e] Any structure that does not comply with Note (1) above. For example a skew structure, bridge with significant torsional behaviour, half through structure with significant floor and main girder vibration modes etc.

NOTE The National Annex may specify additional requirements relating to the application of HSLM-A and HSLM-B to continuous and complex structures.

Load Model and physical properties of HSLM-A and HSLM-B trains such as coach length, axle distance, etc. was shown in Figure 3.5 and Figure 3.6.

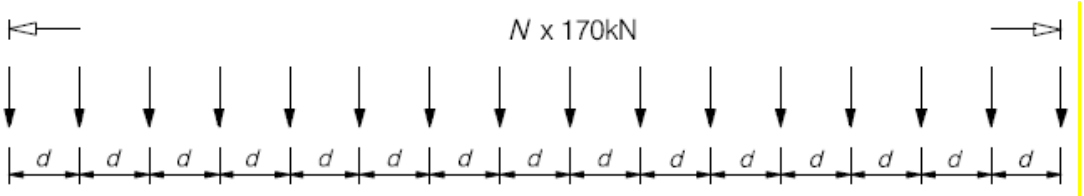

Figure 3.5 HSLM-B Type High Speed Train Model [22]

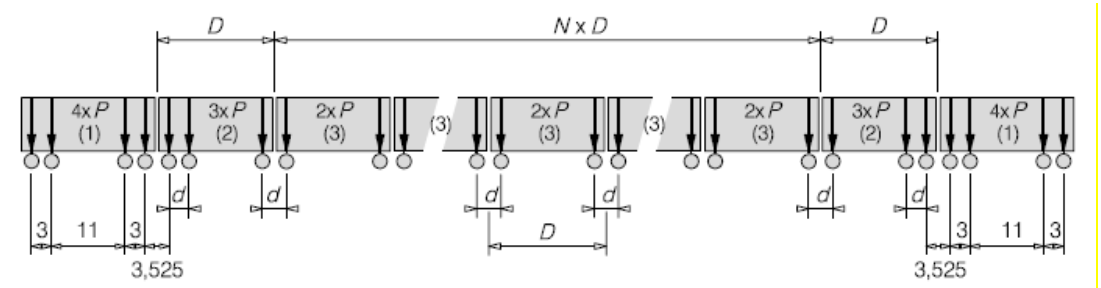

Key

(1) Power car (leading and trailing power cars identical)
(2) End coach (leading and trailing end coaches identical)
(3) Intermediate coach

Figure 3.6 HSLM-A Type High Speed Train Model [22]

HSLM-A Train has also 10 different models based on number of intermediate coaches, coach length and point force values. The critical HSLM-A train was determined according to the procedure defined in EN 1991-2 Annex E. The procedure defines the critical HSLM-A train as a function of the critical wavelength excitation by using the wave length excitation at maximum design speed, the span length of bridge and the maximum value of aggressivity. The wavelength excitation at maximum design speed is defined as,

$$\lambda_v = u_{DS}/n_o \quad \text{.....(3.22)}$$

where,

n_o is the first natural frequency of the simply supported span (Hz),

u_{DS} is maximum design speed (m/s),

The critical wavelength of excitation λ_c should be determined from Figures E.4 to E.17 in EN 1991-2 Annex E according to the value of λ corresponding to the maximum value of aggressivity for the span length in the range of excitation wavelength from 4.5m to λ_v [22].

Length of coaches can be determined by Eurocode chart given in Figure 3.7.

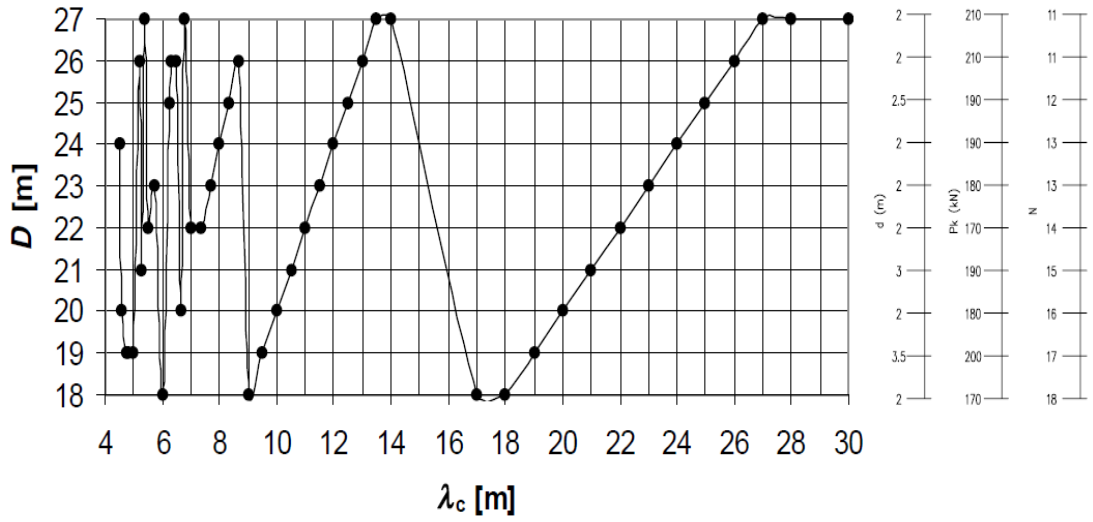

Figure 3.7 Parameters defining critical Universal Train in HSLM-A as a function of critical wavelength of excitation λ_C (m) [22]

Physical properties of HSLM A Universal Trains are given in Table 3.4.

Table 3.4 HSLM-A Train Types Properties [22]

Universal Train	Number of Intermediate coaches N	Coach Length D (m)	Bogie axle spacing d (m)	Point Force P (kN)
A1	18	18	2.00	170
A2	17	19	3.50	200
A3	16	20	2.00	180
A4	15	21	3.00	190
A5	14	22	2.00	170
A6	13	23	2.00	180
A7	13	24	2.00	190
A8	12	25	2.50	190
A9	11	26	2.00	210
A10	11	27	2.00	210

HSLM-B Universal Train comprises of N number point forces of 170 kN at uniform spacing d which are given in Figure 3.8.

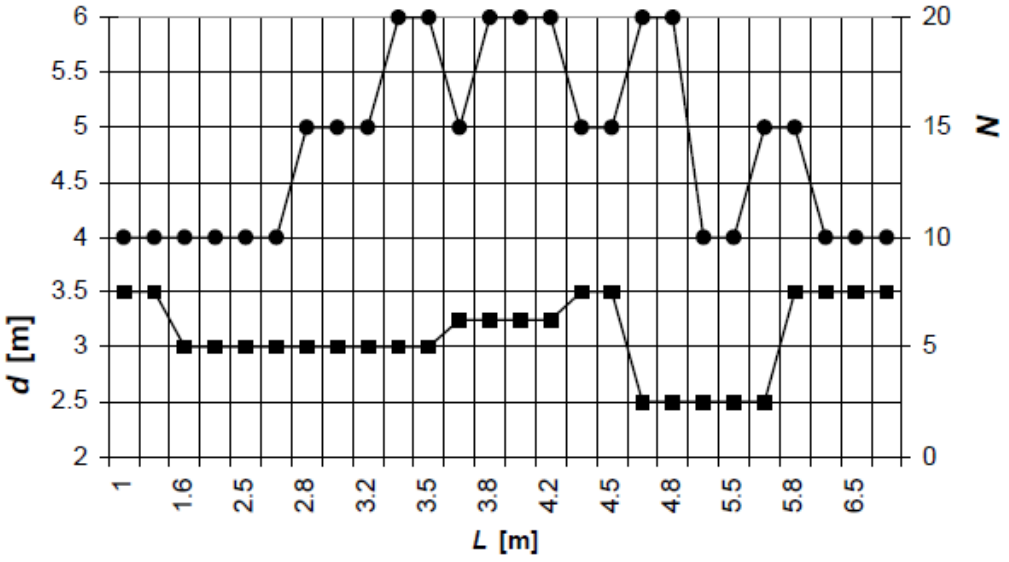

Figure 3.8 HSLM B Train Type Properties [22]

3.3. Passenger Comfort Criteria

3.3.1. Eurocode Passenger Comfort Criteria

Passenger comfort criteria are defined in Annex A2 Application for Bridges of EN1990 Basis of Structural Design. Vertical accelerations of deck, vertical deflection of deck and twist of the deck are major concerns of passenger comfort.

The maximum permitted peak value of bridge deck acceleration calculated along each track is recommended as 3.5 m/s^2 for ballasted tracks in EN1990 Annex A2 item A2.4.4.2.1. The specified levels of comfort and associated limiting values for the vertical acceleration are given in Table 3.5.

Table 3.5 Indicative Levels of Comfort [24]

Level of Comfort	Vertical Acceleration, b_v (m/s^2)
Very Good	1.0
Good	1.3
Acceptable	2.0

The maximum total vertical deflection is limited as 1/600 of span length. Vertical deflection limit for passenger comfort level is defined in Annex A2 item A2.4.4.3.1. as function of span length and vehicle speed as shown in Figure 3.9.

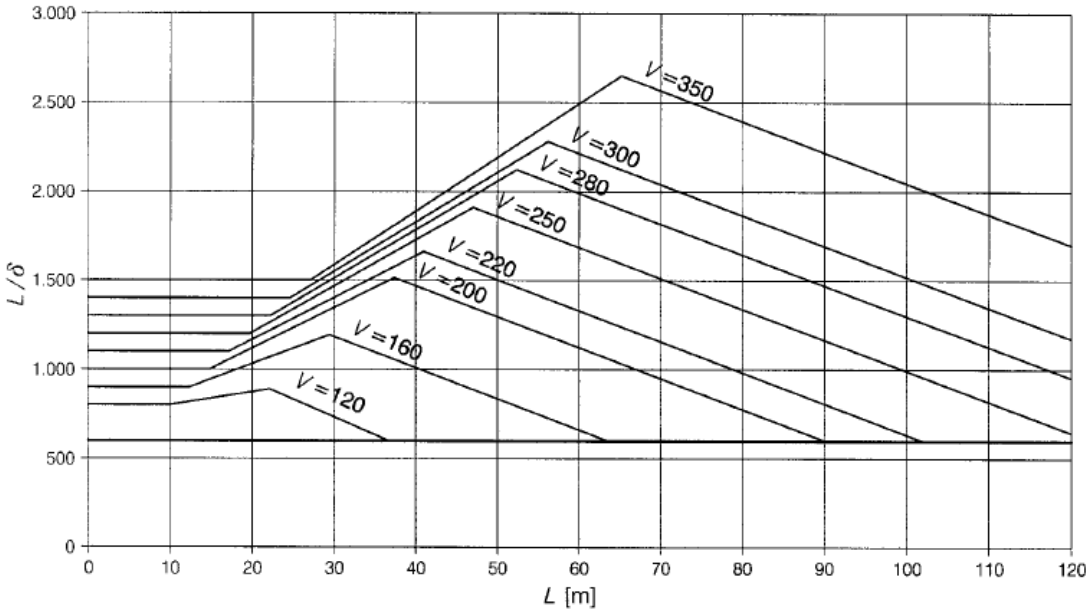

Figure 3.9 Maximum permissible vertical deflection, δ for railway bridges with 3 or more successive simply supported spans corresponding to a permissible vertical acceleration of b_v = 1 m/s² in a coach for speed V (km/h) [24]

The maximum joint rotation which is defined as twist of deck relatively calculated from joint 3 m far away from the track in transverse direction is bounded as shown in Table 3.6.

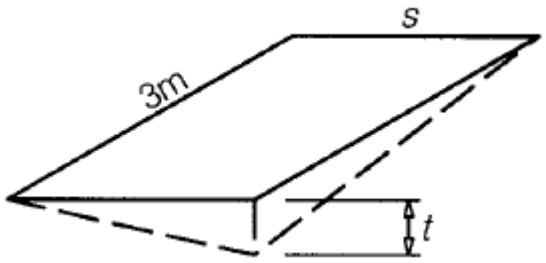

Figure 3.10 Definition of Deck Twist [24]

Table 3.6 Limiting Values of Deck Twist [24]

Speed Range, V (km/h)	Maximum Twist, t (mm/3m)
$V \leq 120$	$t \leq t_1$
$120 < V \leq 200$	$t \leq t_2$
$V > 200$	$t \leq t_3$

The recommended values for the set of t are defined as 4.5 mm/3m for t_1, 3.0 mm/3m for t_2, and 1.5 mm/3m for t_3 in EN1990 Annex A2 item A2.4.4.2.2.

3.3.2. A.R.E.M.A Passenger Comfort Criteria

Passenger comfort criteria are not clearly defined in A.R.E.M.A. which generally focuses the performance of bridge. Serviceability of bridge is only defined for seismic loads. Three levels such as serviceability limit state, ultimate limit state and survivability limit state is used for classification of bridge performance in A.R.E.M.A., 2006 Chapter 9 Part 2 item C-1.3.3.

The vibration criterion is based on natural periods. When natural periods of bridges in transverse direction are over 1 second, there is a possibility of derailment event. Consequently the only bridges having natural periods less than 1 second are classified as serviceable bridge.

The maximum vertical deflection computed using composite section for live load and impact load condition cannot exceed L/640 where L is defined as span length [23].

The maximum lateral deflection limit is calculated as squared proportion of the span lengths by given measurements in A.R.E.M.A. Chapter 15 Part 1 item 1.2.5. Lateral deflection is limited to 10 mm for 19 m track length in tangent track condition.

3.4. Computational Analysis Methods

3.4.1 Non-Linear Force-Time Analysis

The non-linear force-time analysis method was used in analysis of moving force in various train speeds. Although linear force-time analysis method can be accepted as an analysis approach, it is not preferred to use for design verification. Non-linear force-time analysis provides the most accurate results for computation of inelastic deformations and determination of higher mode effects. Despite accuracy and effectiveness, a large number of subjective modeling decisions are needed and this makes non-linear force-time analysis difficult to be handled. The importance of choices should be properly understood before analysis which requires large computational time and effort.

Analysis software used in this study, LARSA 4D uses Newmark-Beta time integration algorithm with the Newton-Raphson method in execution of the non-linear force-time analysis. Software provides two options as Full Newton-Raphson method and modified Newton-Raphson method. A new tangent stiffness matrix is calculated in each iteration in Full Newton Raphson method. However, Modified Newton-Raphson method involves fewer stiffness reformations. The choice depends on the degree of nonlinearity in the structure response, that is, the more nonlinear the response, the more often updating should be performed [26]. In this study, Full Newton-Raphson method was used as recommended by software manual.

The solutions were carried out by step-by-step analysis in varying time periods. This requires iterative solutions of the equations of motion in each load function time steps. Before analysis, the most adequate time-step for the time integration was determined. In order to illustrate the importance of time-step, a small study case was evaluated. In this study case, an example model was analyzed by non-linear force-time analysis in 0.025 s, 0.010 s, 0.005 s and 0.001 s. Analysis executed by 0.025 s time-step differed 10% than analysis of 0.001 s. Results of time-step analysis with 0.001 s were very close to results of 0.005 s time-step analysis. The study case results in an observation that the more time-step size is reduced, the more results obtained converge to the solution which could be considered exact. In non-linear analysis of this thesis, 0.005 s was used as integration time-step.

3.4.2 Eigenvalue Analysis

The Eigenvalue analysis was carried out to get the undamped free-vibration mode shapes and frequencies of bridges. Bridges dynamic characteristics and behaviors were realized by Eigenvalue analysis. The number of speeds caused resonance in analysis was determined by Eigenvalue analysis.

CHAPTER 4

CASE STUDY AND COMPUTER MODELING

4.1. Description of the Bridge

The investigated composite steel I-girder railroad bridge in this thesis is a nonexistent bridge which is a mix design of two existing railroad bridges, one steel girder suburban railway bridge and other precast concrete girder high speed railway bridge as shown in Figure 4.1. Investigated railroad bridge was formed by the steel I-girders, cross beams and piers of existing suburban railroad bridge and concrete deck, ballast layer, sleepers and rails of existing high speed railway bridge. The material and geometrical properties were taken from the suburban railway bridge, since investigated composite bridge had steel I-girders.

The suburban railway bridge is at Kurtuluş Region in Ankara and located on Kayaş-Sincan Railway Line. The railway bridge, constructed in 1953 has two spans of 8.75 m length and 3.00 m height. The width of the deck is 2.80 m. A highway and also two walkways pass under the bridge. Structural steel elements of the bridge are made of S235JR class steel material.

The suburban railway bridge is formed by three main steel I-girders in the direction of railway. Each built-up I-girder has 9.35 m length and 0.75 m height. In transverse direction, six lateral beams are connected to the main girders. Steel plates cover the span above lateral beams. At the top, the railway bridge has two rails continue along the bridge. The rails stand on

timber sleepers in transverse direction. There is a 30 cm thick ballast layer under timber sleepers and above the steel sheets. The railway bridge has no curvature in both girders and rails, and also has an approximately zero degree slope. One of the spans was renewed in 2006 and replacement of whole bridge by a new single span bridge was planned at time of site visit.

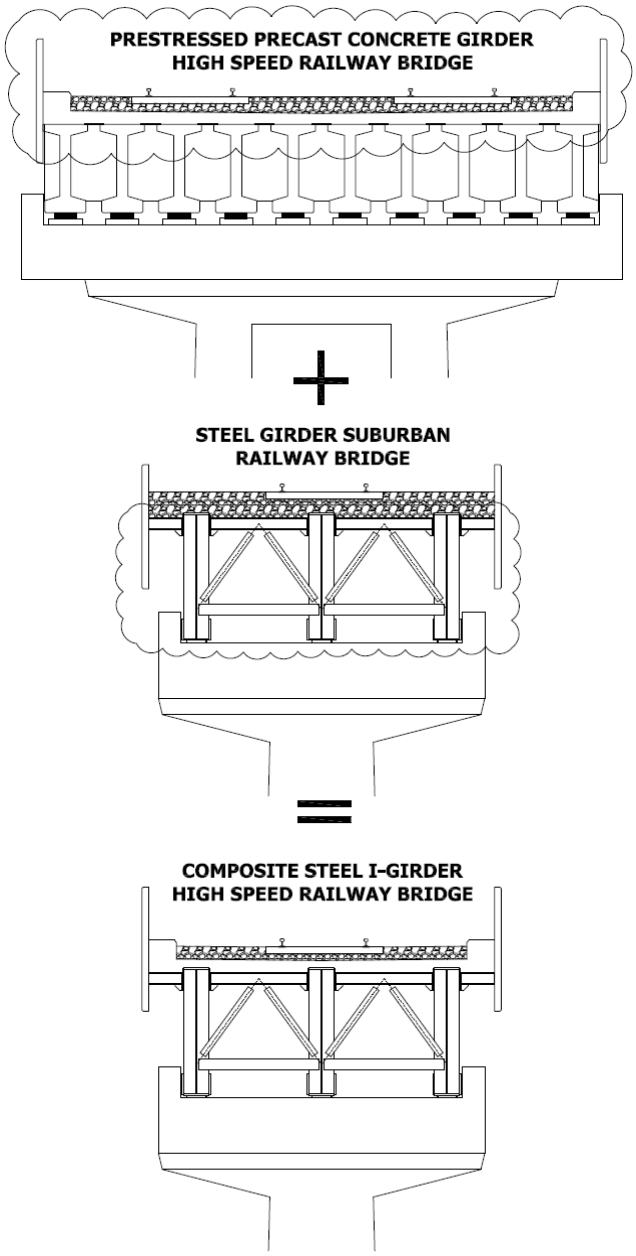

Figure 4.1 Formation of Non-Existing Composite Steel I-Girder Railway Bridge

Figure 4.2 General View of Steel I-Girder Suburban Railway Bridge

Figure 4.3 Views of Steel I-Girder Suburban Railway Bridge Members

Precast concrete girder high speed railway bridge is on Ankara-Eskişehir Highway near Polatlı country as a part of Ankara-Eskişehir High Speed Railway Line. High Speed Railway Line from Ankara to Eskisehir is generally parallel to the state highway except in two points. The precast concrete girder high speed railway bridge is the first point that crosses the Ankara-Eskişehir State Highway. Nonstructural elements and composite parts of the bridge investigated in this study are taken from this railway bridge. Construction of the bridge was completed in 2007 and opened to service in 2009. The bridge has two spans, however spans are not continuous. Deck and straight beams are shifted on middle pier as seen in Figure 4.4.

Figure 4.4 General View of Precast Concrete I-Girder High Speed Train Bridge

The precast concrete girder high speed railway bridge has twelve precast I-girders and a 25 cm thick reinforced concrete deck. Sub-ballast and ballast layers are laid over concrete deck. Total thickness of well graded ballast layers is approximately 75 cm. Precast concrete sleepers are placed on ballast layer. There is no specific placement technique for sleepers, such that in some zones sleepers are buried in ballast layer as in some zones sleepers are on ballast layer. Rails are installed above sleepers by special rail clips. Thickness of sleepers increases at place where rails are installed. Therefore rails are always over ballast layer whether sleepers are buried or not. Although the high speed railroad bridge is skewed bridge, girders and rails are straight. Curvature of rails starts after bridge.

Figure 4.5 Views of Precast Concrete I-Girder High Speed Train Bridge Members and Rail Curvature

The bridge analyzed in this study was the composition of steel girders, cross beams and piers of steel I-girder suburban railway bridge and concrete deck, ballast layer, sleepers and rails of precast concrete I-girder high speed railway bridge. Suburban railway bridge was the main bridge since investigated bridge had partially composite steel I-girder. Geometric properties of composite bridge were taken from the suburban railway bridge. Accordingly, the bridge had 8.75 m span length and 2.80 m span width. The superstructure consisted of three steel I-girders spaced by 1.40 m center to center. Each girder was 9.35 m in length and 0.75 m in height. In transverse direction, 0.30 m high I-shaped cross beams connected to main girder web at sections 5 cm under top flange of built up main girder. Properties of reinforced concrete deck and non-structural elements above cross beams were taken from high speed railway bridge. Concrete deck was assumed over cross beams in order to provide composite behavior. Deck had 3.12 m width and 25 cm uniform thickness as such in high speed railway bridge. The geometrical and material properties of superstructure were given in Table 4.1. The composite bridge also had 30 cm thick ballast layer. The thickness of ballast layer affects the stiffness of ballast. Two case studies were developed with linear spring models both for 30 cm thick ballast and for 75 cm thick ballast. It was observed that thickness has no effect as spring length; stiffness of ballast was only affected by thickness. Consequently, 30 cm thickness was assumed for ballast layer of composite bridge. Concrete sleepers were placed at each 0.75 m over ballast layer as similar to high speed railway bridge. Concrete sleepers were considered as B70 type which is common type for high speed railway lines. Two UIC-60 type rails were fixed to concrete sleepers. Piers of the composite bridge had 3.00 m height. The composite bridge additionally had K-braces at supports in transverse direction unlike both suburban train bridge and high speed railway bridge.

K-Braces were added in order to assure lateral stability of bridge and get more realistic modal behavior.

The span length of investigated bridge was extended to 24.5 m as second case study. All geometric properties and material properties of bridge investigated in first case study were same with one investigated in second case study except span length. Railway bridge in second case study was developed by just only extension of girders, deck, rails and ballast layers and replication of cross beams and sleepers.

The composite bridge was considered as a simple span bridge in order to define a methodology for common type simple span bridges.

Table 4.1 Geometrical and Material Properties of Superstructure

Items	I Girder	Cross Beam	Deck
Number	3	6 or 15	1
Material	SJR235	SJR235	C30
Young's Modulus (N/mm^2)	200,000	200,000	24,837
Mass Density (kg/m^3)	7,850	7,850	2,400
Poisson's Ratio	0.300	0.300	0.167
Height (mm)	750	300	250
Flange Width (mm)	320	125	-
Flange Thickness (mm)	35.0	16.2	-
Web Thickness (mm)	12.0	10.8	-
Section Area (mm^2)	30,560	6,900	-
Strong axis Moment of Inertia (mm^4) (for a steel girder)	$3.1796x10^9$	$9.8000x10^7$	-
Weak axis Moment of Inertia (mm^4) (for a steel girder)	$1.9124x10^8$	$5.6800x10^5$	-
Strong axis Moment of Inertia (mm4) (for a composite girder)	$9.2977x10^9$		-
Weak axis Moment of Inertia (mm4) (for a composite girder)	$1.0845x10^9$		-

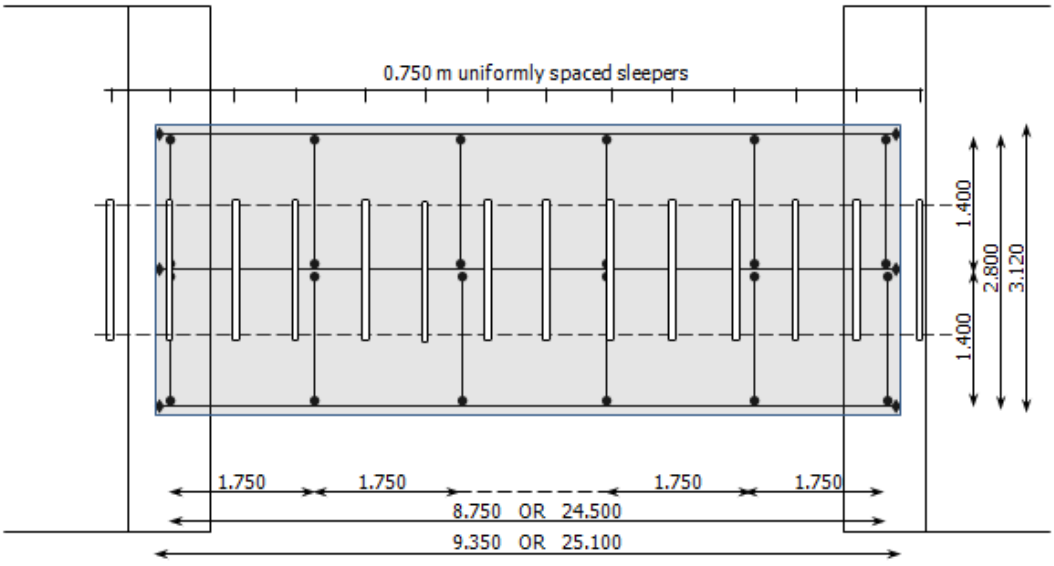

Figure 4.6 General Layout of Analyzed Composite Bridges

4.2. Computer Modeling

A 3-D frame and shell analysis model was developed by LARSA 4D analysis program. The computer model consists of the elements of pier columns, cap beams, elastomeric bearings, main girders, cross beams, bracings, deck, ballast, sleepers and rails as shown in Figure 4.7.

The railway bridge having 8.75 m long span and 0.75 m high girders was initially modeled as main analysis model. The main analysis model was reproduced for two span length, two ballast stiffness and eight bridge stiffness in order to investigate effects of span length, ballast stiffness and stiffness of bridge. As a result, 32 different bridge models were developed by combination of these parameters as listed in Table 4.3.

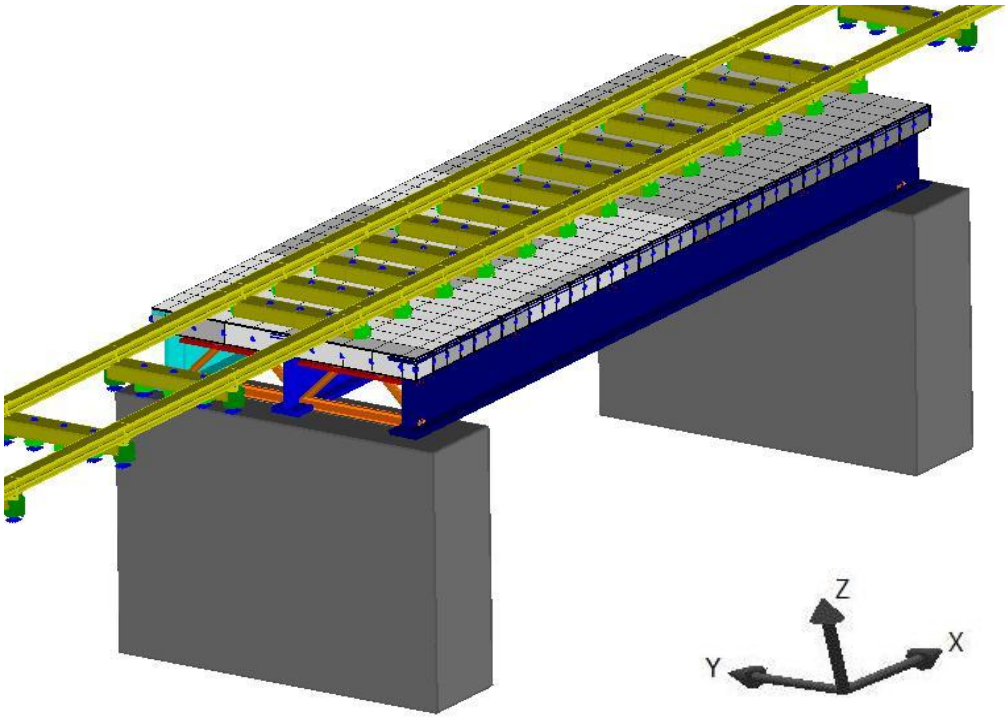

Figure 4.7 General View of 3-D Frame and Shell Analysis Bridge Model

The bridge length was the first parameter that determines the difference of computer models. Bridge length is an important design parameter in aspects of dynamic impact factors, natural frequency and critical damping percentage limitations for bridges designed according to Eurocode or AREMA. Upper limits of bridge length distinction are 24.4 m in AREMA and 20.0 m in Eurocode. In AREMA, formulation of dynamic factor for rolling equipment stated in Section 3.1 Analysis Guideline, changes for the span length larger than 24.4 m. In Eurocode, lower limit percentage of critical damping formulation stated in Section 3.2.1. Structural Damping Ratio, changes for span length larger than 20 m. The main bridge model span length was extended to 24.5 m which satisfies distinction requirements of design codes.

Railway bridges generally have ballast layers in different thickness and different particle sizes. As well-known, ballast stiffness has direct effect on vertical acceleration of railway bridge superstructure. 700 MPa and 350 MPa ballast stiffness were defined as upper and lower limit respectively in computer model in order to evaluate effects of ballast.

The rigidities of railway bridge in longitudinal direction are determinant parameter in the rail-bridge interaction analysis. Additional rail stresses and rails movements by deformation of bridge are mostly depend on the rigidities of beams [25]. Bridge stiffness variation was provided by change in main girder height. Four different girder heights were modeled to investigate bridge stiffness effect on vertical acceleration. Heights of girders were chosen as 0.75 m, 0.90 m, 1.10 m and 1.30 m, by the way increase in bridge stiffness was kept constant. In analysis, 4 more girder stiffness was also evaluated in order to expand the results. Additional girder stiffness's were selected as 10, 100, 400 and 1000 times the stiffness of existing girder, 0.75 m height girder. The multiplier of 400 was determined as back calculation of existing reinforced concrete box girder bridge vertical acceleration results. The level of comfort of reinforced concrete box girder bridge was determined as good. Therefore required rigidity for span length and then required stiffness for steel I-girder bridge were calculated. It was observed that 400 times larger stiffness of existing girder required for good level of comfort. Other multipliers were selected to investigate very good, acceptable and permitted limit of comfort levels in trial and error method. Furthermore, previously stated girder heights and additional girder stiffness were expressed by composite span flexural rigidity, i.e. multiplication of strong axis inertia of composite girder, elastic modulus and number of girders as shown in Table 4.2. Therefore, analyses results can be interpreted for different materials, different geometrical shapes and number of girder.

Table 4.2 Flexural Rigidity of Analyzed Composite Spans

		SINGLE STEEL GIRDER		SINGLE COMPOSITE GIRDER		COMPOSITE SPAN	
Girder Height H (m)	Elastic Modulus E (MPa)	Strong Axis Moment of Inertia I (m^4)	Flexural Rigidity EI ($kN.m^2$)	Strong Axis Moment of Inertia I (m^4)	Flexural Rigidity EI ($kN.m^2$)	Strong Axis Moment of Inertia I (m^4)	Flexural Rigidity EI ($kN.m^2$)
0.75	200,000	3.1796×10^{-3}	635,920	7.9882×10^{-3}	1,597,648	22.1078×10^{-3}	4,421,563
0.90	200,000	4.7641×10^{-3}	952,820	11.2553×10^{-3}	2,251,053	31.2239×10^{-3}	6,244,779
1.10	200,000	7.4467×10^{-3}	1,489,340	16.6647×10^{-3}	3,332,947	46.2998×10^{-3}	9,259,963
1.30	200,000	10.8244×10^{-3}	2,164,880	23.3507×10^{-3}	4,670,136	64.9061×10^{-3}	12,981,221
2.10	200,000	31.7960×10^{-3}	6,359,200	41.9394×10^{-3}	8,387,875	118.7546×10^{-3}	23,750,916
5.45	200,000	317.9600×10^{-3}	63,592,000	329.4103×10^{-3}	65,882,054	979.4908×10^{-3}	195,898,160
9.30	200,000	$1,271.8000 \times 10^{-3}$	254,368,000	$1,283.4087 \times 10^{-3}$	256,681,744	$3,841.3193 \times 10^{-3}$	768,263,855
13.15	200,000	$3,179.6000 \times 10^{-3}$	635,920,000	$3,191.1812 \times 10^{-3}$	638,236,245	$9,564.6028 \times 10^{-3}$	1,912,920,565

Table 4.3 Properties of Investigated Bridge Models

Model No.	Span Length (m)	Flexural Rigidity ($kN.m^2$)	Ballast Stiffness (MPa)
1	8.75	4,421,563	350
2	8.75	6,244,779	350
3	8.75	9,259,963	350
4	8.75	12,981,221	350
5	8.75	23,750,916	350
6	8.75	195,898,160	350
7	8.75	768,263,855	350
8	8.75	1,912,920,565	350
9	8.75	4,421,563	700
10	8.75	6,244,779	700
11	8.75	9,259,963	700
12	8.75	12,981,221	700
13	8.75	23,750,916	700
14	8.75	195,898,160	700
15	8.75	768,263,855	700
16	8.75	1,912,920,565	700
17	24.5	4,421,563	350
18	24.5	6,244,779	350
19	24.5	9,259,963	350
20	24.5	12,981,221	350
21	24.5	23,750,916	350
22	24.5	195,898,160	350
23	24.5	768,263,855	350
24	24.5	1,912,920,565	350
25	24.5	4,421,563	700
26	24.5	6,244,779	700
27	24.5	9,259,963	700
28	24.5	12,981,221	700
29	24.5	23,750,916	700
30	24.5	195,898,160	700
31	24.5	768,263,855	700
32	24.5	1,912,920,565	700

The dynamic loads due to train passage were modeled by train-bridge interaction system which was mainly composed of a train model and a bridge model. Train-bridge interaction is a phenomenon that takes place when the bridge oscillations or the rail-surface roughness excite the motion of the train forces [8]. The train is composed of given number of vehicles which are mainly defined as power car, intermediate coaches and end coach.

When a railway line passes over bridge, track is laid on the bridge deck and the forces from the wheels of a train are transmitted to the bridge deck through the track [11].

In literature, the most common models used in analysis of dynamic vehicle reactions are static load model multiplied by dynamic factors, moving force model and moving mass model.

4.2.1. Static Load Model Multiplied By Dynamic Factors

The train axle loads multiplied by dynamic factors were statically modeled to explore dynamic reactions of high speed trains according to commonly used railroad bridge specifications. Structural elements of the bridge like beam, deck and track were modeled by finite elements. Frame elements were used to model steel members. Concrete piers and cap beams were also modeled by frame elements. A frame element has three degrees of freedom for translational displacements and three degrees of freedom for rotational displacements at each end joint. The frame element is capable of exactly representing constant axial deformation along the beam with constant torsional shear deformation and linear bending deformations within the element. This is sufficient for analyzing structures with loads applied at joint points [26]. The concrete

deck was modeled by finite shell elements. The shell element is the most general form of the plate element. A shell element has both in-plane membrane and out-of-plane bending [26]. These properties make shell element more efficient for deck modeling of composite structure. Fictitious rigid line elements were defined to figure piers in width and to figure beams in height in three-dimensional model. The most important issue is to simulate the nonslip accurate bonding between concrete deck and steel beams. Composite behavior can only be provided by nonslip accurate bonding. The model created for dynamic analysis was well-suit to example model given in Figure 4.8 which is basically defined based upon item 6.5.4.4. Figure 6.19 of EN 1991-2 for the determination of load effects in the combined track/structure systems.

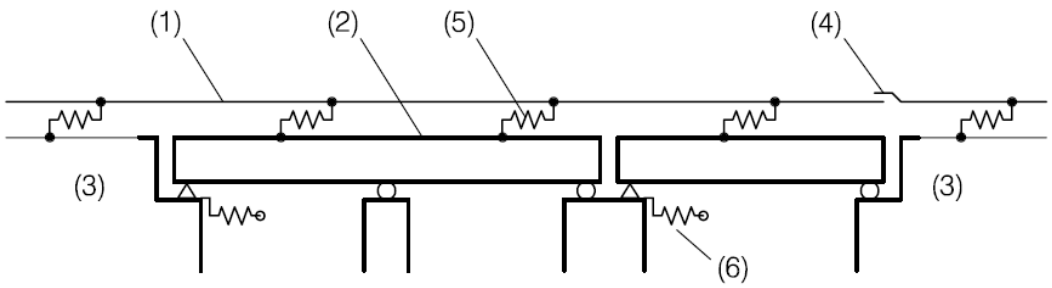

Figure 4.8 Example of a model of a track/structure system [22]

In example model, figures are defined as;

(1) Track

(2) Superstructure (a single deck comprising two spans and a single deck with one span shown)

(3) Embankment

(4) Rail expansion device (if present)

(5) Longitudinal non-linear springs reproducing the longitudinal load/ displacement behavior of the track

(6) Longitudinal springs reproducing the longitudinal stiffness K of a fixed support to the deck taking into account the stiffness of the foundation, piers and bearings etc. [22]

Track shown as first element was represented as UIC 60 type rails and sleepers. In model, rails were directly fixed to sleepers. In real situation, rails were also fastened to sleepers by rail fastening equipments, however between rail and sleeper, rubber pad was placed as shown in Figure 4.8. In this thesis, rubber pad was neglected, so fastening springs were not modeled. UIC 60 is very widely used type in Turkish State Railways. Besides, EN 1991-2 item 6.5.4.5.1 also states UIC 60 rails as design track. Track models were extended a locomotive length after bridge supports to investigate the approaching effect of train as required in UIC code [27].

The dynamic interactions between bridge and train not only depend on the property of bridge like span length and stiffness of girders, but also depend on track irregularity as well. Track irregularities have different influence on bridge-track interaction and past researches indicate that the great influence of the track geometry on dynamic bridge-track interactions in high speed situations [4]. The influences of the track irregularities did not include to scope of this thesis.

Rail expansion device is not present, since the bridge has short span. As a result, 4^{th} element was not modeled in Figure 4.8.

Bearing stiffness in multi direction was taken into account instead of longitudinal springs called as 6^{th} element in Figure 4.8. Bearing material was

assumed as elastomeric rubber as frequently used in literature. Elastomeric bearing was modeled by linear springs. Linear spring stiffness was calculated so as the elastomeric bearing makes 1 mm elastic deformation in direction of applied force that is the bridge total mass subjected to natural ground acceleration in multi direction. In railway bridges, one of the supports is fixed by support locking device. For the stiffness of this fixed support, elastomeric bearing stiffness was amplified by 10000 times as rule of thumb.

- **Ballast Model**

Ballast was idealized as linear and non-linear springs. Ballast materials forming part of railway structures are subjected to cyclic loads. As the results of these loads, ballast densification, aggregate degradation, and lateral spread of the ballast material underneath the ties take place inducing permanent deformations on the railways [28]. Permanent deformation of ballast material which is basically formed by crushing of particles occurs in longitudinal direction due to the spread of cycling load influence presented as Figure 4.10. Consequently, non-linear springs were used to simulate the ballast behavior in longitudinal direction. In lateral direction, ballast is functioned to distribute reaction, so linear springs were used.

The force influences are not uniformly distributed, and concentrate in ballast particles underneath the sleepers. Crushing could be expected to occur at these zones. On the other hand, it could be observed that particles located on top of the ballast bed and between the sleepers does not take any load [21]. For this reason, ballast model springs were assigned just under sleepers in computer model.

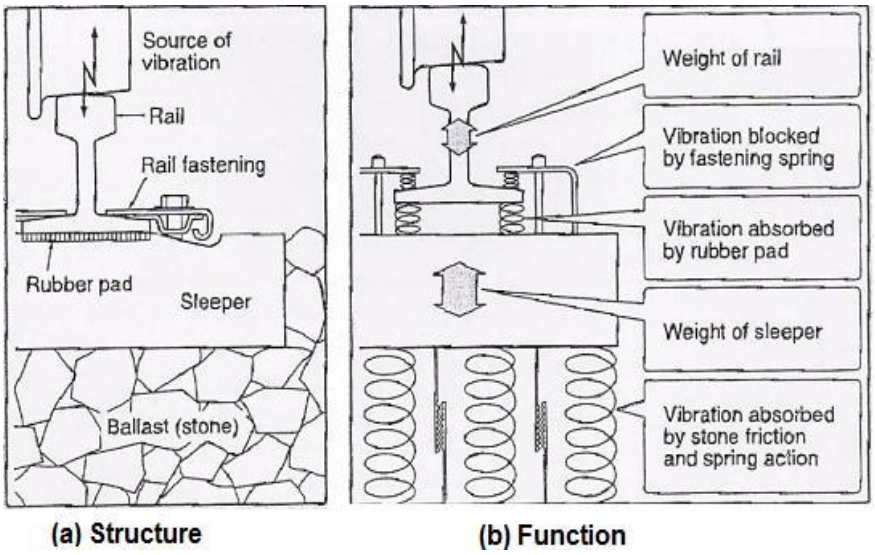

Figure 4.9 Basic Structures and Function of Railway Tracks [29]

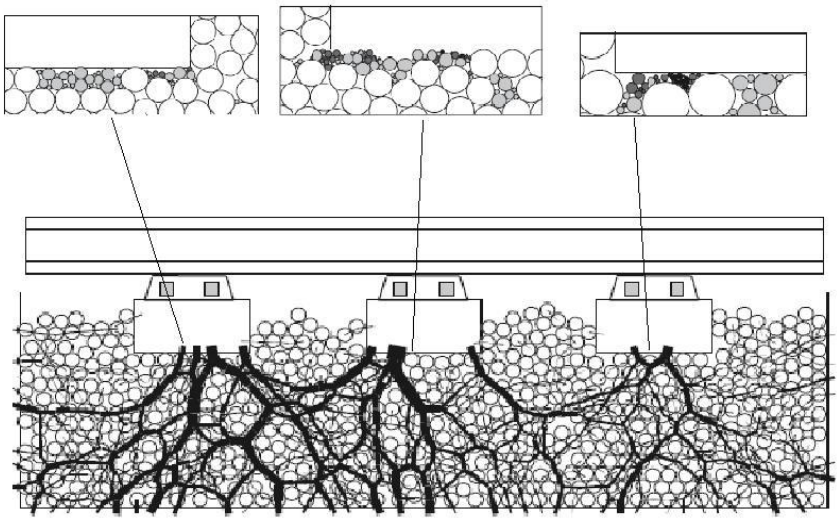

Figure 4.10 Distribution of Cycling Load in Ballast [21]

The non-linear springs which idealize the ballast-track interaction behave elastically up to the displacement, u_0 which is equal to 2 mm for properly maintained ballast. Plastic shear resistance for unloaded track is equal to

20 kN/m and 60 kN/m for loaded track as stated in UIC Leaflet 774-3. The behavior of spring is graphically represented in Figure 4.11.

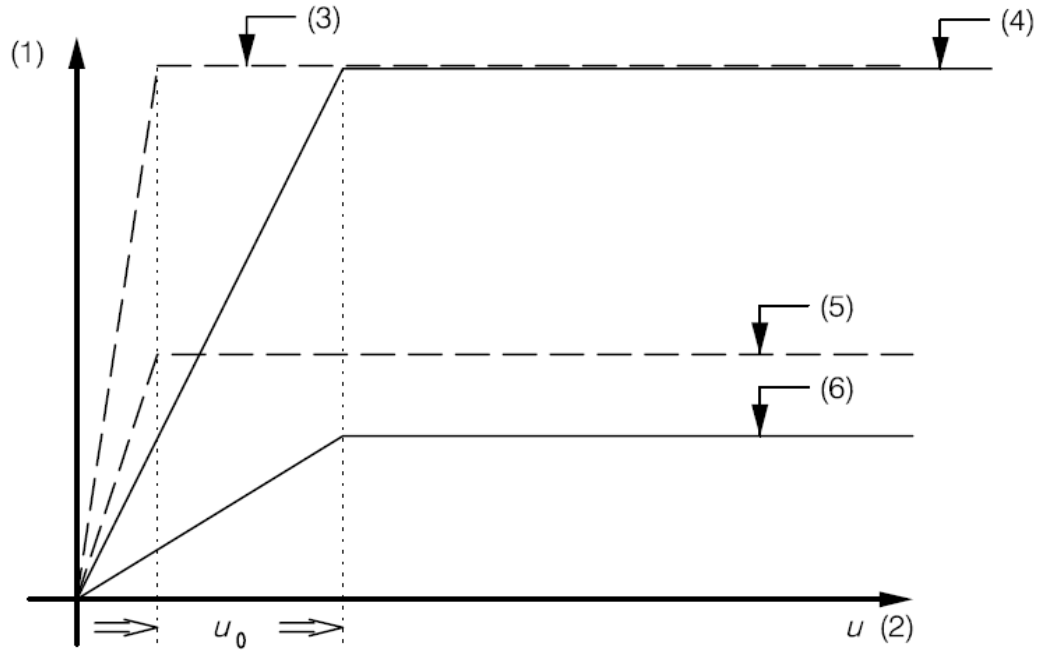

Figure 4.11 Variation of longitudinal shear force per unit length with longitudinal track displacement for one track [22]

Where;

(1) Longitudinal shear force in the track per unit length

(2) Displacement of the rail relative to the top of the supporting deck

(3) Resistance of the rail in sleeper (loaded track) (frozen ballast or track without ballast with conventional fastenings)

(4) Resistance of sleeper in ballast (loaded track)

(5) Resistance of the rail in sleeper (unloaded track) (frozen ballast or track without ballast with conventional fastenings)

(6) Resistance of sleeper in ballast (unloaded track) [22]

Ballast behavior in lateral direction was modeled by linear springs. Stiffness of linear springs was determined according to material classification and gradation. A range of material classification is defined for ballast materials ranging from high quality crushed stone, G1 and G2 to in-situ sub-grade quality material, G10. Quality of ballast generally falls in the upper material categories ranging from G1 to G3 for base and G4 to G6 for sub-base [20]. Material classification depends on many parameters like density, degree of saturation, percentage of humidity, etc., but the main parameter is particle size. Classification of ballast material according to particle size was given in Table 4.4.

Table 4.4 Classification of ballast material based on particle size. [20]

Material Class	Maximum Particle Size
G1	26.5 mm
G2 – G3	37.5 mm
G4	53.0 mm
G5-G6	63.0 mm

Particle size of railway ballast is limited as 50-60 mm for upper bond and 31.5 mm for lower bond in Turkish State Railway Technical Specifications for Material, Construction, Control and Maintenance. Normally, G5 and G6 material is used in sub-base layers and a G2 and G3 material in base layers as seen on site investigation of high speed railway bridge.

In literature, stress condition of well graded ballast layers was represented by the effect of dry density and degree of saturation, the confining pressure, which tends to cause stress-stiffening behavior, and the stress ratio, which causes a reduction in effective stiffness as shown in Table 4.5.

Table 4.5 Effective Stiffness of Ballast Material at Different Combinations of Density and Saturation. [20]

Dry Density (% of apparent density)	Degree of Saturation (%)	Confining Stress (kPa)	Stress Ratio (% of maximum shear strength)	Effective Stiffness (MPa)
84.5	100.0	80	73	357
84.5	100.0	80	92	360
84.5	100.0	80	51	377
80.7	78.0	140	90	380
84.5	100.0	140	74	390
80.7	78.0	80	93	392
80.7	78.0	140	52	447
84.5	100.0	140	91	447
84.5	100.0	140	53	461
80.7	78.0	80	73	468
80.7	33.4	80	94	476
80.7	33.4	140	73	502
80.7	78.0	140	74	512
80.7	33.4	140	52	564
80.7	33.4	140	93	569
84.5	43.5	140	72	620
84.5	43.5	140	52	651

The range of effective stiffness values for ballast is expected to vary from about 350 to 700 MPa. A major portion of this variation in effective stiffness for well graded ballast layer was explained by variation in the relative density and the degree of saturation of the material and stress condition imposed on the material.

4.2.2. Moving Force Model

Moving force method are based on the direct time integration of the dynamic equations of the bridge, under the actions corresponding to a train of moving loads of fixed values which are representative of each axle of the train.

The basic solution of the dynamic equations for known vibration modes is the response of the structure to a single moving load as shown in Figure 4.12. The differential equation for a point load F crossing the beam of length ℓ, model shape $\varphi_t\ (x)$, model mass M_t, eigen frequency of the i-th mode at a constant speed v is defined as,

$$M_t \ddot{y}_t + 2\zeta_t \omega_t M_t \dot{y}_t + \omega_t^2 M_t y_t = F(\varphi_t(vt)) \quad \text{.....(4.1)}$$

Where y_t is the modal amplitude of the i-th mode, ζ_t the damping fraction with respect to the critical value and $(\varphi_t\ (vt))$ indicates that,

$$(\varphi(vt)) = \begin{cases} \varphi(vt) & \text{if} \quad 0 < vt < 1 \\ 0 & \text{otherwise} \end{cases} \quad \text{.....(4.2)}$$

After obtaining the response for a single moving load, the response for a train load can be assembled as the superposition of the responses for the point loads F_k.

$$M_i \ddot{y}_i + 2\zeta_i \omega_i M_i \dot{y}_i + \omega_i^2 M_i y_i = \sum_k^n F_k(\varphi_i(vt_k - vt_{k-1})) \quad \text{.....(4.3)}$$

Dynamic analysis of railway bridges based on moving load models may also be performed through finite element methods. These methods are applicable to arbitrary structures and can include nonlinear effects [30].

In finite element method, the analysis can be carried out by the direct time integration of the complete model or alternatively through modal reduction. In both cases, the system of differential equations can be defined as,

$$[m][\ddot{u}] + [c][\dot{u}] + [k][u] = \{F(t)\} \quad \text{.....(4.4)}$$

where [m] is the mass matrix, [c] the damping matrix, [k] the stiffness matrix, {F(t)} the external load vector and [u] the vector of nodal displacements.

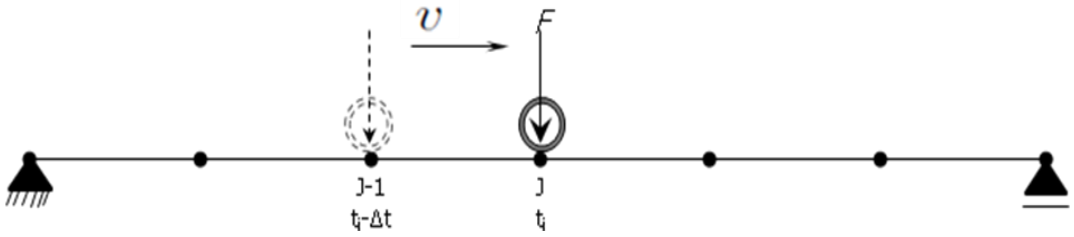

Figure 4.12 Single Moving Force for an Axle Load F Moving at Velocity V

The bridge models were analyzed through a reduction of the number of axles; that is, degrees of freedom which reduces the number of equations instead of the complete discrete system. The procedure to define the train loads is applying load histories in each node. For time step t_i and an axle load F, a nodal load F_J was assigned to the node J if the axle was above an element that contains node J. The magnitude of F_J depends linearly on the distance from the axle to the node [30]. This procedure was outlined in Figure 4.13 for a single load.

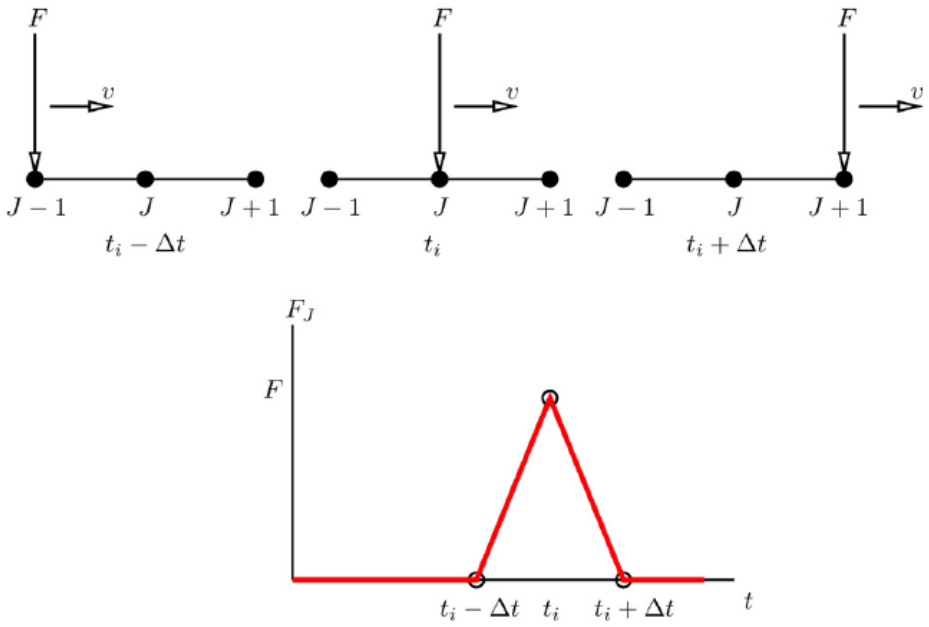

Figure 4.13 Nodal Moving Force Definition for an Axle Load F Moving at Velocity V [30]

4.2.3. Moving Mass Model

Moving mass model is the integration of moving force method and vehicle inertial forces. Vehicle is modeled as moving mass elements and springs at each axle node. The moving force and moving mass models are particular cases of the moving suspension mass model. When the suspension stiffness is rigid, the vehicle acceleration is equal to the acceleration where the vehicle is located. On the other hand, when the suspension stiffness is very soft, this represents the moving force model [19]. The ratio of the mass of the vehicle and the bridge and the ratio of the natural frequency of the vehicle and the bridge, damping coefficients and stiffness of axle are identified as significant factors that determine the effect of dynamic train–bridge interaction in moving mass model. Properties of commonly used high speed trains were given in Table 4.6.

Table 4.6 Properties of German ICE, Japanese SKS, and French TGV High-Speed Railway Trains [19].

Train properties	ICE	SKS	TGV
Number of bogie	52	64	52
Car spacing, d (m)	26.4	25.0	18.7
$(v_c)_{n=1}$ (km/h)	338	320	240
$(v_c)_{n=2}$ (km/h)	169	160	120
m_v (kg)	27,000	20,875	27,000
c_v (N s/m)	22,700	90,200	96,700
k_v (N/m)	660,000	530,000	664,000
m_b (kg)	3,000	3,040	3,000
I_b (kg-m^2)	4,000	3,930	4,000
c_b (N s/m)	78,400	78,400	78,400
k_b (N/m)	2,360,000	2,360,000	2,360,000
m_w (kg)	1,800	1,780	1,800
l_w (m)	1.5	1.25	1.5

Notations denote;

m_v	:	Half mass of a train car
c_v	:	Damping coefficient of vertical bolster spring
k_v	:	Stiffness coefficient of vertical bolster spring
m_b	:	Mass of bogie
I_b	:	Moment of inertia of bogie
c_b	:	Damping coefficient of axle spring
k_b	:	Stiffness coefficient of axle spring
m_w	:	Mass of wheel set
l_w	:	Half distance of wheel base

Moving mass model should be revised or redeveloped for mechanical properties of each train type. Therefore moving mass model solution cannot be generalized. Although moving mass model gives better results, in this thesis moving force model was only developed to generalize the results.

Moving mass model can also be defined as direct time integration of dynamic equations of bridge. Both moving force model and moving mass model are based on the Euler–Bernoulli beam with all degrees of freedom of beam and an additional degree of freedom corresponding to the axle of the train as shown in Figure 4.14. The degrees of freedom of the beam were denoted as W1, θ1, w2, θ2, and the degrees of freedom of the suspended mass, m_v and the non–suspended one, m_w were denoted as y and b respectively. In literature, the dynamical equilibrium equations of the beam were defined as [30]:

$$\mathrm{M}_{\mathrm{interac}}\begin{Bmatrix}\ddot{\mathrm{y}}\\ \ddot{\mathrm{b}}\end{Bmatrix}+\mathrm{C}_{\mathrm{interac}}\begin{Bmatrix}\dot{\mathrm{y}}\\ \dot{\mathrm{b}}\end{Bmatrix}+\mathrm{K}_{\mathrm{interac}}\begin{Bmatrix}\mathrm{y}\\ \mathrm{b}\end{Bmatrix}=\begin{Bmatrix}\mathrm{F}_{\mathrm{y}}\\ \mathrm{F}_{\mathrm{b}}\end{Bmatrix} \quad \text{..... (4.5)}$$

$$\mathrm{M}_{\mathrm{interac}}=\begin{pmatrix}m_v & 0\\ 0 & m_w\end{pmatrix} \quad \text{..... (4.6)}$$

$$\mathrm{C}_{\mathrm{interac}}=\begin{pmatrix}c_v & -c_v\\ -c_v & c_v\end{pmatrix} \quad \text{..... (4.7)}$$

$$\mathrm{K}_{\mathrm{interac}}=\begin{pmatrix}k_v & -k_v\\ -k_v & k_v\end{pmatrix} \quad \text{..... (4.8)}$$

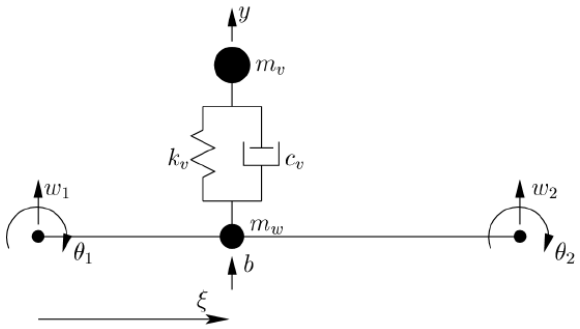

Figure 4.14 Bernoulli beam with simplified vehicle–bridge interaction model [30]

The displacement of the non–suspended mass b was interpolated as [30]

$$b = \begin{bmatrix} N_1 & N_2 & N_3 & N_4 \end{bmatrix} \begin{Bmatrix} w_1 \\ \theta_1 \\ w_2 \\ \theta_2 \end{Bmatrix} \quad \text{..... (4.9)}$$

By using the transformation matrix T,

$$T = \begin{pmatrix} 0 & 0 & 1 & 0 & 0 \\ N_1 & N_2 & 0 & N_3 & N_4 \end{pmatrix} \quad \text{..... (4.10)}$$

The Equation of motion of system can be formulated as [31]:

$$\begin{Bmatrix} F_1 \\ M_1 \\ F_y \\ F_2 \\ M_2 \end{Bmatrix} = M \begin{Bmatrix} \ddot{w}_1 \\ \ddot{\theta}_1 \\ \ddot{y} \\ \ddot{w}_2 \\ \ddot{\theta}_2 \end{Bmatrix} + C \begin{Bmatrix} \dot{w}_1 \\ \dot{\theta}_1 \\ \dot{y} \\ \dot{w}_2 \\ \dot{\theta}_2 \end{Bmatrix} + K \begin{Bmatrix} w_1 \\ \theta_1 \\ y \\ w_2 \\ \theta_2 \end{Bmatrix} \quad \text{..... (4.11)}$$

$$M = T^T M_{interac} T \quad \text{..... (4.12)}$$

$$C = T^T C_{interac} T \quad \text{..... (4.13)}$$

$$K = T^T K_{interac} T \quad \text{..... (4.14)}$$

$$M = T^T M_{interac} T \quad \text{..... (4.15)}$$

Equations 4.12, 4.13, 4.14 and 4.15 must be assembled with the standard matrix of the Bernoulli beam element in order to obtain the stiffness matrix of the interaction element. The element matrix must be re-computed in each time step. In this study, moving force models were analyzed by finite element analysis software and no numerical calculation was done.

4.3. Dynamic Analysis Parameters

Dynamic analysis parameters of case study bridges were calculated according to Section 3.2. Dynamic Analysis Parameters.

4.3.1. Structural Damping Ratio

Structural damping ratio was calculated as summation of critical damping and additional damping caused by vehicle-bridge mass interaction.

Lower limit percentage of critical damping for composite bridges having 8.75 m and 24.5 m span lengths are calculated as 1.91% and 0.5% respectively according to the Table 3.2.

Additional damping values were calculated as 0.26% for bridge having 8.75 m span length and 0.07% for bridge having 24.5 m span length by either Equation 3.12 or Figure 3.3.

Total damping ratio is equal to 2.16% for bridge having 8.75 m span length and 0.57% for bridge having 24.5 m span length. Total damping ratios were decomposed to Rayleigh damping coefficients as mass proportional damping coefficient and stiffness proportional damping coefficient according to natural frequencies of bridges. Rayleigh damping coefficients and natural frequencies of bridges were tabulated as shown in Table 4.7.

Table 4.7 Rayleigh damping coefficients and natural frequencies

Model No.	f_1	f_2	w_1	w_2	Rayleigh Damping Coefficients	
					Mass Proportional Coefficient, a_0	Stiffness Proportional Coefficient, a_1
1 & 9	9.55	12.82	60.00	80.55	1.487	3.08×10^{-4}
2 & 10	10.47	12.83	65.78	80.61	1.566	2.95×10^{-4}
3 & 11	11.72	12.84	73.64	80.68	1.665	2.80×10^{-4}
4 & 12	12.83	12.93	80.61	81.24	1.750	2.67×10^{-4}
5 & 13	12.76	15.59	80.17	97.95	1.906	2.43×10^{-4}
6 & 14	7.07	7.69	44.42	48.32	1.001	4.66×10^{-4}
7 & 15	3.51	4.11	22.05	25.82	0.514	9.03×10^{-4}
8 & 16	2.38	2.92	14.95	18.35	0.356	1.30×10^{-3}
17 & 25	1.82	3.84	11.44	24.13	0.089	3.22×10^{-4}
18 & 26	1.99	3.93	12.50	24.69	0.095	3.08×10^{-4}
19 & 27	2.25	4.06	14.14	25.51	0.104	2.89×10^{-4}
20 & 28	2.52	4.21	15.83	26.45	0.113	2.71×10^{-4}
21 & 29	3.04	4.07	19.10	25.57	0.125	2.56×10^{-4}
22 & 30	2.52	4.21	15.83	26.45	0.113	2.71×10^{-4}
23 & 31	1.99	2.15	12.50	13.51	0.074	4.40×10^{-4}
24 & 32	1.45	1.46	9.11	9.17	0.052	6.26×10^{-4}

4.3.2. Train Analysis Speed

Train analysis speeds were chosen as speeds cause resonance of structure. Resonance speeds can be estimated by first natural frequency and principle wavelength of frequency as stated in Eurocode or structural natural frequencies cause peak model displacements determined through modal analysis.

Estimated train speeds which cause resonance were given in Table 4.8.

Table 4.8 Estimated Train Speeds Cause Resonance of Bridge

Model No.	Eurocode Estimation				Analytical Peak Frequencies	
	V_1 (m/s)	V_2 (m/s)	V_3 (m/s)	V_4 (m/s)	V_5 (m/s)	V_6 (m/s)
1 & 9	137.50	68.75	45.83	34.38	55.92	44.13
2 & 10	141.13	38.49	19.25	12.83	46.59	86.10
3 & 11	141.24	38.52	19.26	12.84	49.92	87.42
4 & 12	141.24	38.52	19.26	12.84	38.49	53.10
5 & 13	141.35	38.55	19.28	12.85	38.28	46.77
6 & 14	141.90	38.70	19.35	12.90	67.17	76.26
7 & 15	142.34	38.82	19.41	12.94	38.94	73.53
8 & 16	142.45	38.85	19.43	12.95	53.88	74.73
17 & 25	54.27	27.14	18.09	13.57	61.68	76.08
18 & 26	29.70	24.20	19.80	14.85	67.17	82.11
19 & 27	33.35	27.17	22.23	16.67	36.39	67.17
20 & 28	37.40	30.47	24.93	18.70	50.91	79.53
21 & 29	37.53	30.58	25.02	18.77	48.45	87.45
22 & 30	37.80	30.80	25.20	18.90	70.65	76.11
23 & 31	38.75	31.57	25.83	19.37	51.03	64.47
24 & 32	39.02	31.79	26.01	19.51	60.42	64.32

Analysis was executed by maximum and minimum design speeds and additionally selected three of resonance speeds. Resonance speeds were selected as maximum speeds in range of maximum and minimum design speeds. One of resonance speeds was selected from analytical peak frequencies, others from Eurocode estimations and analytical peak frequencies of existent girder. Eurocode estimation of resonance speed for existent girder was executed for all rigidities since their resonance speed were lower than minimum limit and also by this way, correlations of rigidities and ballast stiffness' with speed were investigated.

Table 4.9 Train Speeds Selected For Analysis

Model No.	V_1 (m/s)	V_2 (m/s)	V_3 (m/s)	V_4 (m/s)	V_5 (m/s)
1 & 9	40.00	44.13	68.75	55.92	83.30
2 & 10	40.00	44.13	68.75	46.59	83.30
3 & 11	40.00	44.13	68.75	49.92	83.30
4 & 12	40.00	44.13	68.75	53.10	83.30
5 & 13	40.00	44.13	68.75	46.77	83.30
6 & 14	40.00	44.13	68.75	76.26	83.30
7 & 15	40.00	44.13	68.75	73.53	83.30
8 & 16	40.00	44.13	68.75	74.73	83.30
17 & 25	40.00	54.27	76.08	61.68	83.30
18 & 26	40.00	54.27	76.08	82.11	83.30
19 & 27	40.00	54.27	76.08	67.17	83.30
20 & 28	40.00	54.27	76.08	79.53	83.30
21 & 29	40.00	54.27	76.08	48.45	83.30
22 & 30	40.00	54.27	76.08	76.11	83.30
23 & 31	40.00	54.27	76.08	64.47	83.30
24 & 32	40.00	54.27	76.08	64.32	83.30

4.3.3. Train Loading

In dynamic analysis, HSLM train load was used as recommended by Eurocode. Model of HSLM train depends on structural configuration and span length as seen on Table 3.6. Train model was determined as HSLM-A for both of bridges having either 8.75 m or 24.5 m span length since the span lengths are greater than the specified limit of 7 m. Load Model and physical properties of HSLM-A train such as coach length, axle distance, etc. was shown in Figure 4.15.

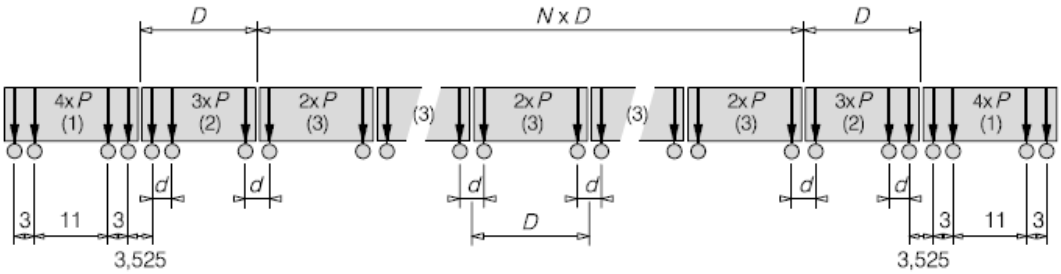

Key
(1) Power car (leading and trailing power cars identical)
(2) End coach (leading and trailing end coaches identical)
(3) Intermediate coach

Figure 4.15 HSLM-A Type High Speed Train Model [22]

HSLM-A Train has also 10 different models based on number of intermediate coaches, coach length and point force values. The critical HSLM-A train was determined according to the procedure depends on wavelength excitation, aggresivity and critical wavelenght excitation.

Data of procedure defined to determine the critical HSLM-A train was given in Table 4.10.

Table 4.10 Data of critical HSLM-A Train Determination Procedure

Bridge Span Length (m)	Wavelength Excitation (m)	Aggressivity (kN/m)	Critical Wavelength Excitation (m)	Length of Coaches (m)
8.75	10.47	600	10.00	20
24.5	54.92	140	27.00	27

Data given in Table 4.10 indicates that HSLM-A3 train model is critical for bridge having 8.75 m span length while HSLM-A10 train model is critical for bridge having 24.5 m span length. HSLM-A10 train model was used for both bridges with the intension of direct comparison and analysis simplification.

CHAPTER 5

ANALYSIS RESULTS

5.1. Introduction

The results quantify the accelerations, displacements, twist and stresses. Mid-span joint accelerations, mid-span joint displacements and deck twist at mid-span values of moving force models were provided to identify the passenger comfort level. Flexural stresses in girders were determined to compare the usage of flexural capacity for static models and moving force models. Mode shapes and frequencies were determined to understand dynamic behavior of bridges.

Analyses were executed for 2 span lengths, 2 ballast stiffness, 5 vehicle speeds for each span length and 8 different bridge stiffness. 1260 different graphics were obtained as the results of analyses. These can be decomposed as 800 graphics for flexural strength capacity, 32 graphics for mode shapes and frequencies and 428 graphics for passenger comfort level parameters. 96 selective graphics of passenger comfort level parameters were reported for critical vehicle speeds of analyses in Appendix A.

Dynamic analyses of moving force model were carried out by the Non-Linear Force-Time Analysis Method. Total of 160 non-linear force-time analysis cases were run for 22 different vehicle speeds of HSLM A10 train. Selected vehicle speeds indicated as V_{select} according to flexural rigidities are given in Table 5.1.

All reported values and calculations represent the maximum values of mid-span joints which were marked at Figures 5.1, 5.2, 5.3, 5.4 and 5.5. Selected joint ID numbers were 171 for 8.75 m span length and 827 for 24.5 m span length.

Table 5.1 Selected Vehicle Speeds, V_{select} (m/s) for Flexural Rigidities

Span Flexural Rigidity ($kN.m^2$)	Selected Vehicle Speeds , V_{select} (m/s)	
	8.75 m Span Length	24.5 m Span Length
4,421,563	55.92	61.68
6,244,779	46.59	82.11
9,259,963	49.92	67.17
12,981,221	53.10	79.53
23,750,916	46.77	48.45
195,898,160	76.26	76.11
768,263,855	73.53	64.47
1,912,920,565	74.73	64.32

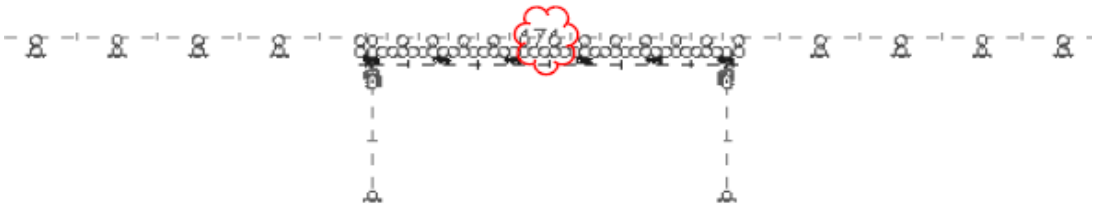

Figure 5.1 Longitudinal Cross-Section of Model for 8.75 m Span Length

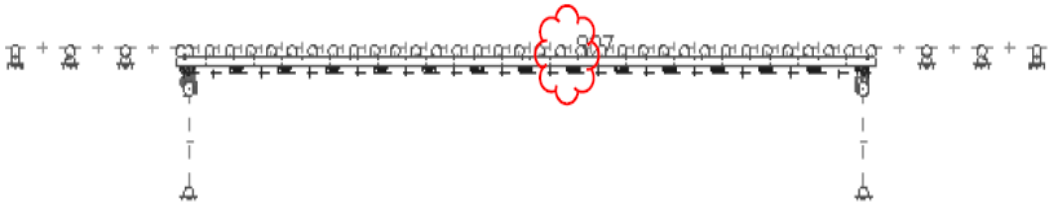

Figure 5.2 Longitudinal Cross-section of Model for 24.5 m Span Length

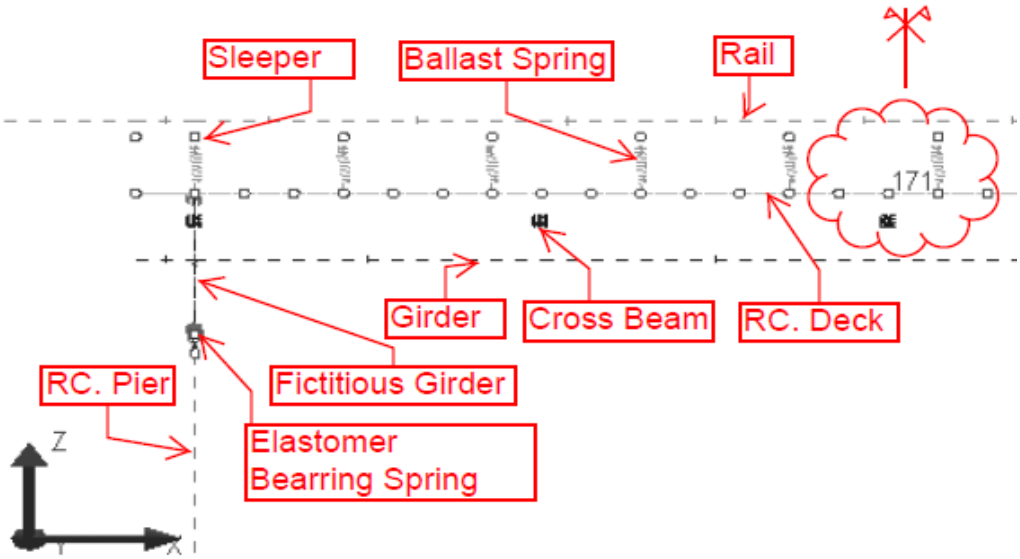

Figure 5.3 Structural Members of Bridge Model for 8.75 m Span Length

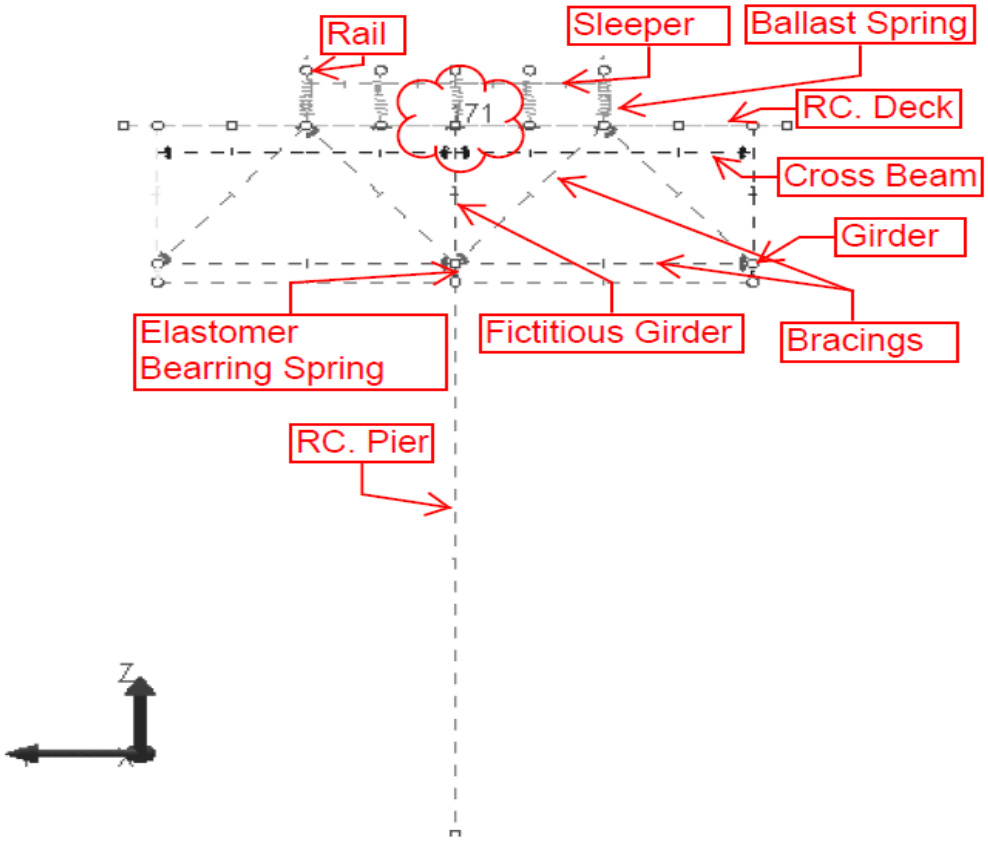

Figure 5.4 Vertical Cross-section of Bridge Model for 8.75 m Span Length

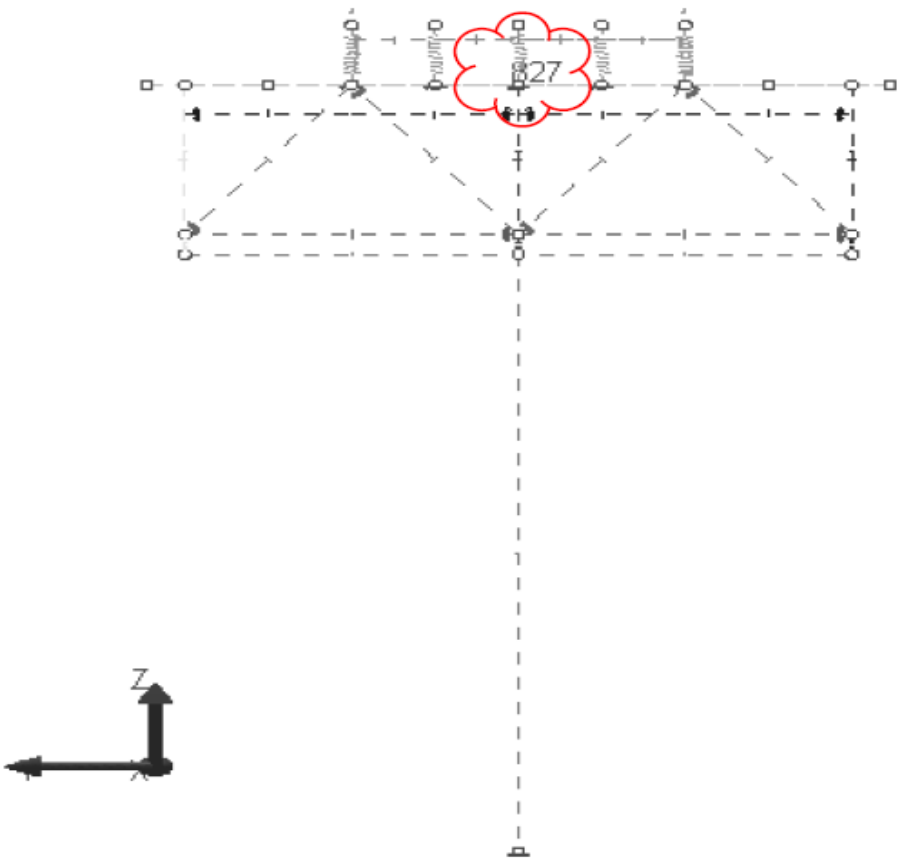

Figure 5.5 Vertical Cross-section of Bridge Model for 24.5 m Span Length

5.2. Mid-Span Joint Acceleration Results

Mid-Span joint accelerations were calculated by non-linear force-time method of Larsa 4D analysis software. Software provides the joint acceleration results graphically as shown in Figure 5.6 for 8.75 m span length and Figure 5.7 for 24.5 m span length. Time versus joint acceleration graphs for selected case studies were given in Appendix A. The maximum mid-span joint acceleration values were reported. Correlation of acceleration with span length, ballast stiffness, vehicle speeds and flexural rigidity were provided. Correlation of mid-span joint acceleration and flexural rigidity for a constant speed was also provided in this section for maximum and minimum design speeds and in

Appendix C for other design speeds. Mid-span accelerations of reinforced concrete box girder railway bridge in Taiwan and prestressed precast girder railway bridge in Turkey were also marked for comparison.

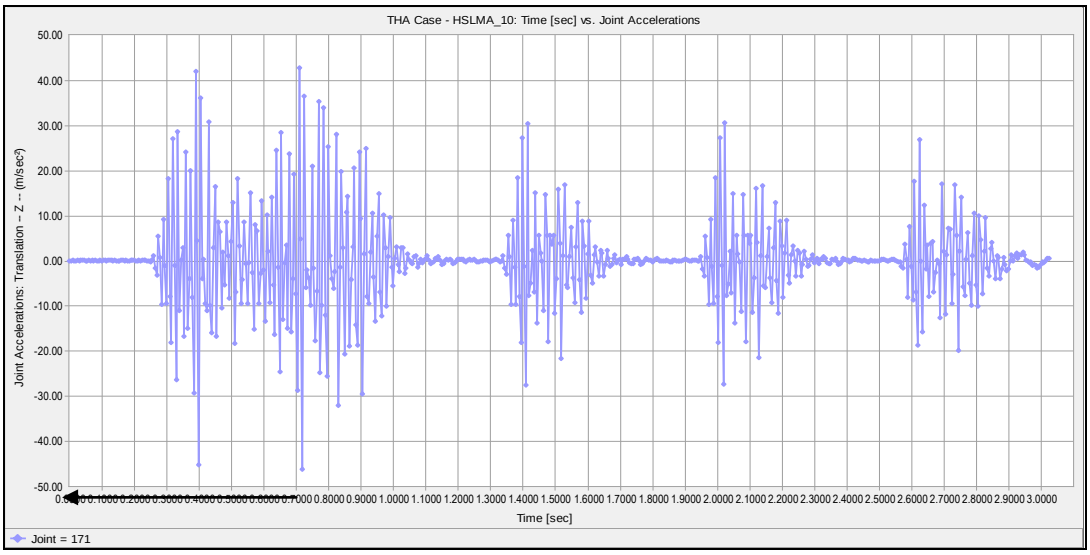

Figure 5.6 Joint Acceleration vs. Time graph of the bridge having 8.75 m span length, 0.75 m girder height for 44.13 m/s vehicle speed.

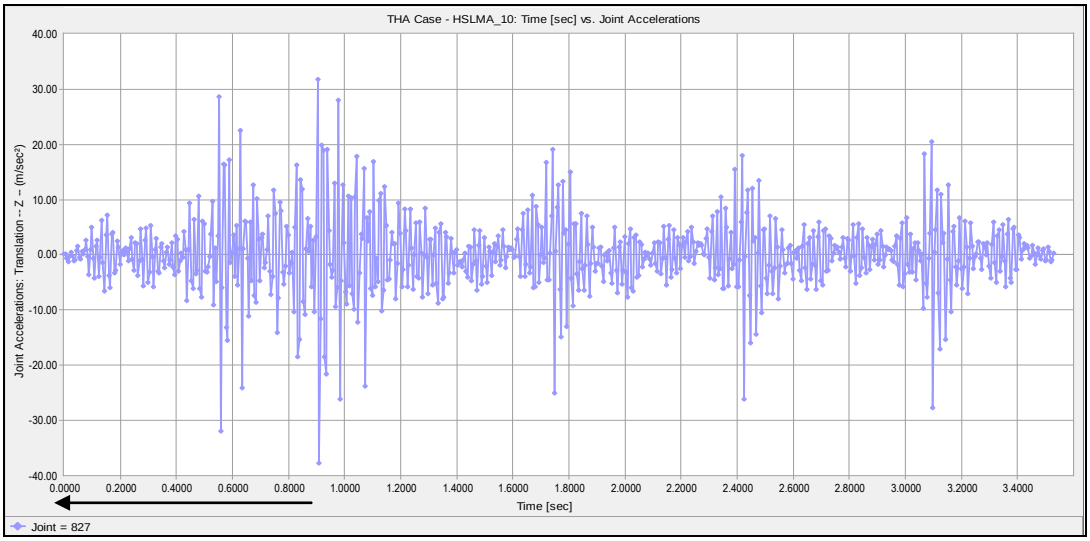

Figure 5.7 Joint Acceleration vs. Time graph of the bridge having 24.5 m span length, 0.75 m girder height for 40 m/s vehicle speed.

Table 5.2 Mid-Span Joint Accelerations (m/s^2) of Bridge Having 8.75m Span Length for Flexural Rigidities and Ballast Stiffness's with varying Vehicle Speeds

Span Flexural Rigidity ($kN.m^2$)	Ballast Stiffness (MPa)	Design Speeds (m/s)				
		40.00	44.13	68.75	83.30	V_{select}
4,421,563	350	31.24	46.18	28.06	28.10	35.56
	700	36.38	50.57	30.97	30.65	36.64
6,244,779	350	35.19	45.04	27.29	27.58	37.02
	700	36.44	48.68	29.89	30.26	36.75
9,259,962	350	32.86	40.30	25.59	26.00	41.76
	700	35.42	47.16	26.93	29.00	43.03
12,981,220	350	29.67	36.97	25.50	25.98	39.48
	700	34.80	42.20	26.86	30.20	45.10
23,750,916	350	18.80	19.34	14.38	13.88	27.19
	700	19.36	22.62	14.57	14.08	25.37
195,898,160	350	3.27	3.80	2.60	4.13	4.25
	700	3.45	2.90	2.40	3.30	1.88
768,263,855	350	0.80	0.71	0.54	0.83	0.36
	700	0.81	0.85	0.66	0.84	0.42
1,912,920,565	350	0.42	0.30	0.29	0.37	0.15
	700	0.44	0.31	0.30	0.32	0.11

Table 5.3 Mid-Span Joint Accelerations (m/s^2) of Bridge Having 24.5m Span Length for Flexural Rigidities and Ballast Stiffness's with varying Vehicle Speeds

Span Flexural Rigidity ($kN.m^2$)	Ballast Stiffness (MPa)	Design Speeds (m/s)				
		40	54.27	76.08	83.3	V_{select}
4,421,563	350	37.82	31.39	34.21	37.07	37.34
	700	40.25	34.49	36.23	37.23	37.50
6,244,779	350	37.61	26.88	31.56	35.33	32.12
	700	39.72	32.29	33.26	35.54	36.20
9,259,962	350	35.62	26.78	30.24	30.45	37.68
	700	39.59	29.06	31.55	31.20	37.01
12,981,220	350	35.58	26.30	29.54	30.40	28.90
	700	39.04	30.21	31.16	31.07	30.27
23,750,916	350	20.48	18.91	14.65	18.49	17.31
	700	19.99	20.94	14.84	18.10	18.22
195,898,160	350	3.15	3.97	2.48	3.71	2.79
	700	3.77	3.91	2.28	4.35	2.58
768,263,855	350	0.89	1.16	0.70	0.77	0.62
	700	1.00	1.10	0.86	0.78	0.45
1,912,920,565	350	0.42	0.45	0.29	0.35	0.17
	700	0.44	0.47	0.30	0.30	0.19

Table 5.4 Maximum Mid-Span Joint Accelerations (m/s^2) of Bridge Having 8.75m Span Length for Flexural Rigidities and Ballast Stiffness's

Span Flexural Rigidity ($kN.m^2$)	Ballast Stiffness (MPa)	Max. Acceleration (m/s^2)
4,421,563	**350**	46.18
	700	50.57
6,244,779	**350**	45.04
	700	48.68
9,259,962	**350**	41.76
	700	47.16
12,981,220	**350**	39.48
	700	45.10
23,750,916	**350**	27.19
	700	25.37
195,898,160	**350**	4.25
	700	3.45
768,263,855	**350**	0.83
	700	0.85
1,912,920,565	**350**	0.42
	700	0.44

Table 5.5 Maximum Mid-Span Joint Accelerations (m/s^2) of Bridge Having 24.5m Span Length for Flexural Rigidities and Ballast Stiffness's

Span Flexural Rigidity ($kN.m^2$)	Ballast Stiffness (MPa)	Max. Acceleration (m/s^2)
4,421,563	**350**	37.82
	700	40.25
6,244,779	**350**	37.61
	700	39.72
9,259,962	**350**	37.68
	700	39.59
12,981,220	**350**	35.58
	700	39.04
23,750,916	**350**	20.48
	700	20.94
195,898,160	**350**	3.97
	700	4.35
768,263,855	**350**	1.16
	700	1.10
1,912,920,565	**350**	0.45
	700	0.47

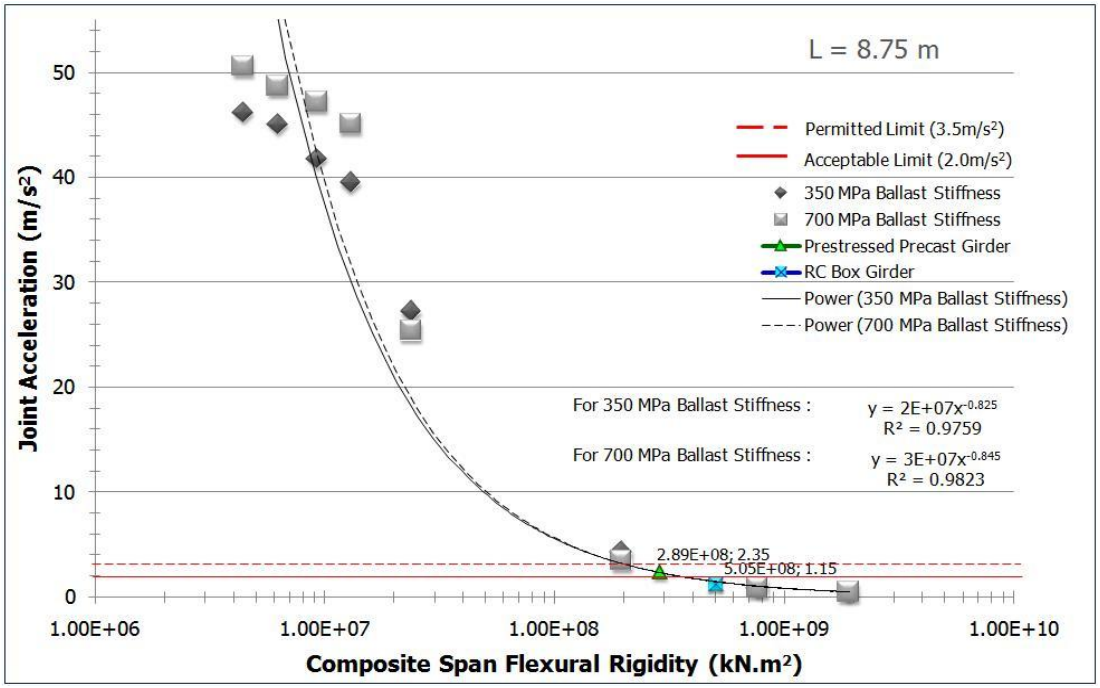

Figure 5.8 Correlations of Max. Joint Acceleration with Span Flexural Rigidity for Bridge Having 8.75 m Span Length

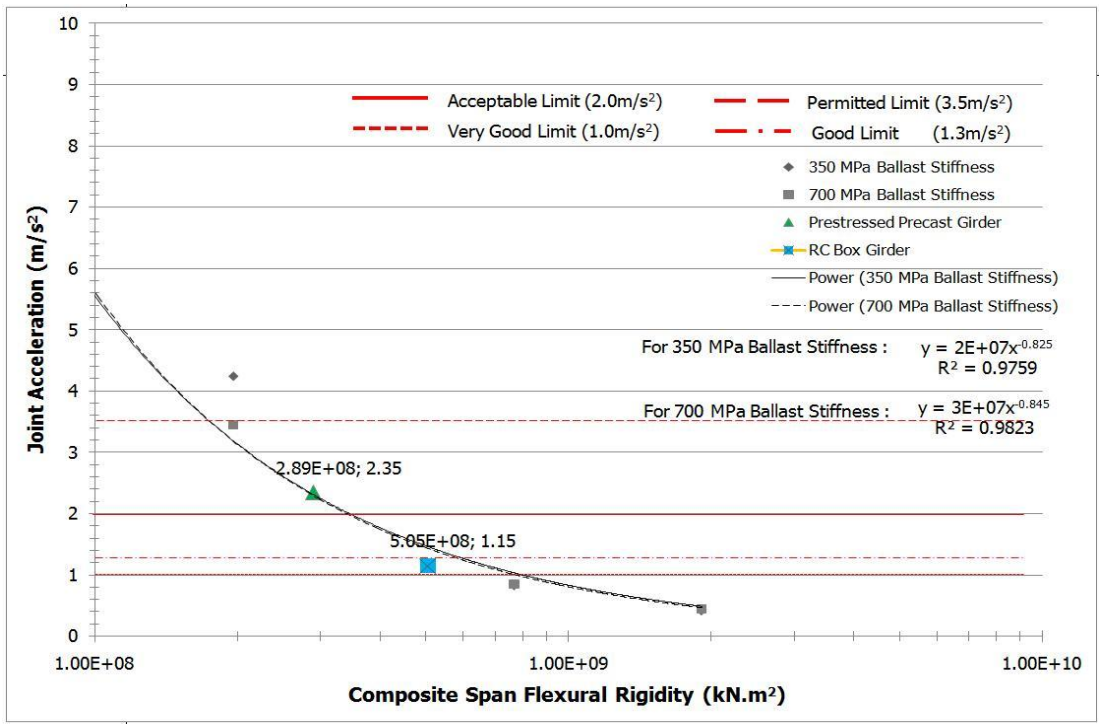

Figure 5.9 Correlations of Max. Joint Acceleration in Limits with Span Flexural Rigidity for Bridge Having 8.75 m Span Length

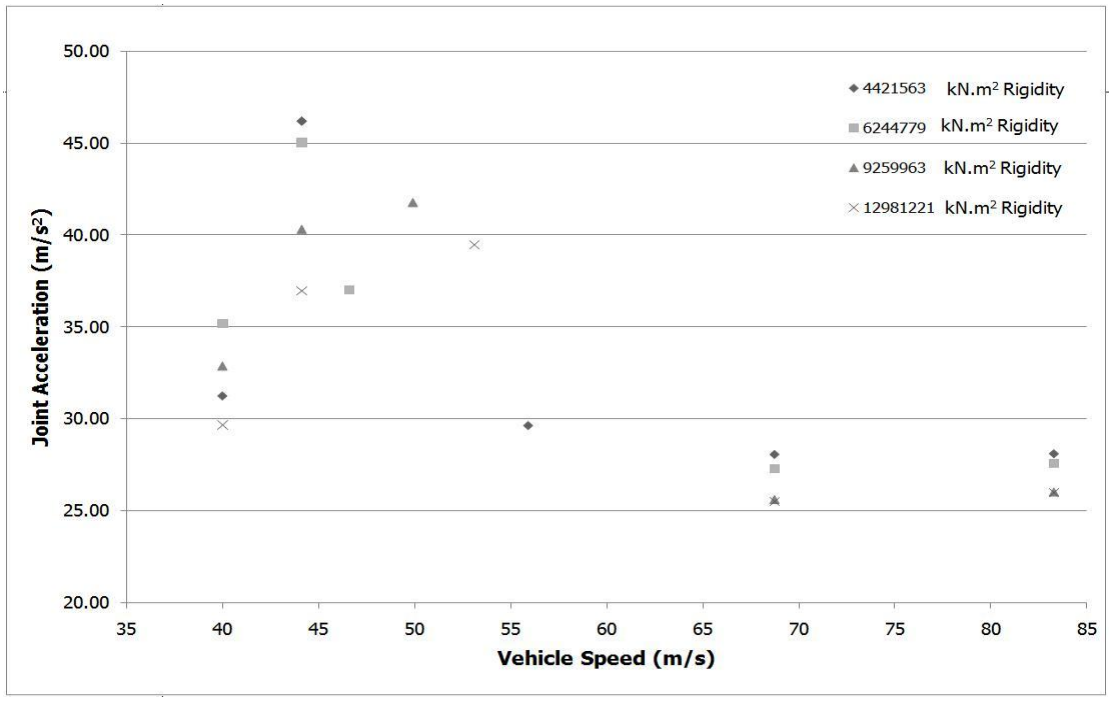

Figure 5.10 Correlations of Max. Joint Acceleration with Vehicle Speed for Bridge Having 8.75 m Span Length & 350 MPa Ballast Stiffness

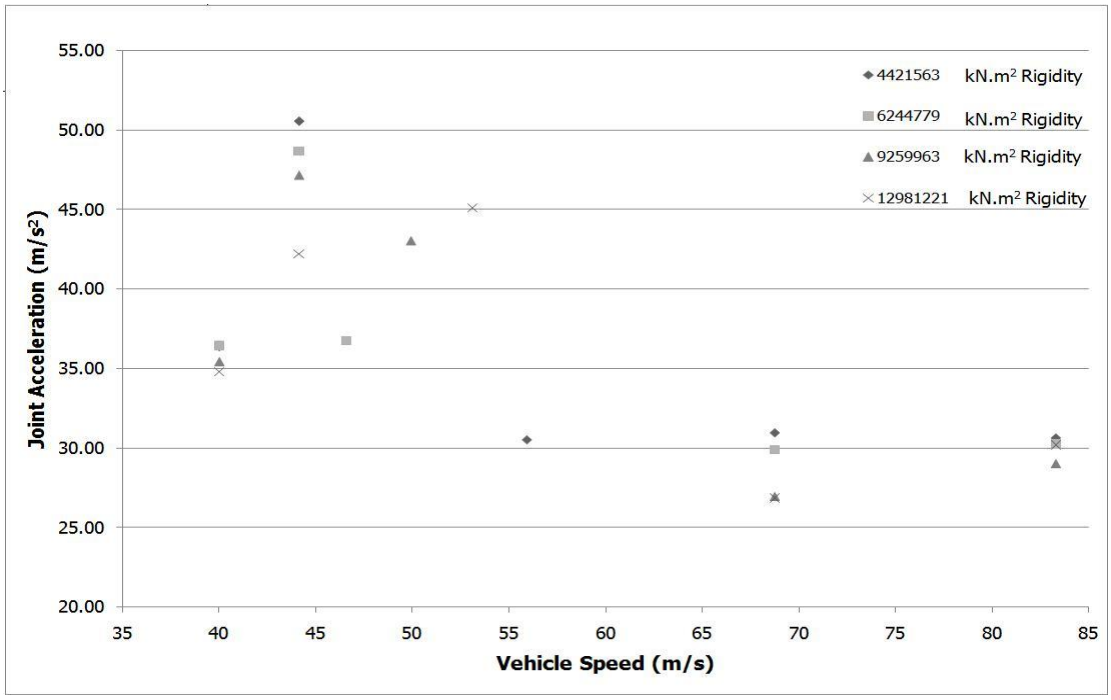

Figure 5.11 Correlations of Max. Joint Acceleration with Vehicle Speed for Bridge Having 8.75 m Span Length & 700 MPa Ballast Stiffness

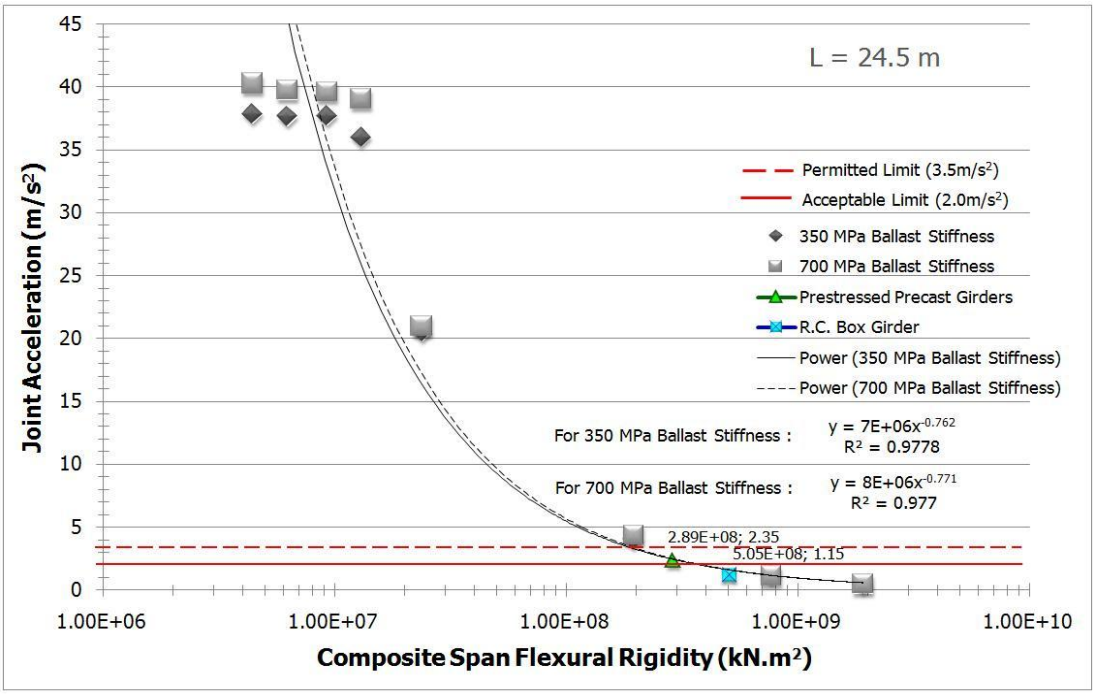

Figure 5.12 Correlations of Max. Joint Acceleration with Span Flexural Rigidity for Bridge Having 24.5 m Span Length

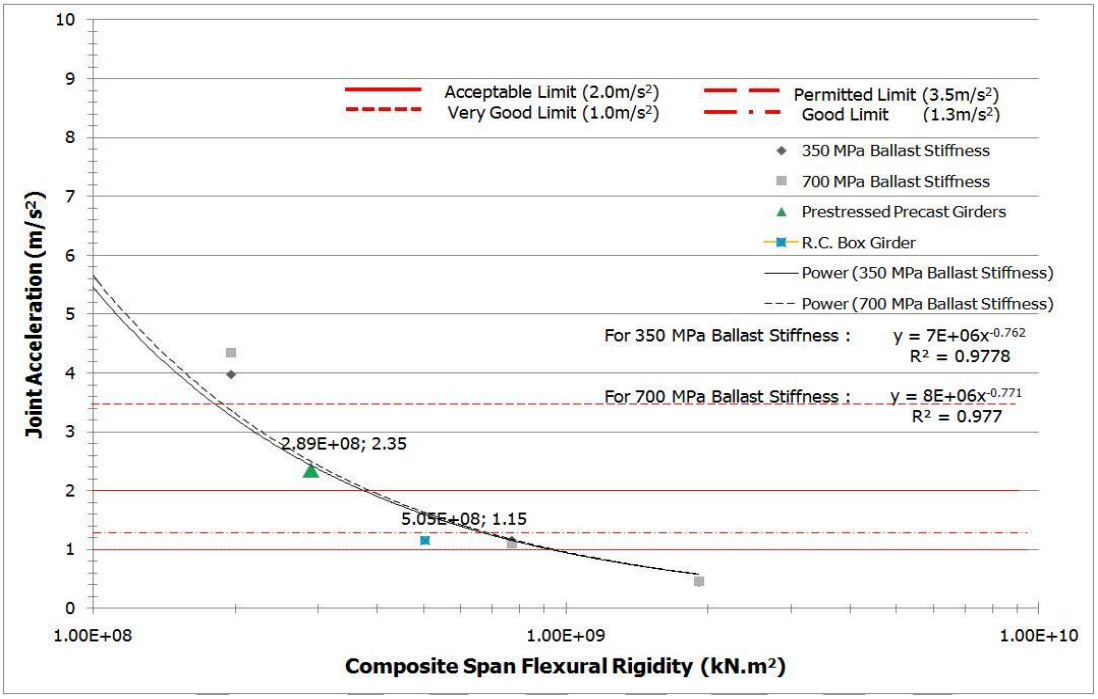

Figure 5.13 Correlations of Max. Joint Acceleration in Limits with Span Flexural Rigidity for Bridge Having 24.5 m Span Length

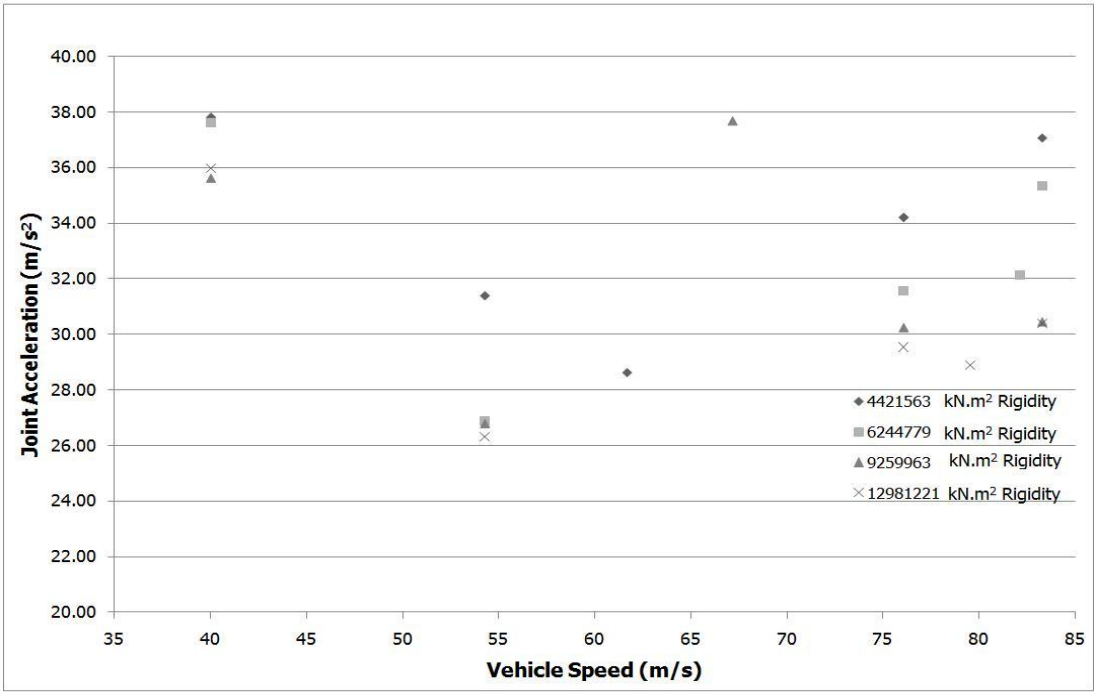

Figure 5.14 Correlations of Max. Joint Acceleration with Vehicle Speed for Bridge Having 24.5 m Span Length & 350 MPa Ballast Stiffness

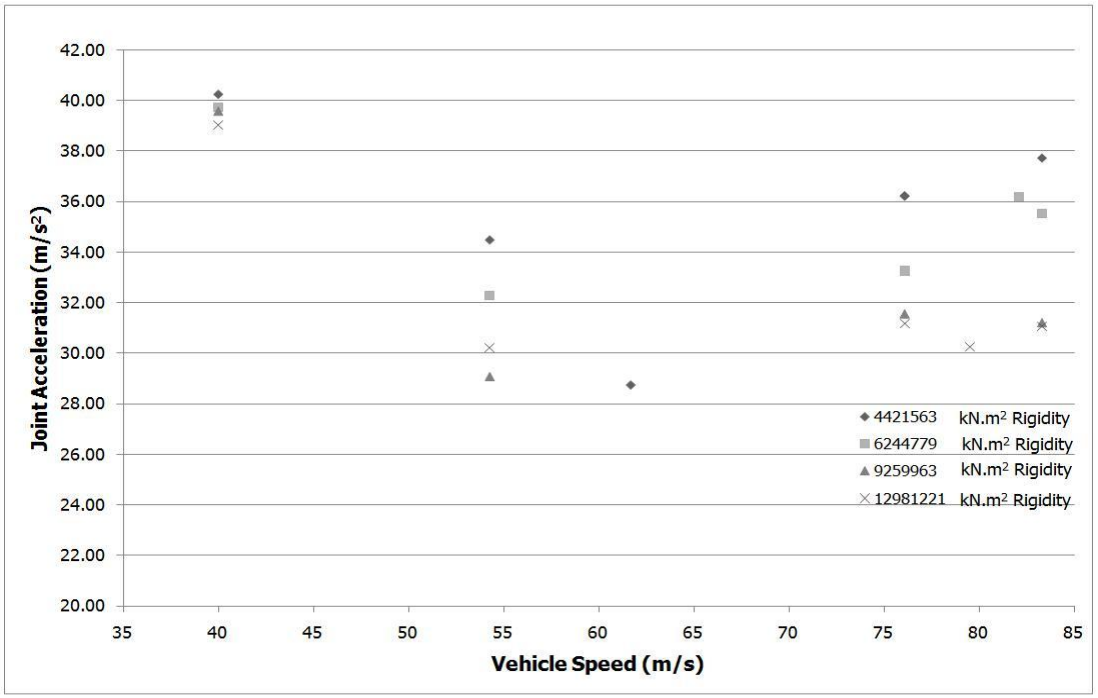

Figure 5.15 Correlations of Max. Joint Acceleration with Vehicle Speed for Bridge Having 24.5 m Span Length & 700 MPa Ballast Stiffness

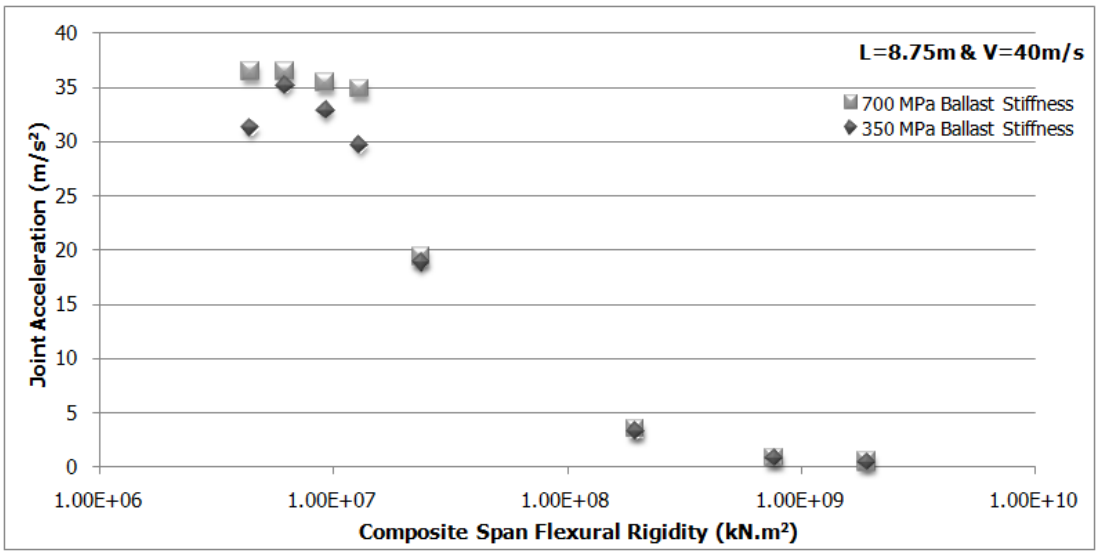

Figure 5.16 Correlations of Max. Joint Acceleration with Span Flexural Rigidity for 40m/s Constant Design Speed and Bridge Having 8.75 m Span Length

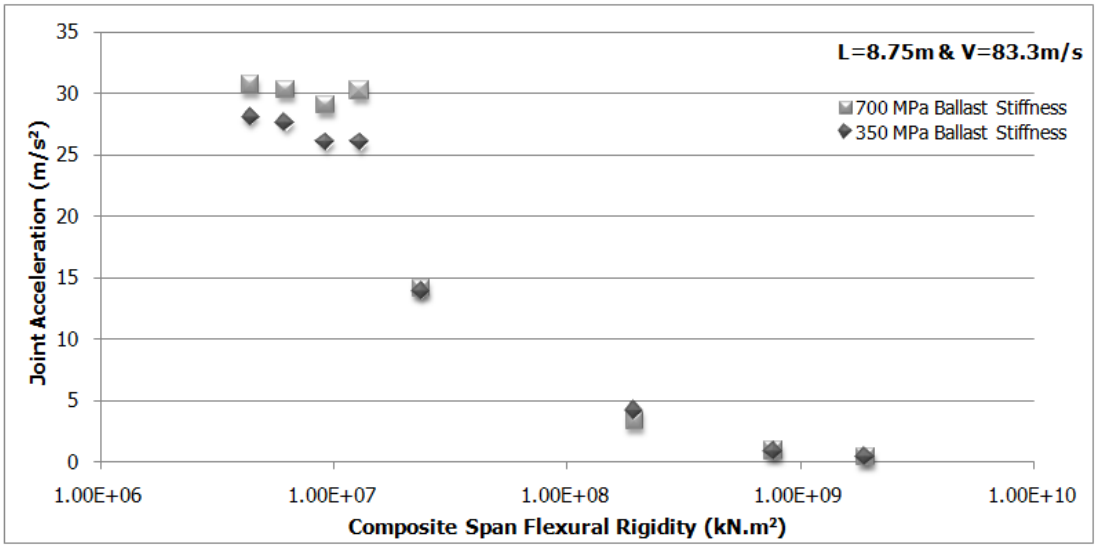

Figure 5.17 Correlations of Max. Joint Acceleration with Span Flexural Rigidity for 83.3m/s Constant Design Speed and Bridge Having 8.75 m Span Length

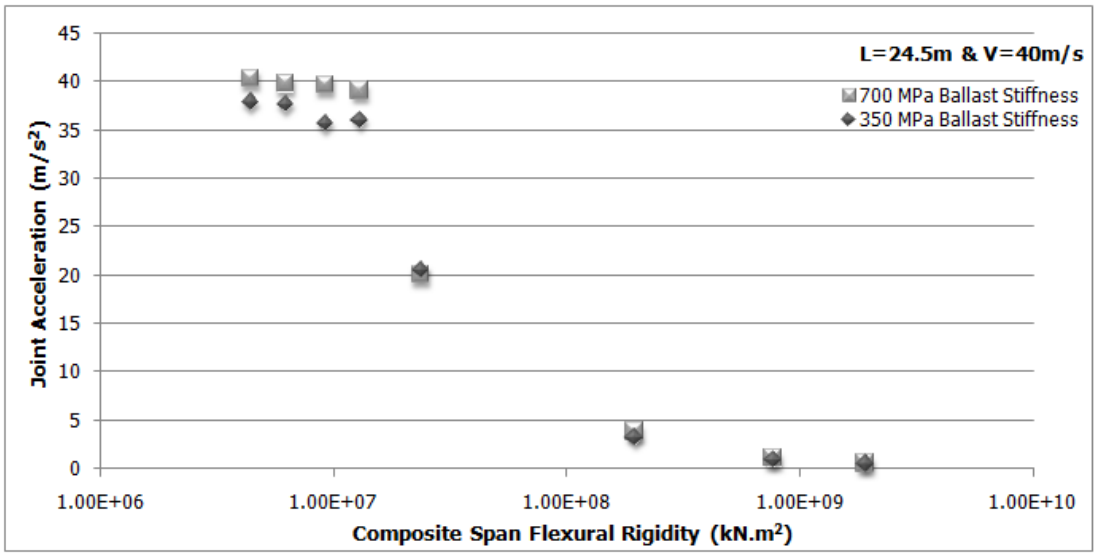

Figure 5.18 Correlations of Max. Joint Acceleration with Span Flexural Rigidity for 40m/s Constant Design Speed and Bridge Having 24.5 m Span Length

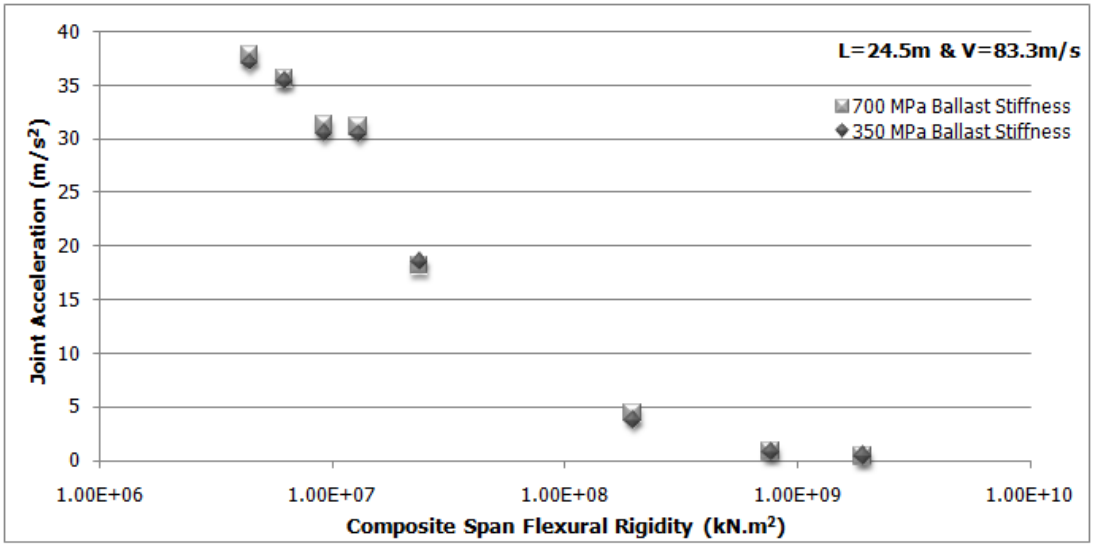

Figure 5.19 Correlations of Max. Joint Acceleration with Span Flexural Rigidity for 83.3m/s Constant Design Speed and Bridge Having 24.5 m Span Length

5.3. Mid-Span Joint Displacement Results

The maximum mid-span joint vertical displacements were reported. The joint vertical displacement results were presented graphically by analysis software as shown in Figure 5.20 for 8.75 m span length and Figure 5.21 for 24.5 m span length. Time versus joint displacement graphs for selected case studies were given in Appendix A. Correlation of vertical displacement with span length, ballast stiffness, vehicle speeds and flexural rigidity were provided. Correlation of joint vertical displacement and flexural rigidity for a constant speed was also provided in this section for maximum and minimum design speeds and in Appendix C for other design speeds.

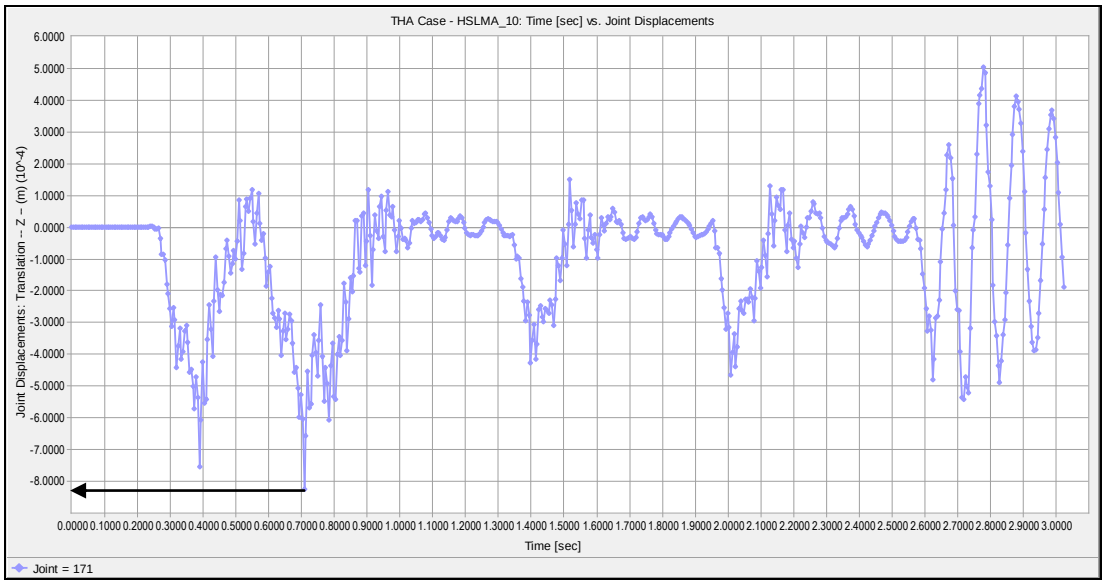

Figure 5.20 Joint Displacement vs. Time graph of the bridge having 8.75 m span length, 0.75 m girder height for 44.13 m/s vehicle speed.

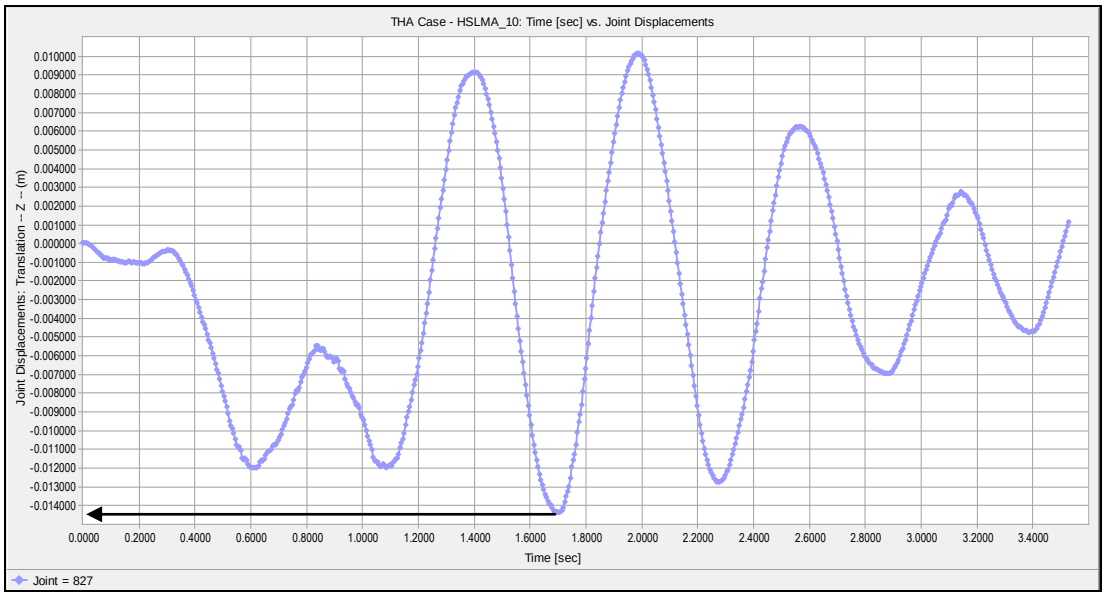

Figure 5.21 Joint Displacement vs. Time graph of the bridge having 24.5 m span length, 0.75 m girder height for 40 m/s vehicle speed.

Table 5.6 Mid-Span Joint Displacements (mm) of Bridge Having 8.75m Span Length for Flexural Rigidities and Ballast Stiffness's with varying Vehicle Speeds

Span Flexural Rigidity ($kN.m^2$)	Ballast Stiffness (MPa)	Design Speeds (m/s)				
		40.00	44.13	68.75	83.30	V_{select}
4,421,563	350	0.710	0.800	1.000	1.810	0.850
	700	0.730	0.820	1.000	1.600	0.800
6,244,779	350	0.700	0.700	0.820	1.100	0.700
	700	0.680	0.680	0.800	1.050	0.650
9,259,962	350	0.700	0.610	0.670	0.820	0.500
	700	0.660	0.600	0.620	0.800	0.471
12,981,220	350	0.450	0.600	0.580	0.660	0.511
	700	0.423	0.550	0.540	0.640	0.535
23,750,916	350	0.267	0.250	0.330	0.307	0.380
	700	0.360	0.213	0.308	0.273	0.320
195,898,160	350	0.067	0.055	0.120	0.140	0.153
	700	0.064	0.052	0.083	0.130	0.100
768,263,855	350	0.030	0.034	0.040	0.045	0.047
	700	0.028	0.033	0.045	0.041	0.041
1,912,920,565	350	0.020	0.025	0.038	0.060	0.036
	700	0.020	0.023	0.038	0.057	0.038

Table 5.7 Mid-Span Joint Displacements (mm) of Bridge Having 24.5m Span Length for Flexural Rigidities and Ballast Stiffness's with varying Vehicle Speeds

Span Flexural Rigidity ($kN.m^2$)	Ballast Stiffness (MPa)	Design Speeds (m/s)				
		40.00	54.27	76.08	83.30	V_{select}
4,421,563	350	14.370	24.300	28.110	32.000	22.000
	700	14.500	24.300	28.000	32.000	23.000
6,244,779	350	11.200	23.100	22.200	25.400	25.000
	700	12.000	23.000	22.000	25.000	25.000
9,259,962	350	9.450	15.200	16.940	19.000	20.300
	700	10.000	15.000	16.990	18.400	21.000
12,981,220	350	7.300	9.650	16.330	16.130	15.100
	700	7.400	9.570	17.500	14.000	15.000
23,750,916	350	2.800	4.200	0.910	14.900	3.650
	700	2.950	4.200	9.100	14.500	3.600
195,898,160	350	0.375	0.550	0.700	0.710	0.700
	700	0.385	0.540	0.690	0.700	0.680
768,263,855	350	0.125	0.190	0.217	0.252	0.207
	700	0.145	0.184	0.244	0.230	0.198
1,912,920,565	350	0.090	0.095	0.158	0.206	0.113
	700	0.090	0.087	0.158	0.196	0.110

Table 5.8 Maximum Mid-Span Joint Displacements (mm) of Bridge Having 8.75m Span Length for Flexural Rigidities and Ballast Stiffness's

Span Flexural Rigidity ($kN.m^2$)	Ballast Stiffness (MPa)	Max. Displacement (mm)
4,421,563	350	1.810
	700	1.600
6,244,779	350	1.100
	700	1.050
9,259,962	350	0.820
	700	0.800
12,981,220	350	0.660
	700	0.640
23,750,916	350	0.380
	700	0.360
195,898,160	350	0.153
	700	0.130
768,263,855	350	0.047
	700	0.045
1,912,920,565	350	0.060
	700	0.057

Table 5.9 Maximum Mid-Span Joint Displacements (mm) of Bridge Having 24.5m Span Length for Flexural Rigidities and Ballast Stiffness's

Span Flexural Rigidity ($kN.m^2$)	Ballast Stiffness (MPa)	Max. Displacement (mm)
4,421,563	**350**	32.000
	700	32.000
6,244,779	**350**	25.400
	700	25.000
9,259,962	**350**	20.300
	700	21.000
12,981,220	**350**	16.330
	700	17.500
23,750,916	**350**	14.900
	700	14.500
195,898,160	**350**	0.710
	700	0.700
768,263,855	**350**	0.252
	700	0.244
1,912,920,565	**350**	0.206
	700	0.196

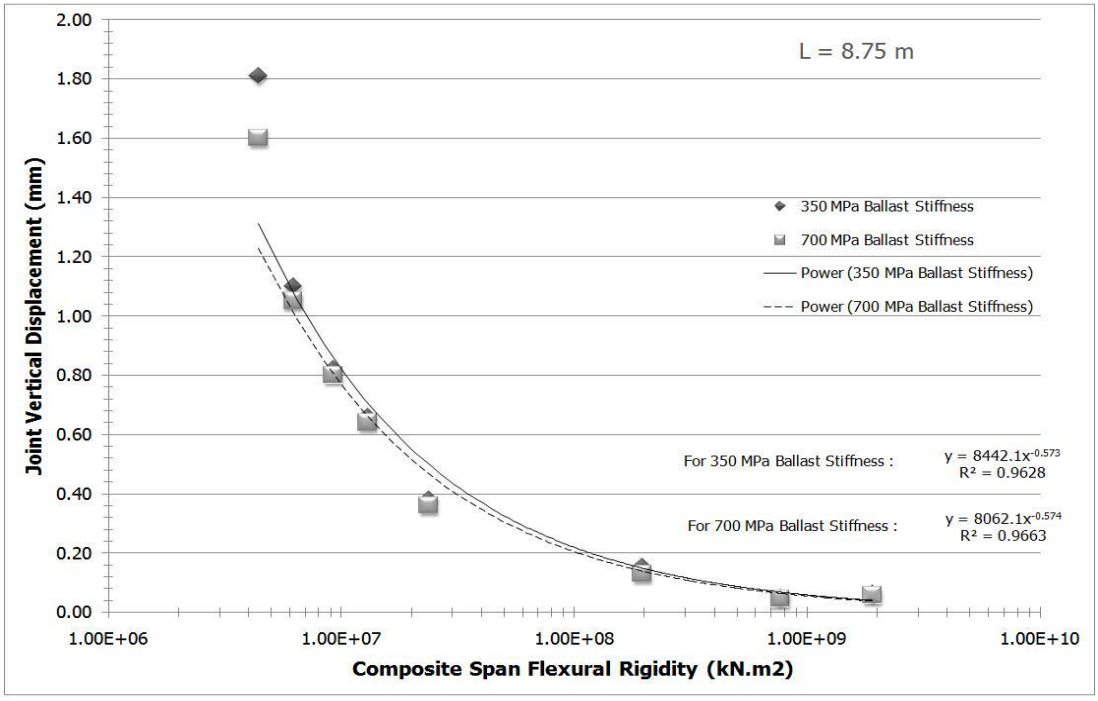

Figure 5.22 Correlations of Max. Joint Displacement with Span Flexural Rigidity for Bridge Having 8.75 m Span Length

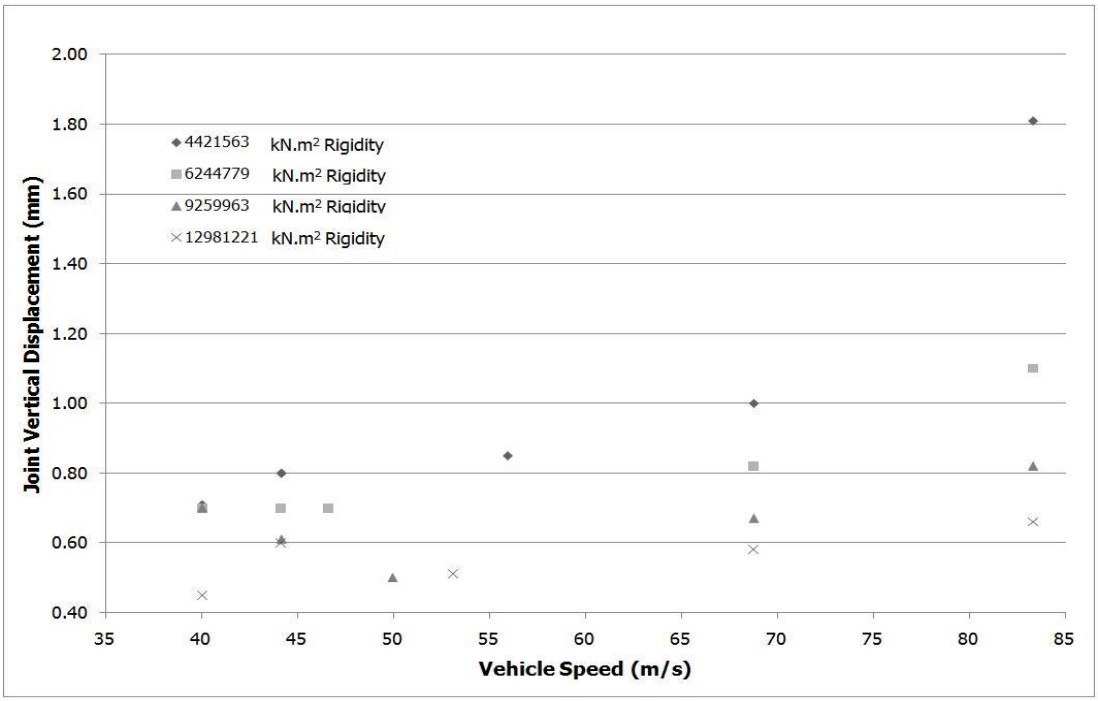

Figure 5.23 Correlations of Max. Joint Displacement with Vehicle Speed for Bridge Having 8.75 m Span Length & 350 MPa Ballast Stiffness

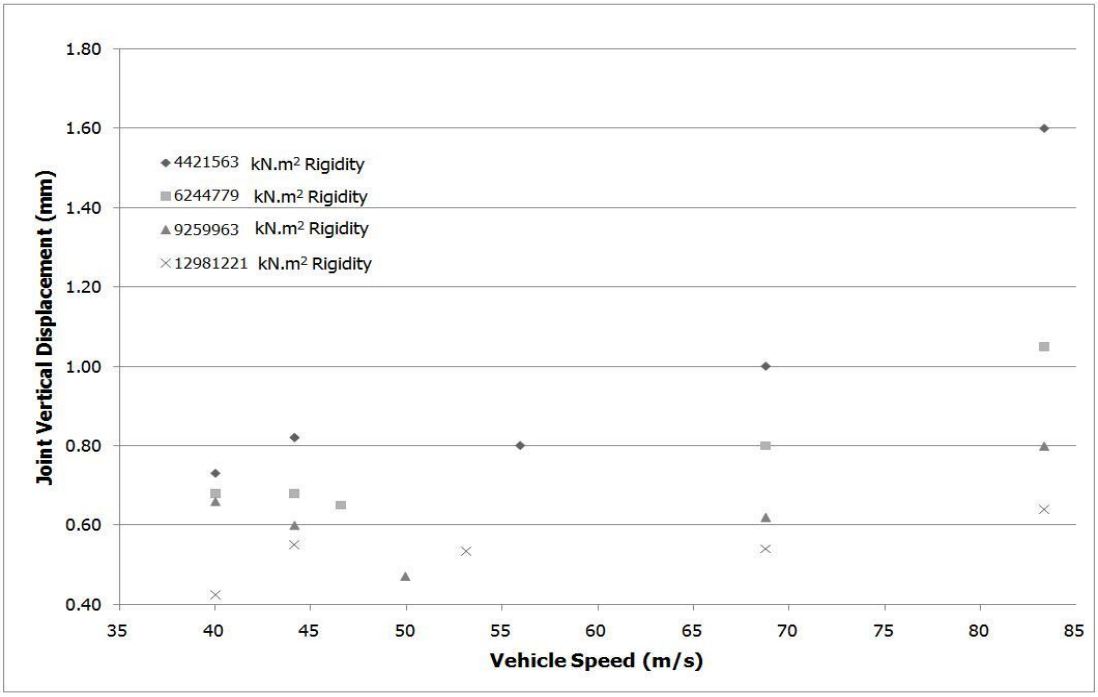

Figure 5.24 Correlations of Max. Joint Displacement with Vehicle Speed for Bridge Having 8.75 m Span Length & 700 MPa Ballast Stiffness

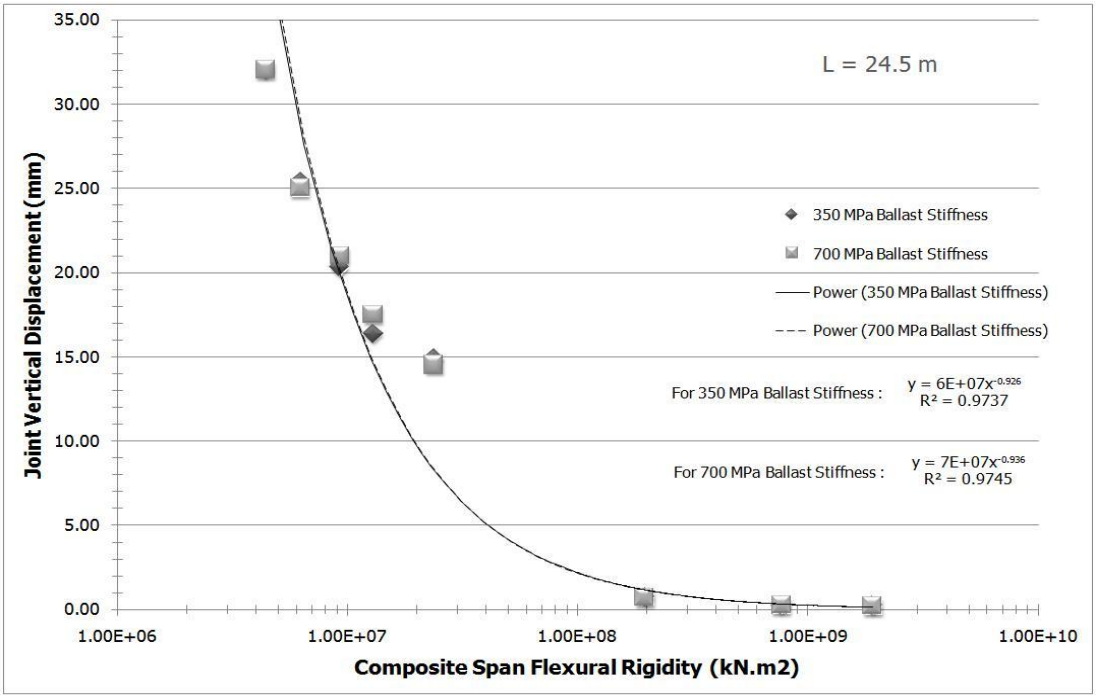

Figure 5.25 Correlations of Max. Joint Displacement with Span Flexural Rigidity for Bridge Having 24.5 m Span Length

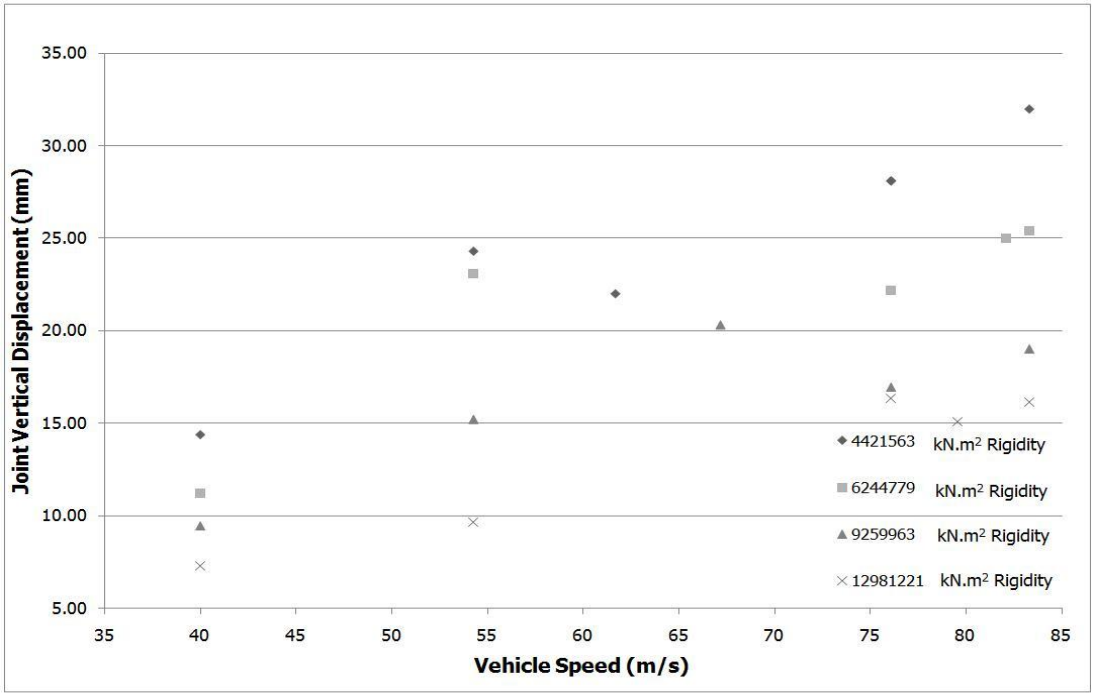

Figure 5.26 Correlations of Max. Joint Displacement with Vehicle Speed for Bridge Having 24.5 m Span Length & 350 MPa Ballast Stiffness

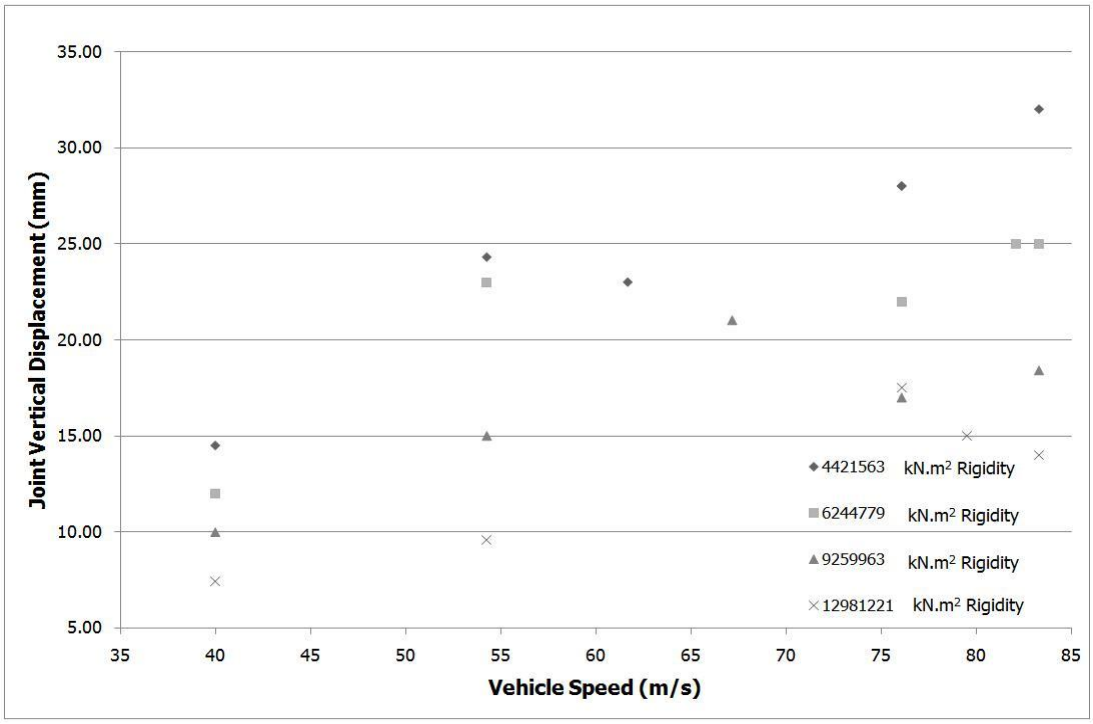

Figure 5.27 Correlations of Max. Joint Displacement with Vehicle Speed for Bridge Having 24.5 m Span Length & 700 MPa Ballast Stiffness

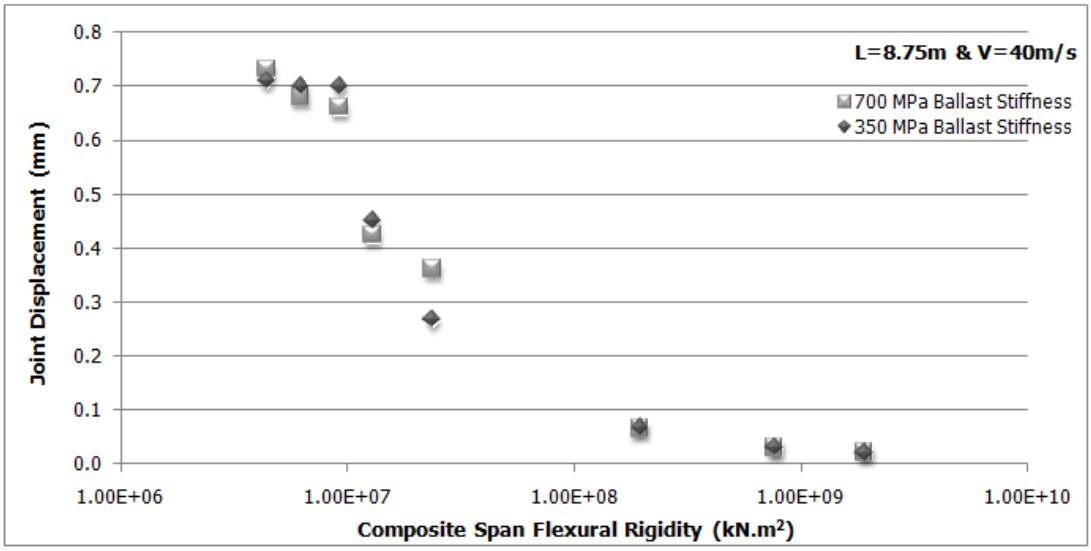

Figure 5.28 Correlations of Max. Joint Displacement with Span Flexural Rigidity for 40m/s Constant Design Speed and Bridge Having 8.75 m Span Length

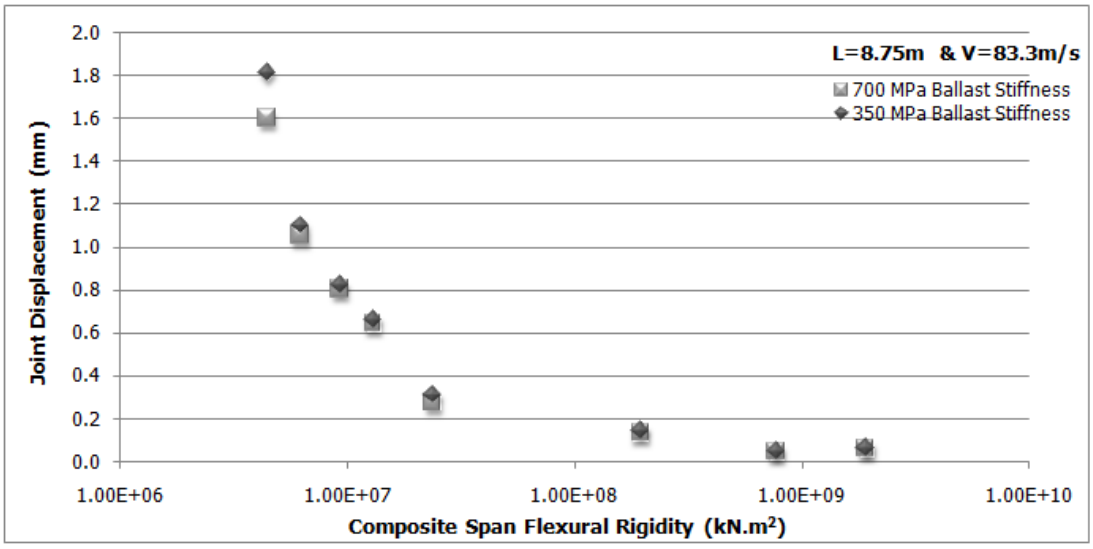

Figure 5.29 Correlations of Max. Joint Displacement with Span Flexural Rigidity for 83.3m/s Constant Design Speed and Bridge Having 8.75 m Span Length

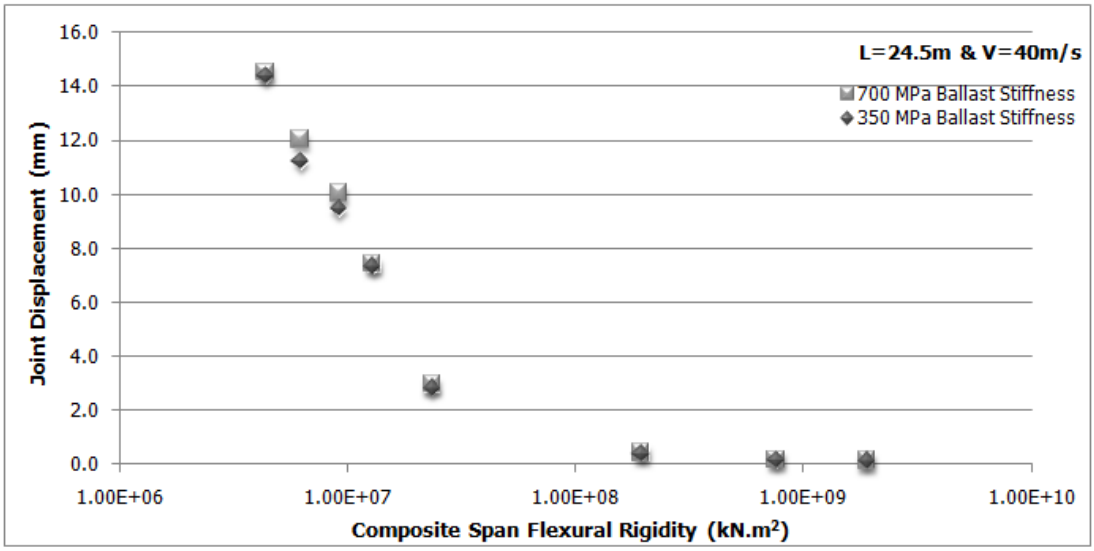

Figure 5.30 Correlations of Max. Joint Displacement with Span Flexural Rigidity for 40m/s Constant Design Speed and Bridge Having 24.5 m Span Length

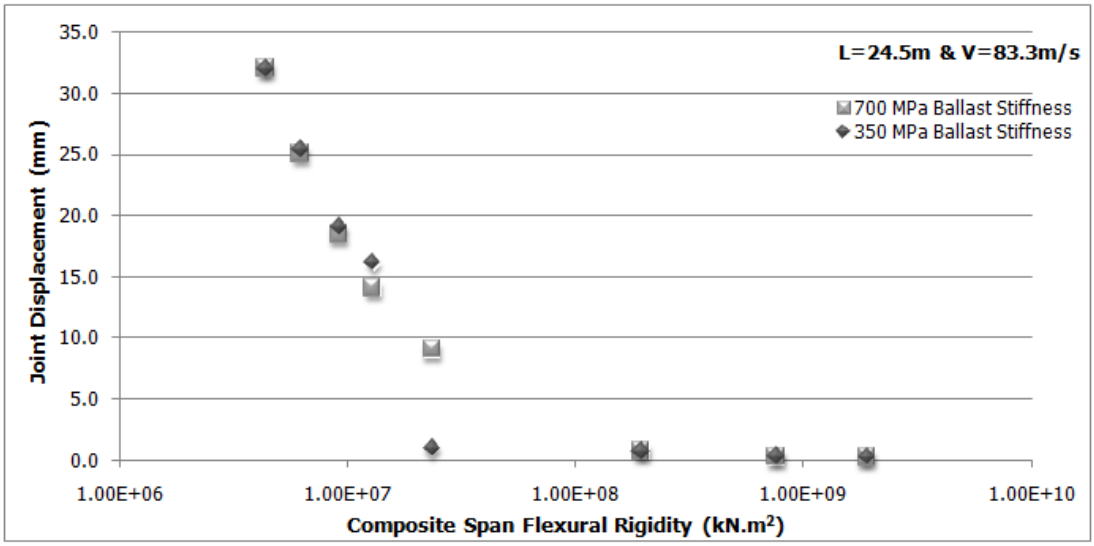

Figure 5.31 Correlations of Max. Joint Displacement with Span Flexural Rigidity for 83.3m/s Constant Design Speed and Bridge Having 24.5 m Span Length

5.4. Mid-Span Deck Twist Results

The maximum deck twist values were reported. The joint rotation relative to the joint 3 m away from track in transverse direction is defined as twist of deck. The deck twist results were presented graphically by analysis software as shown in Figure 5.32 for 8.75 m span length and Figure 5.33 for 24.5 m span length. Time versus deck twist graphs for selected case studies were given in Appendix A. Correlation of deck twist with span length, ballast stiffness, vehicle speeds and flexural rigidity were provided. Correlation of deck twist and flexural rigidity for a constant speed was also provided in this section for maximum and minimum design speeds and in Appendix C for other design speeds.

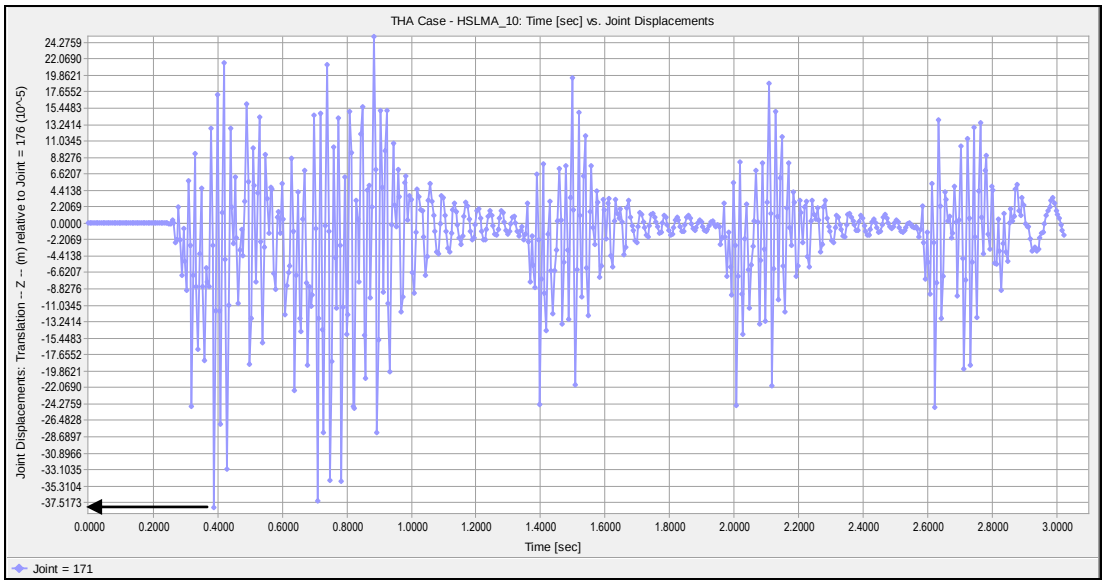

Figure 5.32 Deck Twist vs. Time graph of the bridge having 8.75 m span length, 0.75 m girder height for 44.13 m/s vehicle speed.

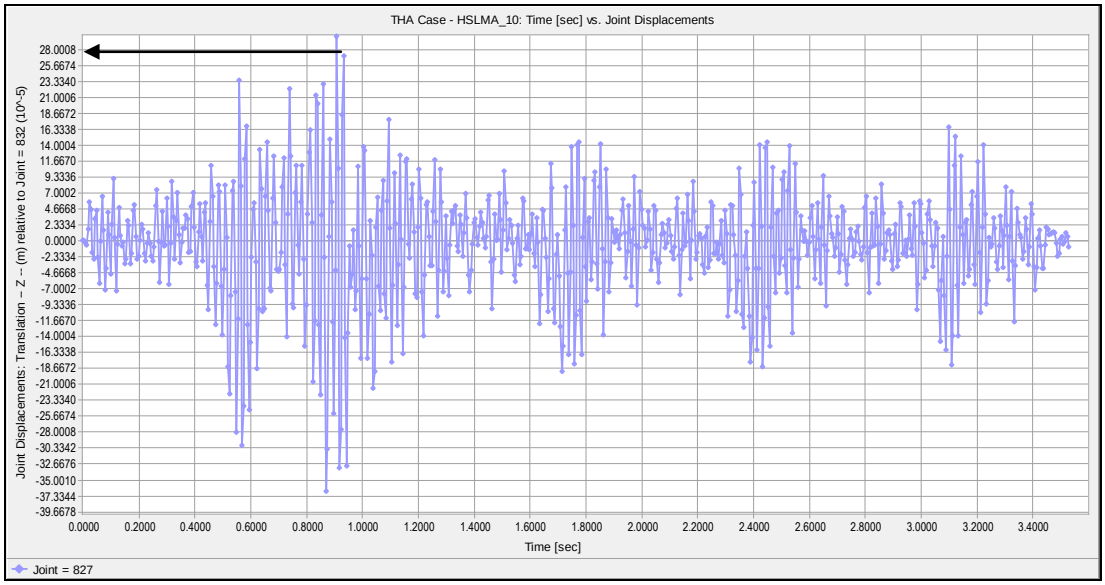

Figure 5.33 Deck Twist vs. Time graph of the bridge having 24.5 m span length, 0.75 m girder height for 40 m/s vehicle speed.

Table 5.10 Mid-Span Deck Twist (mm/3m) of Bridge Having 8.75m Span Length for Flexural Rigidities and Ballast Stiffness's with varying Vehicle Speeds

Span Flexural Rigidity ($kN.m^2$)	Ballast Stiffness (MPa)	Design Speeds (m/s)				
		40.00	44.13	68.75	83.30	V_{select}
4,421,563	350	0.352	0.400	0.300	0.320	0.230
	700	0.350	0.363	0.290	0.330	0.290
6,244,779	350	0.340	0.397	0.240	0.290	0.373
	700	0.300	0.365	0.272	0.260	0.355
9,259,962	350	0.320	0.430	0.240	0.350	0.216
	700	0.310	0.360	0.260	0.240	0.209
12,981,220	350	0.310	0.373	0.240	0.382	0.386
	700	0.320	0.306	0.270	0.228	0.462
23,750,916	350	0.240	0.260	0.155	0.266	0.215
	700	0.190	0.249	0.175	0.233	0.217
195,898,160	350	0.070	0.070	0.150	0.175	0.215
	700	0.056	0.055	0.125	0.140	0.108
768,263,855	350	0.280	0.030	0.038	0.035	0.134
	700	0.029	0.029	0.045	0.034	0.033
1,912,920,565	350	0.168	0.018	0.023	0.000	0.118
	700	0.016	0.002	0.025	0.026	0.021

Table 5.11 Mid-Span Deck Twist (mm/3m) of Bridge Having 24.5m Span Length for Flexural Rigidities and Ballast Stiffness's with varying Vehicle Speeds

Span Flexural Rigidity ($kN.m^2$)	Ballast Stiffness (MPa)	Design Speeds (m/s)				
		40.00	44.13	68.75	83.30	V_{select}
4,421,563	350	0.367	0.240	0.265	0.348	0.270
	700	0.290	0.219	0.215	0.280	0.280
6,244,779	350	0.362	0.255	0.340	0.310	0.285
	700	0.285	0.250	0.215	0.290	0.310
9,259,962	350	0.410	0.220	0.240	0.340	0.309
	700	0.397	0.210	0.215	0.300	0.217
12,981,220	350	0.400	0.222	0.286	0.351	0.285
	700	0.360	0.222	0.270	0.295	0.331
23,750,916	350	0.182	0.210	0.235	0.325	0.207
	700	0.179	0.196	0.279	0.297	0.152
195,898,160	350	0.145	0.174	0.140	0.184	0.145
	700	0.156	0.170	0.197	0.190	0.118
768,263,855	350	0.048	0.070	0.103	0.115	0.098
	700	0.047	0.070	0.122	0.112	0.080
1,912,920,565	350	0.042	0.062	0.100	0.106	0.066
	700	0.004	0.006	0.109	0.110	0.064

Table 5.12 Maximum Mid-Span Deck Twist (mm/3m) of Bridge Having 8.75m Span Length for Flexural Rigidities and Ballast Stiffness's

Span Flexural Rigidity ($kN.m^2$)	Ballast Stiffness (MPa)	Max. Twist (mm/3m)
4,421,563	**350**	0.400
	700	0.363
6,244,779	**350**	0.397
	700	0.365
9,259,962	**350**	0.430
	700	0.360
12,981,220	**350**	0.386
	700	0.462
23,750,916	**350**	0.266
	700	0.249
195,898,160	**350**	0.215
	700	0.140
768,263,855	**350**	0.280
	700	0.045
1,912,920,565	**350**	0.168
	700	0.026

Table 5.13 Maximum Mid-Span Deck Twist (mm/3m) of Bridge Having 24.5m Span Length for Flexural Rigidities and Ballast Stiffness's

Span Flexural Rigidity ($kN.m^2$)	Ballast Stiffness (MPa)	Max. Twist (mm/3m)
4,421,563	**350**	0.367
	700	0.290
6,244,779	**350**	0.362
	700	0.310
9,259,962	**350**	0.410
	700	0.397
12,981,220	**350**	0.400
	700	0.360
23,750,916	**350**	0.325
	700	0.297
195,898,160	**350**	0.184
	700	0.197
768,263,855	**350**	0.115
	700	0.122
1,912,920,565	**350**	0.106
	700	0.110

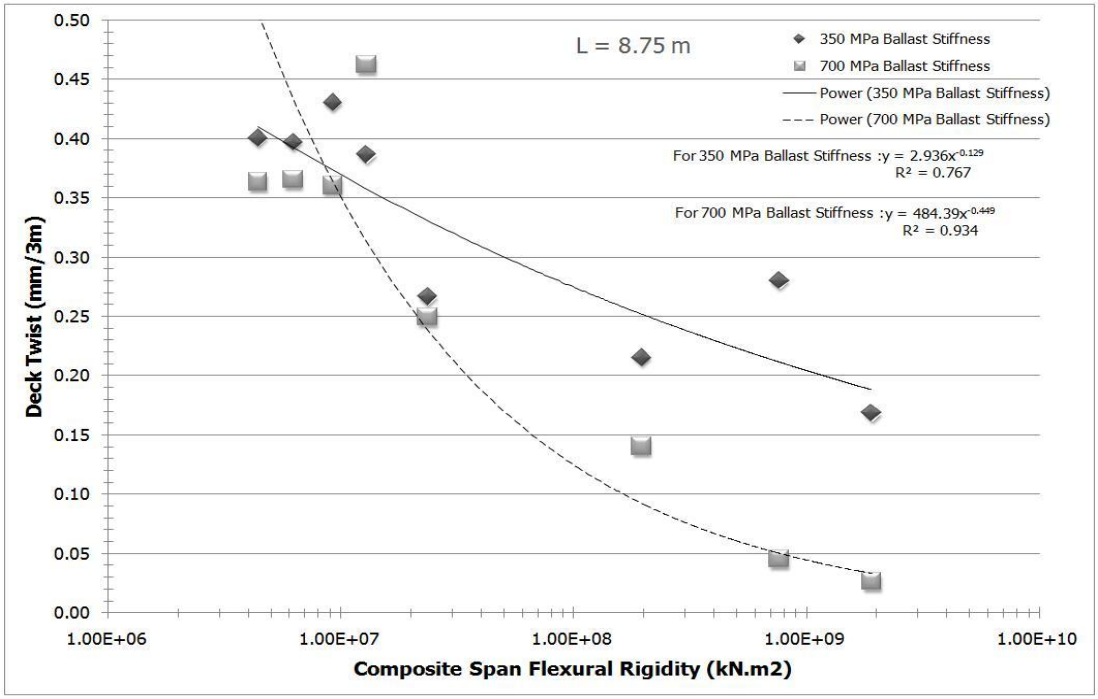

Figure 5.34 Correlations of Max. Deck Twist with Span Flexural Rigidity for Bridge Having 8.75 m Span Length

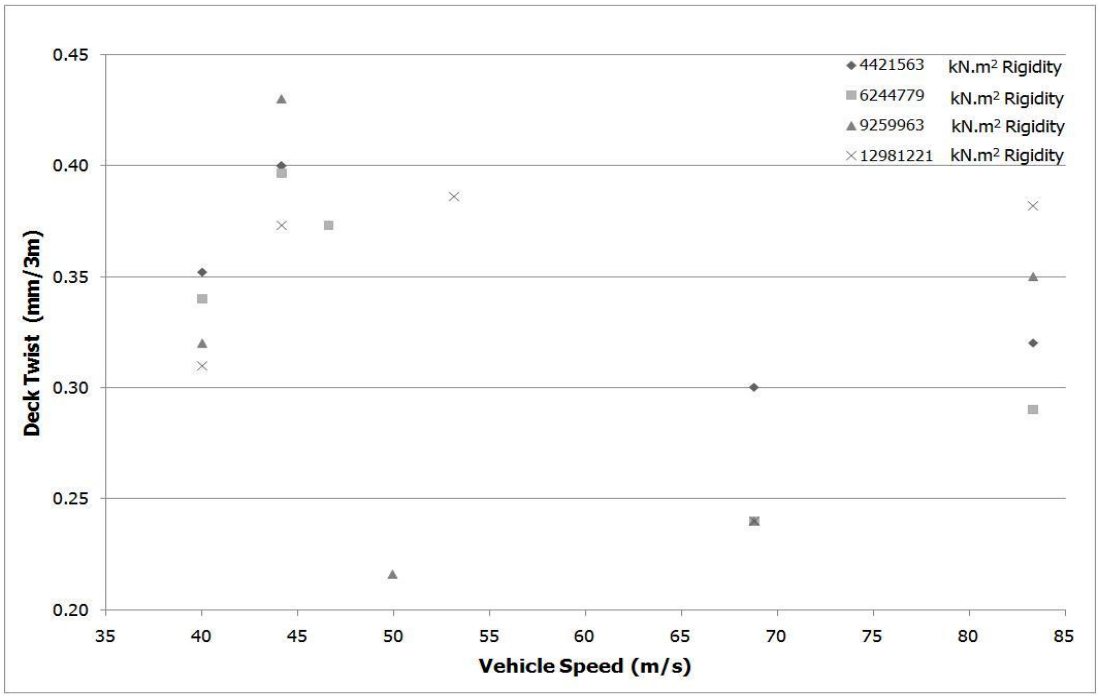

Figure 5.35 Correlations of Max. Deck Twist with Vehicle Speed for Bridge Having 8.75 m Span Length & 350 MPa Ballast Stiffness

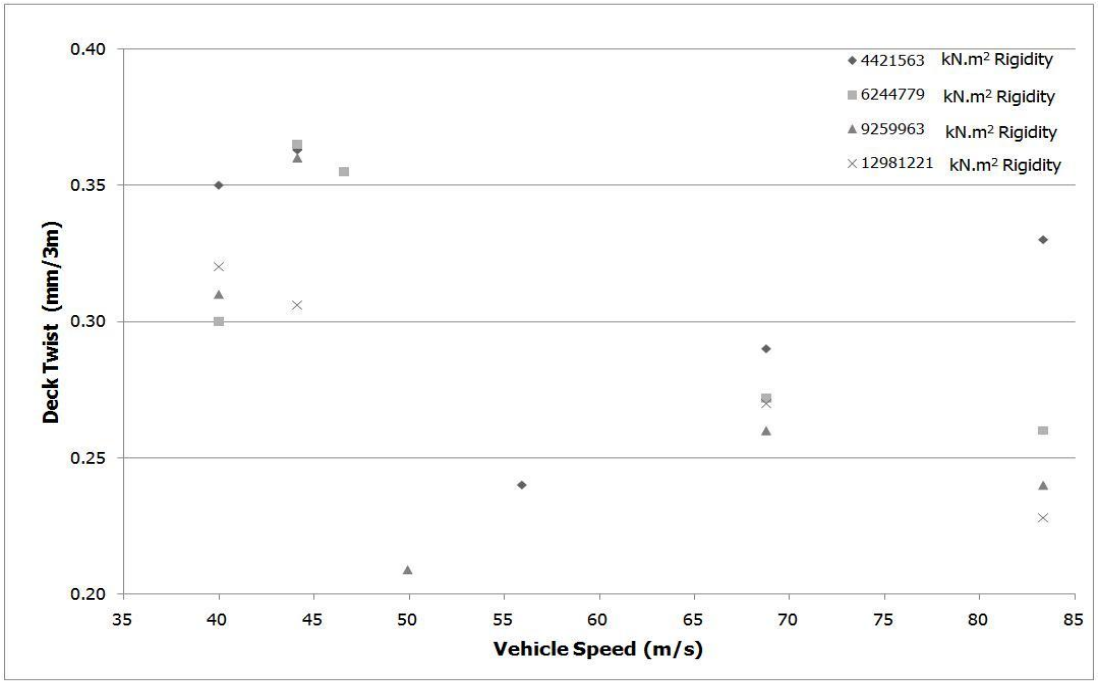

Figure 5.36 Correlations of Max. Deck Twist with Vehicle Speed for Bridge Having 8.75 m Span Length & 700 MPa Ballast Stiffness

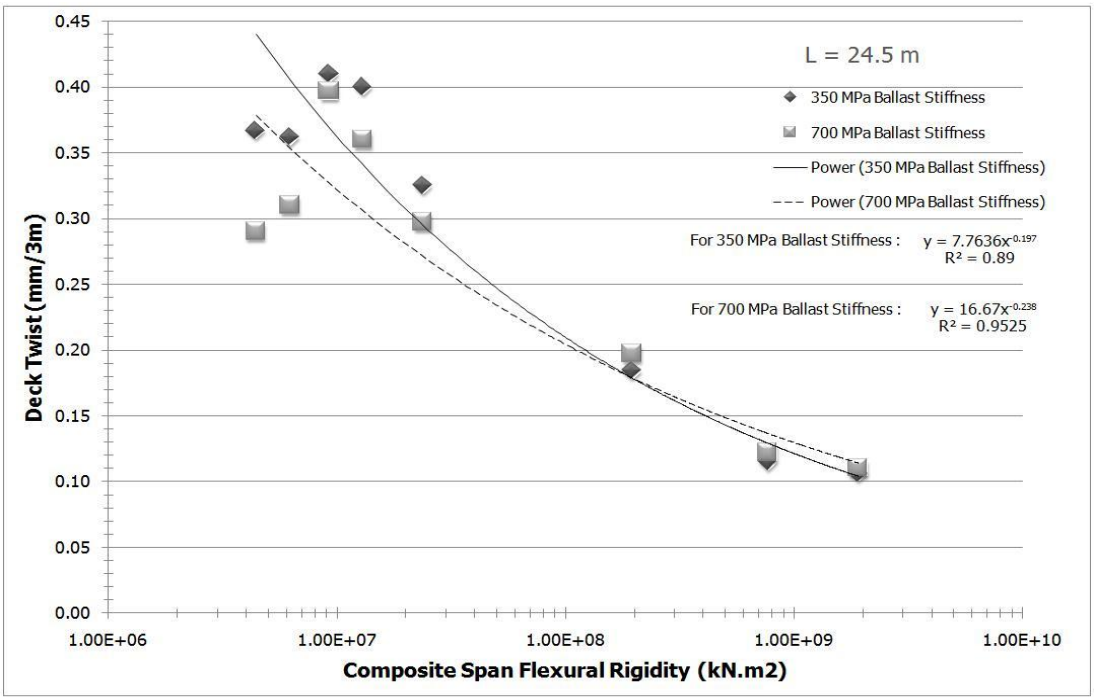

Figure 5.37 Correlations of Max. Deck Twist with Span Flexural Rigidity for Bridge Having 24.5 m Span Length

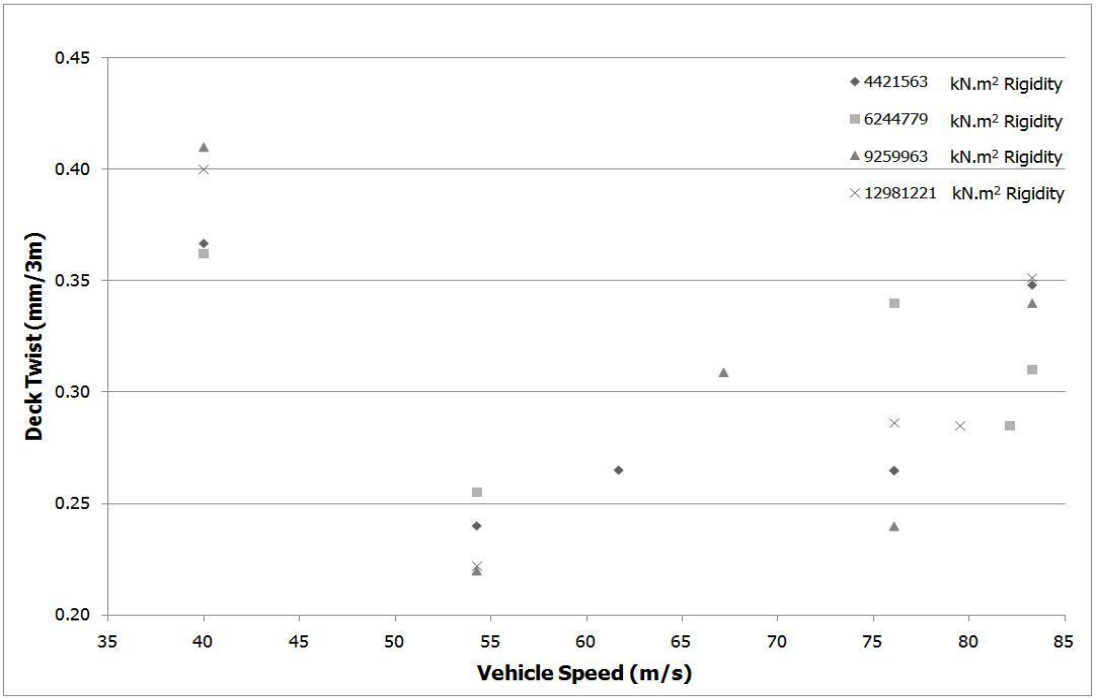

Figure 5.38 Correlations of Max. Deck Twist with Vehicle Speed for Bridge Having 24.5 m Span Length & 350 MPa Ballast Stiffness

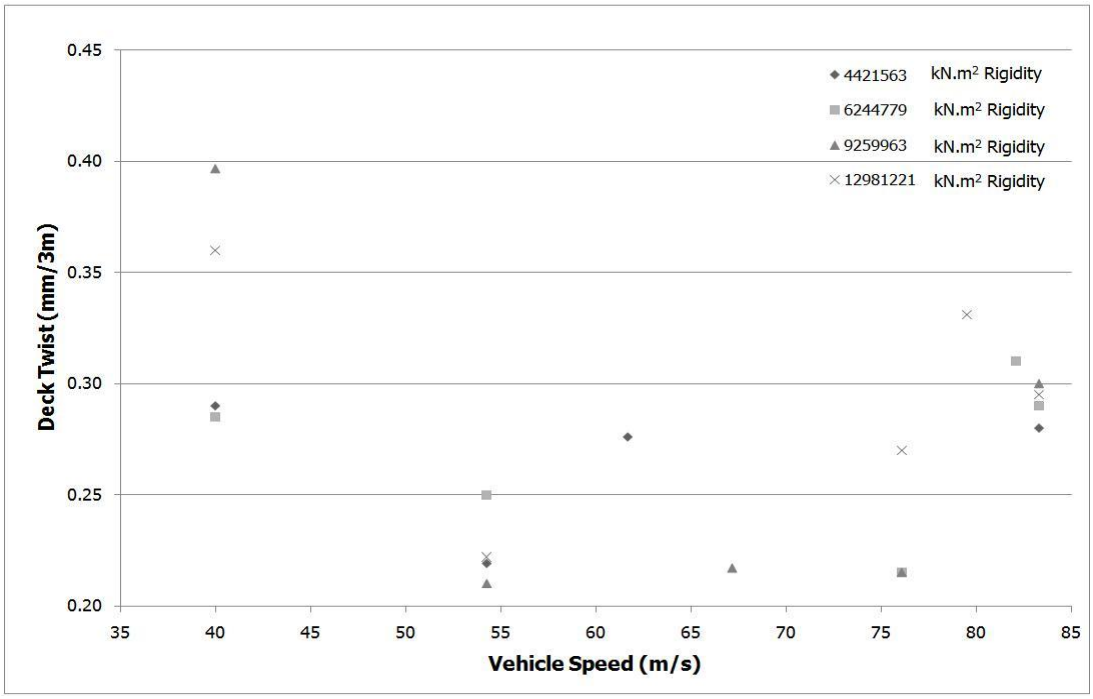

Figure 5.39 Correlations of Max. Deck Twist with Vehicle Speed for Bridge Having 24.5 m Span Length & 700 MPa Ballast Stiffness

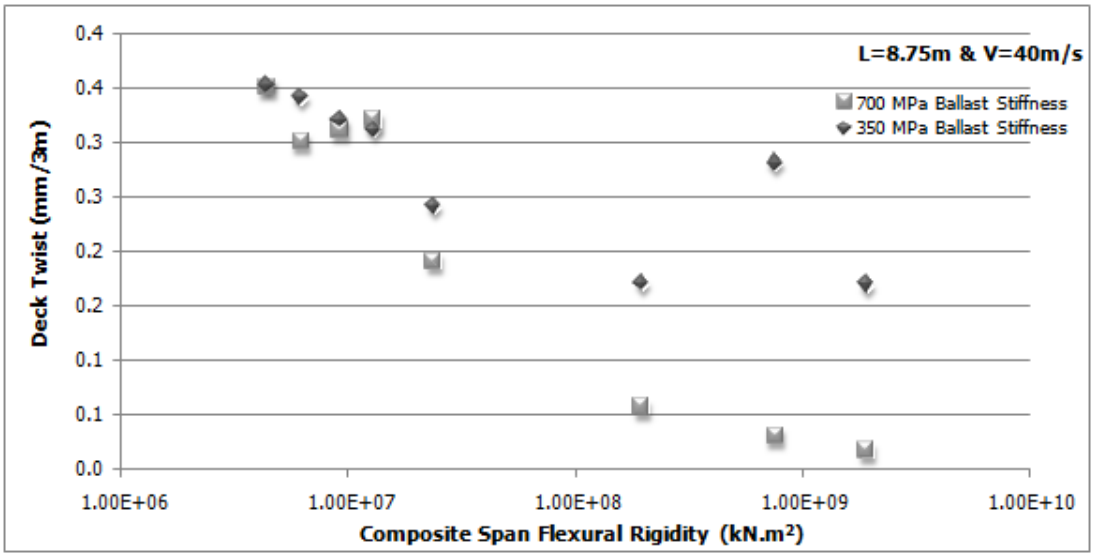

Figure 5.40 Correlations of Max. Deck Twist with Span Flexural Rigidity for 40m/s Constant Design Speed and Bridge Having 8.75 m Span Length

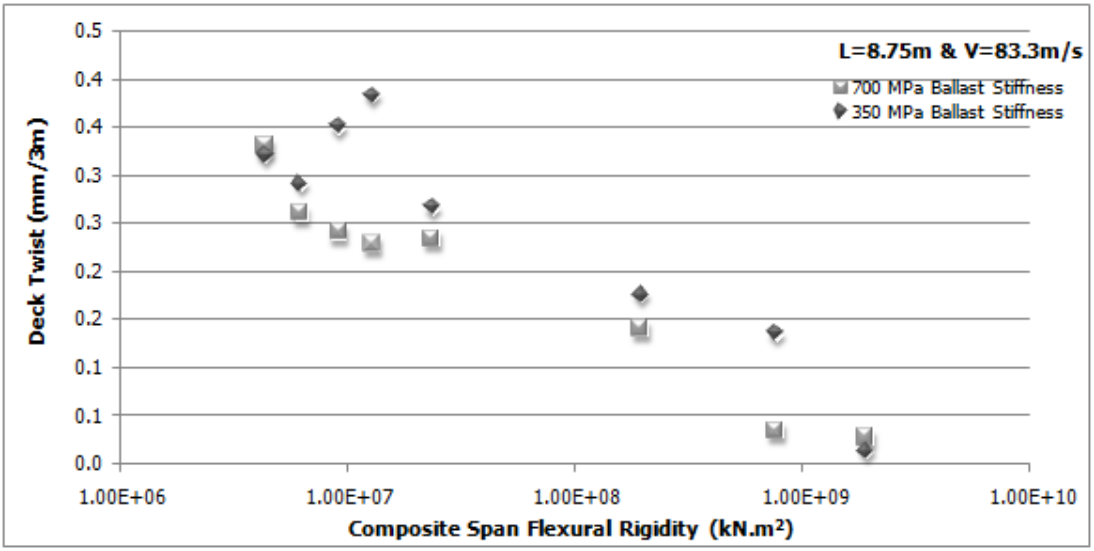

Figure 5.41 Correlations of Max. Deck Twist with Span Flexural Rigidity for 83.3m/s Constant Design Speed and Bridge Having 8.75 m Span Length

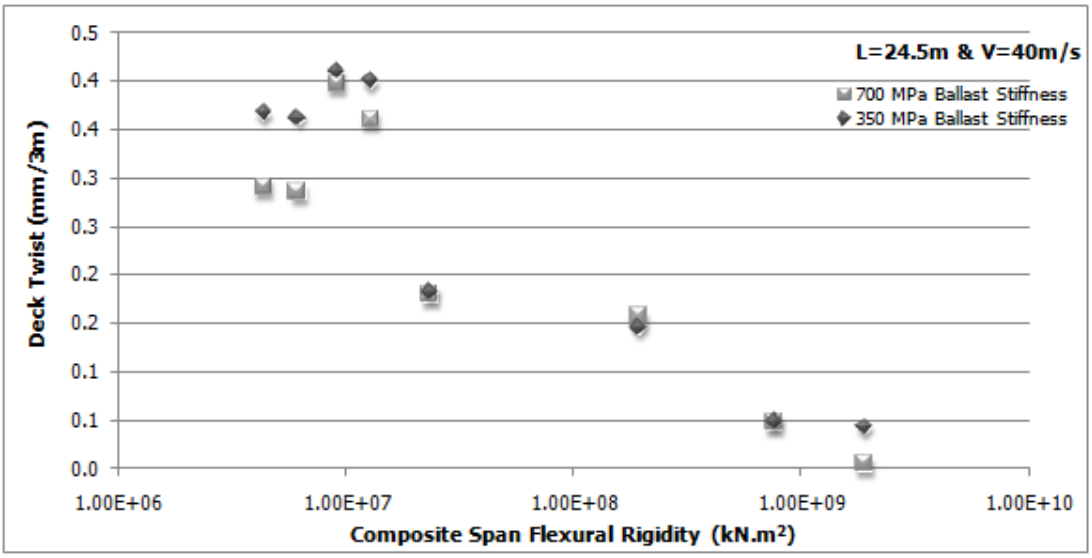

Figure 5.42 Correlations of Max. Deck Twist with Span Flexural Rigidity for 40m/s Constant Design Speed and Bridge Having 24.5 m Span Length

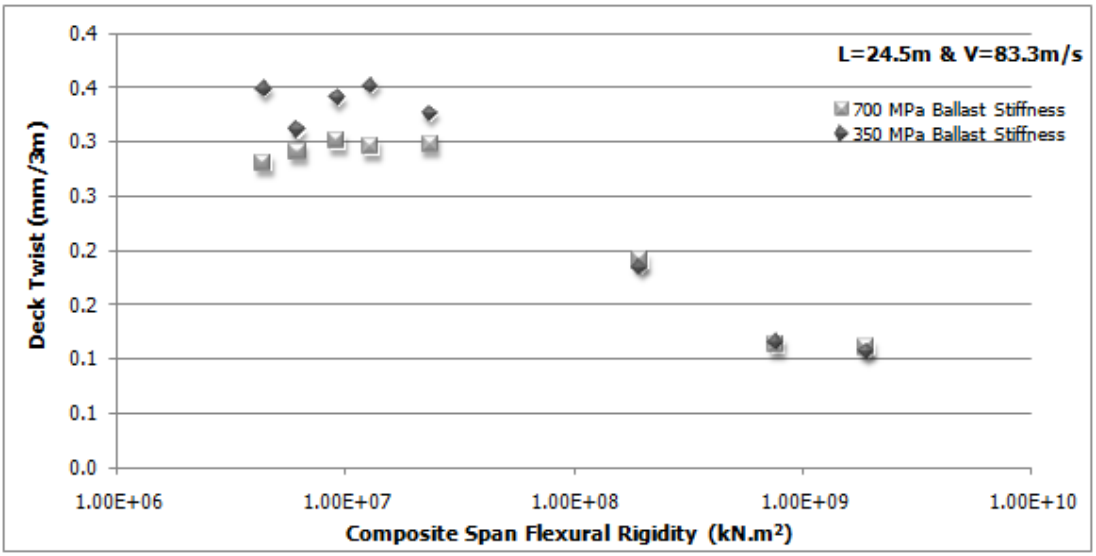

Figure 5.43 Correlations of Max. Deck Twist with Span Flexural Rigidity for 83.3m/s Constant Design Speed and Bridge Having 24.5 m Span Length

5.5. Mid-Span Composite Section Stress Results

The mid-span composite section stresses were calculated for top flange and bottom flange. In calculations, long-term composite action was considered. Calculation spreadsheets for selected case studies were given in Appendix B.

Table 5.14 Composite Section Top Flange Compression Stress (MPa) of Bridge Having 8.75m Span Length for Flexural Rigidities and Ballast Stiffness with varying Vehicle Speeds

Span Rigidity ($kN.m^2$)	Ballast Stiffness (MPa)	Eurocode	AREMA	Design Speeds (m/s)				
				40.00	44.13	68.75	83.30	V_{select}
4,421,563	**350**	12.48	11.70	10.38	10.85	11.01	15.12	10.98
	700	16.22	16.30	10.68	10.85	10.71	14.31	10.92
6,244,779	**350**	14.06	14.13	9.43	9.42	9.11	11.44	9.30
	700	14.52	14.59	9.71	8.78	8.78	11.34	8.76
9,259,962	**350**	11.78	11.84	8.53	8.12	7.61	9.23	6.84
	700	11.73	11.79	8.17	7.94	7.28	9.15	6.71
12,981,220	**350**	10.07	10.12	6.04	7.48	6.61	7.62	6.92
	700	10.02	10.07	5.99	7.06	6.33	7.38	7.01

Table 5.15 Composite Section Bottom Flange Tension Stress (MPa) of Bridge Having 8.75m Span Length for Flexural Rigidities and Ballast Stiffness with varying Vehicle Speeds

Span Rigidity ($kN.m^2$)	Ballast Stiffness (MPa)	Eurocode	AREMA	Design Speeds (m/s)				
				40.00	44.13	68.75	83.30	V_{select}
4,421,563	**350**	25.17	23.60	20.95	21.90	22.21	30.49	21.30
	700	32.72	32.88	21.54	21.88	21.61	28.87	21.28
6,244,779	**350**	29.60	29.75	19.84	19.83	19.18	24.09	19.57
	700	30.56	30.72	20.44	18.47	18.48	23.87	18.44
9,259,962	**350**	25.64	25.77	18.56	17.67	16.56	20.08	14.89
	700	25.54	25.68	17.79	17.29	15.84	19.91	14.60
12,981,220	**350**	22.29	22.41	13.38	16.57	14.63	16.87	15.32
	700	22.19	22.30	13.26	15.62	14.02	16.34	15.57

Table 5.16 Composite Section Top Flange Compression Stress (MPa) of Bridge Having 24.5m Span Length for Flexural Rigidities and Ballast Stiffness with varying Vehicle Speeds

Span Rigidity ($kN.m^2$)	Ballast Stiffness (MPa)	Eurocode	AREMA	Design Speeds (m/s)				
				40.00	54.27	76.08	83.30	V_{select}
4,421,563	**350**	58.75	62.23	45.10	61.45	65.87	74.52	65.87
	700	58.76	62.23	48.70	60.62	65.81	72.81	65.81
6,244,779	**350**	51.37	54.27	34.80	54.34	55.25	59.08	56.70
	700	51.25	54.28	40.27	54.21	53.67	58.57	58.81
9,259,962	**350**	43.29	45.84	35.57	41.59	42.52	46.18	46.54
	700	43.30	45.85	35.03	41.35	36.35	38.91	39.03
12,981,220	**350**	37.07	39.24	29.50	32.40	41.53	39.00	38.00
	700	37.08	39.25	26.09	27.99	34.92	35.40	32.71

Table 5.17 Composite Section Bottom Flange Tension Stress (MPa) of Bridge Having 24.5m Span Length for Flexural Rigidities and Ballast Stiffness with varying Vehicle Speeds

Span Rigidity ($kN.m^2$)	Ballast Stiffness (MPa)	Eurocode	AREMA	Design Speeds (m/s)				
				40.00	54.27	76.08	83.30	V_{select}
4,421,563	**350**	118.5	125.5	91.0	124.0	132.9	150.3	132.9
	700	118.5	125.6	98.3	122.3	132.8	146.9	132.8
6,244,779	**350**	108.1	114.2	73.2	114.4	116.3	124.4	119.3
	700	107.9	114.3	84.8	114.1	113.0	123.3	123.8
9,259,962	**350**	94.2	99.8	77.4	90.5	92.6	100.5	101.3
	700	94.3	99.8	76.3	90.0	79.1	84.7	85.0
12,981,220	**350**	82.1	86.9	65.3	71.8	92.0	86.4	84.1
	700	82.1	86.9	57.8	62.0	77.3	78.4	72.4

5.6. Eigenvalue Analysis Results

The first and second natural frequencies of bridges were reported to investigate change in dynamic behavior.

Table 5.18 First and Second Natural Frequencies (Hz) and Periods (s) of Bridge Having 8.75m Span Length for Flexural Rigidities

Span Rigidity ($kN.m^2$)	First Natural Frequency (Hz)	Second Natural Frequency (Hz)	First Period (s)	Second Period (s)
4,421,563	9.55	12.82	0.105	0.078
6,244,779	10.47	12.83	0.096	0.078
9,259,962	11.72	12.84	0.085	0.078
12,981,220	12.83	12.93	0.078	0.077
23,750,916	12.76	15.59	0.078	0.064
195,898,160	7.07	7.69	0.141	0.130
768,263,855	3.51	4.11	0.285	0.243
1,912,920,565	2.38	2.92	0.420	0.342

Table 5.19 First and Second Natural Frequencies (Hz) and Periods (s) of Bridge Having 24.5m Span Length for Flexural Rigidities

Span Rigidity ($kN.m^2$)	First Natural Frequency (Hz)	Second Natural Frequency (Hz)	First Period (s)	Second Period (s)
4,421,563	1.82	3.84	0.549	0.260
6,244,779	1.99	3.93	0.503	0.254
9,259,962	2.25	4.06	0.444	0.246
12,981,220	2.52	4.21	0.397	0.238
23,750,916	3.04	4.07	0.329	0.246
195,898,160	2.52	4.21	0.397	0.238
768,263,855	1.99	2.15	0.503	0.465
1,912,920,565	1.45	1.46	0.690	0.685

CHAPTER 6

SUMMARY & CONCLUSION

6.1. Summary

Passenger discomfort is one of the important factors on limiting train speed rather than derailment. Flexural rigidity and ballast stiffness have critical effects on the comfort of passengers. In this study, a total of 160 analysis runs was carried out to figure the effects of parameters like flexural rigidity, train speed and ballast stiffness on passenger comfort level under high speed train loads. High speed train load defined in Eurocode was analyzed for the railway bridge designed according to A.R.E.M.A. Resonance speed effects due to train passes were investigated through force-time analyses and comparison of dynamic factor approach and force-time approach was done for short span railway bridge. The results quantify the accelerations, displacements, deck twists and stresses were provided. In this chapter, discussion on results and concluding remarks were presented.

6.2. Discussion on Results

Results of accelerations, displacements, deck twists, stresses and their correlation with flexural rigidity of composite span, train speed and ballast stiffness were discussed.

6.2.1. Discussion on Results of Acceleration

Vertical accelerations of investigated railway bridges were approximately 10 times greater than the permitted limit of acceleration stated in railway bridge specifications.

Flexural rigidity has a great effect on vertical acceleration of the railway bridges. Acceleration values decrease approximately 40~45% by a 10 times increase in flexural rigidity as shown in Figure 5.8 and Figure 5.9. Therefore, it can be concluded that stiffer structures can have significantly less vibration amplitudes than lighter ones providing a comfortable ride for high speed train passes. Required rigidity of railway bridge for a comfortable ride should be known in order to avoid time consuming iterations in design stage. Results shown in Figure 5.8 and Figure 5.12 can be generalized to determine required flexural rigidity of bridge. By the way, the structural element dimensions or material properties of railway bridge can be more accurately selected in preliminary design stage. Flexural rigidities of railway bridges in Figure 5.8 and Figure 5.12 were divided to span lengths in order to generalize results. Data of both graphs were combined in Figure 6.1. Coefficient of determination of the graph (R^2) which reveals how closely the estimated values for the trendline correspond to actual data is approximately equal to 0.92. A trendline is most reliable when its R-squared value is at or near 1. Although coefficient of determination of the graph shown in Figure 6.1 is close to 1, vertical acceleration data for flexural stiffness (EI/L) less than $1.0x10^7$ $kN.m^2/m$ scatter. Scattered acceleration data couples were labeled from 1 to 10 in Figure 6.1. Flexural stiffness of data 4 and 6 and also data 5 and 8 are very close to each other, however vertical acceleration magnitudes differ up to 100%.

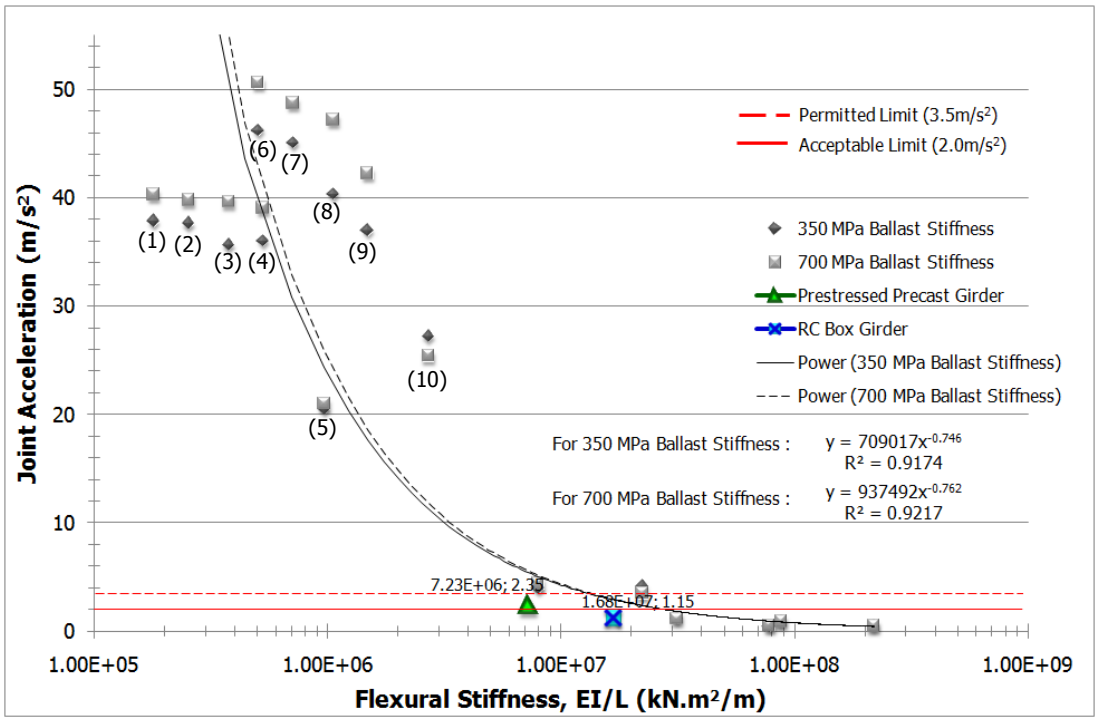

Figure 6.1 Correlations of Max. Joint Acceleration with Span Flexural Stiffness

The fluctuation in vertical acceleration magnitudes can be explained by the proximity effect of peak modal displacement. In the study of vibration, a modal displacement describes the expected response, i.e. acceleration of a surface vibrating at a particular mode [1]. Acceleration magnitude tends to decrease by an increase of flexural stiffness however modal displacement is the second factor that affects the magnitude of acceleration. Acceleration magnitude increases by an increase of modal displacement value of the frequency correspond to vehicle speed that causes the acceleration. That is; although a structure has greater flexural stiffness, it may have larger vertical acceleration due to the magnitude of vertical modal displacement for selected frequency. Ratios of modal displacement values of selected frequency and frequency caused peak modal displacement in the design frequency range were presented in Table 6.1 in order to investigate the effect of modal displacement. The modal displacement values of the closest

natural frequency were taken for frequencies that do not match the natural frequencies of bridge.

Table 6.1 Ratio of Modal Displacements of Selected Frequency and Frequency Caused Peak Modal Displacement in the Design Frequency Range

No	**L** (m)	**EI** ($kN.m^2$)	**EI/L** ($kN.m^2/m$)	**V** (m/s)	**n** (Hz)	**a_{max}** (m/s^2)		$\frac{u_{select}}{u_{peak}}$
						B350	**B700**	
1	24.5	4,421,563	180,472	40.00	13.33	37.82	40.25	7.93
2	24.5	6,244,779	254,889	40.00	13.33	37.61	39.72	2.80
3	24.5	9,259,963	377,958	40.00	13.33	35.62	39.59	0.45
4	24.5	12,981,221	529,846	40.00	13.33	35.58	39.04	0.21
5	24.5	23,750,916	969,425	40.00	13.33	20.48	20.94	0.00
6	8.75	4,421,563	505,322	44.13	14.71	46.18	50.57	1.00
7	8.75	6,244,779	713,689	44.13	14.71	45.04	48.68	1.00
8	8.75	9,259,963	1,058,281	44.13	14.71	40.30	47.16	1.00
9	8.75	12,981,221	1,483,568	44.13	14.71	36.97	42.20	118
10	8.75	23,750,916	2,714,390	44.13	14.71	27.19	25.37	0.13

where;

L : span length (m)

EI : flexural rigidity ($kN.m^2$)

EI/L : flexural stiffness ($kN.m^2/m$)

V : vehicle velocity that corresponds to maximum vertical acceleration (m/s)

n : frequency that corresponds to vehicle velocity (Hz)

a_{max} : maximum vertical acceleration (m/s^2)

B350 : vertical acceleration for analysis model having 350 MPa ballast stiffness

B700 : vertical acceleration for analysis model having 700 MPa ballast stiffness

$\frac{u_{select}}{u_{peak}}$: Ratio of modal displacements of selected frequency and frequency caused peak modal displacement in the design frequency range

Flexural stiffness of 4^{th} data couple is 5% larger than the flexural stiffness of 6^{th} data couple. However, the acceleration magnitude of 4^{th} data couple is 22% smaller than the acceleration magnitude of 6^{th} data couple. Because modal displacement of 6^{th} data couple is equal to the peak modal displacement in design frequency range, however modal displacement of 4^{th} data couple is 21% of peak modal displacement in design frequency range. That is; 6^{th} data couple is more close to the peak modal displacement than 4^{th} data couple. Therefore response for 6^{th} data couple is greater than 4^{th} data couple. Same phenomenon is valid for 5^{th}, 7^{th} and 8^{th} data couples. Flexural stiffness of 8^{th} data couple is 8% larger than the flexural stiffness of 5^{th} data couple which is 26% larger than 7^{th} data couple. However, the acceleration magnitude of 5^{th} data couple is 55% and 50% smaller than the acceleration magnitude of 7^{th} and 8^{th} data couples respectively. Because modal displacement of 7^{th} 8^{th} data couples are equal to the peak modal displacement in design frequency range, however modal displacement of 5^{th} data couple is approximately 0% of peak modal displacement in design frequency range. Therefore, although flexural stiffness of 5^{th} data couple is smaller than flexural stiffness of 8^{th} data couple, response for 8^{th} data couple is greater than 5^{th} data couple due to the ratio of modal displacements of selected frequency and frequency caused peak modal displacement in the design frequency range. The sharp decrease in acceleration magnitudes of 5^{th} and 7^{th} data couples can be explained in same way.

Maximum vertical acceleration magnitude gradually decreases by an increase in flexural stiffness for a constant frequency; i.e. for a constant vehicle speed according to the data provided in Table 6.1. However it was observed that it was not correct when the correlation of vertical acceleration and flexural stiffness investigated for a constant speed. Figures 6.2 and 6.3 show the

correlation of vertical acceleration and flexural stiffness for minimum analysis speed, 40 m/s and maximum analysis speed, 83.3 m/s respectively.

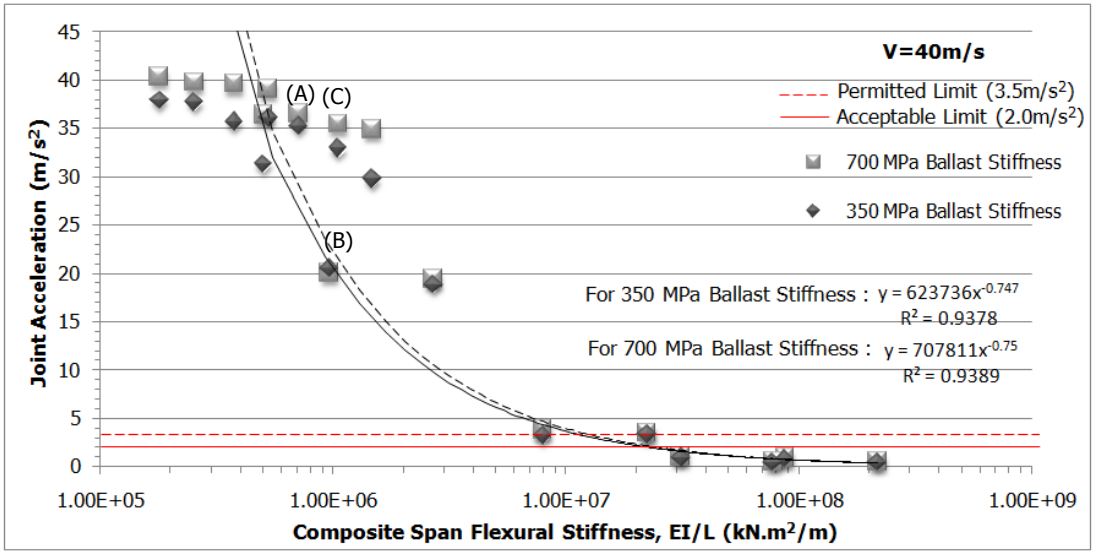

Figure 6.2 Correlations of Joint Acceleration with Span Flexural Stiffness for minimum Analysis Speed, 40 m/s

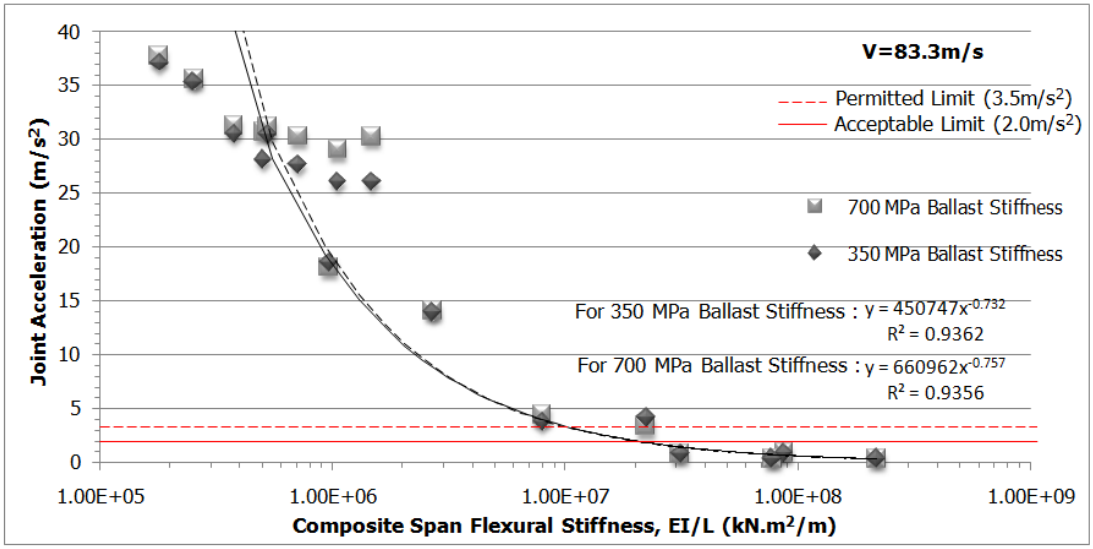

Figure 6.3 Correlations of Joint Acceleration with Span Flexural Stiffness for maximum Analysis Speed, 83.3 m/s

In spite of a constant speed, acceleration data were similarly scattered for both minimum and maximum speeds. Ratios of modal displacement values of the closet natural frequency to selected frequency and frequency caused peak modal displacement in the design frequency range were presented in Table 6.2 for data labeled as A, B and C in Figure 6.2. Ratios of all other flexural stiffness for all analysis speeds were provided in Appendix D.

Table 6.2 Ratios of Modal Displacements of the Closet Natural Frequency and Frequency Caused Peak Modal Displacement in the Design Frequency Range for Minimum Design Speed, 40 m/s and 13.33 Hz Frequency.

No	**EI/L** ($kN.m^2/m$)	**a_{max}** (m/s^2)		**n_{close}** (Hz)	**u_{close}** (10^{-3})	**n^r_{peak}** (Hz)	**u^r_{peak}** (10^{-3})	**$\frac{u_{close}}{u^r_{peak}}$**
		B350	**B700**					
A	713,689	35.19	36.44	12.83	11.70	15.53	4.40	2.66
B	969,425	20.48	19.99	13.33	0.10	22.39	49.26	0.00
C	1,058,281	32.86	35.42	12.84	10.20	16.64	2.29	4.45

where;

EI/L : flexural stiffness ($kN.m^2/m$)

a_{max} : maximum vertical acceleration (m/s^2)

B350 : vertical acceleration for analysis model having 350 MPa ballast stiffness

B700 : vertical acceleration for analysis model having 700 MPa ballast stiffness

n_{close} : natural frequency which is the closest frequency to selected frequency

n^r_{peak} : natural frequency caused peak modal displacement in the design frequency range (Hz)

u_{close} : vertical modal displacement that corresponds to n_{close}

n^r_{peak} : peak vertical modal displacement in the design frequency range

$\frac{u_{close}}{u^r_{peak}}$: Ratio of modal displacements of n_{close} frequency and frequency caused peak modal displacement in the design frequency range

Vertical modal displacement that corresponds to n_{close}, u_{close} and peak vertical modal displacement in the design frequency range, n^r_{peak} were presented in Figures 6.4, 6.5 and 6.6 for data A, B and C respectively.

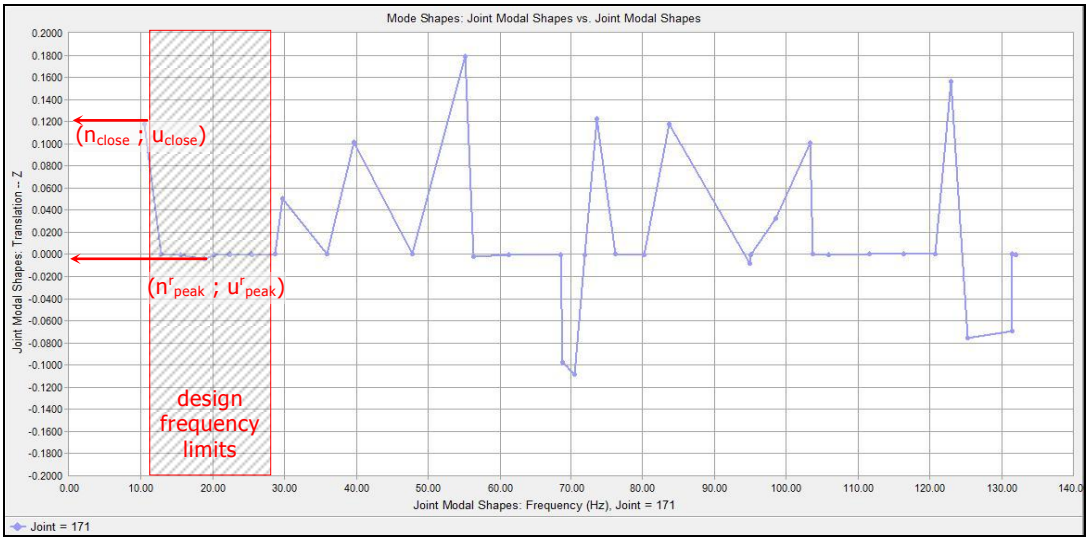

Figure 6.4 Joint Modal Displacement vs. Mode Shape Frequency graph of bridge having 713,689 kN.m^2/m Span Flexural Stiffness.

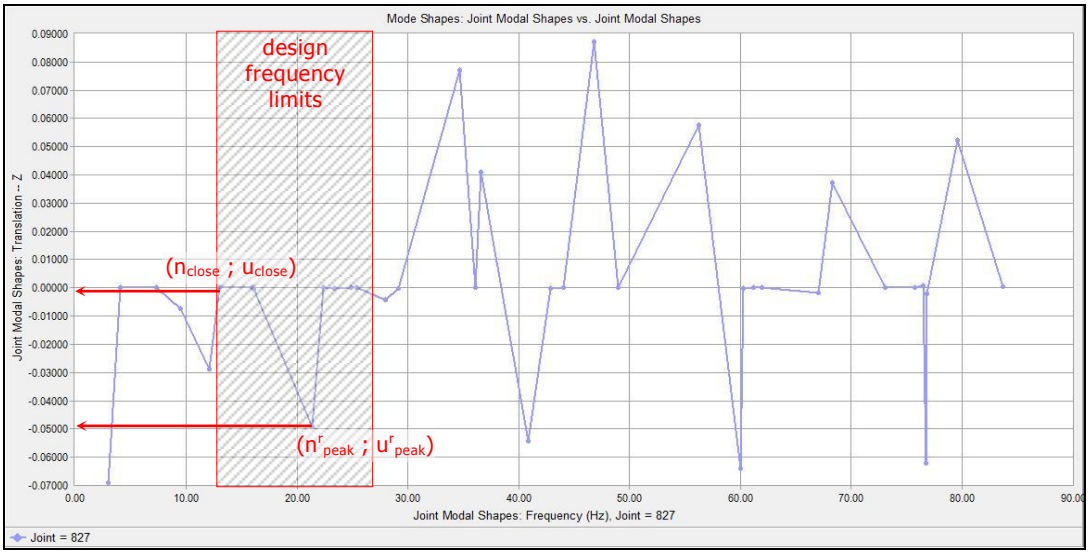

Figure 6.5 Joint Modal Displacement vs. Mode Shape Frequency graph of bridge having 969,425 kN.m^2/m Span Flexural Stiffness.

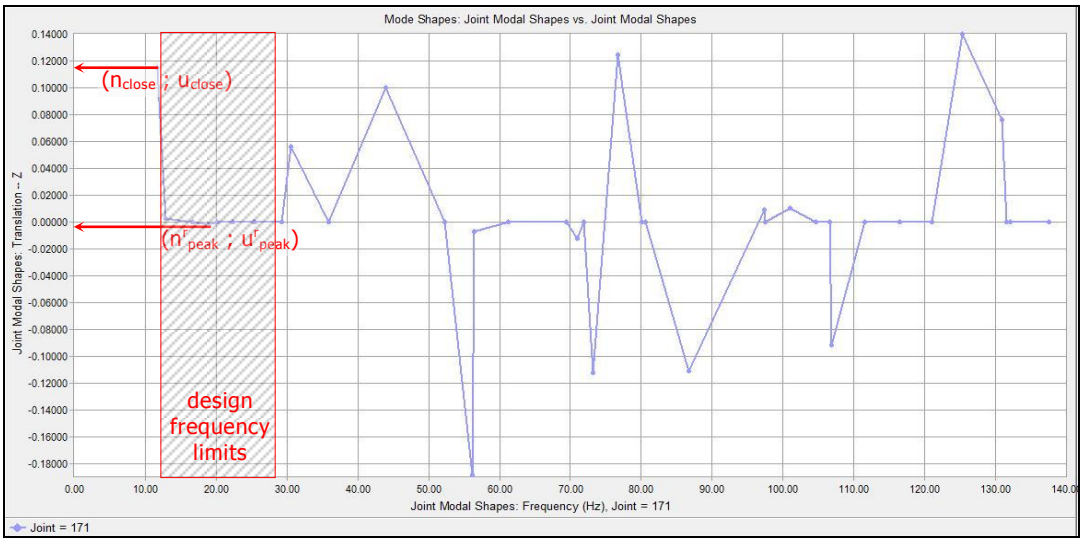

Figure 6.6 Joint Modal Displacement vs. Mode Shape Frequency graph of bridge having 1,058,281 kN.m^2/m Span Flexural Stiffness.

Flexural stiffness of data C is 8% larger than the flexural stiffness data B which is 26% larger than data A. One other hand, the acceleration magnitude of data B is 53% and 38% smaller than the acceleration magnitude of data A and C respectively. Because modal displacement magnitudes of data A and C are respectively 2.66 and 4.45 times larger than the peak modal displacement in design frequency range, however modal displacement magnitude of data B is approximately 0% of peak modal displacement in design frequency range. Despite an increase in flexural stiffness, there is an increase in vertical acceleration magnitude.

A resonance frequency is defined as the forcing frequency at which the largest response amplitude occurs. Therefore it is expected that the maximum vertical accelerations can be obtained by analysis of resonance frequencies, i.e. resonance speeds. However, maximum vertical accelerations were calculated for speeds different than the resonance speeds as seen in Tables 5.2 and 5.3. Non-resonance speeds caused

maximum vertical displacement can be explained by frequency-response curve.

Frequency-response curve can be defined as a plot of the amplitude of a response quantity against the excitation frequency which is the frequency of the forced vibration or steady-state vibration. The steady-state dynamic response can be interpreted as a sinusoidal oscillation at forcing frequency. The amplitude of the steady-state response of a system with $n=n_0$ and the rate at which steady state is attained is strongly influenced by damping [32]. The steady state motion occurs at the forcing period $T=2\Pi/n$, but with a time lag $ø/2\Pi$ for the frequency ratio n/n_n as shown in Figure 6.7.

In Figure 6.7, response factors were plotted for constant frequency ratios and damping ratios. These lagged response graphs can be generalized as a function of frequency ratio for various damping ratios by frequency-response curves. Frequency response curves for the ratio of the amplitude of the vibratory acceleration to the acceleration due to applied force are given in Figure 6.8.

If the frequency ratio, $n/n_0 \ll 1$, implying that the force is slowly varying, response factor, R_a tends to zero as n/n_0 increases and is essentially unaffected by damping. This implies that the response is controlled by the mass of the system [32].

If the frequency ratio, $n/n_0 \gg 1$, implying that the force is rapidly varying, response factor, R_a is only slightly larger than 1 and is essentially independent of damping. This implies that the amplitude of dynamic response is controlled by the stiffness of the system [32].

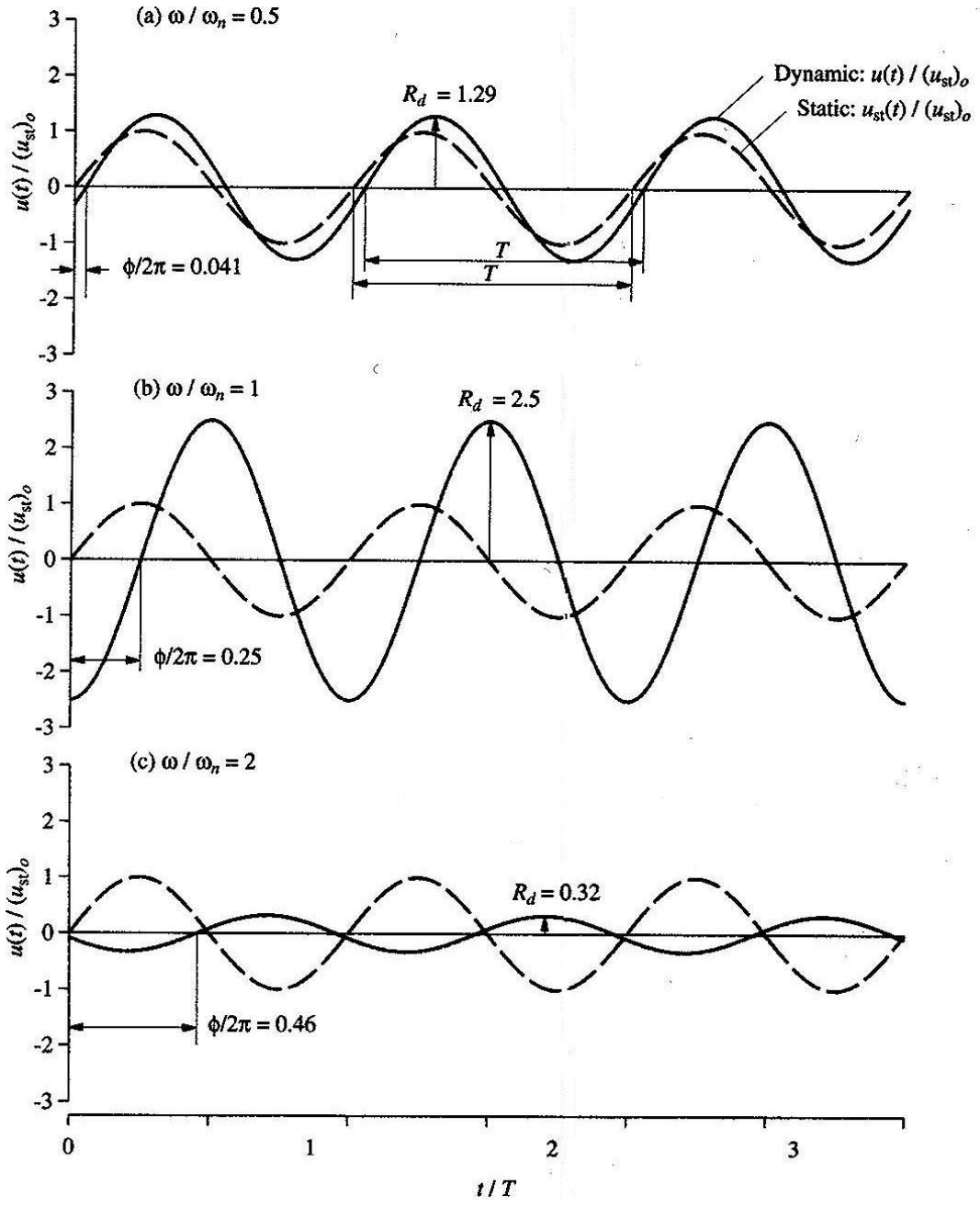

Figure 6.7 Steady state responses of damped systems for three values of the frequency ratio [32].

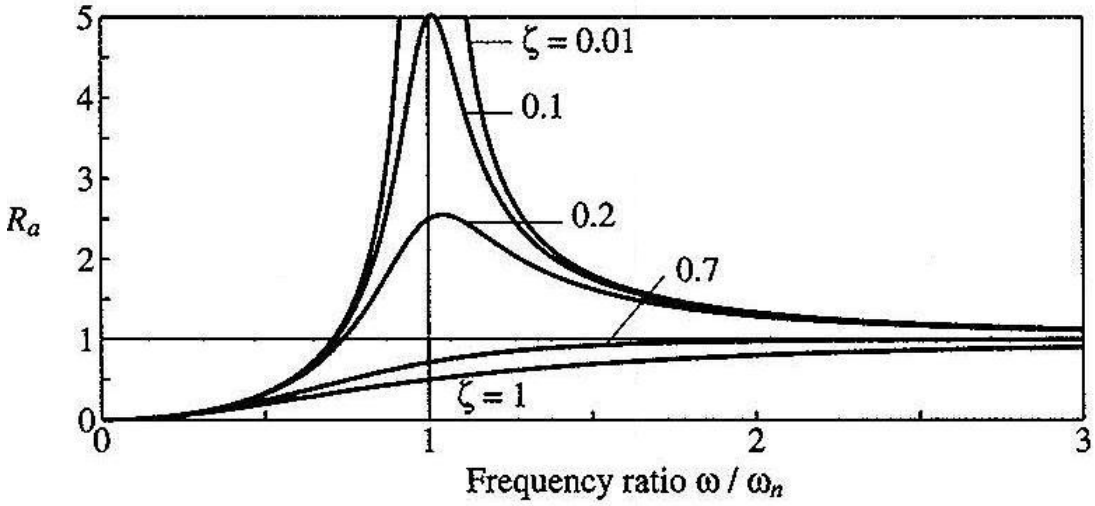

Figure 6.8 Frequency-Acceleration Response Curve of damped systems [32].

If the frequency ratio, $n/n_0 = 1$, i.e. the forcing frequency is equal to the natural frequency of the system, response factor, R_a can be several times larger than 1. That is, the largest response amplitude occurs when system natural frequency and forcing frequency are equal to each other, as previously stated as resonance frequency. However response factor for frequency ratio that is not equal but close to 1, $n/n_0 \approx 1$, is also several times larger than 1. This can be summarized as the structure whose forced frequency is close to its natural frequency, $n/n_0 \approx 1$, also has the response amplitudes as larger as the resonance amplitude. Response factor gradually decreases by the change of frequency ratio as shown in Figure 6.8.

Vertical accelerations caused by non resonance speeds are larger than accelerations caused by resonance speeds for some of the case studies. Since the frequencies correspond to these non resonance speeds are close to natural frequencies, response amplitudes are as larger as the

response amplitudes of resonance frequency. On the other hand, the modal displacement magnitude of the resonance frequency to which selected frequency of non resonance speed is close, is larger than the modal displacement magnitude of resonance frequency corresponds to selected vehicle resonance speed in design speed range. As a result, the acceleration magnitude of non resonance speed becomes larger than the acceleration magnitude of resonance speed in design speed range. Frequency ratios and modal displacement magnitudes for selected examples of phenomena described above are given in Table 6.3.

Table 6.3 Frequencies Ratio and Modal Displacements of Non-Resonance Speeds

EI/L	**$V_{nonresonance}$**					**$V_{resonance}$**			
$kN.m^2/m$	**n** (Hz)	**n_0** (Hz)	**$\frac{n}{n_0}$**	**u** (10^{-3})	**a_{max}** (m/s^2)	**n_0** (Hz)	**$\frac{n}{n_0}$**	**u** (10^{-3})	**a_{max}** (m/s^2)
180,472	13.33	12.30	1.08	58.22	37.82	20.56	1.00	50.6	37.34
254,889	13.33	13.72	0.97	59.00	37.61	27.37	1.00	45.1	32.12
713,689	14.71	12.83	1.10	11.70	45.04	15.53	1.00	4.40	37.02

where;

EI/L : flexural stiffness ($kN.m^2/m$)

a_{max} : maximum acceleration for 350MPa Ballast Stiffness (m/s^2)

n_0 : natural frequency which is the closest frequency to selected frequency

n : frequency corresponds to non resonance speed caused maximum acceleration (Hz)

n/n_0 : frequency ratio

u : vertical modal displacement that corresponds to n_0

$V_{nonresonance}$: Non resonance vehicle speed, it is equal to 40 m/s for first and second data and 44.13 m/s for third data

$V_{resonance}$: Resonance vehicle speed in design speed range, it is equal to 61.68 m/s for first data, 82.11 m/s for second data and 46.59 m/s for third data

Frequency ratios of non resonance speeds are very close to 1; that is the frequencies correspond to selected speeds are slightly different than the resonance frequency. Since the modal displacements of resonance frequencies to which selected frequency of non resonance speed is close, is larger than the modal displacement magnitude of resonance frequency in design frequency range, the acceleration magnitudes of non resonance speeds are larger than the resonance speeds in design speed range.

Stiffer ballast layer causes slightly high acceleration than lighter one; however this difference disappears when flexural rigidity of bridge increases. Ballast effect on acceleration is almost negligible for flexural rigidity required for acceptable limit of passenger comfort.

Although vertical acceleration data for flexural stiffness (EI/L) less than $1.0x10^7$ $kN.m^2/m$ scatter in the graph shown in Figure 6.1, there is a trendline for vertical acceleration data for flexural stiffness (EI/L) larger than $1.0x10^7$ $kN.m^2/m$. Therefore, threshold values for flexural stiffness can be determined by the trendline equation of the acceleration data for flexural stiffness (EI/L) larger than $1.0x10^7$ $kN.m^2/m$ as shown in Figure 6.9. As a result, it can be stated that railway bridge should have $2.5x10^7$ $kN.m^2/m$ flexural stiffness in order to satisfy the acceptable limit of vertical acceleration and $1.5x10^7$ $kN.m^2/m$ flexural stiffness in order to satisfy the permitted limit of vertical acceleration. Required flexural rigidities per span length were tabulated for passenger comfort levels in Table 6.4.

Table 6.4 Required Flexural Stiffness for Passenger Comfort Levels

Level of Comfort	Vertical Acceleration, b_v (m/s^2)	Required Flexural Stiffness, EI/L (kN.m^2/m)
Very Good	1.0	6.0 x 10^7
Good	1.3	4.5 x 10^7
Acceptable	2.0	2.5 x 10^7
Permitted	3.5	1.5 x 10^7

Coefficient of determination of the joint acceleration versus vehicle speed graphs given in Figure 5.10, Figure 5.11, Figure 5.14 and Figure 5.15 is nearly equal to 0.55. This implies that there is no remarkable correlation between vehicle speed and acceleration.

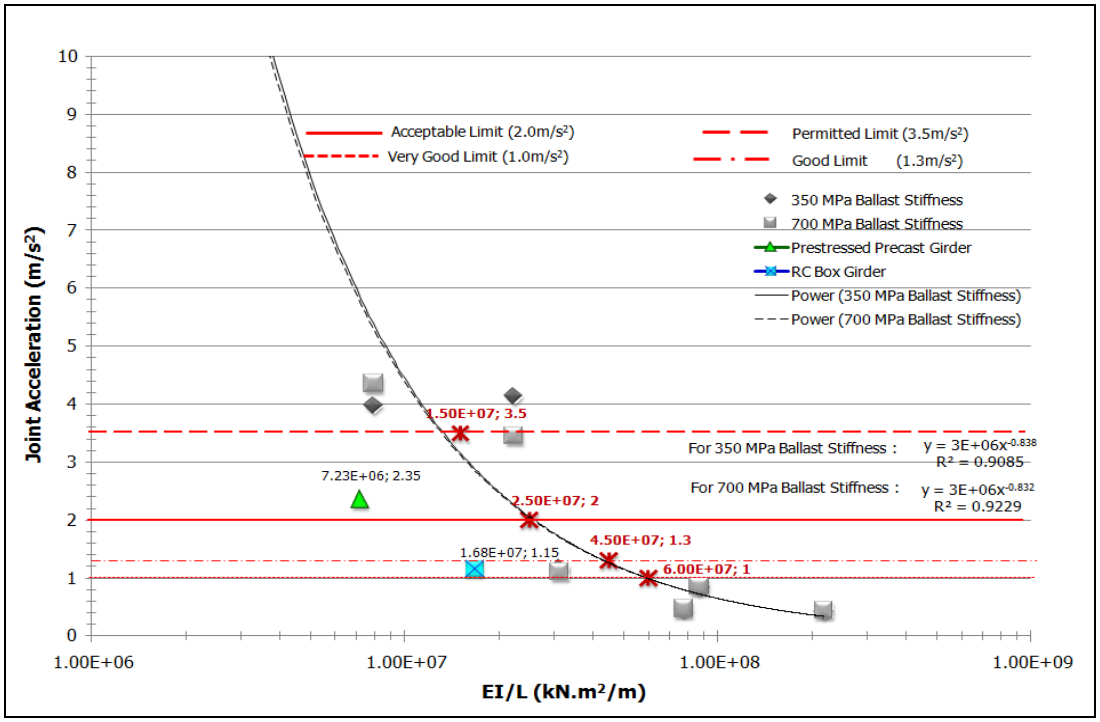

Figure 6.9 Threshold values of Span Flexural Stiffness for Acceleration Limits of Passenger Comfort Levels

6.2.2. Discussion on Results of Displacement

Displacements of investigated railway bridges were approximately 1/750 of span length and this ratio gets smaller for shorter span lengths. Displacements are not critical in serviceability design for short span bridges.

Displacements decrease by an increase in flexural rigidity of railway bridge. Coefficient of determination of the displacement versus flexural rigidity is equal to 0.97 in average. This implies that displacement is well correlated with flexural rigidity.

Displacements increase by an increase in vehicle speed as expected. Coefficient of determination of the displacement versus vehicle speed is nearly equal to 0.85. The rate of increase in displacement due to increase in vehicle speed is also controlled by rigidity. That is, the increase rate in displacement reduces by an increase in rigidity.

Ballast stiffness has a reverse effect on displacement. Stiffer ballast layer causes smaller displacements. However, rate of change in displacement due to ballast stiffness becomes negligible for large flexural rigidities.

6.2.3. Discussion on Results of Deck Twist

Deck twists were approximately 4 times smaller than the allowable deck twist, 1.5mm/3m.

Deck twist is not a critical serviceability parameter for short span railway bridges. Stiffer structures have less deck twist than lighter ones. There is also no remarkable correlation between vehicle speed and deck twist. The

maximum deck twists were occurred at resonance speeds. Ballast stiffness is not effective as much as flexural rigidity and vehicle speed, however deck twist decreases by an increase in ballast stiffness.

6.2.4. Discussion on Results of Stresses

Girder stresses were smaller than allowable stress value for girders whose rigidities provide permitted limit of passenger comfort level. Stresses calculated according to Eurocode and AREMA were smaller than stresses calculated according to moving force method as seen in Tables 5.14, 5.15, 5.16 and 5.17. Therefore, it was observed that Eurocode and AREMA were more conservative than moving force method and also girder stresses calculated according to AREMA were larger than the girder stresses calculated according to Eurocode. That is, AREMA is also more conservative than Eurocode.

6.3. Conclusion

Train-bridge interaction has a considerable influence in the dynamic behavior of short span railway bridges. It was observed that acceleration is the most critical parameter in design rather than flexural capacity and other serviceability parameters. The moving high-speed train often produces significant ground vibrations, especially at the resonance speeds or speeds close to resonance speeds, so how to avoid resonance and reduce the vibrations induced by high-speed trains has become an important issue. To avoid resonance, the dominated train frequencies and the bridge natural frequencies should be as different as possible, especially for the first dominated train frequency and the first bridge natural frequency. Increasing flexural stiffness is the effective rehabilitation method to avoid resonance

and reduce the vibrations. Isolators or mass dampers are also used to reduce vibration of bridges like Taiwan High-Speed Railway Bridge. The most effective technique of rehabilitation by dampers is the usage of multiple tuned mass dampers, MTMD. However, MTMD are effective to reduce acceleration in range of 15% to 45% as well. Therefore rehabilitation of bridge by increase in flexural stiffness may be inevitable for the bridges having acceleration amplitudes several times larger than the permitted limit. Ballast stiffness is effective to provide passenger comfort levels for small stiffness, but the effect becomes negligible for railway bridges having large stiffness.

As a conclusion of this thesis, existing short span railway bridges may not be appropriate for the high speed train passage. Dynamic behavior of railway bridge and also effective rehabilitation methods should be carefully analyzed with more accurate preliminary design.

REFERENCES

[1] Wikipedia Community, 12 October 2008, "High-Speed Rail-Wikipedia The Free Encyclopedia", http://en.wikipedia.org/wiki/High-speedrail, September 2007.

[2] Keating, O., 12 October 2008, "High Speed Rail", http://www.o-keating.com/hsr, November 1997.

[3] Patrick, J., 12 October 2008, "A Short History of Turkish Railways", http://www.trainsofturkey.com/w/pmwiki.php/History/History, September 2007.

[4] Zhai, W.M., Cai, C.B., 2002, "Train/Track/Bridge Dynamic Interactions: Simulation and Applications", Vehicle System Dynamics Supplement, 37, 653-665.

[5] Song, K., M., Noh, H., C., and Choi, C., K., 2003, "A New Three-Dimensional Finite Element Analysis Model of High-Speed Train-Bridge Interactions", Journal of Engineering Structures, 25, 1611-1626.

[6] Frýba, L., 2001, "A Rough Assessment of Railway Bridges for High Speed Trains", Journal of Engineering Structures, 23, 448-556.

[7] Geier, R., Österreicher, M., "Dynamic Investigations of Railway Bridges", Vienna, Austria.

[8] Museros, P., Romero, M.L., Poy, A., and Alarcon, E., 2002, "Advances in the Analysis of Short Span Railway Bridges for High-Speed Lines", Journal of Computers and Structures, 80, 2121-2132.

[9] Biondi, B., Muscolino, G., and Sofi, A., 2005, "A Substructure Approach for the Dynamic Analysis of Train-Track-Bridge System", Journal of Computer and Structures, 83, 2271-2281.

[10] De Roeck, G., Maeck, J., and Teughels, A., "Validation of Numerical Models by Experiments on a High Speed Railway Bridge in Antoing" Belgium.

[11] Xia, H., Zhang, N., 2005, "Dynamic Analysis of Railway Bridge Under High-Speed Trains", Journal of Computers and Structures, 83, 1891-1901.

[12] Cheung, Y. K., Au,F. T. K., Zheng, D. Y. and Cheng, 1998, "Vibration and Stability of Non-uniform Beams with Abrupt Changes of Cross-section by using C1 Modified Beam Vibration Functions", Applied Mathematical Modelling, Vol. 23, Issue 1, pp. 19-34.

[13] Heiden, M., Bokan, H., Simôes da Silva, L., Greiner, R., Pirchere, M., Pircher, H., 2003, "Dynamic Effects of Railway Bridges for High Speed Usage: Application Example Steel-Composite Truss Bridge", IV Congresso de Construção Metálica e Mista, Lisbon.

[14] Xia, H., Roeck, G.D., Zhang, N., Maecka, J., 2003, "Experimental analysis of a high-speed railway bridge under Thalys trains", Journal of Sound and Vibration, 268, 103-113.

[15] Delgado, M. R., dos Santos R. C., S. M., 1997, "Modeling of Railway Bridge-Vehicle Interaction on High Speed Tracks", Journal of Computers and Structures, Vol. 63, No. 3 511-523.

[16] Goicolea, J. M., Dominguez, J., Navarro, J. A., Gabaldon, F., 2002, "New Dynamic Analysis Methods for Railway Bridges in Codes IAPF and Eurocode 1", Railway Bridges Design, Construction and Maintenance Spanish Group of IABSE, 2-43, Madrid.

[17] Ju, S. H., Lin, H. T., 2003, "Resonance Characteristics of High-Speed Trains Passing Simply Supported Bridges" Journal of Sound and Vibration, 267, 1127-1141.

[18] Yang, Y. B., Yau, J. D., Hsu, L.C., 1997, " Vibration of Simple Beams Due to Trains Moving at High Speeds", Journal of Engineering Structures, Vol.19, No.11 936-944.

[19] Lin, C.C., Wang, J. F., Chen, B. L., 2005, "Train-Induced Vibration Control of High Speed Railway Bridges Equipped with Multiple Tuned Mass Dampers", Civil Engineering, ASCE.

[20] Theyse, H. L., 2002, "Stiffness, Strength, and Performance of Unbound Aggregate Material: Application of South African HVS and Laboratory Results to California Flexible Pavements", University of California, California

[21] Guerrero, S. L., Vallejo, L. E., 2006, "Discrete element method analysis of rail-track ballast degradation during cyclic loading", Journal of Granular Matter, 8, 195-204.

[22] Eurocode 1991-2:2003 – Eurocode 1: Actions on structures-Part 2, "Traffic loads on bridges", 2003, Brussels.

[23] American Railway Engineering and Maintenance of Way Association Chapter 15, "Steel Structures", 2006

[24] Eurocode 1990:2005-Eurocode: "Basis on structural design", 2005, Brussels.

[25] Chin, W., Choi, E., Park, S., Kang, J., Kwark, J., Kim, Y., and Kim, B., 2003, "Experimental Study on the Rigidities of Bridge Substructures in KHSR", Development of Structural Safety Technology in Korean High Speed Railway Bridge.

[26] LARSA Ins., "LARSA 2000 Reference for LARSA 2000 Finite Element Analysis and Design Software", 2004, Melville, New York.

[27] Güneş, B., 2009, "Track-Bridge Interaction in High Speed Railway Bridges and its Application", International Advance Technology Symposium, Karabük

[28] Raymond, G. P., Bathurst, R. J., 1987, "Performance of Large Scale Model", Transportation Research Record, 1131, 361-1981.

[29] Miura, S., Takai, H., Uchida, M., and Fukada, Y., 1998, "The Mechanism of Railway Tracks", Railway Technology Today 2, EJRCF.

[30] Gabaldon, F., Riquelme, F., Goicolea, J. M., and Arribas, J. J., "Dynamic Analysis of Structures Under High Speed Train Loads: Case Studies in Spain", Dynamics of High-Speed Railway Bridges, pp. 143-165.

[31] Ju, S. and Lin, H. Numerical Investigation of a steel arch bridge and interaction with high-speed trains. Engineering Structures. Vol 25. pp. 241-250, (2003).

[32] Chopra, A., 2000, "Dynamics of Structures", Prentice Hall, New Jersey.

[33] Milliyet, 11 August 2009 and 14 November 2009, "Hızlandırılmış Tren Kazası", http://www.milliyet.com.tr/Yasam/SonDakika.

[34] Caner, A., Oğuz, C., Karcı Topçu, T., 2007, "Bildiriler Kitabı", 1. Bridge and Viaducts Symposium, Antalya

APPENDIX A

SELECTED ANALYSIS RESULTS

A.1. Eigenvalue Analysis Joint Mode Shapes

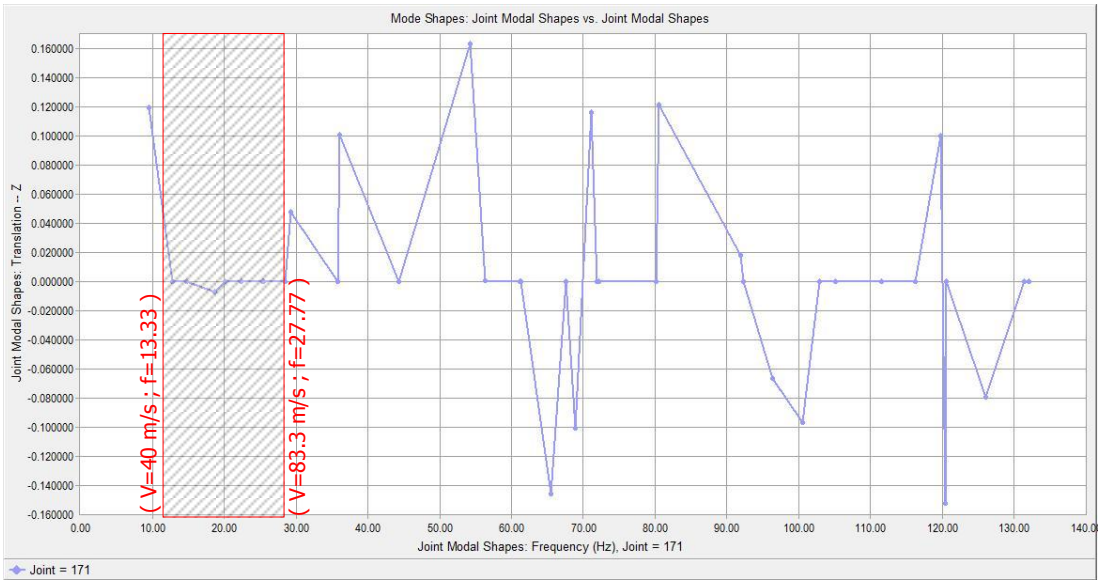

Figure A.1 Joint Modal Shape vs. Mode Shape graph of the bridge having 8.75 m span length, 4.421.563 kN.m^2 Span Flexural Rigidity.

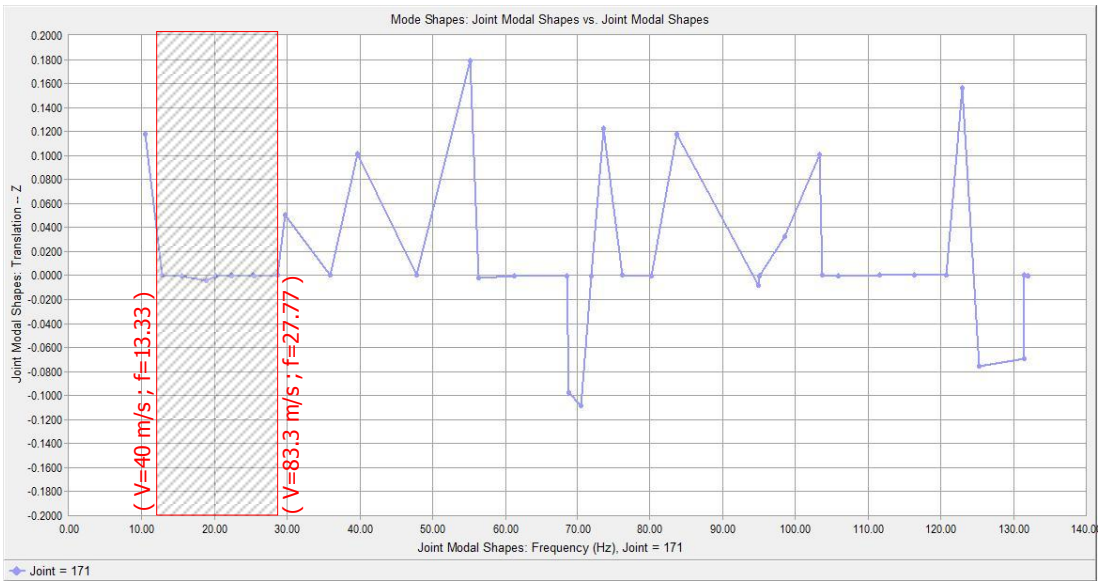

Figure A.2 Joint Modal Shape vs. Mode Shape graph of the bridge having 8.75 m span length, 6.244.779 kN.m^2 Span Flexural Rigidity.

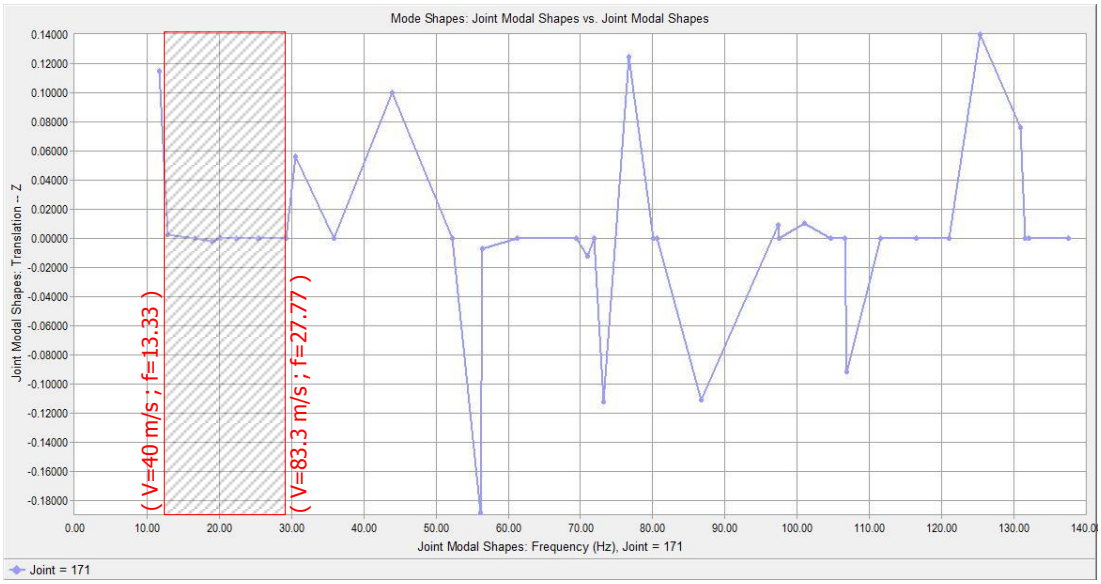

Figure A.3 Joint Modal Shape vs. Mode Shape graph of the bridge having 8.75 m span length, 9.259.963 kN.m^2 Span Flexural Rigidity.

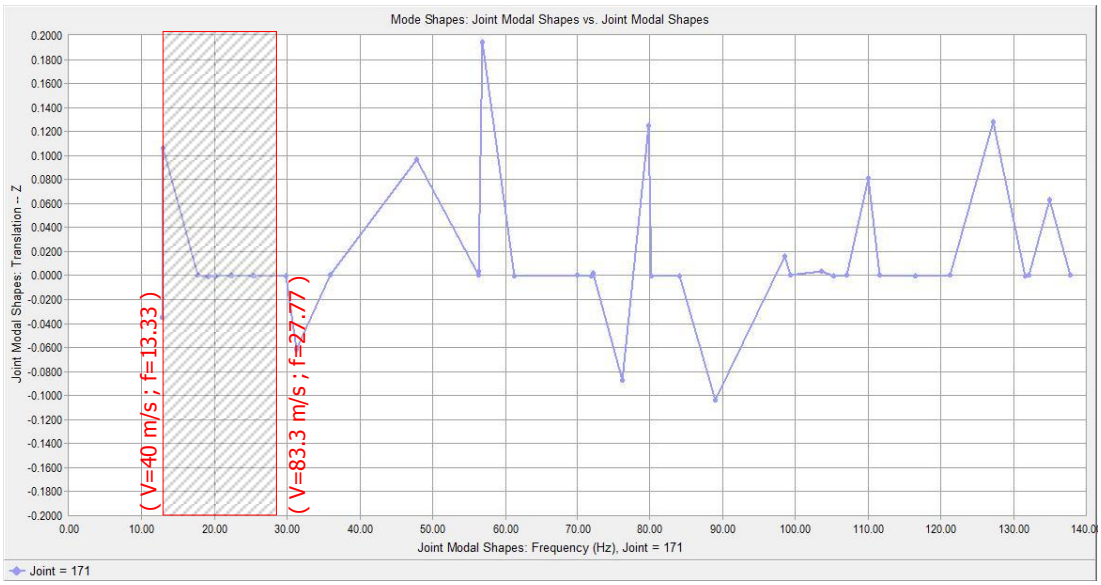

Figure A.4 Joint Modal Shape vs. Mode Shape graph of the bridge having 8.75 m span length, 12.981.221 kN.m^2 Span Flexural Rigidity.

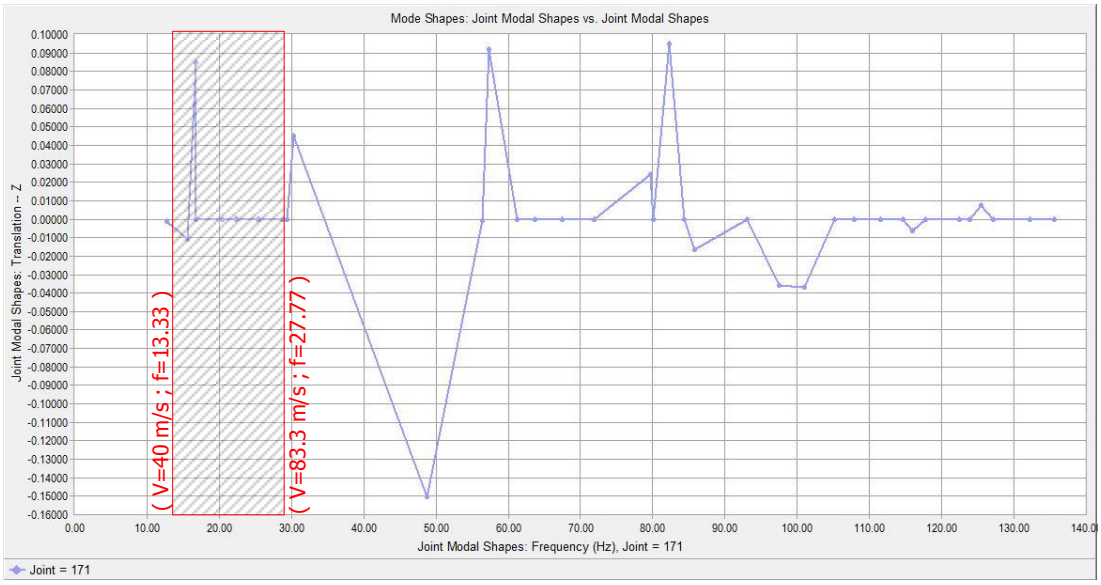

Figure A.5 Joint Modal Shape vs. Mode Shape graph of the bridge having 8.75 m span length, 23.750.916 kN.m^2 Span Flexural Rigidity.

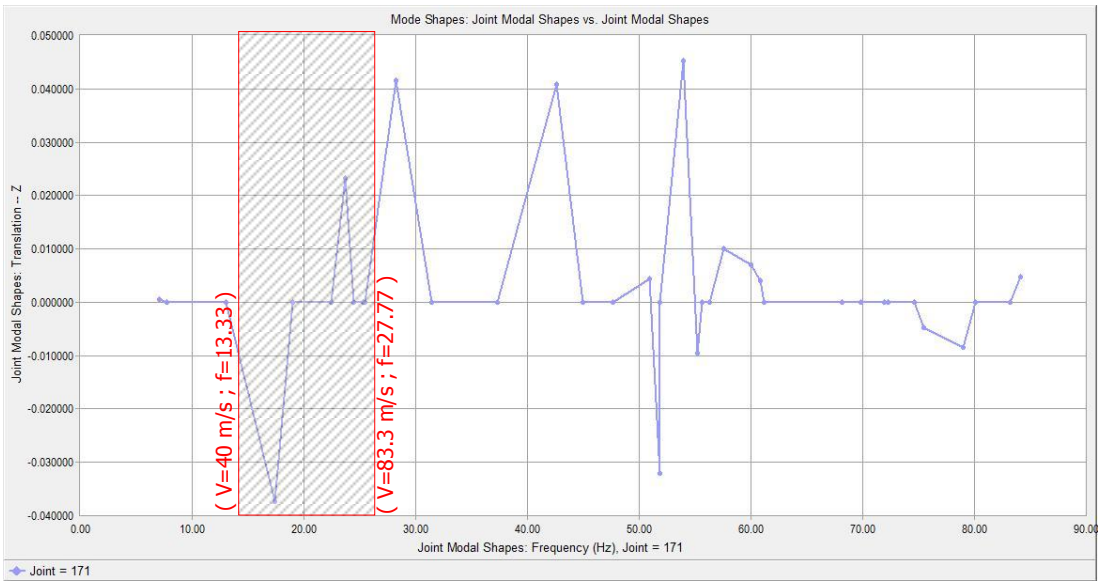

Figure A.6 Joint Modal Shape vs. Mode Shape graph of the bridge having 8.75 m span length, 195.898.160 kN.m^2 Span Flexural Rigidity.

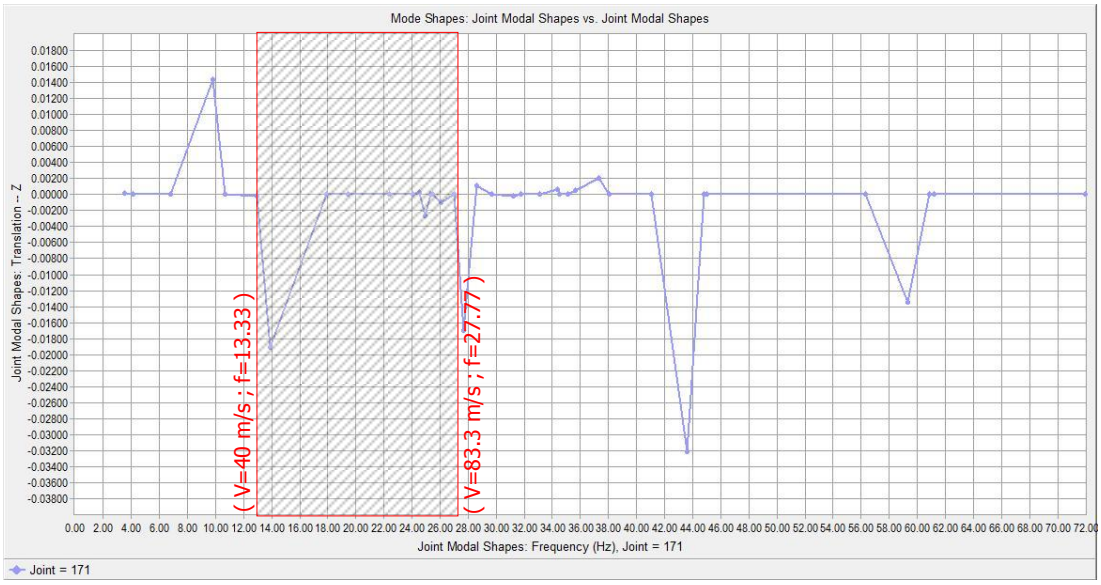

Figure A.7 Joint Modal Shape vs. Mode Shape graph of the bridge having 8.75 m span length, 768.263.855 kN.m^2 Span Flexural Rigidity.

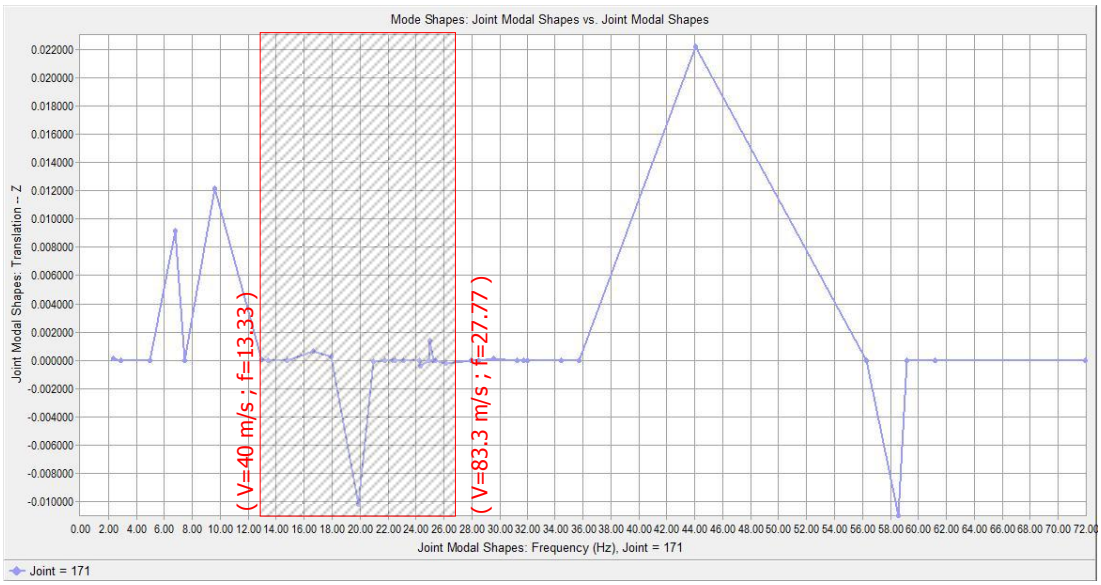

Figure A.8 Joint Modal Shape vs. Mode Shape graph of the bridge having 8.75 m span length, 1.912.920.565 kN.m^2 Span Flexural Rigidity.

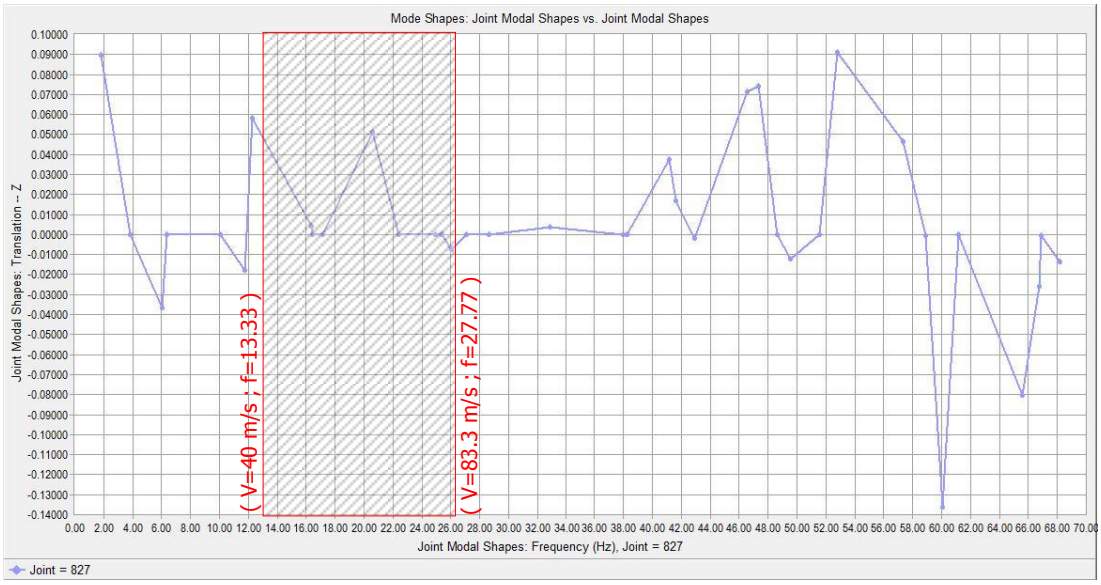

Figure A.9 Joint Modal Shape vs. Mode Shape graph of the bridge having 24.5 m span length, 4.421.563 kN.m^2 Span Flexural Rigidity.

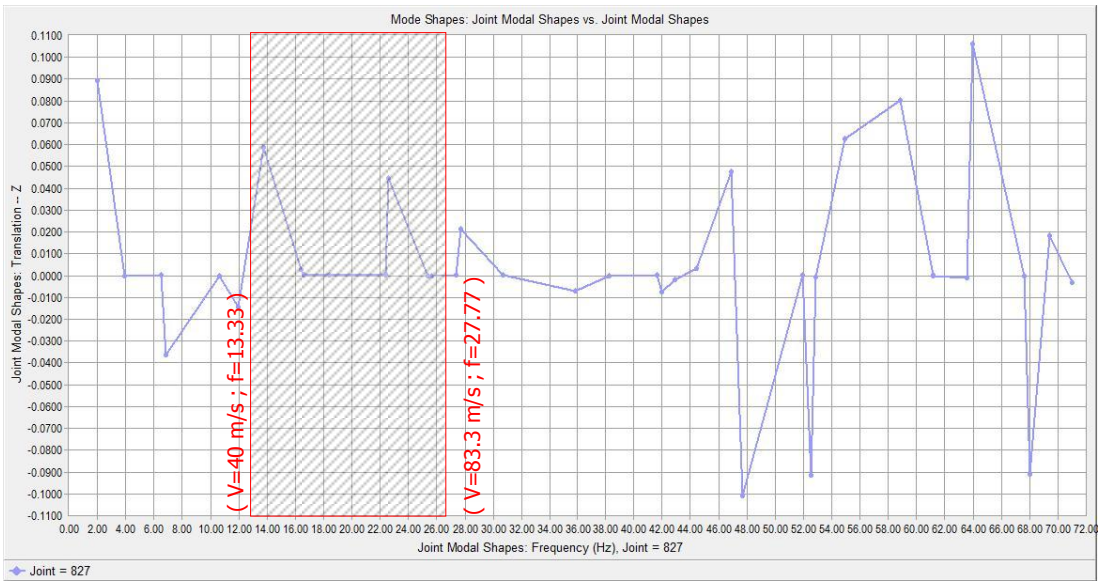

Figure A.10 Joint Modal Shape vs. Mode Shape graph of the bridge having 24.5 m span length, 6.244.779 kN.m^2 Span Flexural Rigidity.

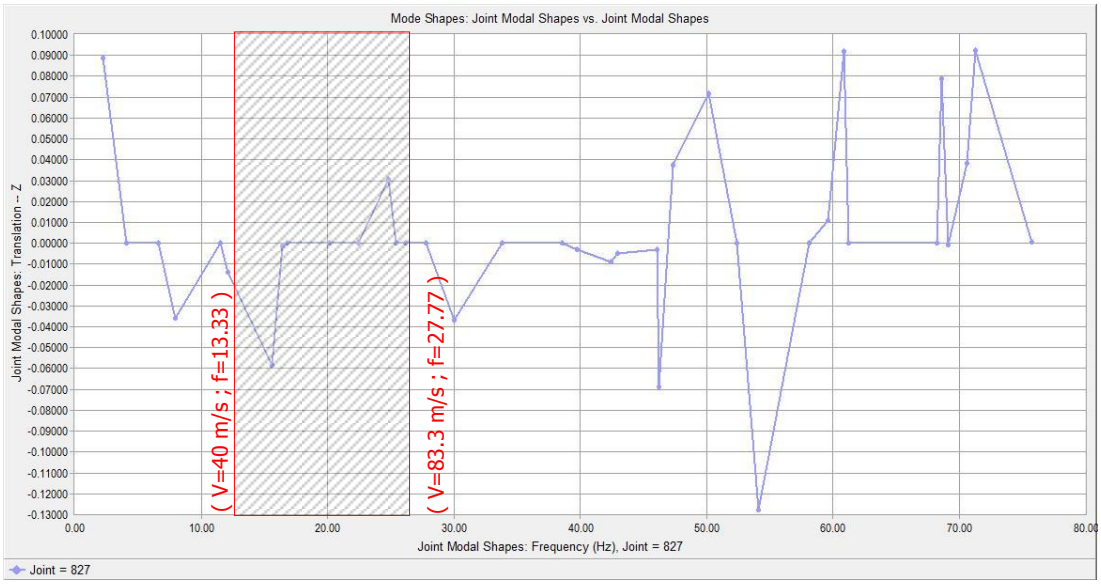

Figure A.11 Joint Modal Shape vs. Mode Shape graph of the bridge having 24.5 m span length, 9.259.963 kN.m^2 Span Flexural Rigidity.

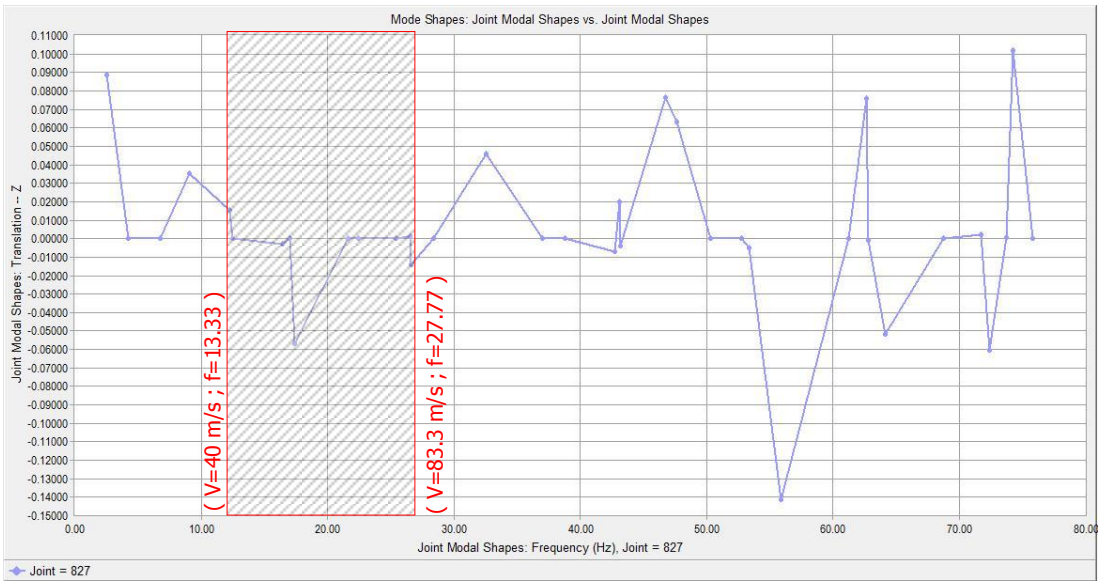

Figure A.12 Joint Modal Shape vs. Mode Shape graph of the bridge having 24.5 m span length, 12.981.221 kN.m^2 Span Flexural Rigidity.

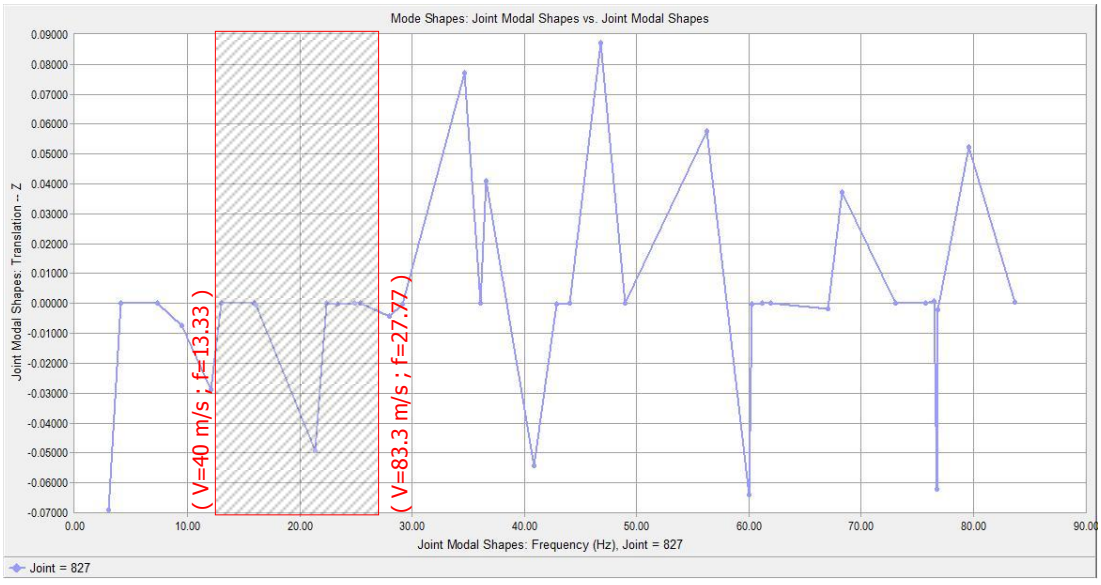

Figure A.13 Joint Modal Shape vs. Mode Shape graph of the bridge having 24.5 m span length, 23.750.916 kN.m^2 Span Flexural Rigidity.

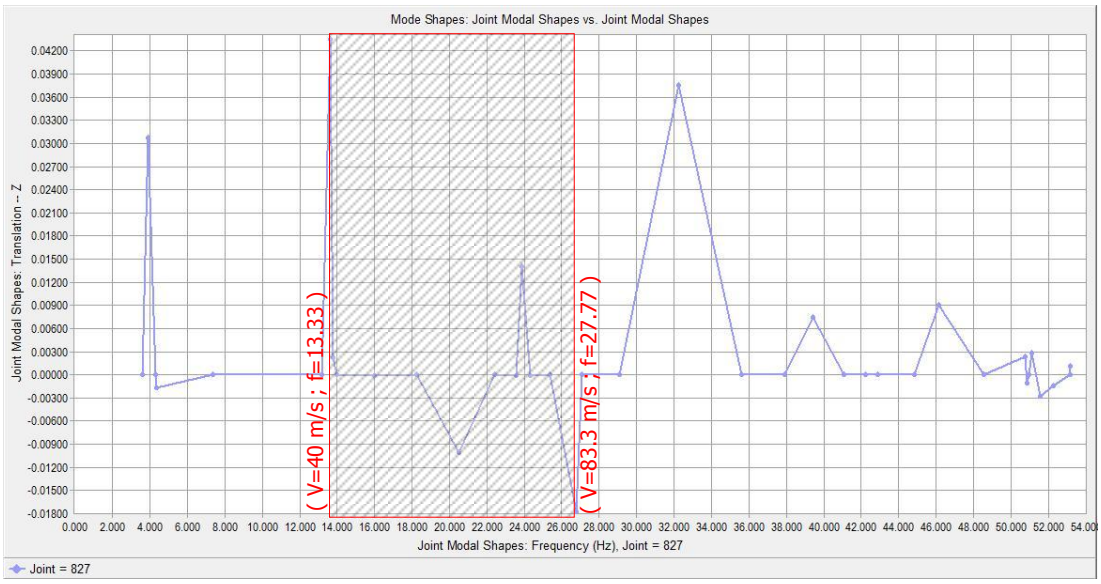

Figure A.14 Joint Modal Shape vs. Mode Shape graph of the bridge having 24.5 m span length, 195.898.160 kN.m^2 Span Flexural Rigidity.

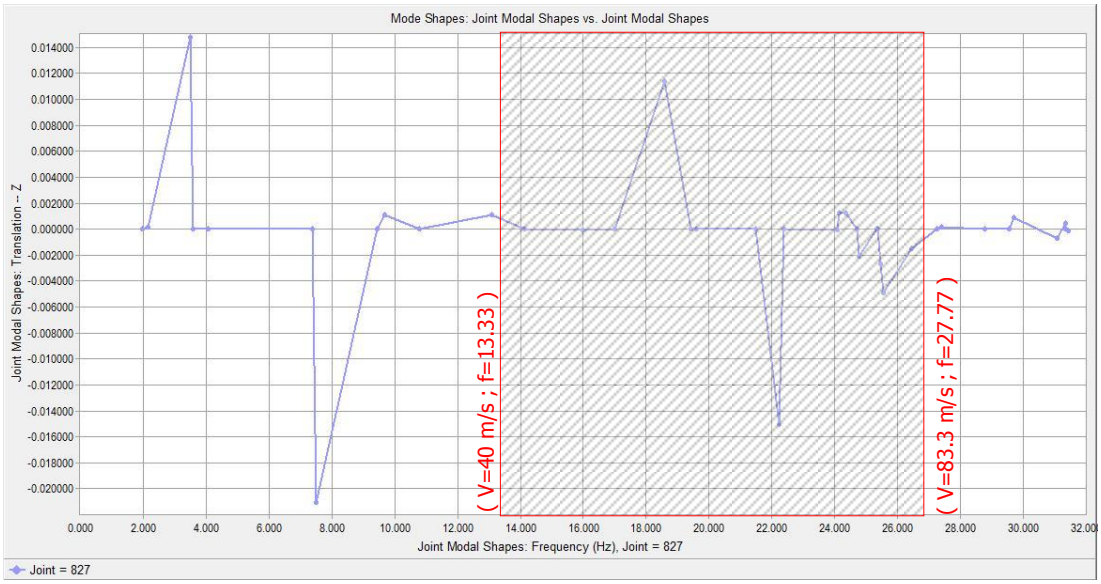

Figure A.15 Joint Modal Shape vs. Mode Shape graph of the bridge having 24.5 m span length, 768.263.855 kN.m^2 Span Flexural Rigidity.

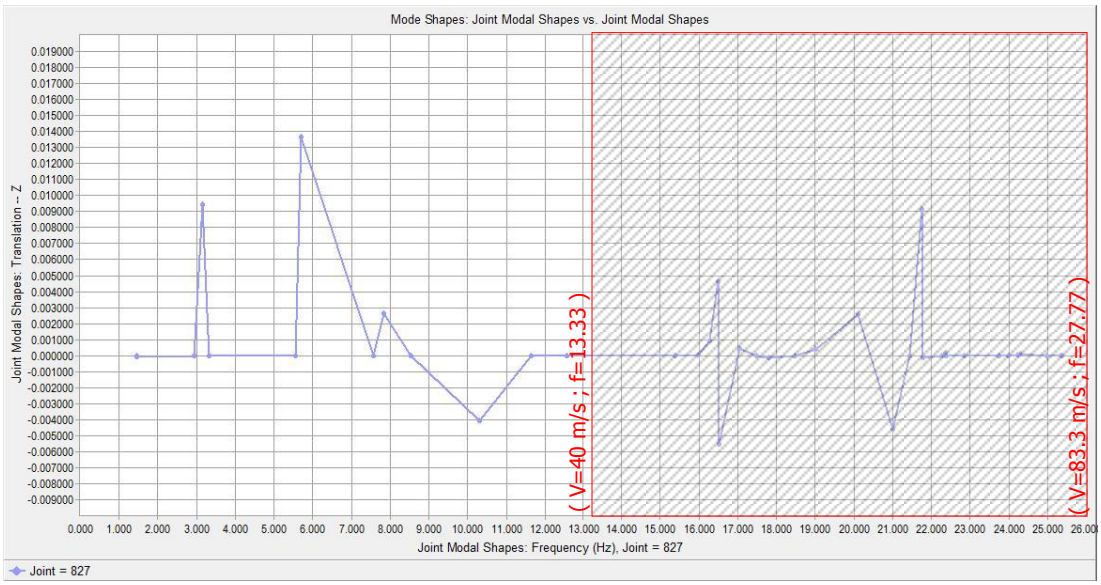

Figure A.16 Joint Modal Shape vs. Mode Shape graph of the bridge having 24.5 m span length, 1.912.920.565 kN.m^2 Span Flexural Rigidity.

A.2. Moving Force Model Joint Acceleration Graphs

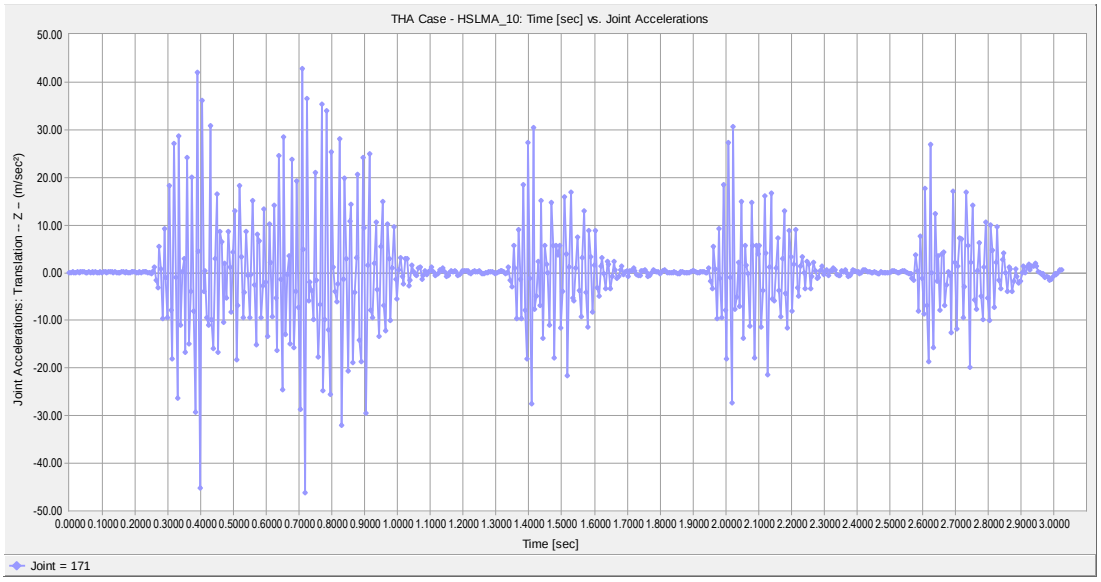

Figure A.17 Joint Acceleration vs. Time graph of the bridge having 8.75 m span length, 0.75 m girder height, 300 MPa ballast stiffness for 44.13 m/s vehicle speed.

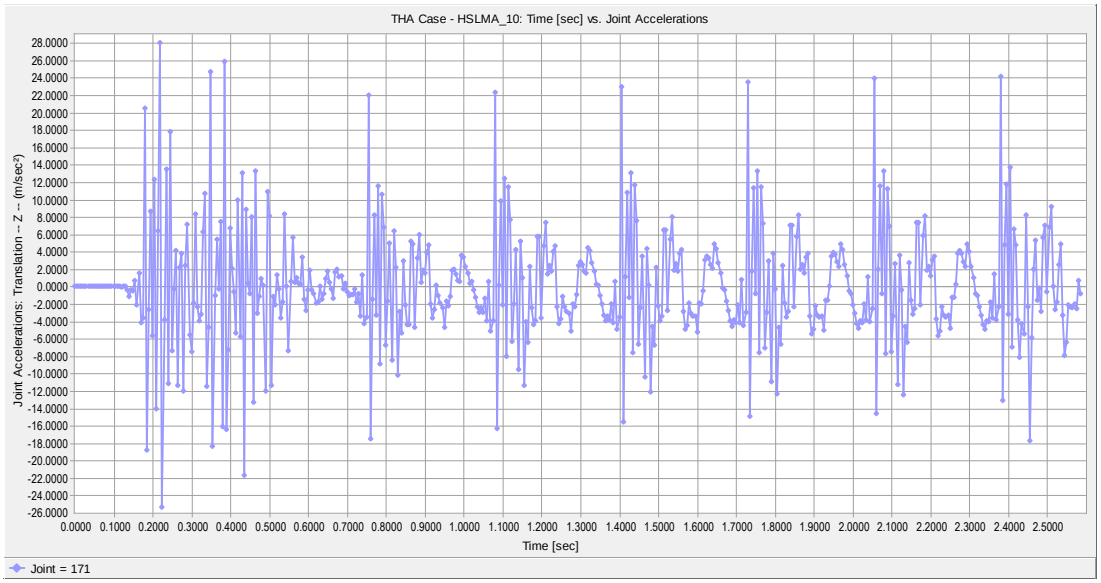

Figure A.18 Joint Acceleration vs. Time graph of the bridge having 8.75 m span length, 0.75 m girder height, 300 MPa ballast stiffness for 83 m/s vehicle speed.

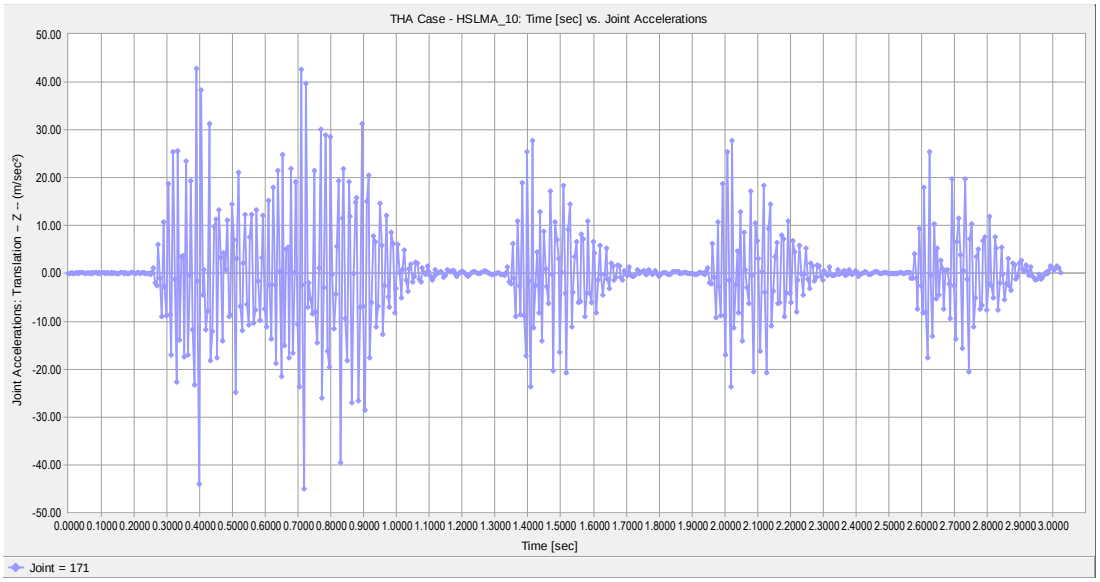

Figure A.19 Joint Acceleration vs. Time graph of the bridge having 8.75 m span length, 0.90 m girder height, 300 MPa ballast stiffness for 44.13 m/s vehicle speed.

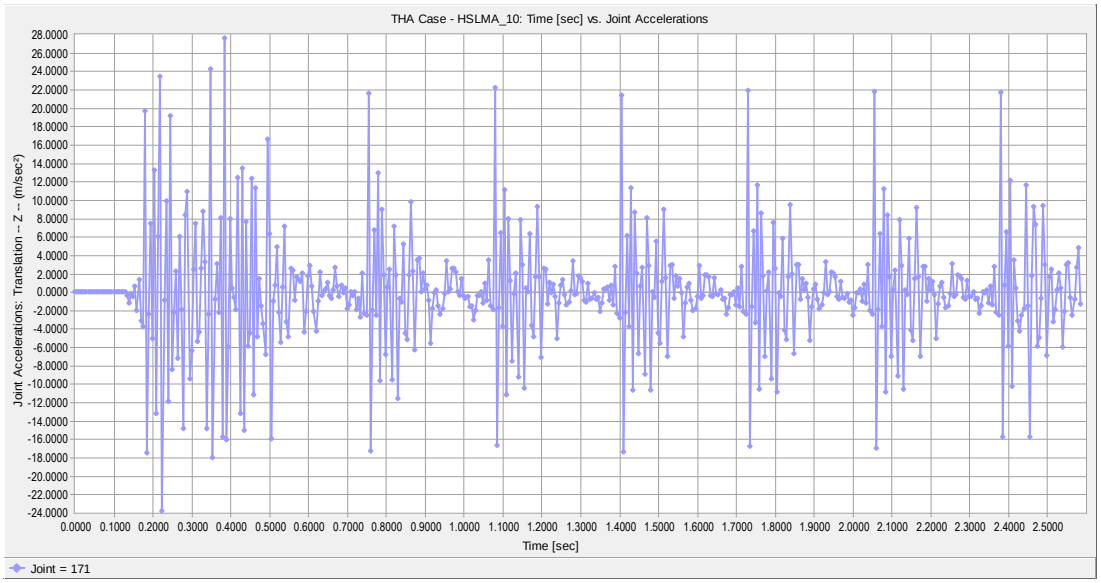

Figure A.20 Joint Acceleration vs. Time graph of the bridge having 8.75 m span length, 0.90 m girder height, 300 MPa ballast stiffness for 83 m/s vehicle speed.

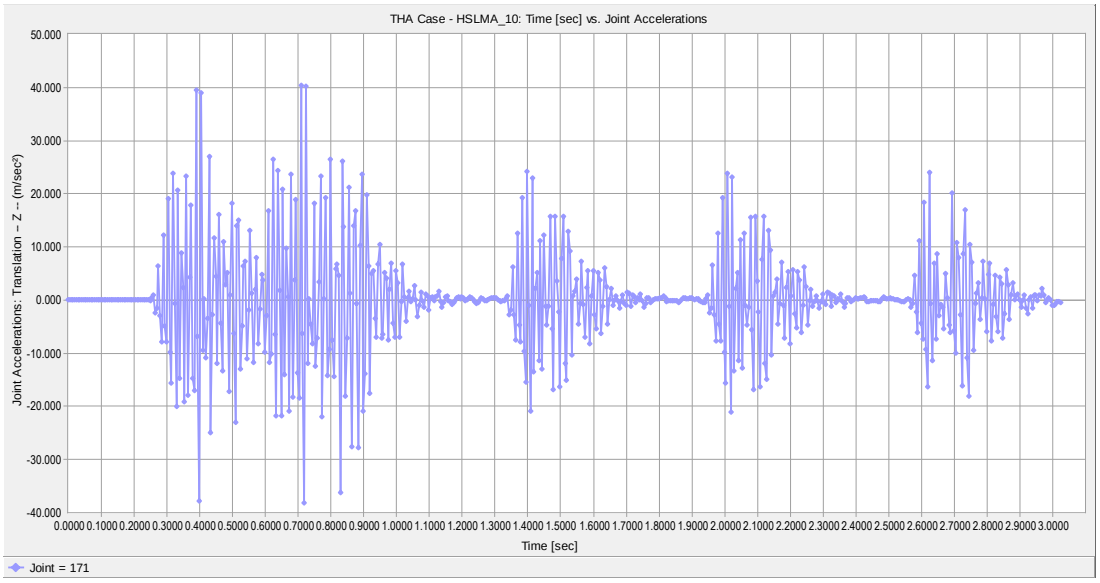

Figure A.21 Joint Acceleration vs. Time graph of the bridge having 8.75 m span length, 1.10 m girder height, 300 MPa ballast stiffness for 44.13 m/s vehicle speed.

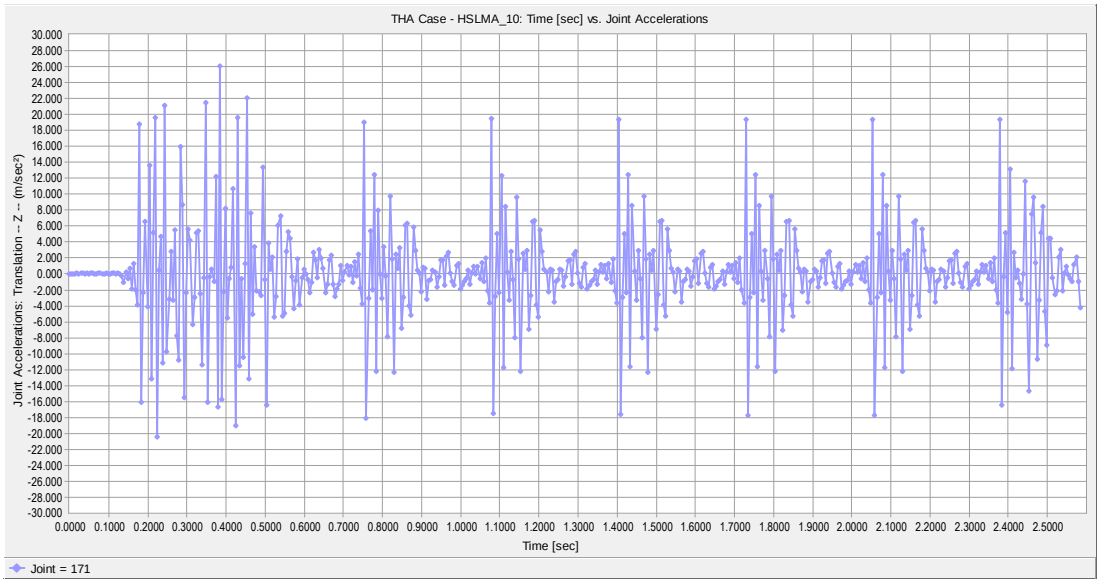

Figure A.22 Joint Acceleration vs. Time graph of the bridge having 8.75 m span length, 1.10 m girder height, 300 MPa ballast stiffness for 83 m/s vehicle speed.

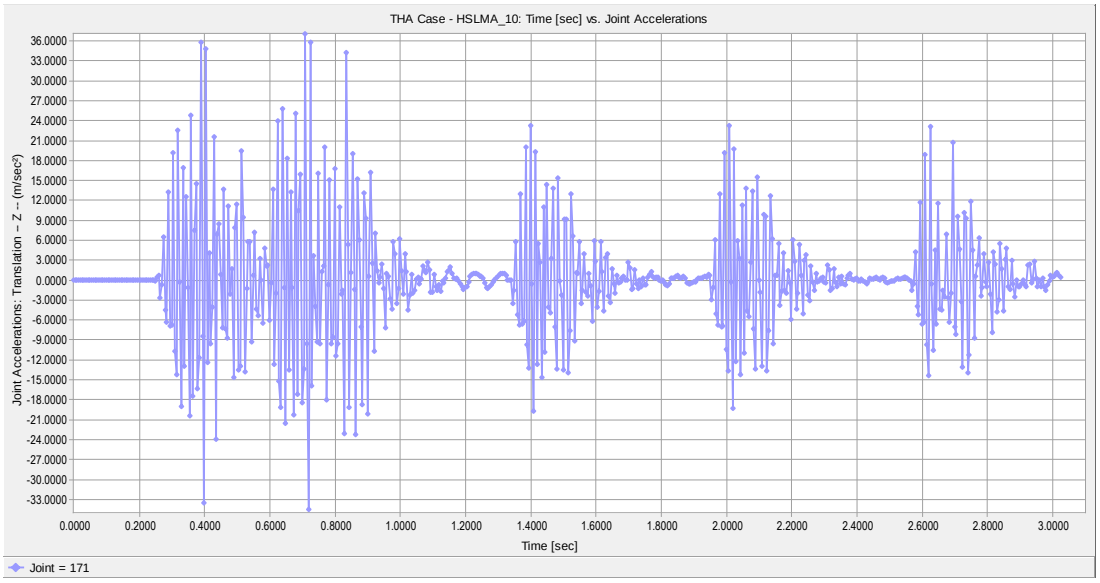

Figure A.23 Joint Acceleration vs. Time graph of the bridge having 8.75 m span length, 1.30 m girder height, 300 MPa ballast stiffness for 44.13 m/s vehicle speed.

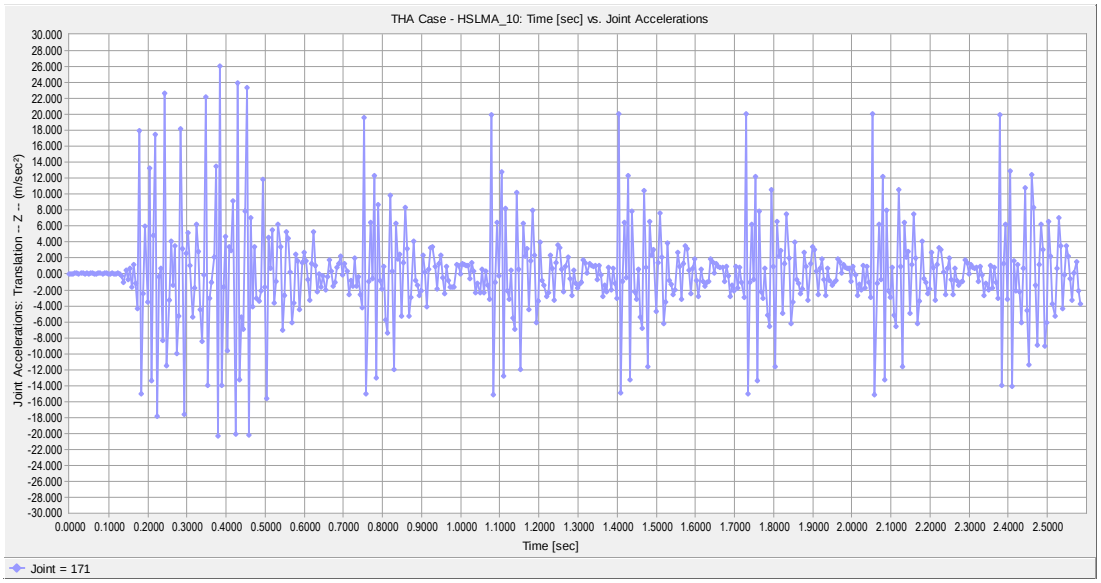

Figure A.24 Joint Acceleration vs. Time graph of the bridge having 8.75 m span length, 1.30 m girder height, 300 MPa ballast stiffness for 83 m/s vehicle speed.

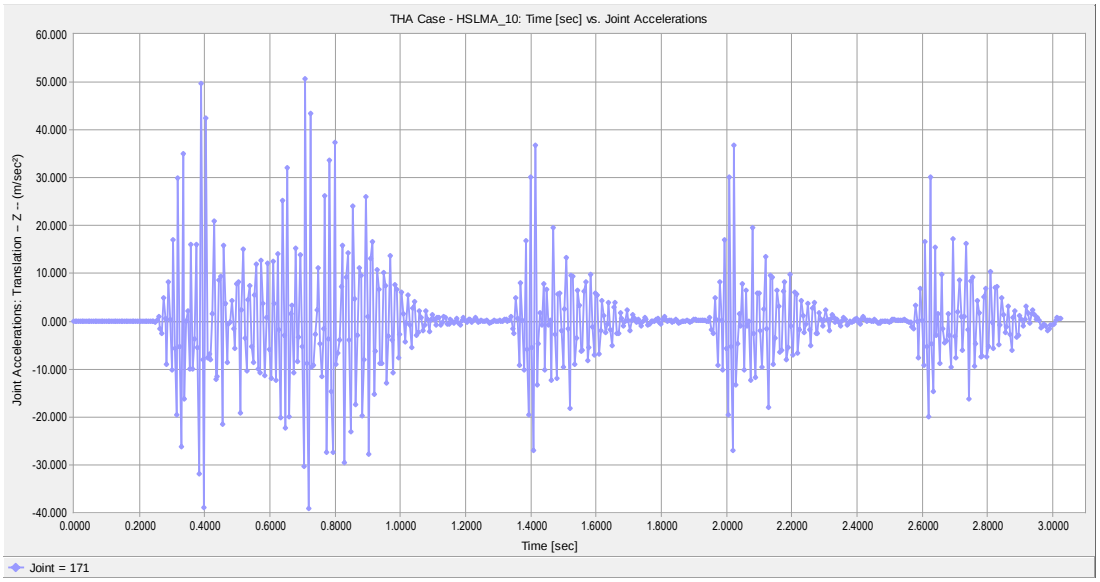

Figure A.25 Joint Acceleration vs. Time graph of the bridge having 8.75 m span length, 0.75 m girder height, 700 MPa ballast stiffness for 44.13 m/s vehicle speed.

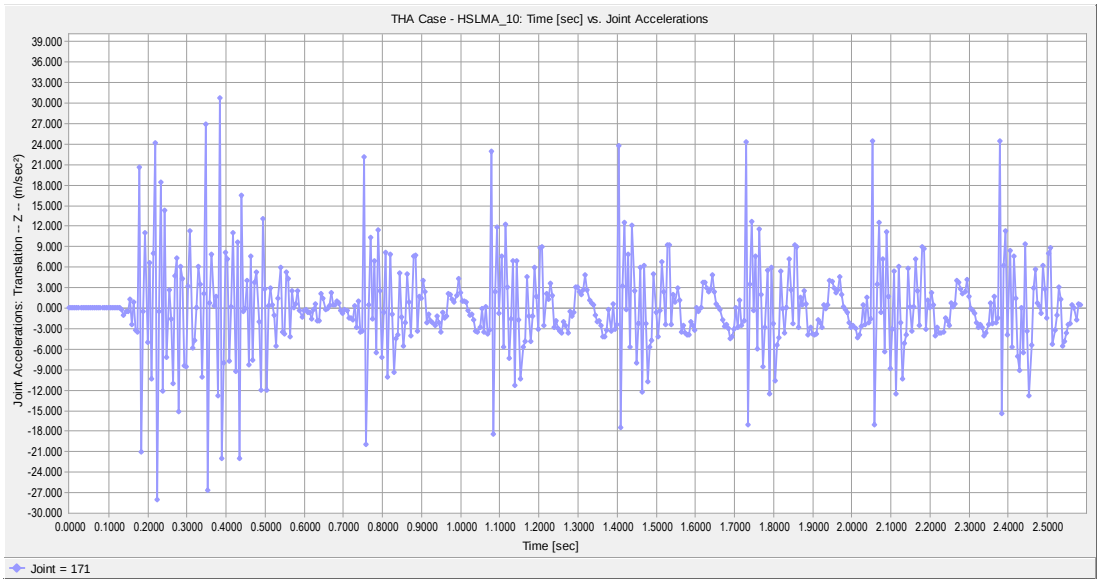

Figure A.26 Joint Acceleration vs. Time graph of the bridge having 8.75 m span length, 0.75 m girder height, 700 MPa ballast stiffness for 83 m/s vehicle speed.

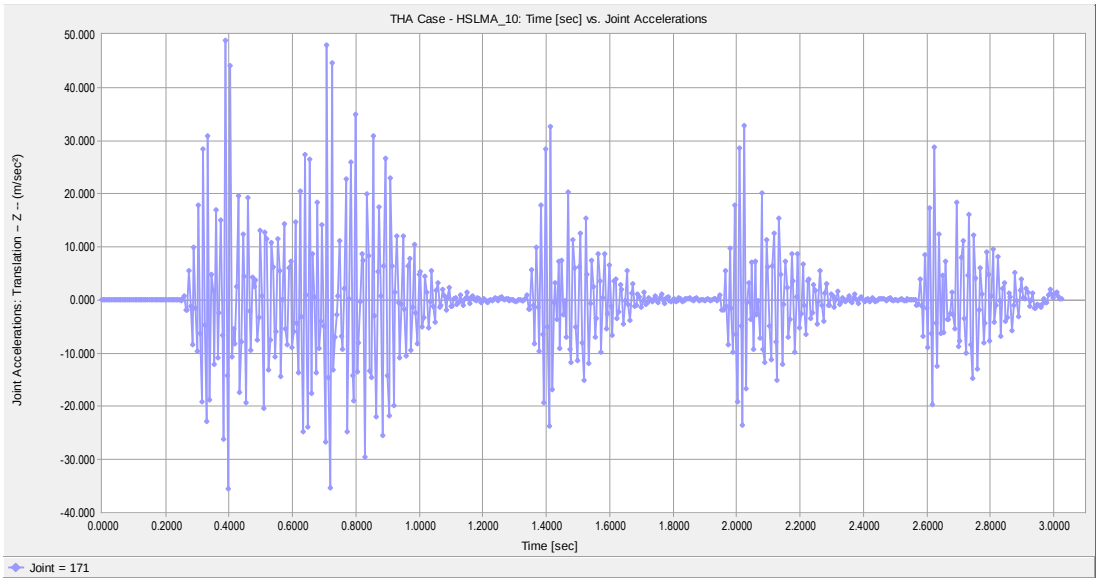

Figure A.27 Joint Acceleration vs. Time graph of the bridge having 8.75 m span length, 0.90 m girder height, 700 MPa ballast stiffness for 44.13 m/s vehicle speed.

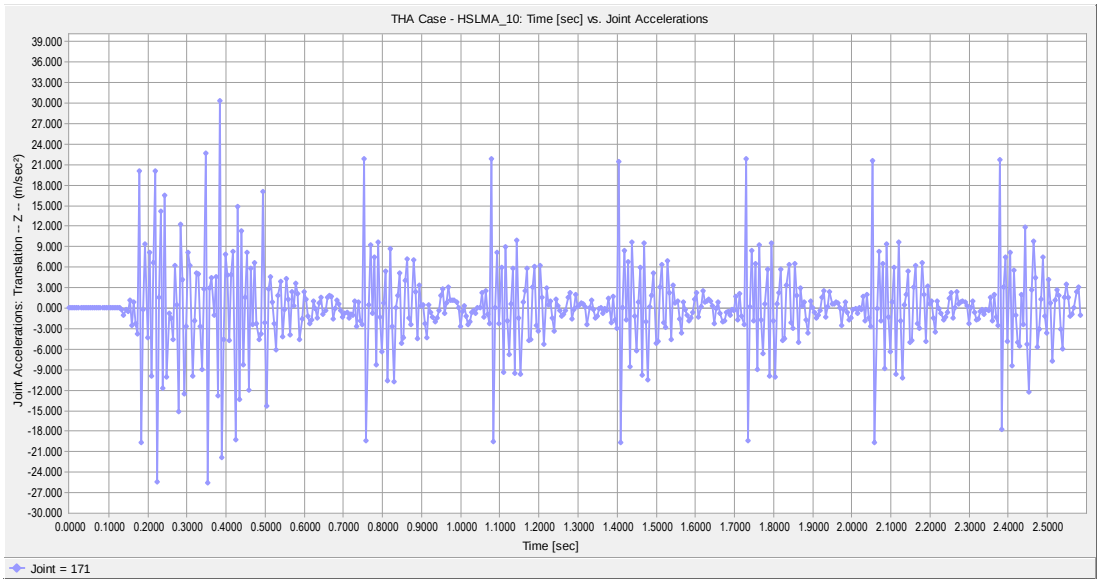

Figure A.28 Joint Acceleration vs. Time graph of the bridge having 8.75 m span length, 0.90 m girder height, 700 MPa ballast stiffness for 83 m/s vehicle speed.

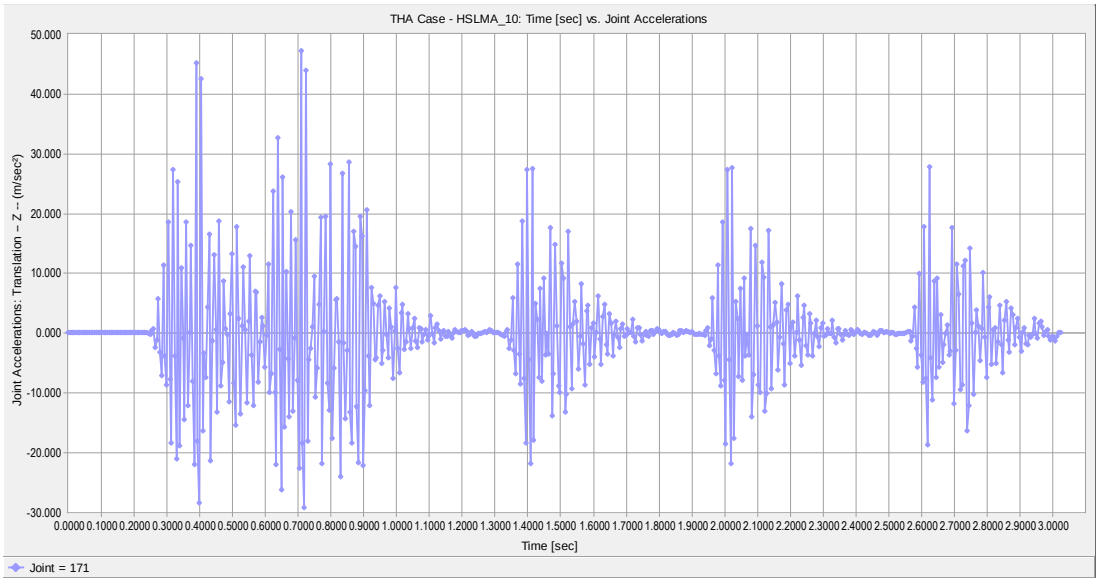

Figure A.29 Joint Acceleration vs. Time graph of the bridge having 8.75 m span length, 1.10 m girder height, 700 MPa ballast stiffness for 44.13 m/s vehicle speed.

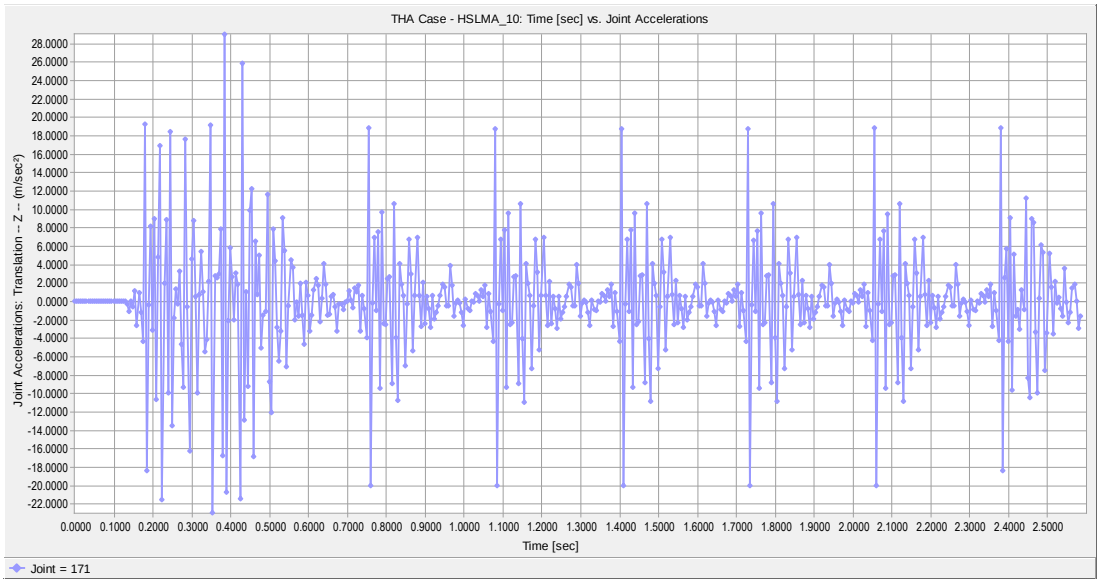

Figure A.30 Joint Acceleration vs. Time graph of the bridge having 8.75 m span length, 1.10 m girder height, 700 MPa ballast stiffness for 83 m/s vehicle speed.

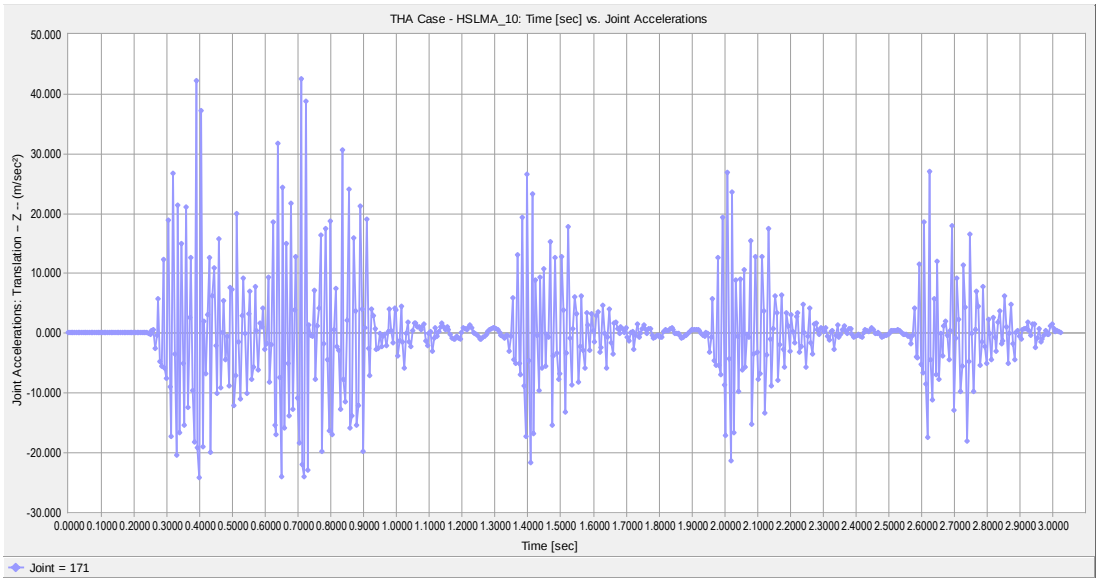

Figure A.31 Joint Acceleration vs. Time graph of the bridge having 8.75 m span length, 1.30 m girder height, 700 MPa ballast stiffness for 44.13 m/s vehicle speed.

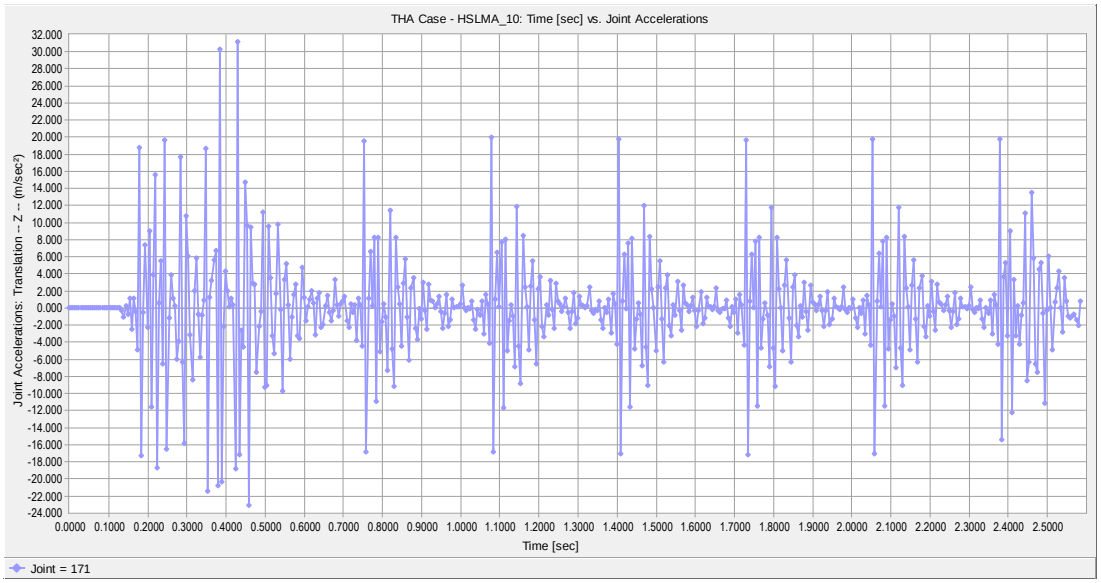

Figure A.32 Joint Acceleration vs. Time graph of the bridge having 8.75 m span length, 1.30 m girder height, 700 MPa ballast stiffness for 83 m/s vehicle speed.

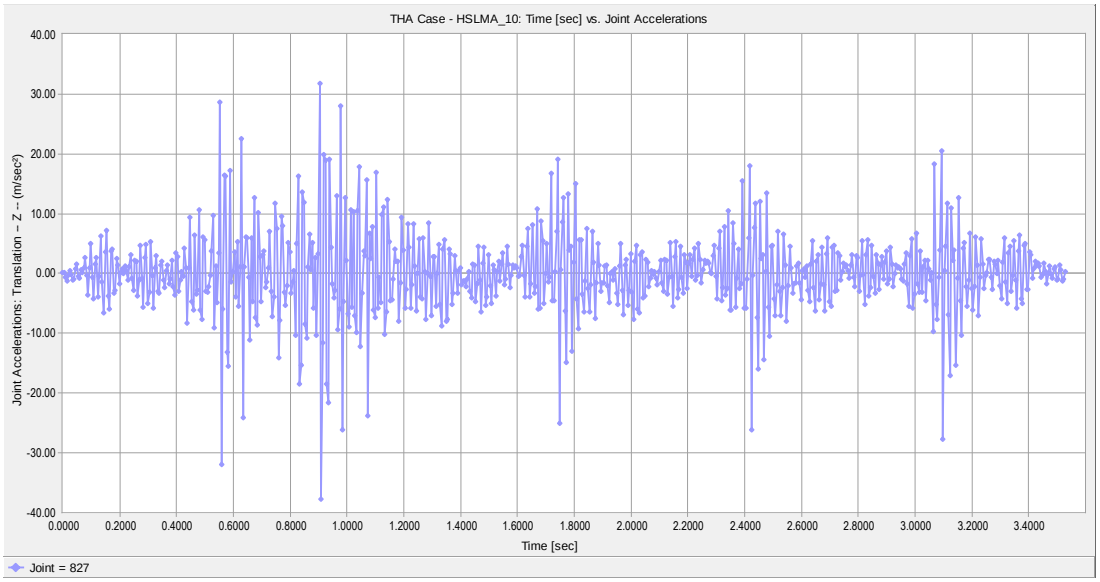

Figure A.33 Joint Acceleration vs. Time graph of the bridge having 24.5 m span length, 0.75 m girder height, 300 MPa ballast stiffness for 40 m/s vehicle speed.

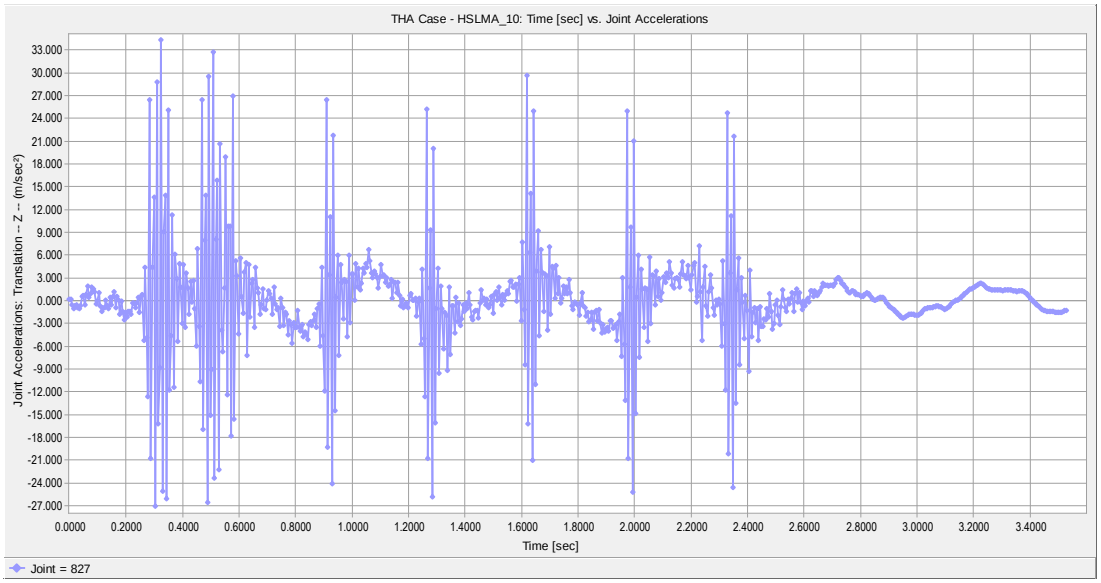

Figure A.34 Joint Acceleration vs. Time graph of the bridge having 24.5 m span length, 0.75 m girder height, 300 MPa ballast stiffness for 76.08 m/s vehicle speed.

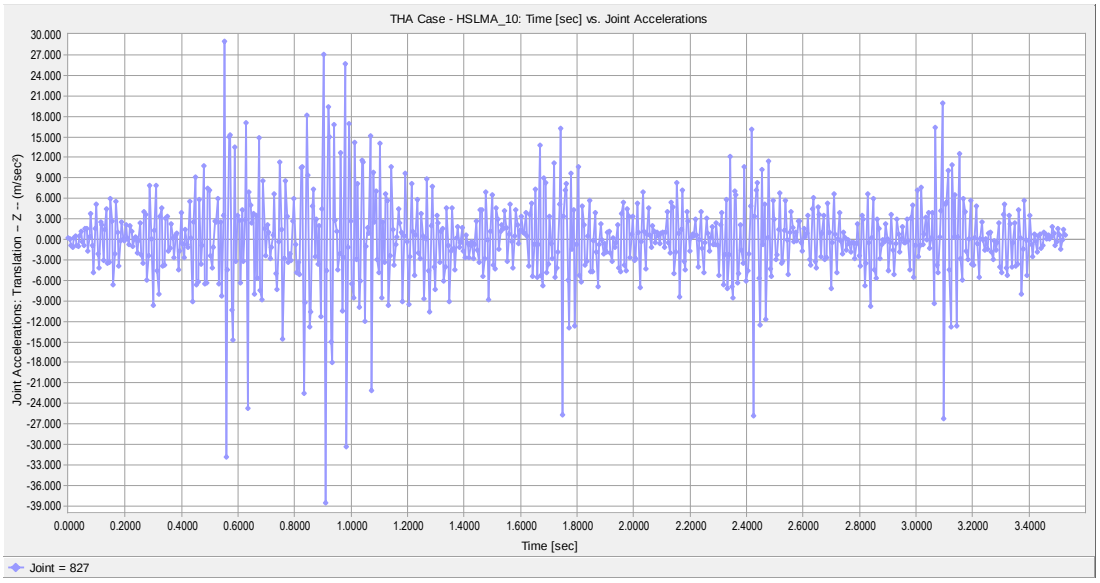

Figure A.35 Joint Acceleration vs. Time graph of the bridge having 24.5 m span length, 0.90 m girder height, 300 MPa ballast stiffness for 40 m/s vehicle speed.

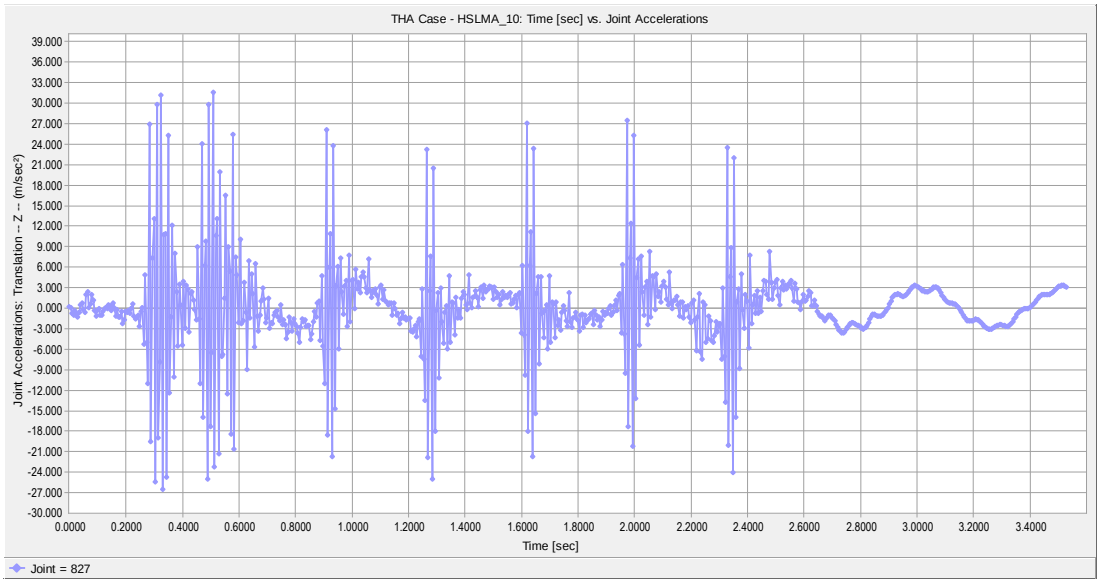

Figure A.36 Joint Acceleration vs. Time graph of the bridge having 24.5 m span length, 0.90 m girder height, 300 MPa ballast stiffness for 76.08 m/s vehicle speed.

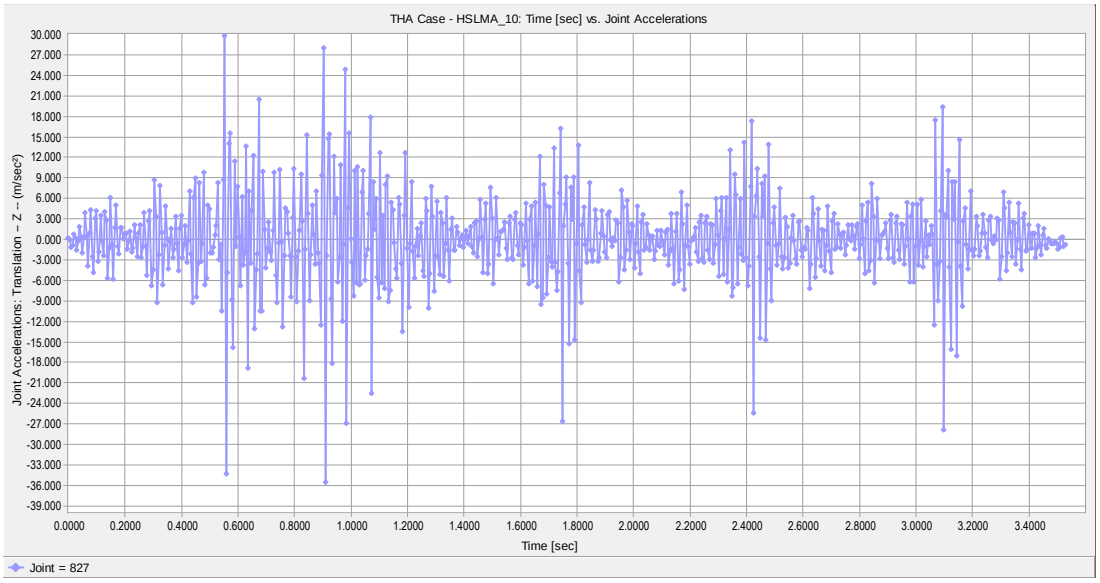

Figure A.37 Joint Acceleration vs. Time graph of the bridge having 24.5 m span length, 1.10 m girder height, 300 MPa ballast stiffness for 40 m/s vehicle speed.

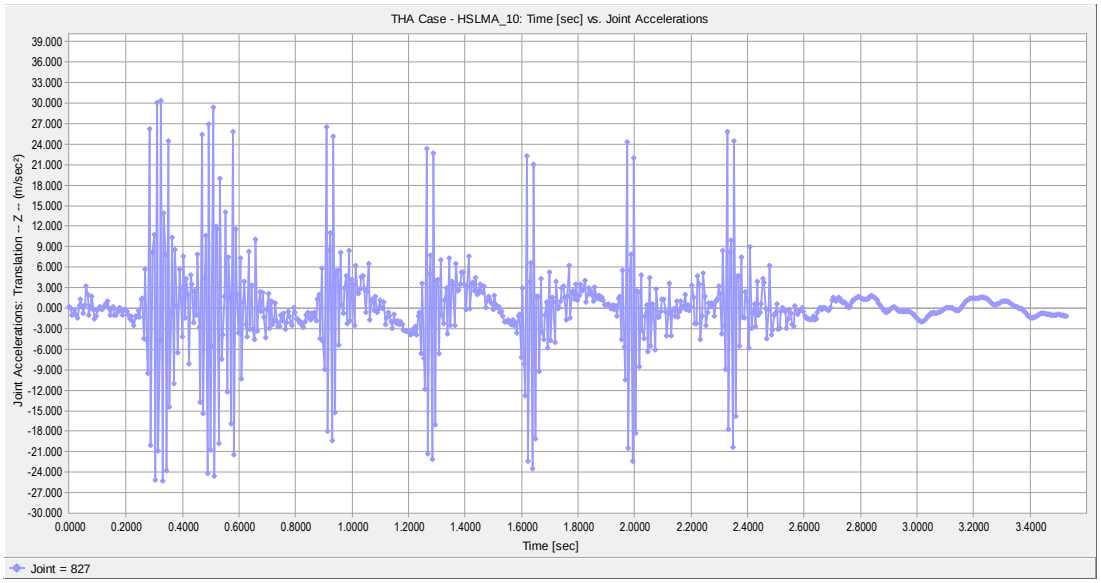

Figure A.38 Joint Acceleration vs. Time graph of the bridge having 24.5 m span length, 1.10 m girder height, 300 MPa ballast stiffness for 76.08 m/s vehicle speed.

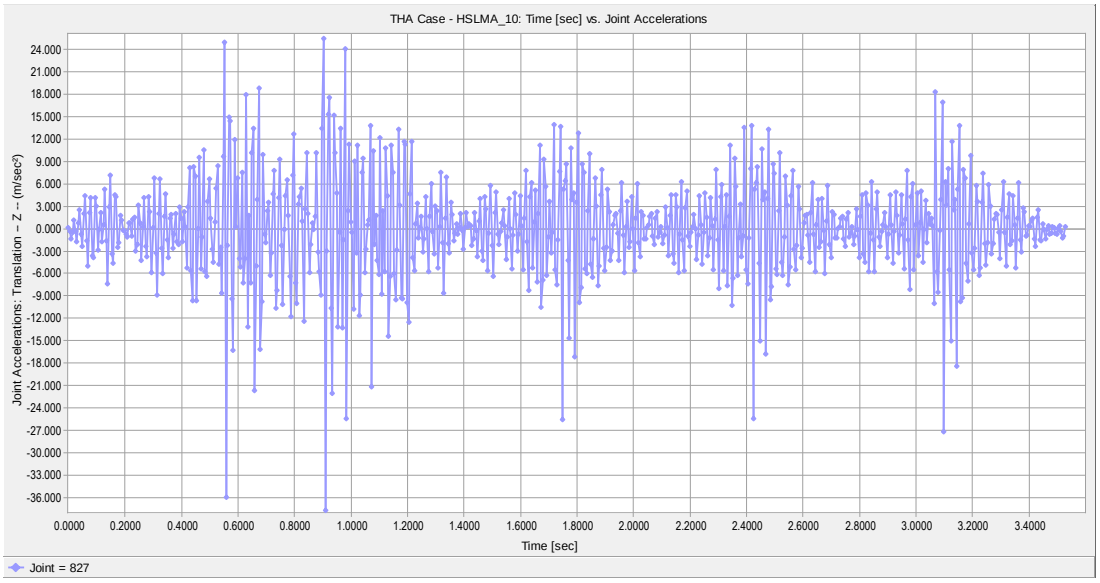

Figure A.39 Joint Acceleration vs. Time graph of the bridge having 24.5 m span length, 1.30 m girder height, 300 MPa ballast stiffness for 40 m/s vehicle speed.

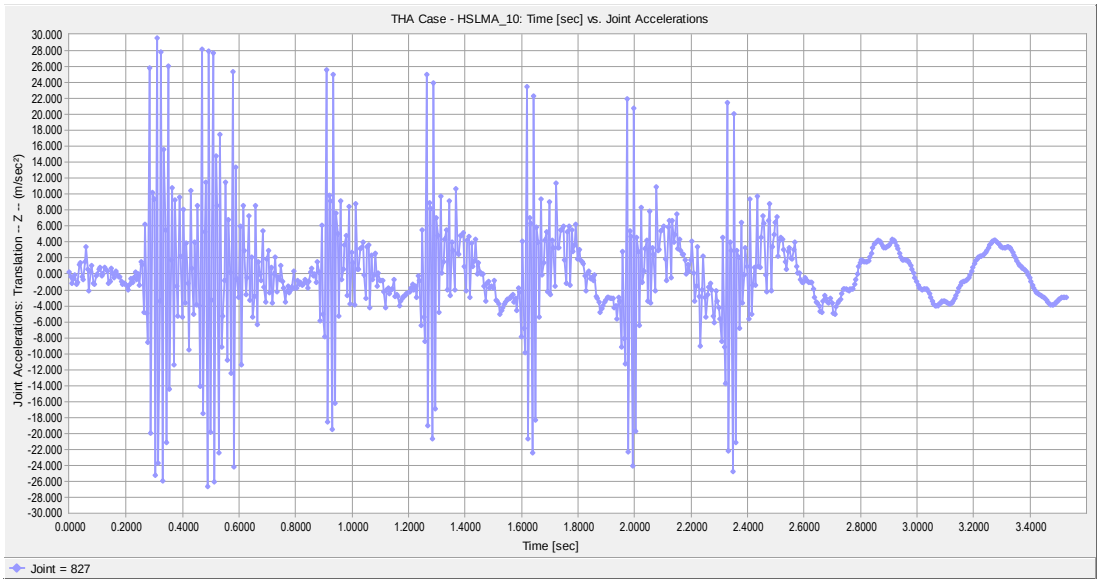

Figure A.40 Joint Acceleration vs. Time graph of the bridge having 24.5 m span length, 1.30 m girder height, 300 MPa ballast stiffness for 76.08 m/s vehicle speed.

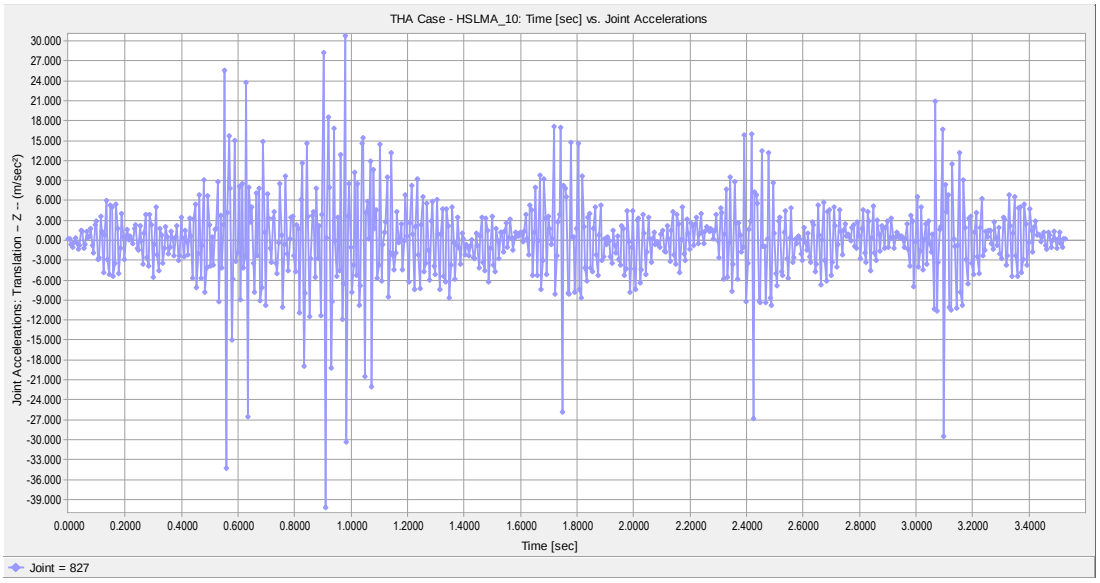

Figure A.41 Joint Acceleration vs. Time graph of the bridge having 24.5 m span length, 0.75 m girder height, 700 MPa ballast stiffness for 40 m/s vehicle speed.

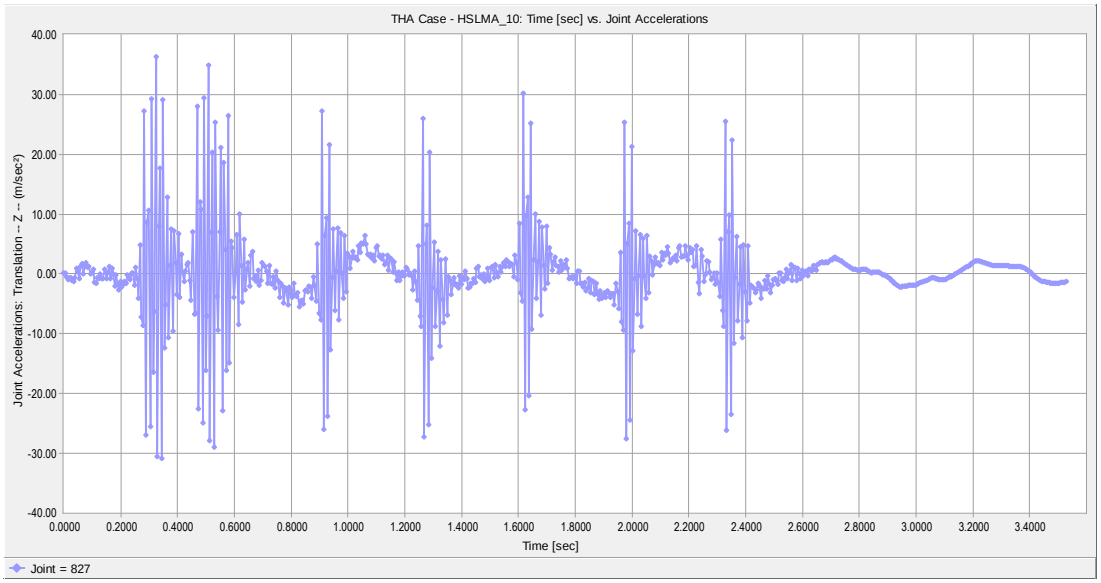

Figure A.42 Joint Acceleration vs. Time graph of the bridge having 24.5 m span length, 0.75 m girder height, 700 MPa ballast stiffness for 76.08 m/s vehicle speed.

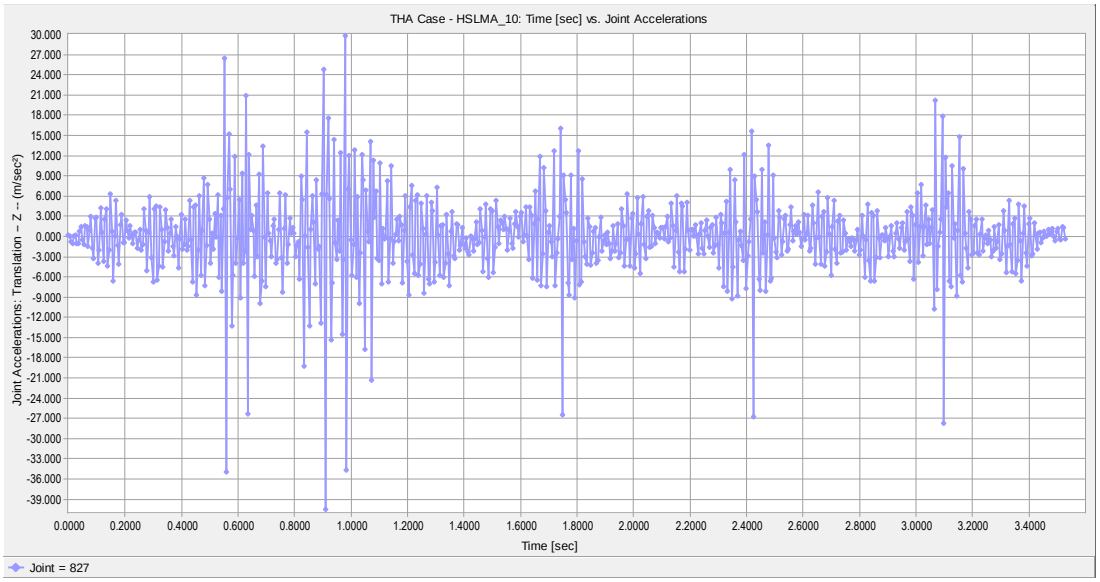

Figure A.43 Joint Acceleration vs. Time graph of the bridge having 24.5 m span length, 0.90 m girder height, 700 MPa ballast stiffness for 40 m/s vehicle speed.

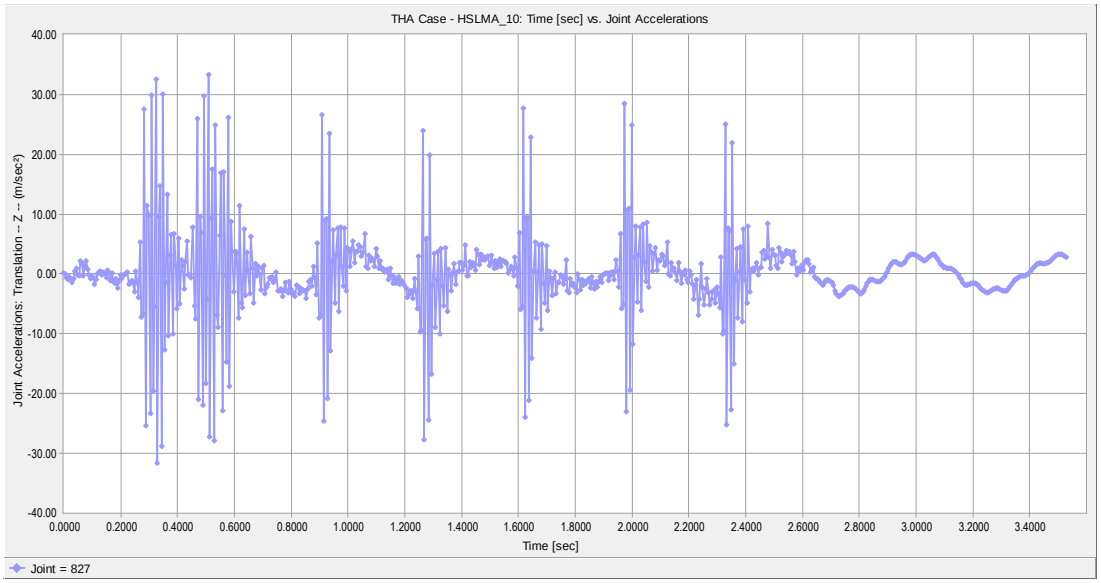

Figure A.44 Joint Acceleration vs. Time graph of the bridge having 24.5 m span length, 0.90 m girder height, 700 MPa ballast stiffness for 76.08 m/s vehicle speed.

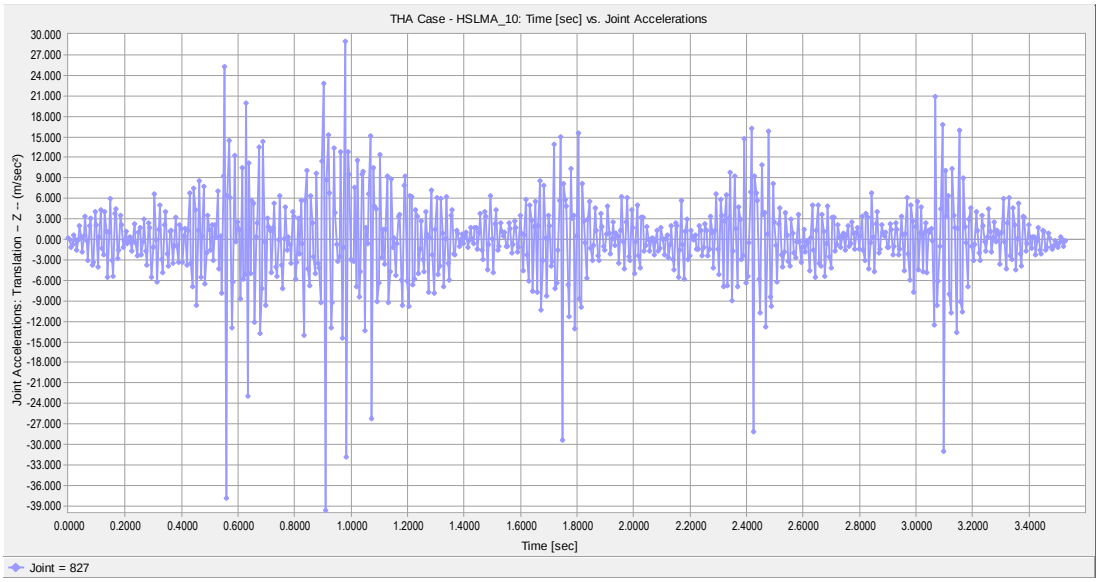

Figure A.45 Joint Acceleration vs. Time graph of the bridge having 24.5 m span length, 1.10 m girder height, 700 MPa ballast stiffness for 40 m/s vehicle speed.

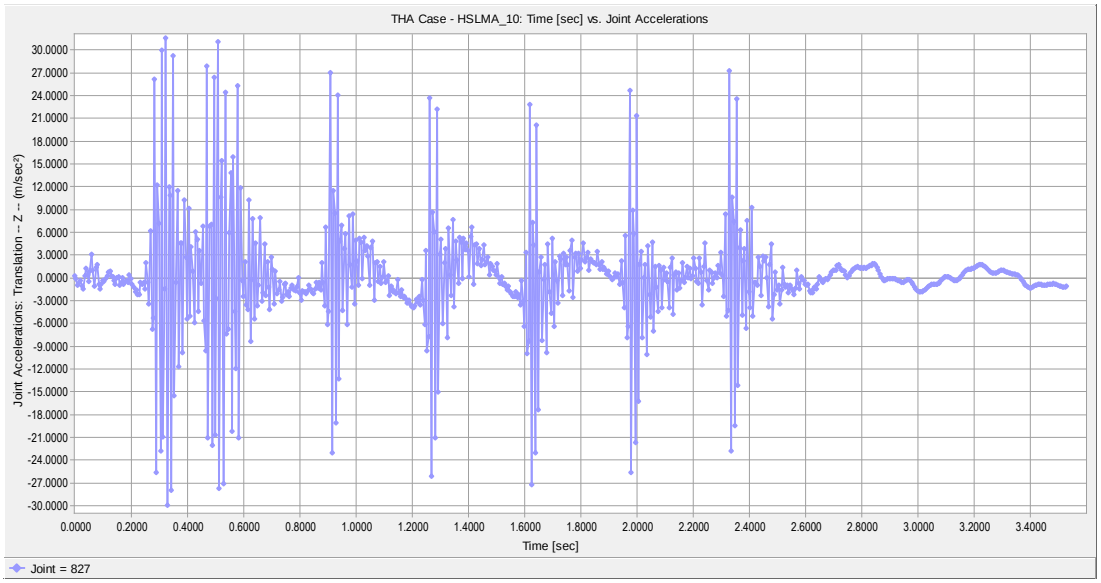

Figure A.46 Joint Acceleration vs. Time graph of the bridge having 24.5 m span length, 1.10 m girder height, 700 MPa ballast stiffness for 76.08 m/s vehicle speed.

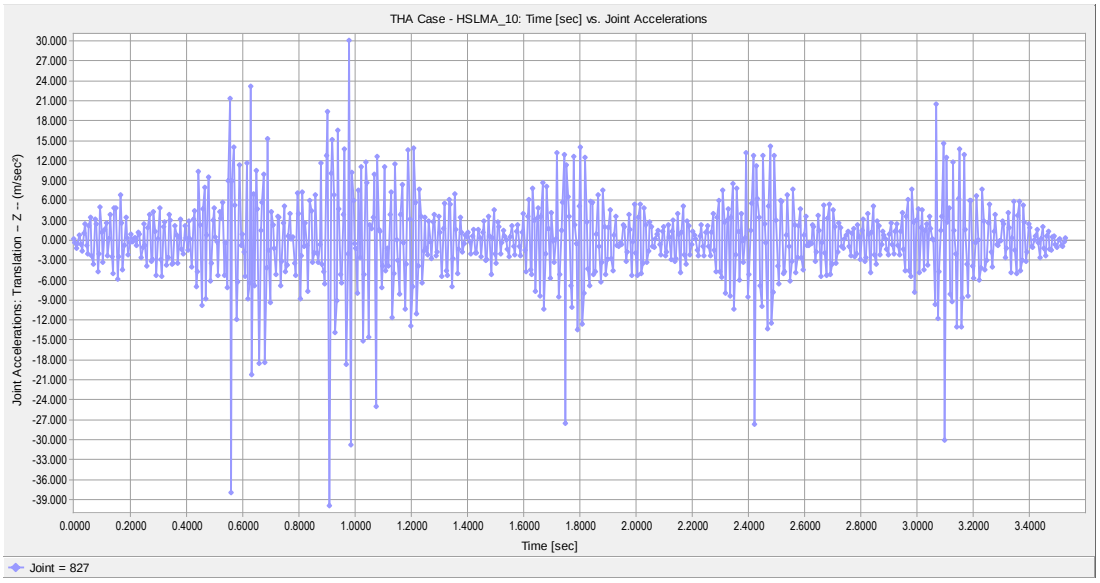

Figure A.47 Joint Acceleration vs. Time graph of the bridge having 24.5 m span length, 1.30 m girder height, 700 MPa ballast stiffness for 40 m/s vehicle speed.

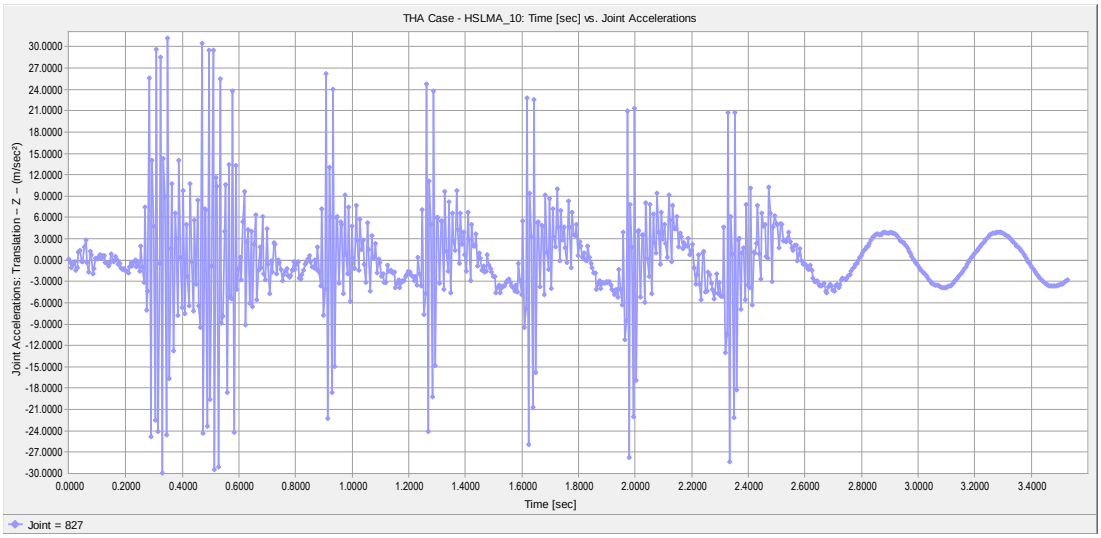

Figure A.48 Joint Acceleration vs. Time graph of the bridge having 24.5 m span length, 1.30 m girder height, 700 MPa ballast stiffness for 76.08 m/s vehicle speed.

A.3 Moving Force Model Joint Displacement Graphs

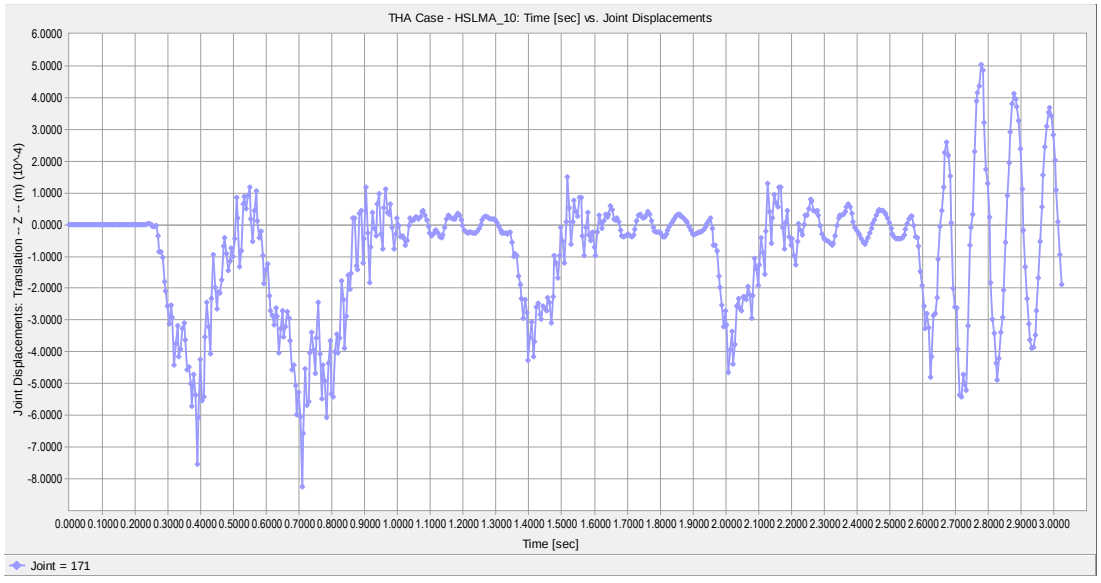

Figure A.49 Joint Displacement vs. Time graph of the bridge having 8.75 m span length, 0.75 m girder height, 300 MPa ballast stiffness for 44.13 m/s vehicle speed.

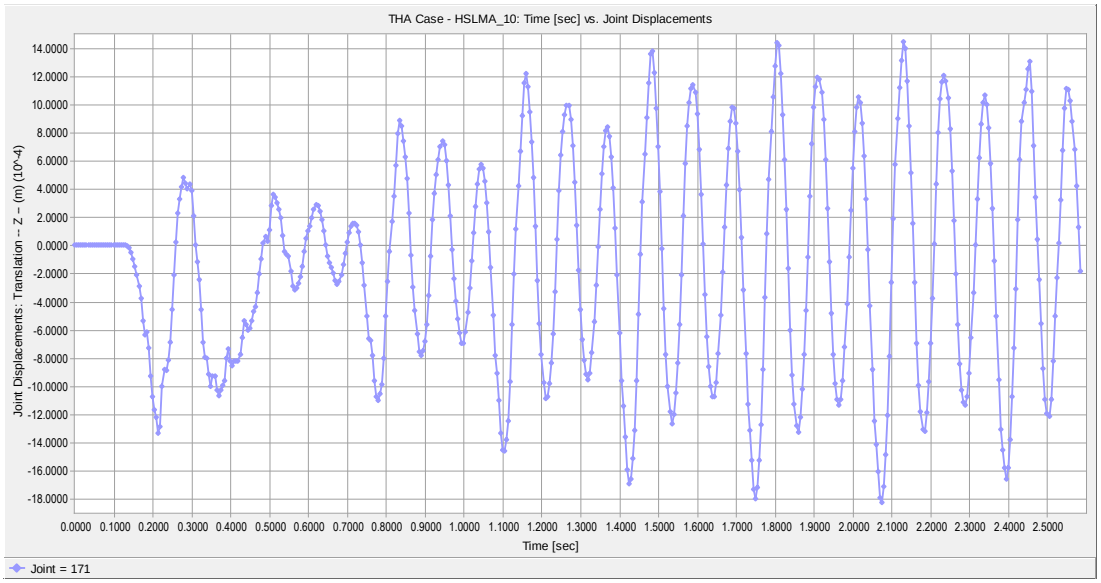

Figure A.50 Joint Displacement vs. Time graph of the bridge having 8.75 m span length, 0.75 m girder height, 300 MPa ballast stiffness for 83 m/s vehicle speed.

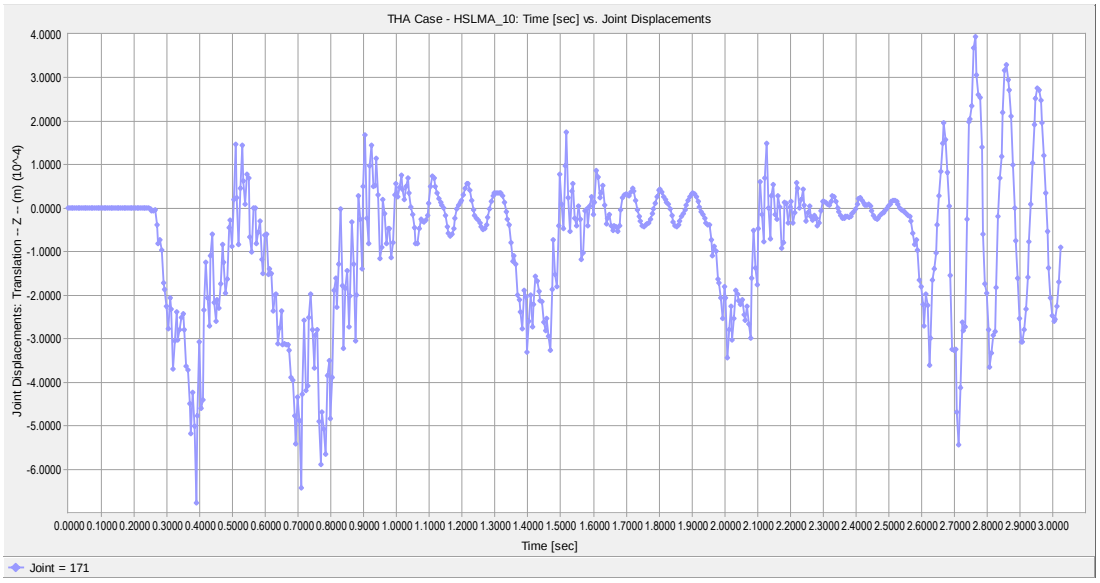

Figure A.51 Joint Displacement vs. Time graph of the bridge having 8.75 m span length, 0.90 m girder height, 300 MPa ballast stiffness for 44.13 m/s vehicle speed.

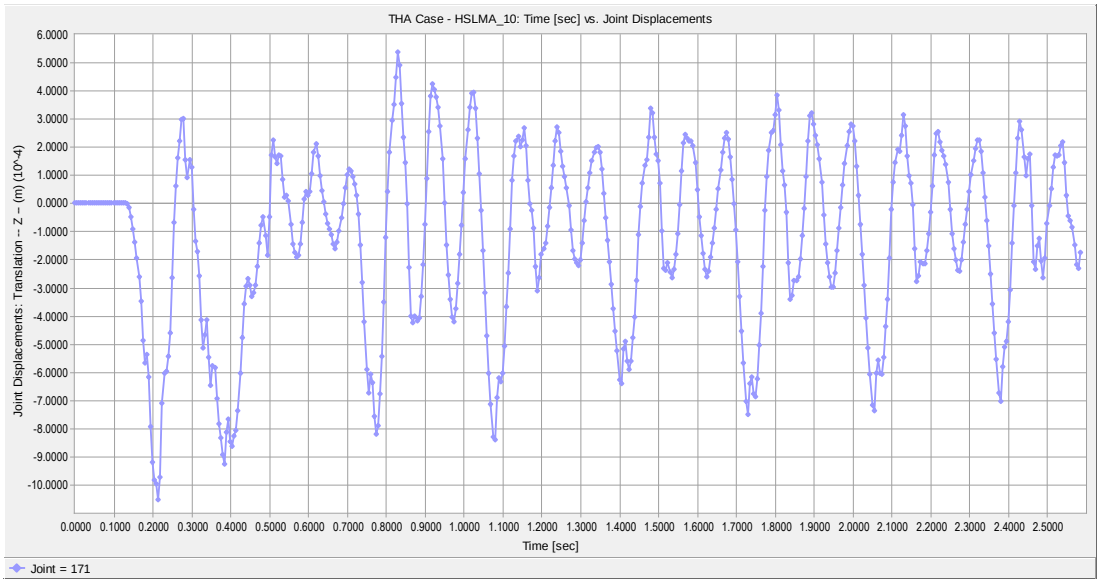

Figure A.52 Joint Displacement vs. Time graph of the bridge having 8.75 m span length, 0.90 m girder height, 300 MPa ballast stiffness for 83 m/s vehicle speed.

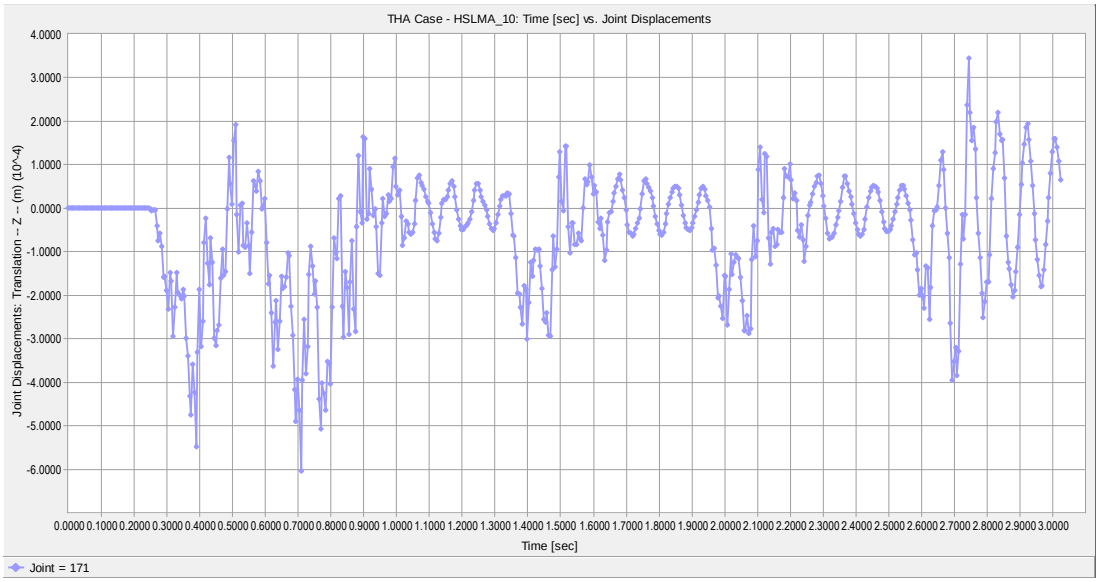

Figure A.53 Joint Displacement vs. Time graph of the bridge having 8.75 m span length, 1.10 m girder height, 300 MPa ballast stiffness for 44.13 m/s vehicle speed.

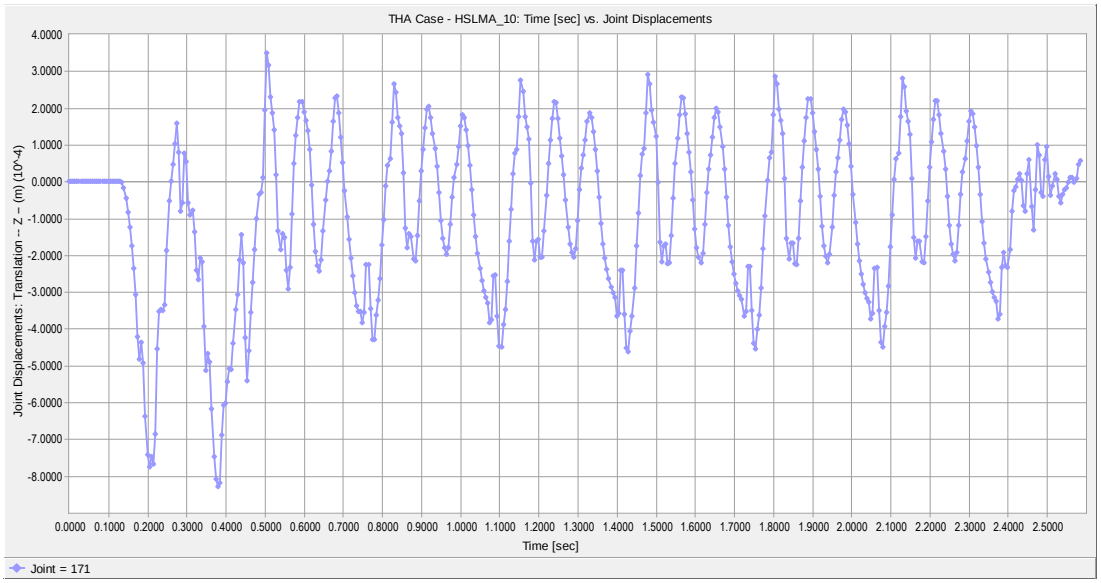

Figure A.54 Joint Displacement vs. Time graph of the bridge having 8.75 m span length, 1.10 m girder height, 300 MPa ballast stiffness for 83 m/s vehicle speed.

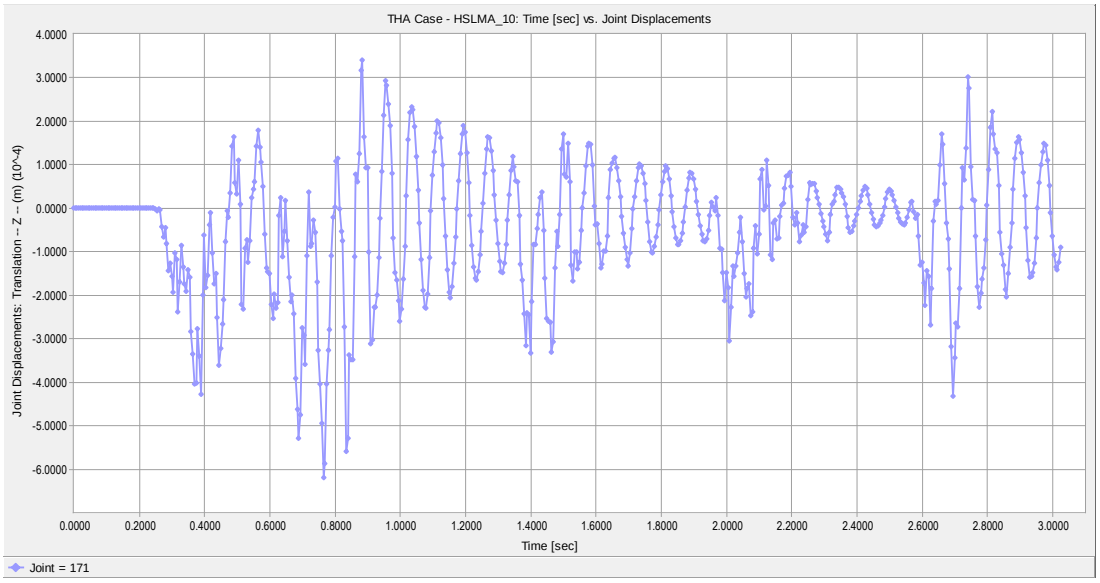

Figure A.55 Joint Displacement vs. Time graph of the bridge having 8.75 m span length, 1.30 m girder height, 300 MPa ballast stiffness for 44.13 m/s vehicle speed.

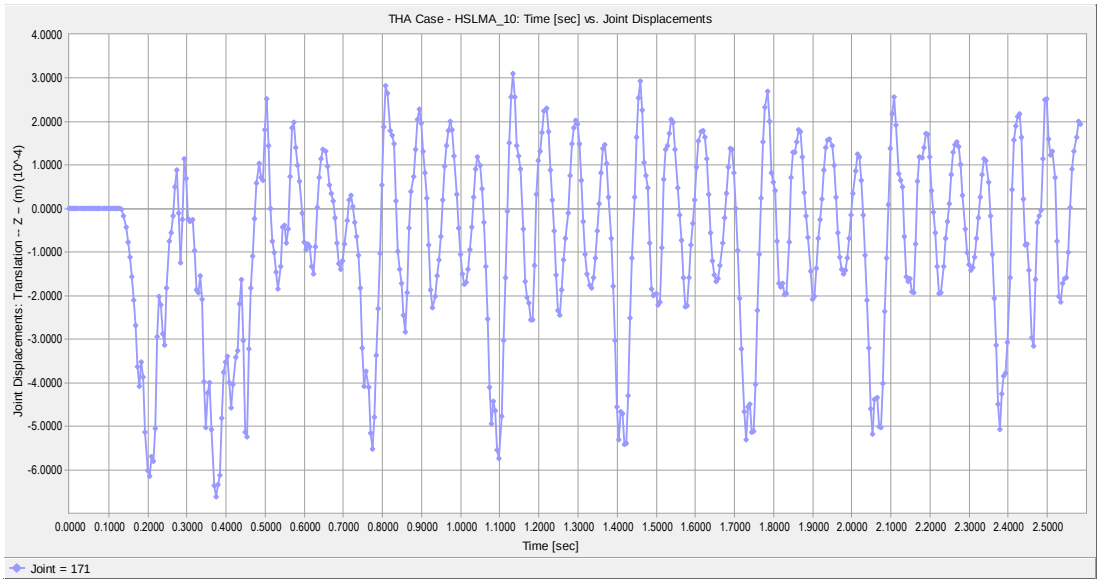

Figure A.56 Joint Displacement vs. Time graph of the bridge having 8.75 m span length, 1.30 m girder height, 300 MPa ballast stiffness for 83 m/s vehicle speed.

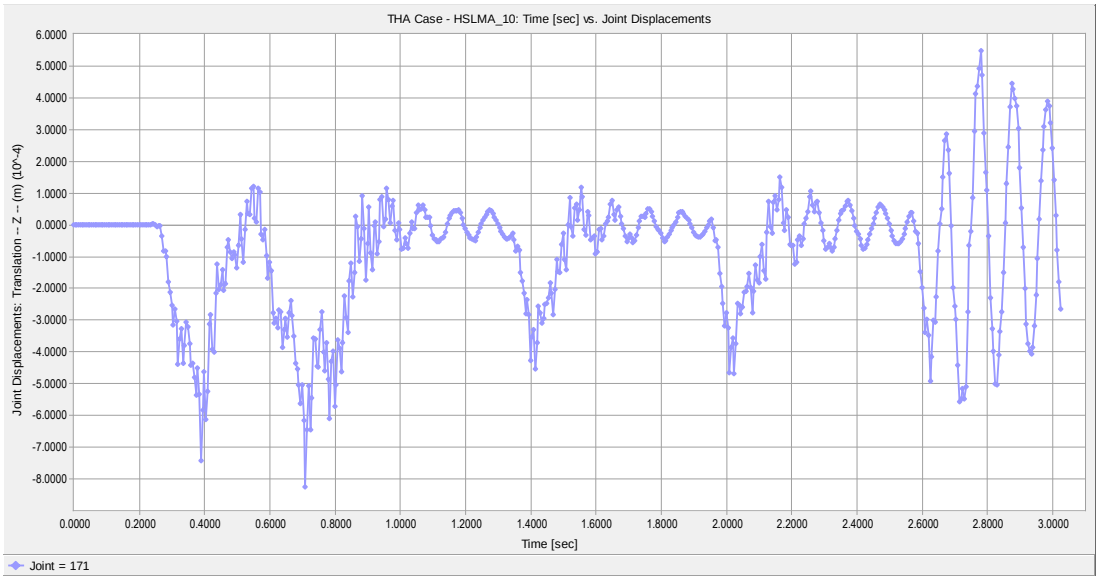

Figure A.57 Joint Displacement vs. Time graph of the bridge having 8.75 m span length, 0.75 m girder height, 700 MPa ballast stiffness for 44.13 m/s vehicle speed.

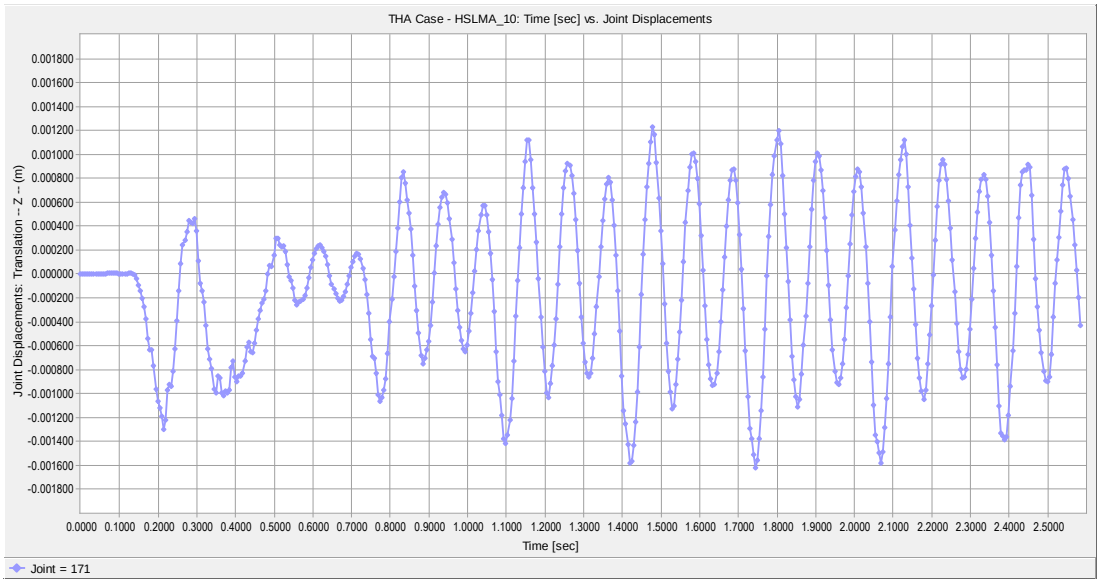

Figure A.58 Joint Displacement vs. Time graph of the bridge having 8.75 m span length, 0.75 m girder height, 700 MPa ballast stiffness for 83 m/s vehicle speed.

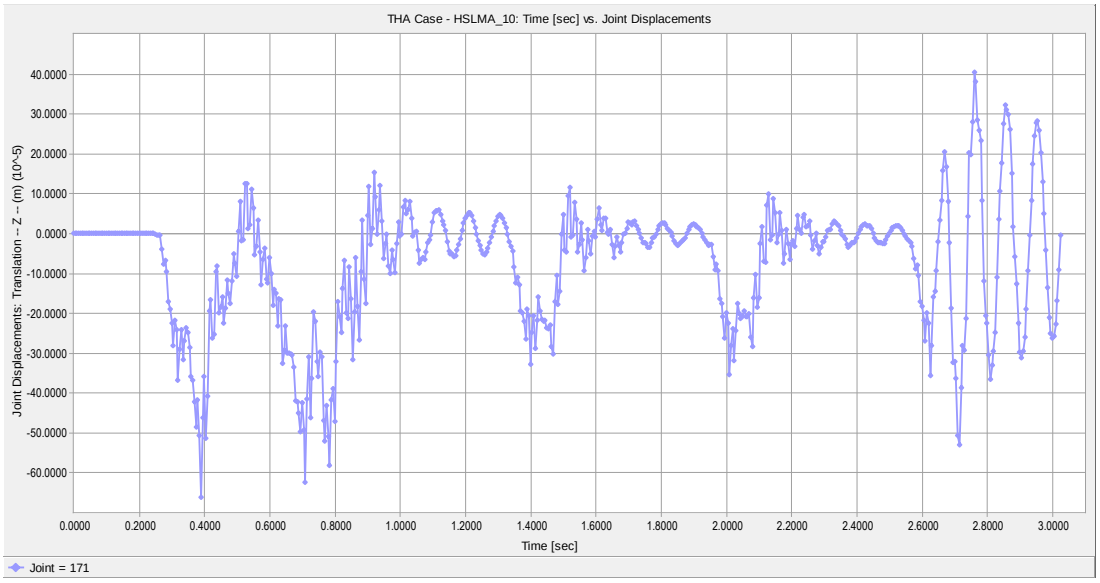

Figure A.59 Joint Displacement vs. Time graph of the bridge having 8.75 m span length, 0.90 m girder height, 700 MPa ballast stiffness for 44.13 m/s vehicle speed.

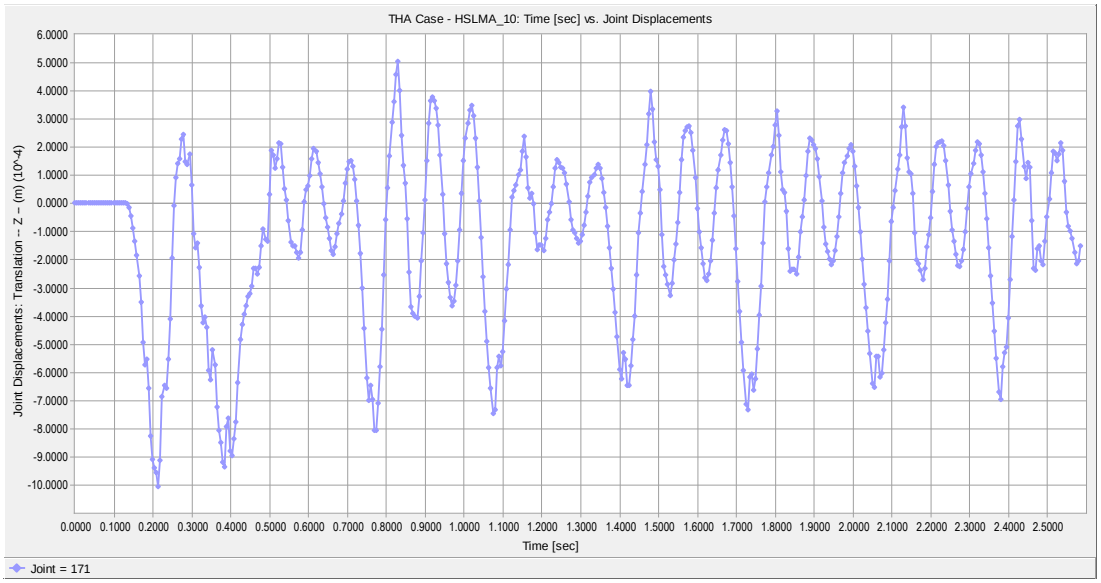

Figure A.60 Joint Displacement vs. Time graph of the bridge having 8.75 m span length, 0.90 m girder height, 700 MPa ballast stiffness for 83 m/s vehicle speed.

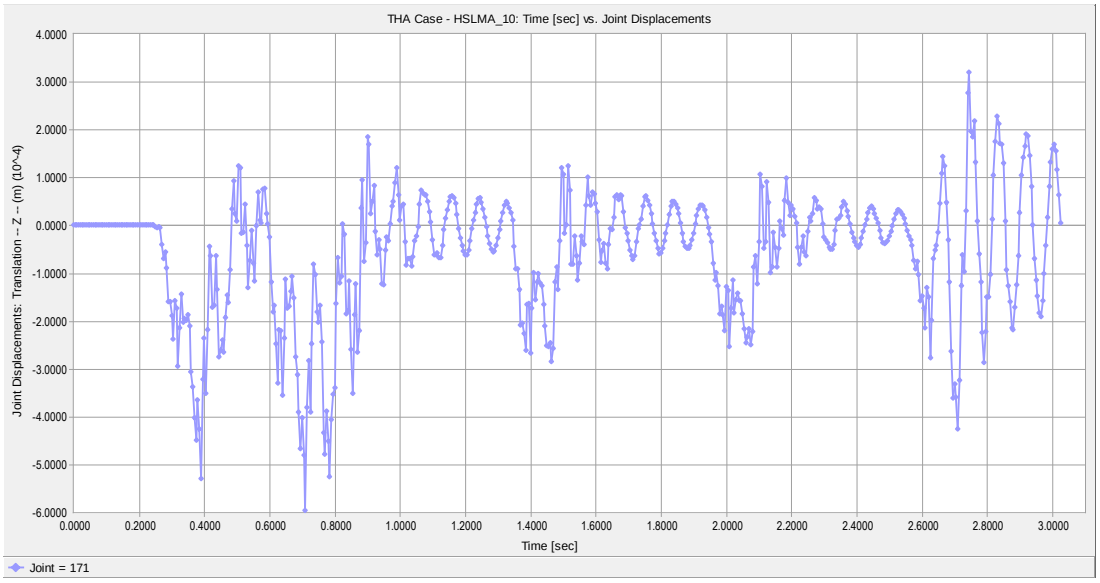

Figure A.61 Joint Displacement vs. Time graph of the bridge having 8.75 m span length, 1.10 m girder height, 700 MPa ballast stiffness for 44.13 m/s vehicle speed.

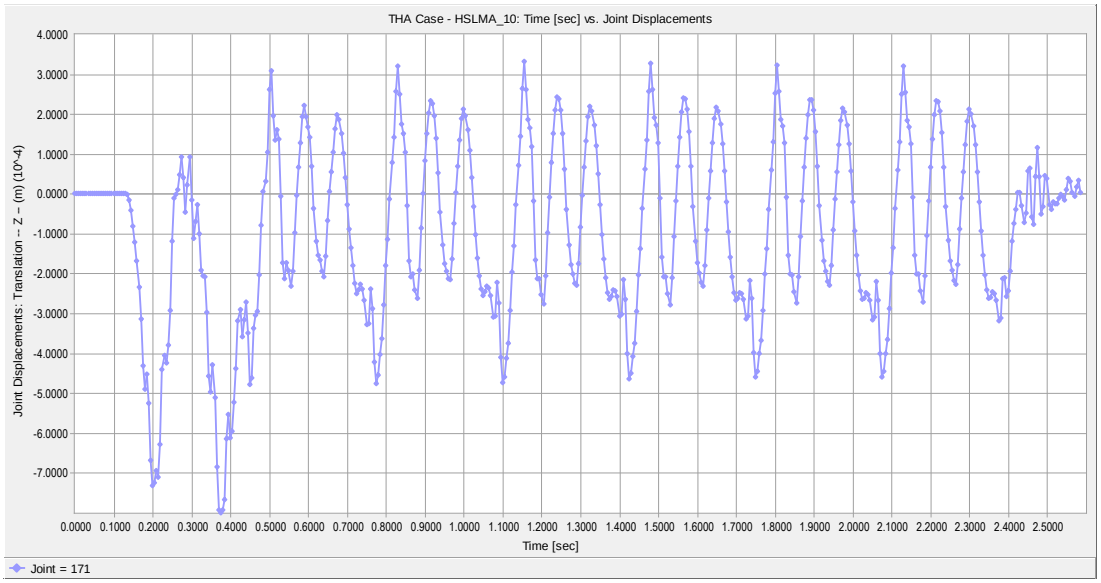

Figure A.62 Joint Displacement vs. Time graph of the bridge having 8.75 m span length, 1.10 m girder height, 700 MPa ballast stiffness for 83 m/s vehicle speed.

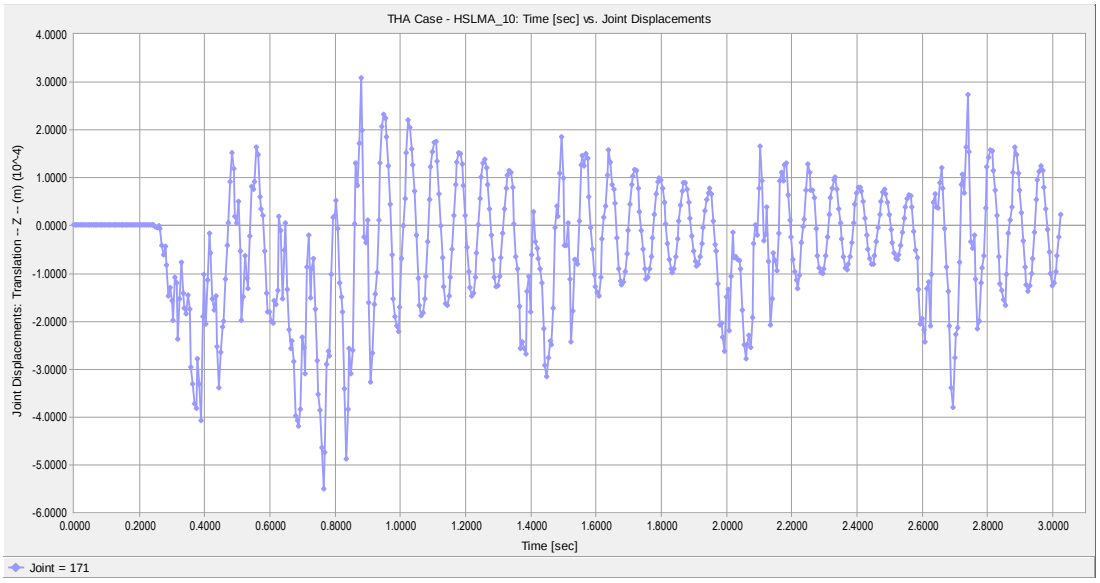

Figure A.63 Joint Displacement vs. Time graph of the bridge having 8.75 m span length, 1.30 m girder height, 700 MPa ballast stiffness for 44.13 m/s vehicle speed.

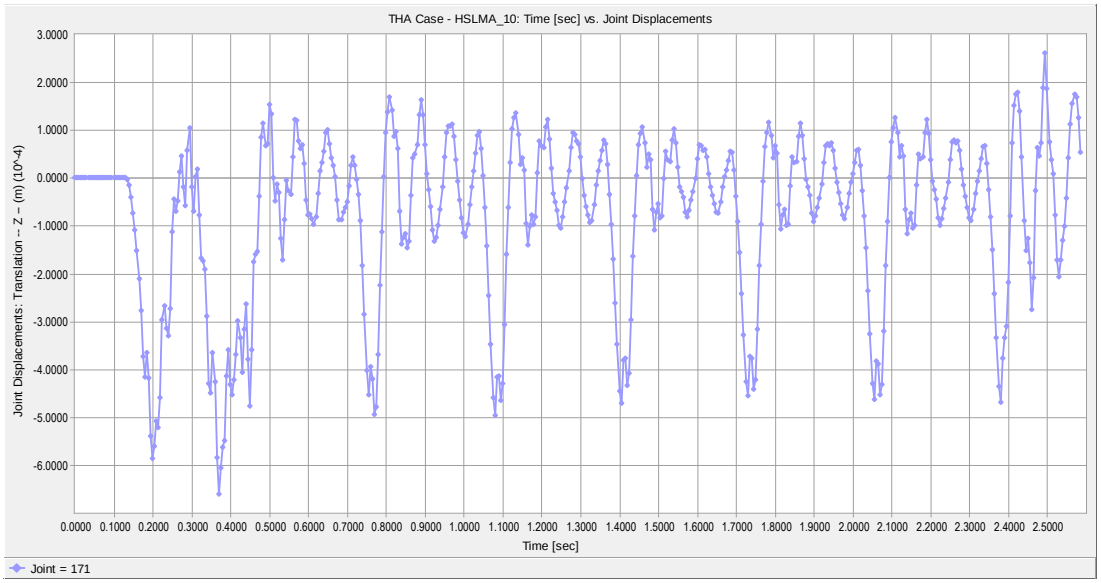

Figure A.64 Joint Displacement vs. Time graph of the bridge having 8.75 m span length, 1.30 m girder height, 700 MPa ballast stiffness for 83 m/s vehicle speed.

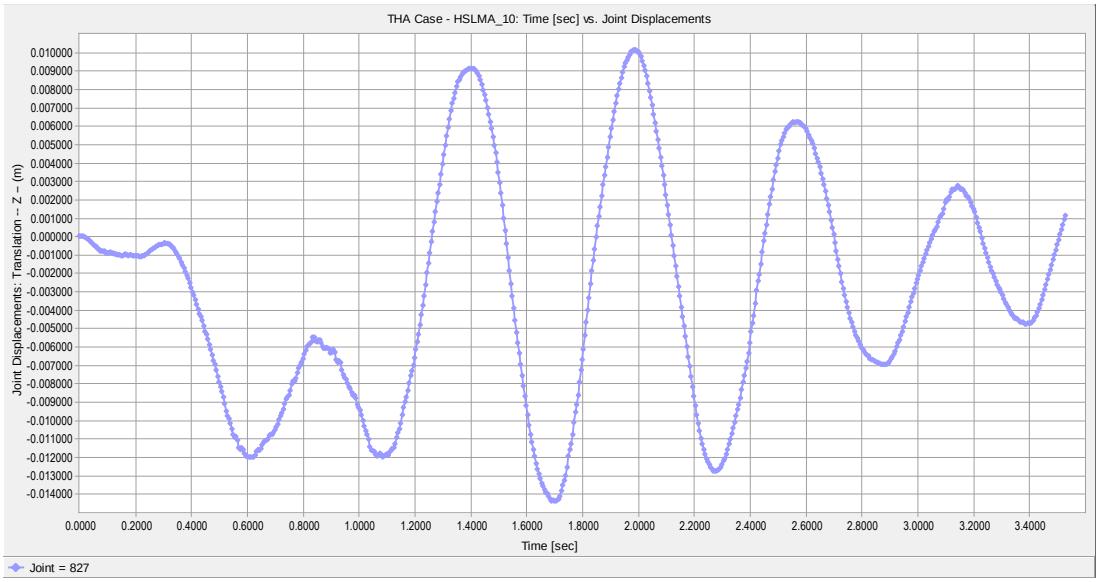

Figure A.65 Joint Displacement vs. Time graph of the bridge having 24.5 m span length, 0.75 m girder height, 300 MPa ballast stiffness for 40 m/s vehicle speed.

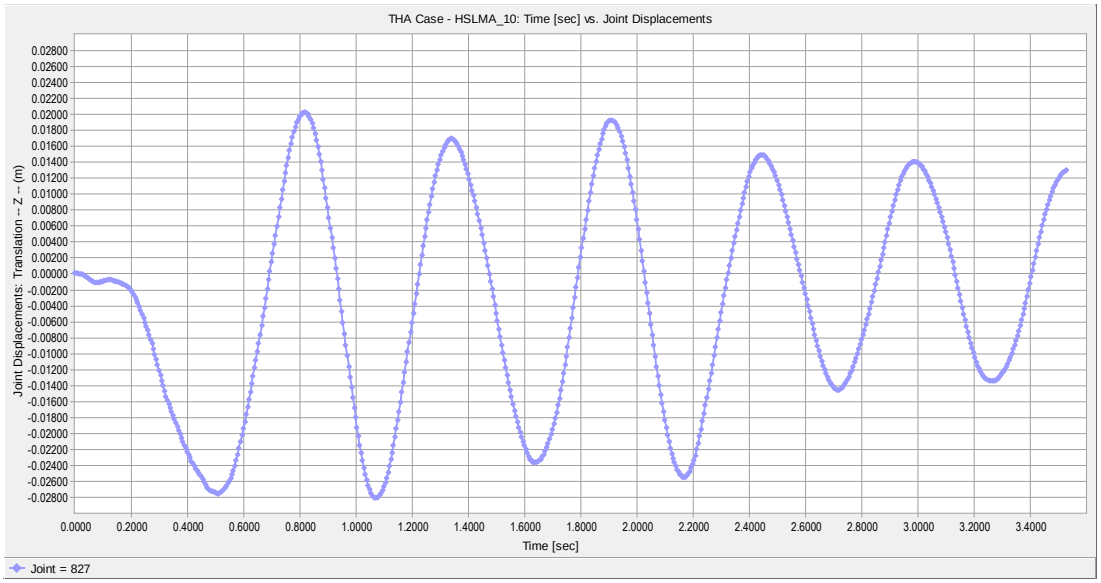

Figure A.66 Joint Displacement vs. Time graph of the bridge having 24.5 m span length, 0.75 m girder height, 300 MPa ballast stiffness for 76.08 m/s vehicle speed.

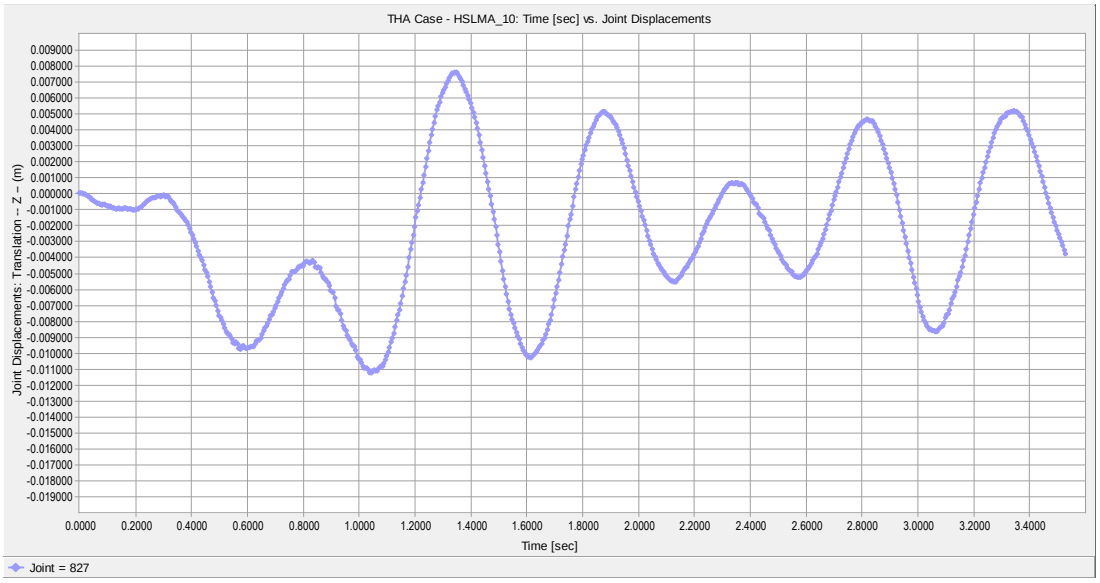

Figure A.67 Joint Displacement vs. Time graph of the bridge having 24.5 m span length, 0.90 m girder height, 300 MPa ballast stiffness for 40 m/s vehicle speed.

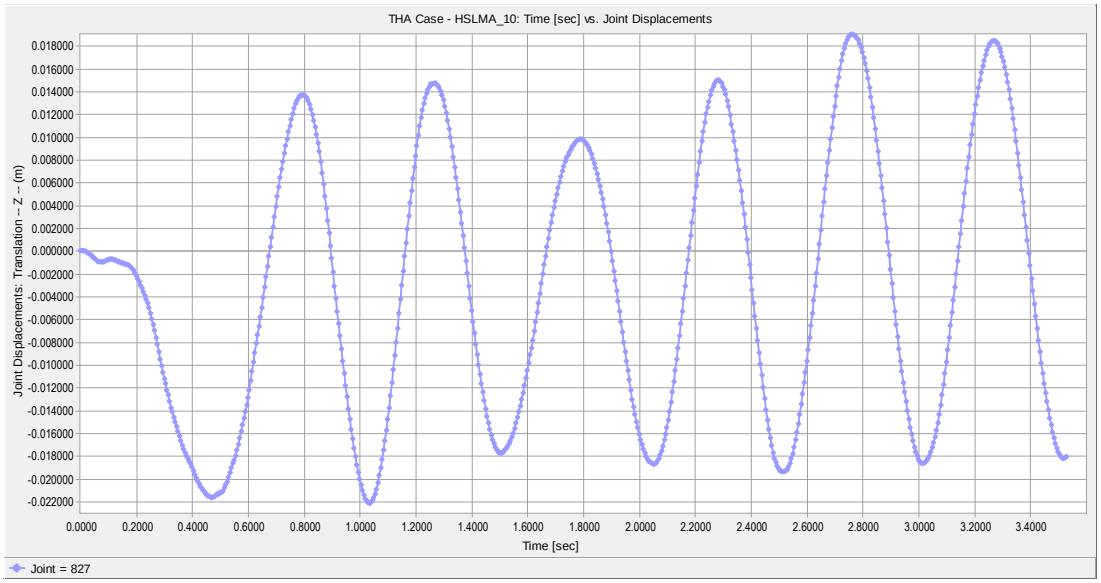

Figure A.68 Joint Displacement vs. Time graph of the bridge having 24.5 m span length, 0.90 m girder height, 300 MPa ballast stiffness for 76.08 m/s vehicle speed.

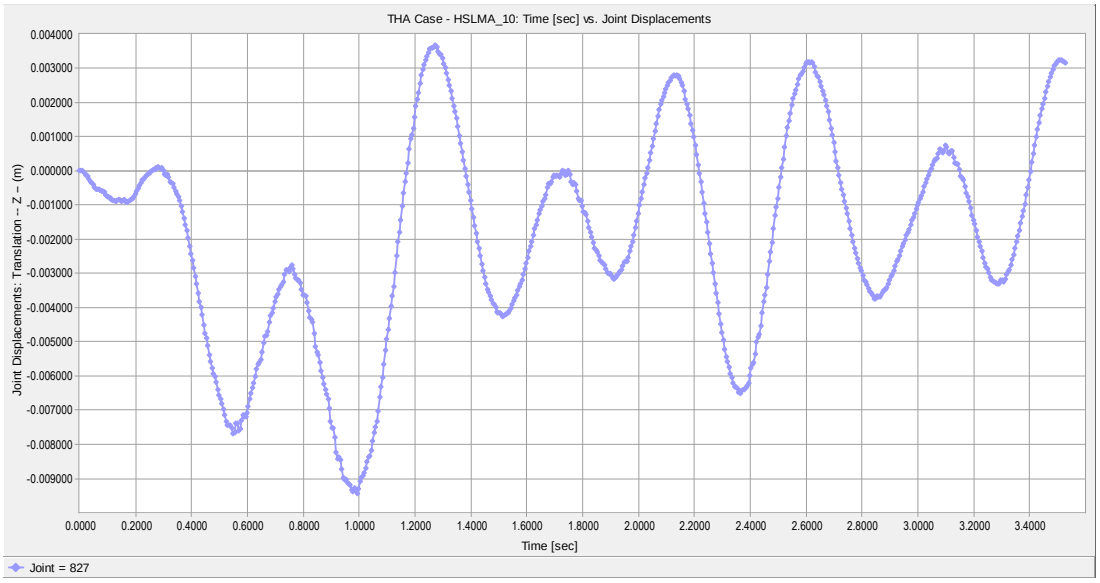

Figure A.69 Joint Displacement vs. Time graph of the bridge having 24.5 m span length, 1.10 m girder height, 300 MPa ballast stiffness for 40 m/s vehicle speed.

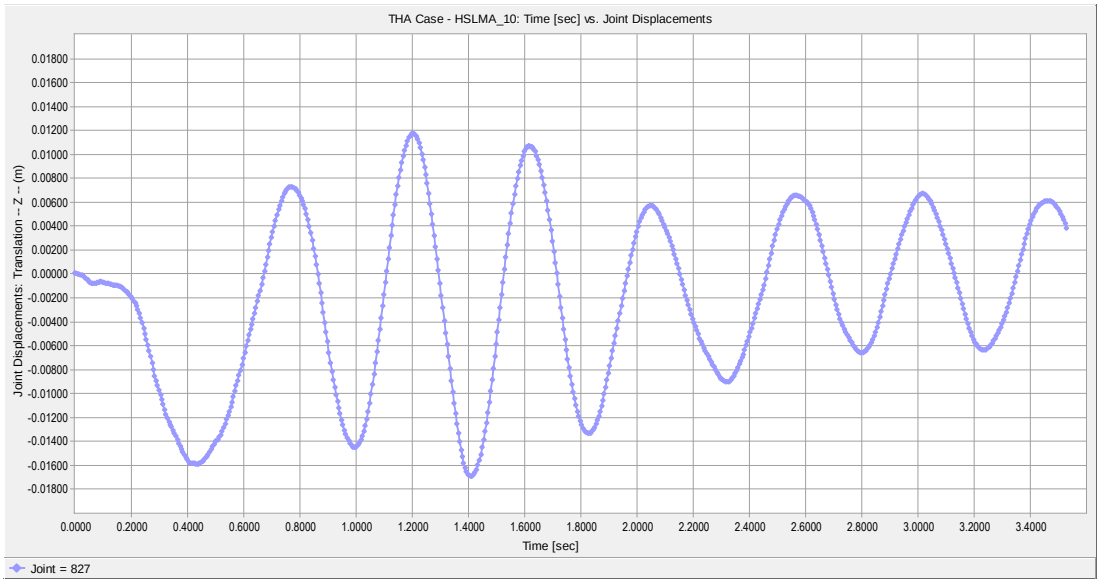

Figure A.70 Joint Displacement vs. Time graph of the bridge having 24.5 m span length, 1.10 m girder height, 300 MPa ballast stiffness for 76.08 m/s vehicle speed.

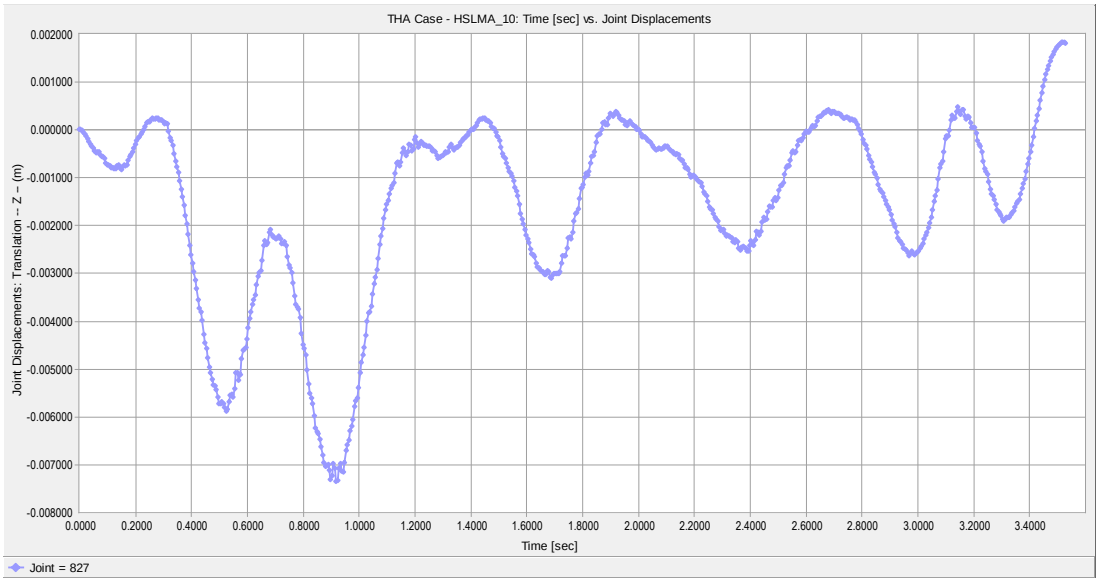

Figure A.71 Joint Displacement vs. Time graph of the bridge having 24.5 m span length, 1.30 m girder height, 300 MPa ballast stiffness for 40 m/s vehicle speed.

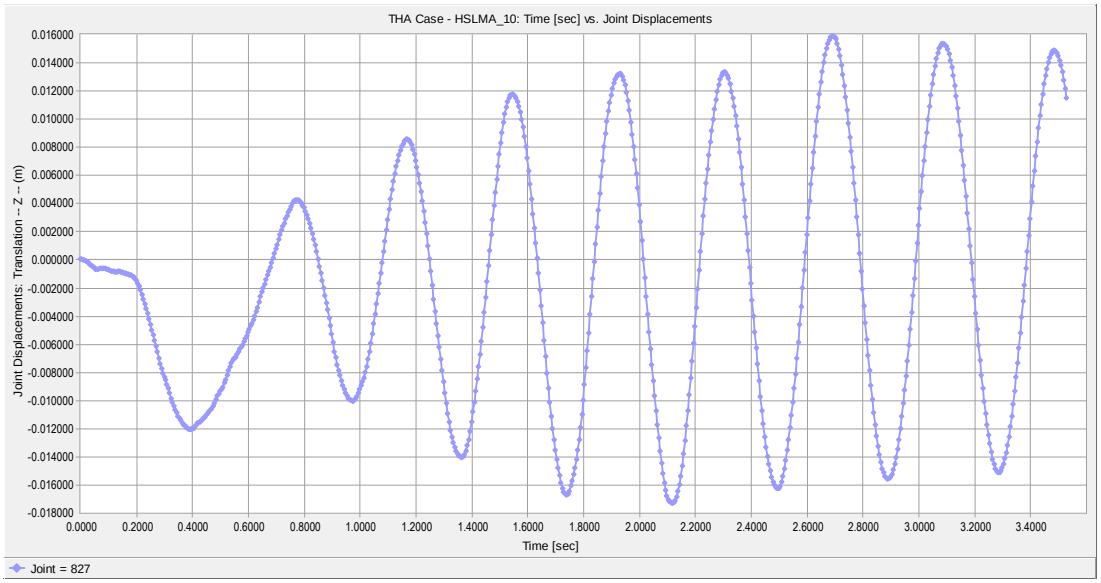

Figure A.72 Joint Displacement vs. Time graph of the bridge having 24.5 m span length, 1.30 m girder height, 300 MPa ballast stiffness for 76.08 m/s vehicle speed.

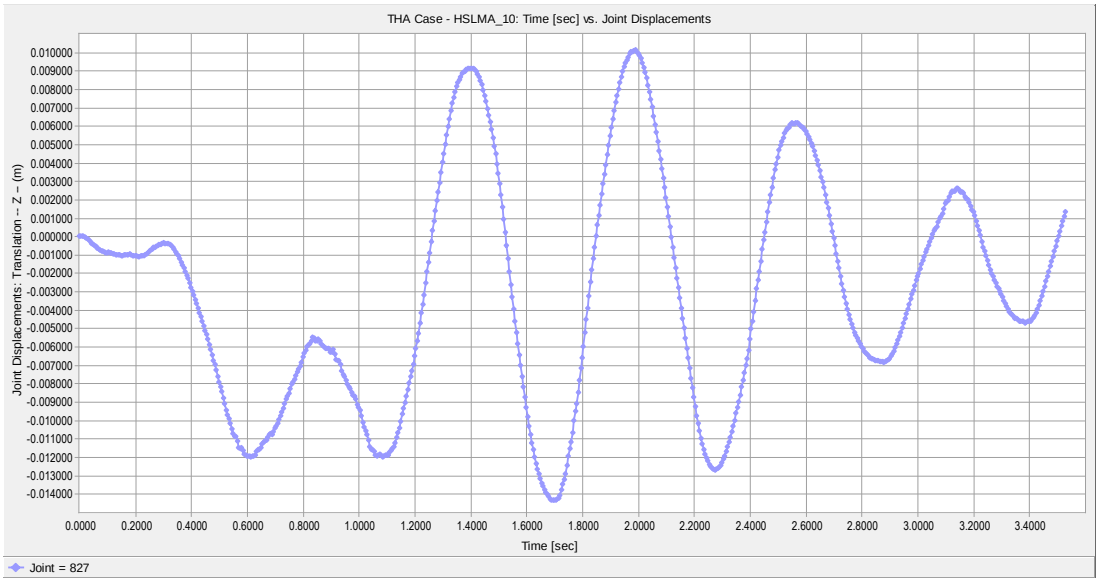

Figure A.73 Joint Displacement vs. Time graph of the bridge having 24.5 m span length, 0.75 m girder height, 700 MPa ballast stiffness for 40 m/s vehicle speed.

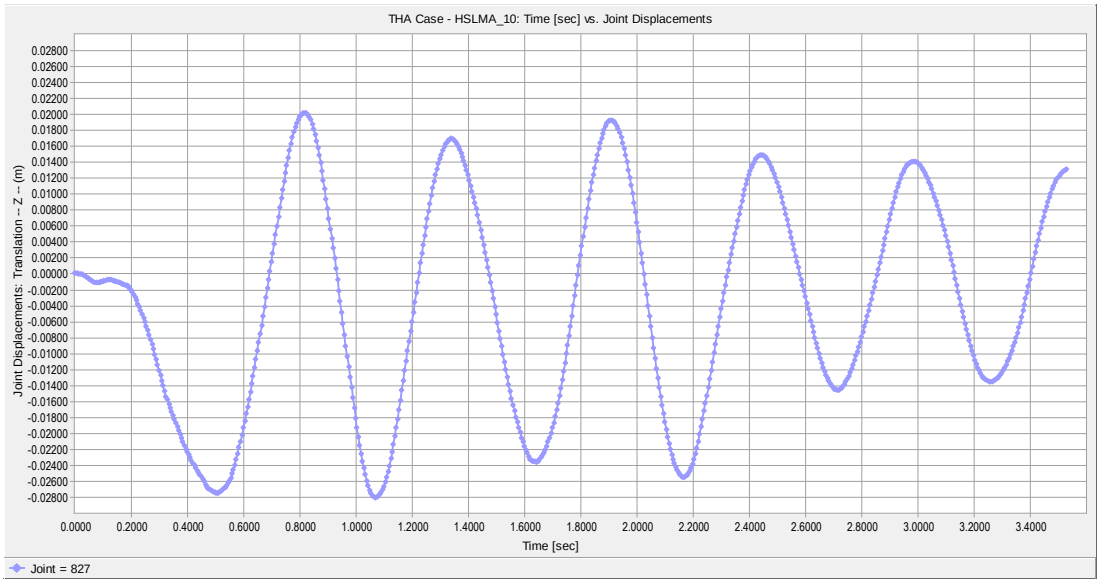

Figure A.74 Joint Displacement vs. Time graph of the bridge having 24.5 m span length, 0.75 m girder height, 700 MPa ballast stiffness for 76.08 m/s vehicle speed.

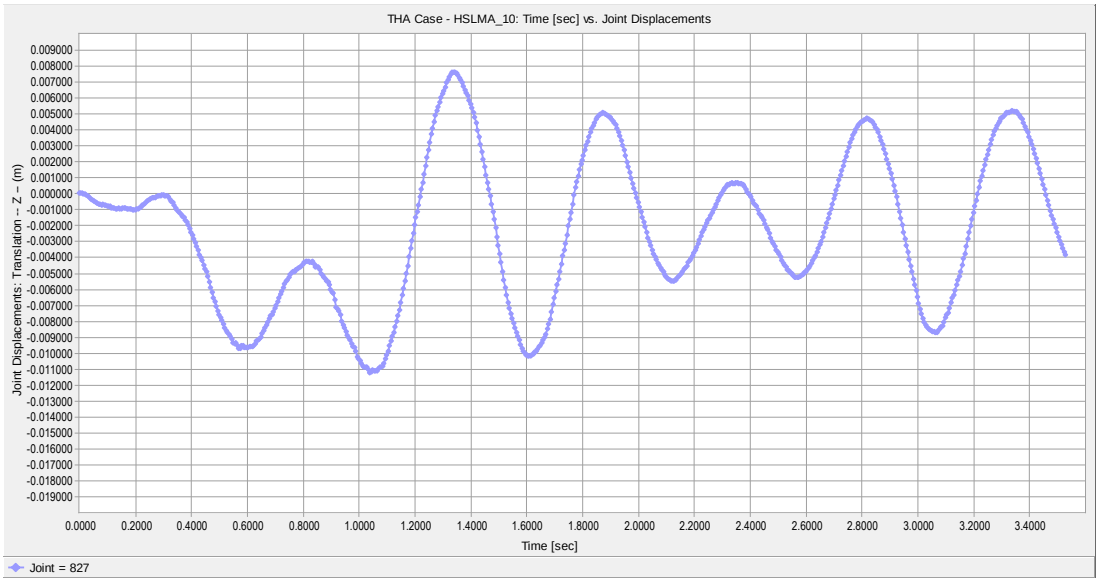

Figure A.75 Joint Displacement vs. Time graph of the bridge having 24.5 m span length, 0.90 m girder height, 700 MPa ballast stiffness for 40 m/s vehicle speed.

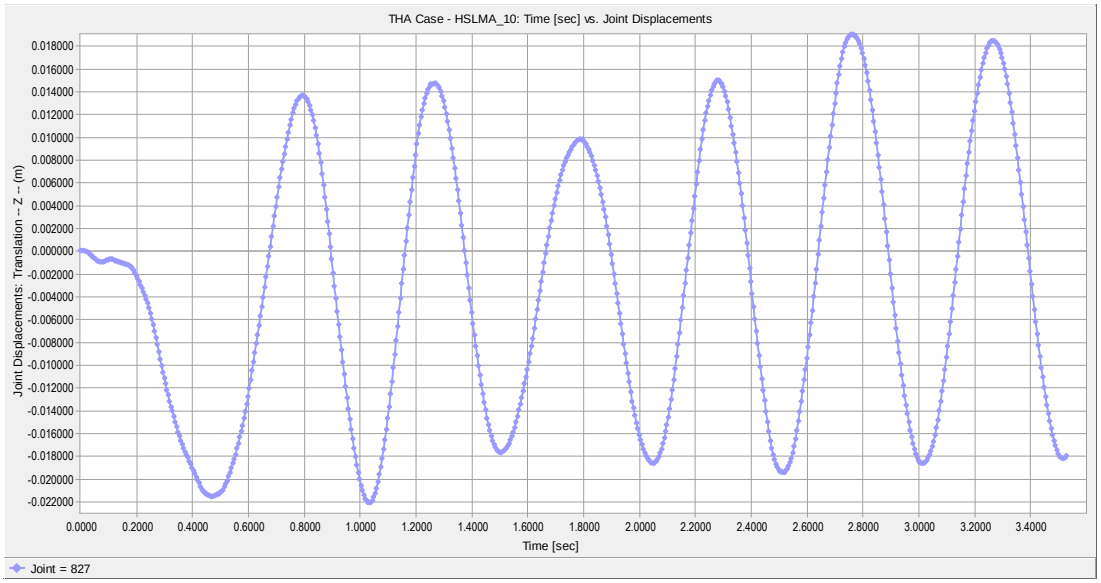

Figure A.76 Joint Displacement vs. Time graph of the bridge having 24.5 m span length, 0.90 m girder height, 700 MPa ballast stiffness for 76.08 m/s vehicle speed.

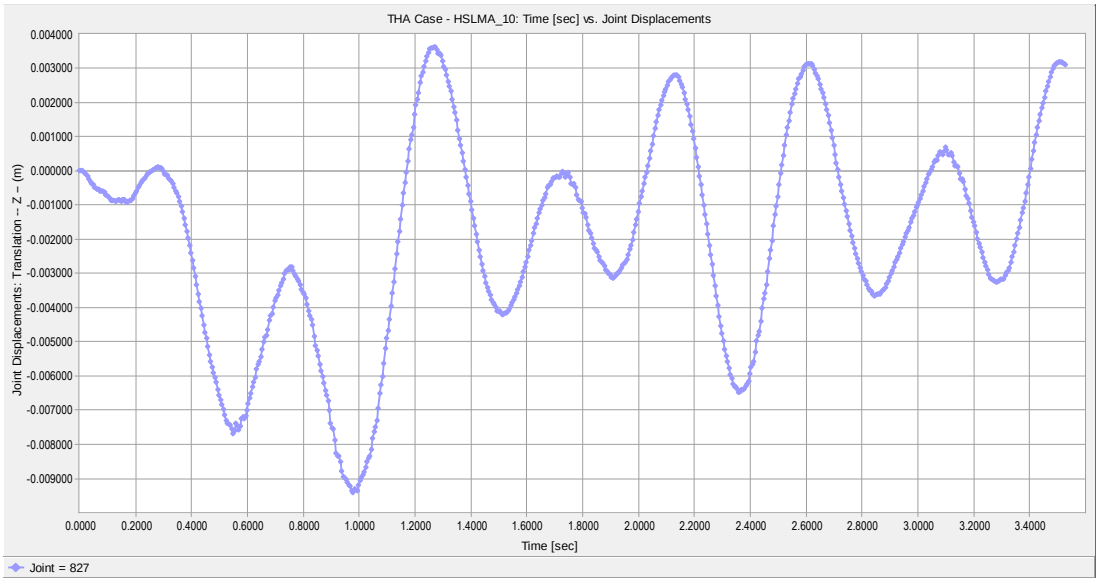

Figure A.77 Joint Displacement vs. Time graph of the bridge having 24.5 m span length, 1.10 m girder height, 700 MPa ballast stiffness for 40 m/s vehicle speed.

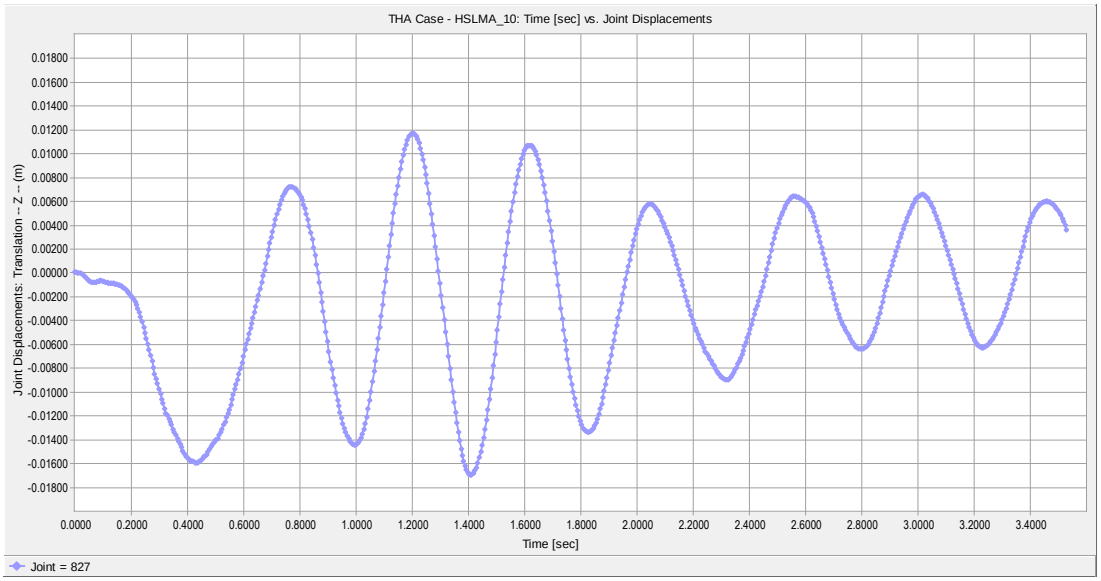

Figure A.78 Joint Displacement vs. Time graph of the bridge having 24.5 m span length, 1.10 m girder height, 700 MPa ballast stiffness for 76.08 m/s vehicle speed.

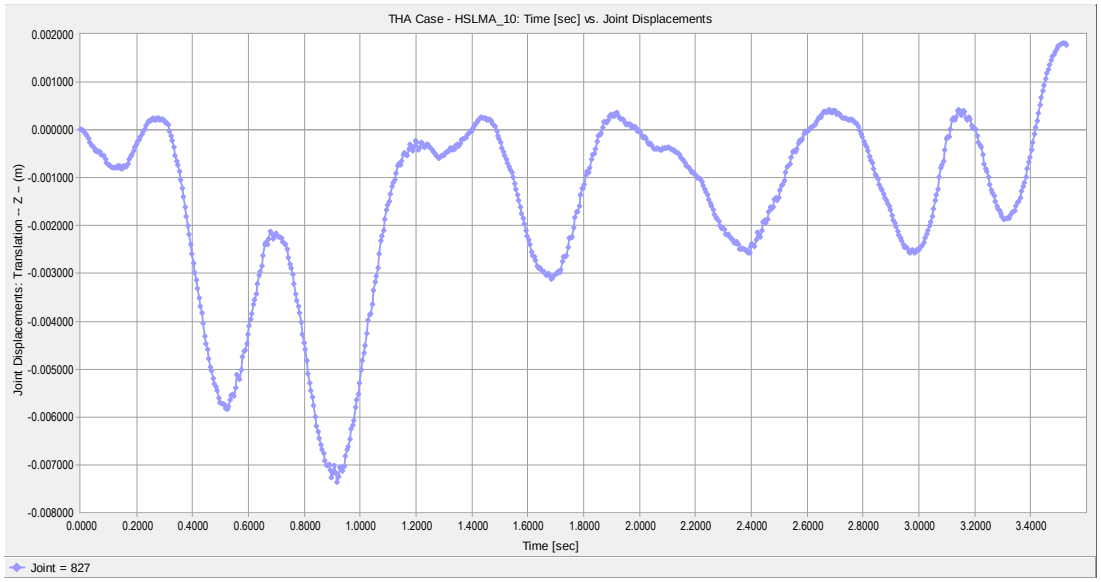

Figure A.79 Joint Displacement vs. Time graph of the bridge having 24.5 m span length, 1.30 m girder height, 700 MPa ballast stiffness for 40 m/s vehicle speed.

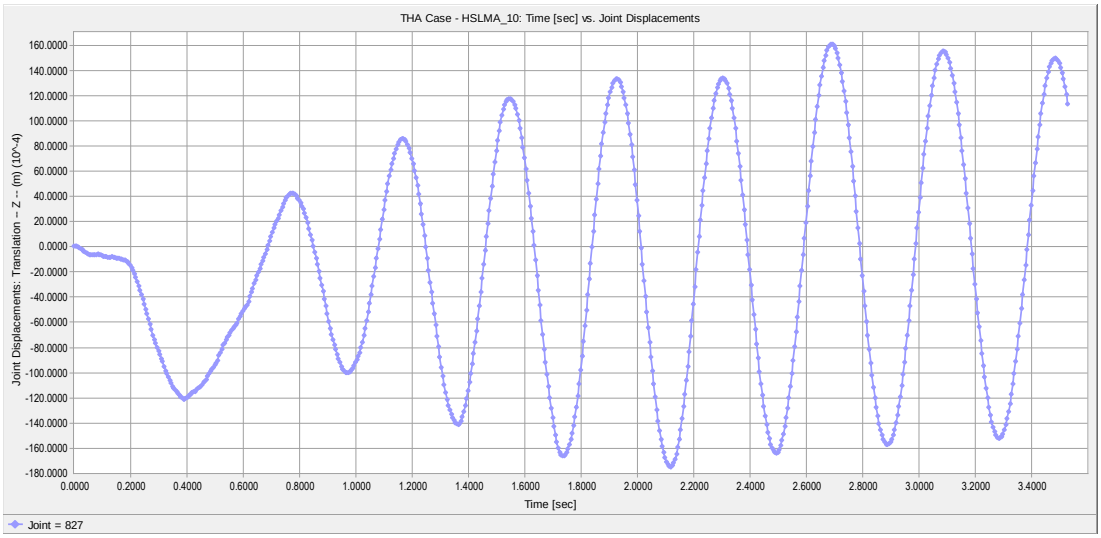

Figure A.80 Joint Displacement vs. Time graph of the bridge having 24.5 m span length, 1.30 m girder height, 700 MPa ballast stiffness for 76.08 m/s vehicle speed.

A.4 Moving Force Model Deck Twist Graphs

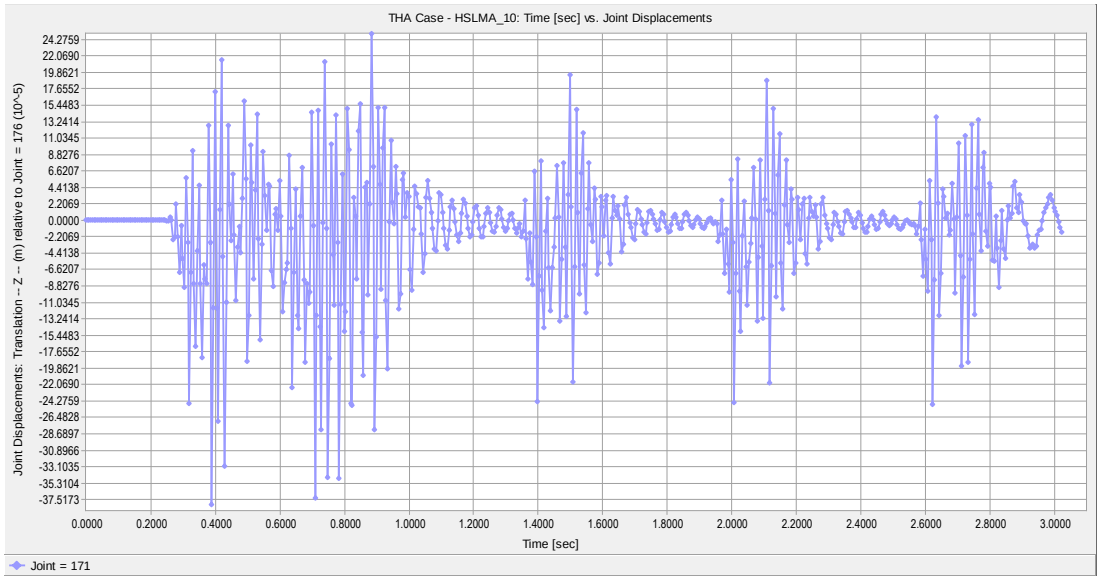

Figure A.81 Deck Twist vs. Time graph of the bridge having 8.75 m span length, 0.75 m girder height, 300 MPa ballast stiffness for 44.13 m/s vehicle speed.

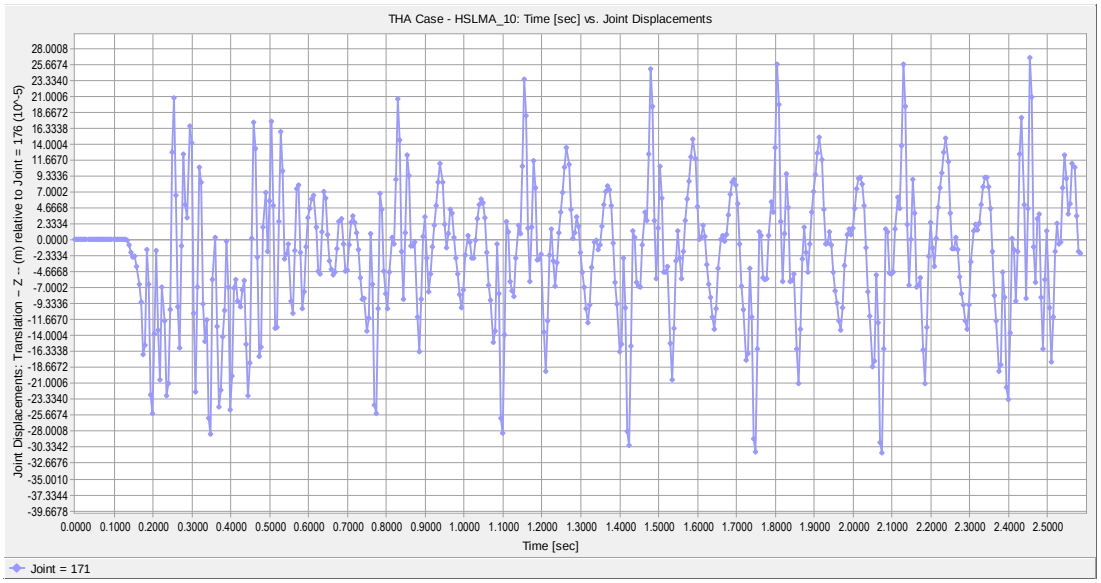

Figure A.82 Deck Twist vs. Time graph of the bridge having 8.75 m span length, 0.75 m girder height, 300 MPa ballast stiffness for 83 m/s vehicle speed.

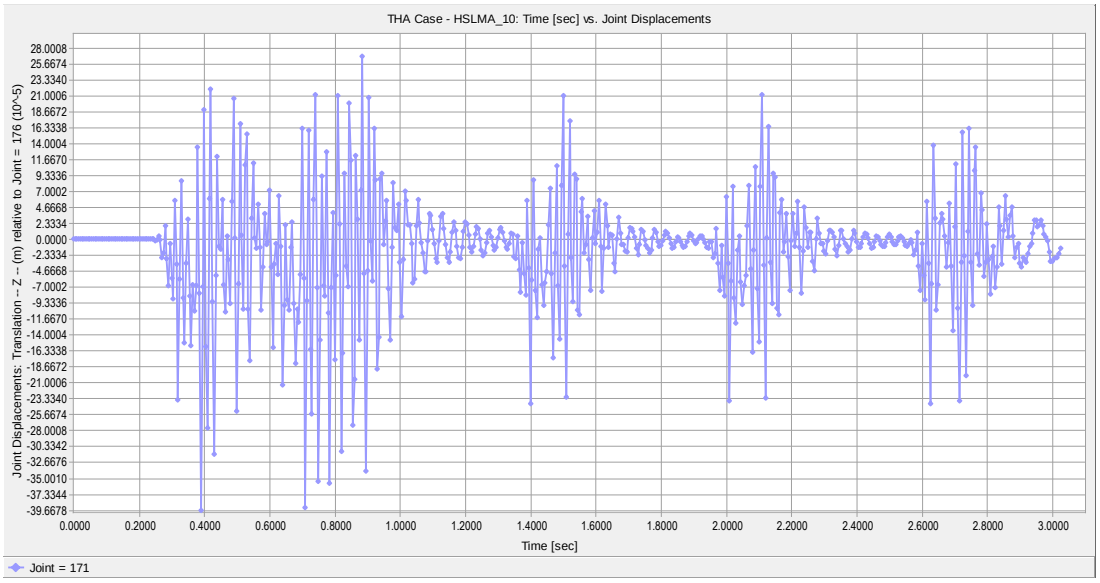

Figure A.83 Deck Twist vs. Time graph of the bridge having 8.75 m span length, 0.90 m girder height, 300 MPa ballast stiffness for 44.13 m/s vehicle speed.

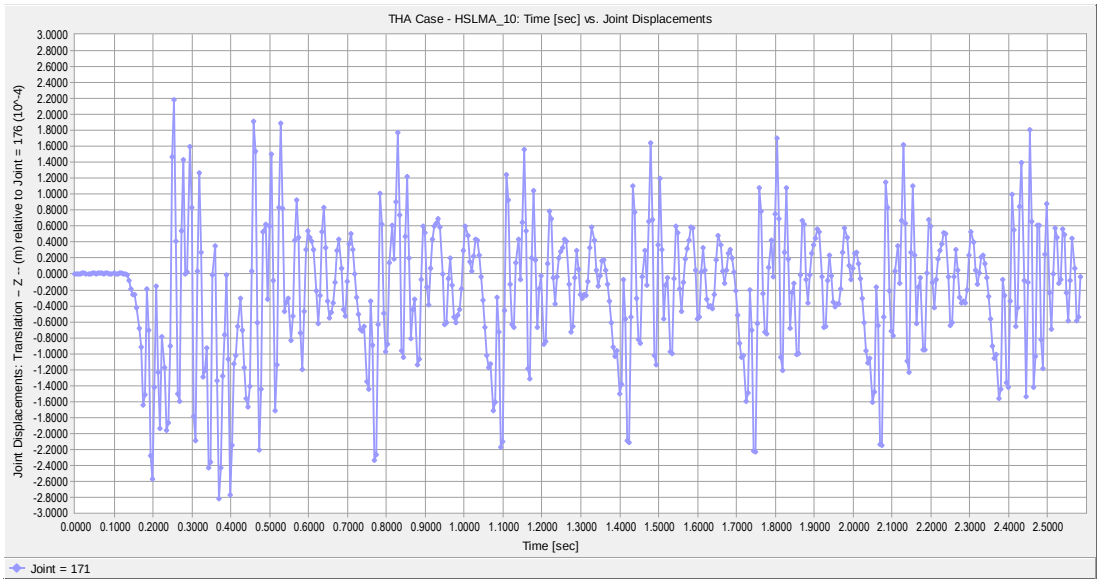

Figure A.84 Deck Twist vs. Time graph of the bridge having 8.75 m span length, 0.90 m girder height, 300 MPa ballast stiffness for 83 m/s vehicle speed.

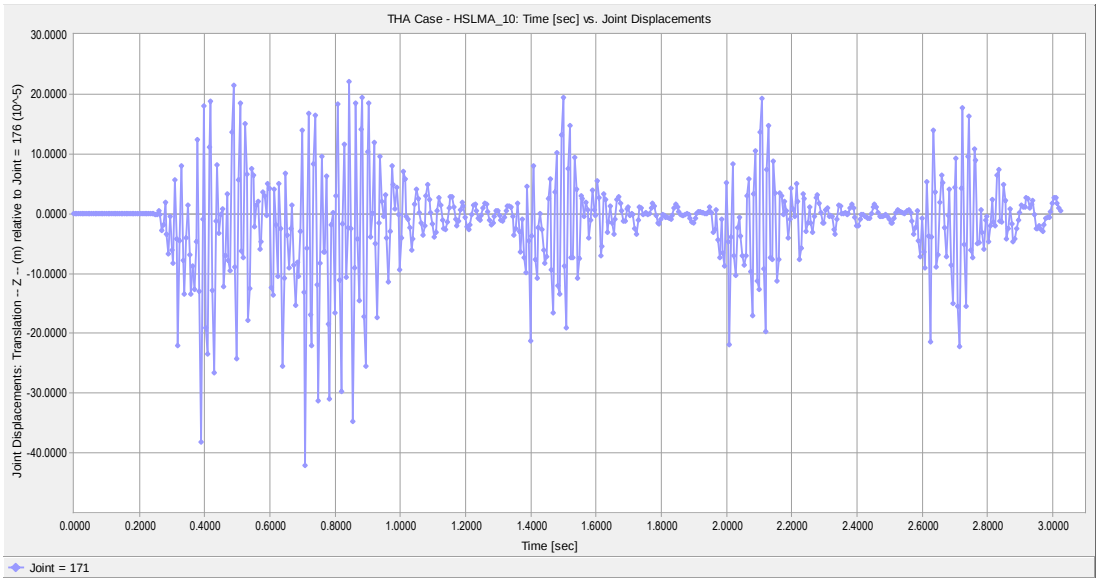

Figure A.85 Deck Twist vs. Time graph of the bridge having 8.75 m span length, 1.10 m girder height, 300 MPa ballast stiffness for 44.13 m/s vehicle speed.

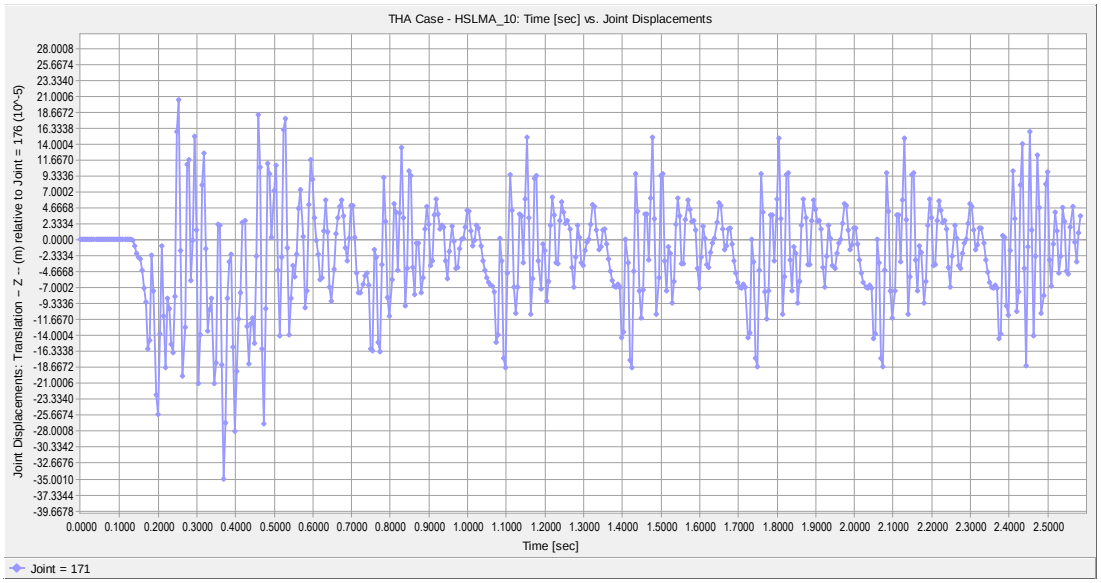

Figure A.86 Deck Twist vs. Time graph of the bridge having 8.75 m span length, 1.10 m girder height, 300 MPa ballast stiffness for 83 m/s vehicle speed.

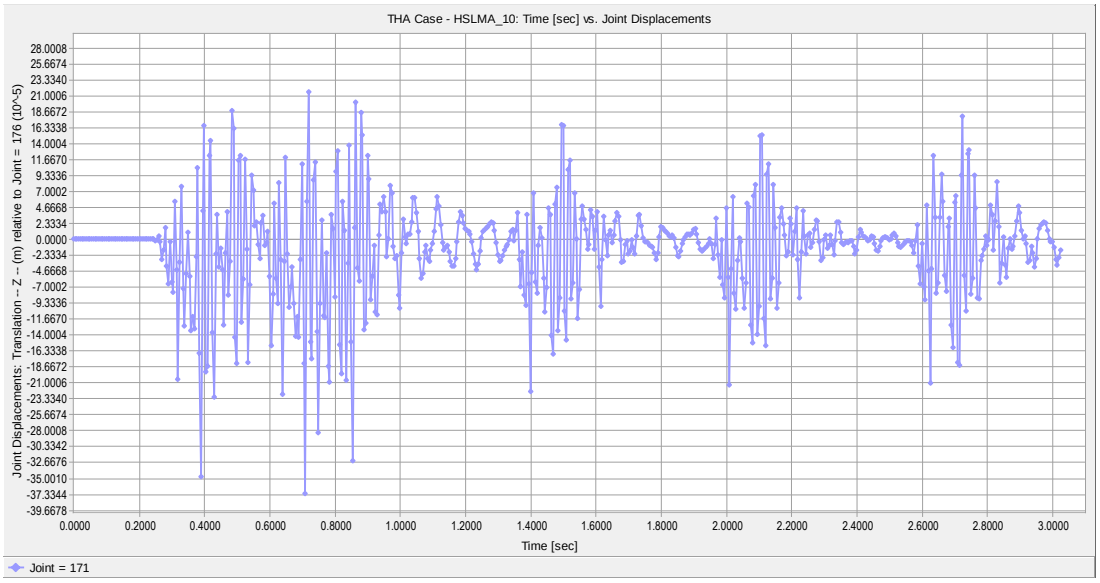

Figure A.87 Deck Twist vs. Time graph of the bridge having 8.75 m span length, 1.30 m girder height, 300 MPa ballast stiffness for 44.13 m/s vehicle speed.

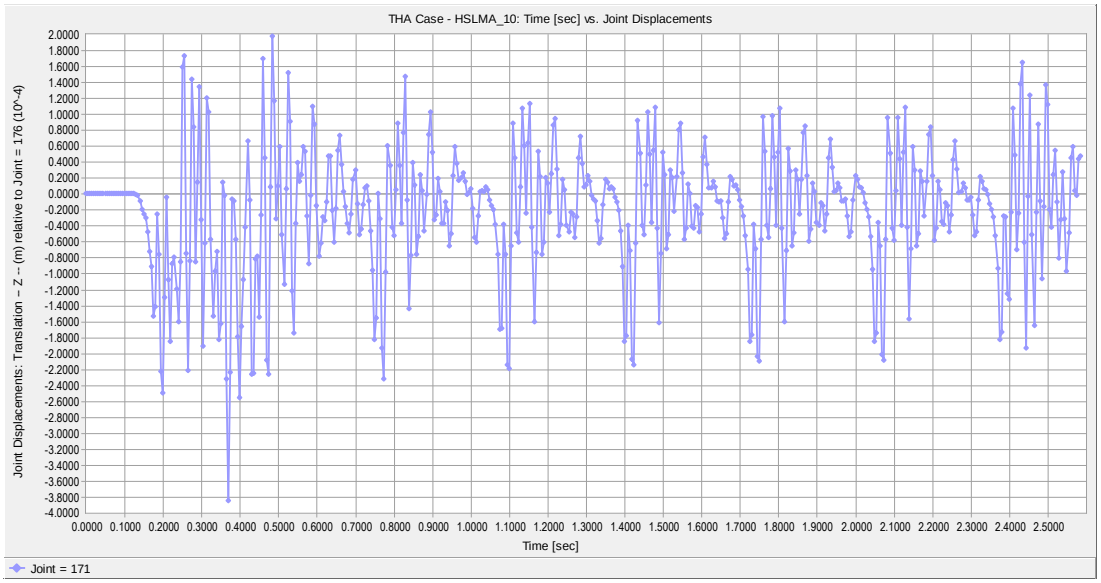

Figure A.88 Deck Twist vs. Time graph of the bridge having 8.75 m span length, 1.30 m girder height, 300 MPa ballast stiffness for 83 m/s vehicle speed.

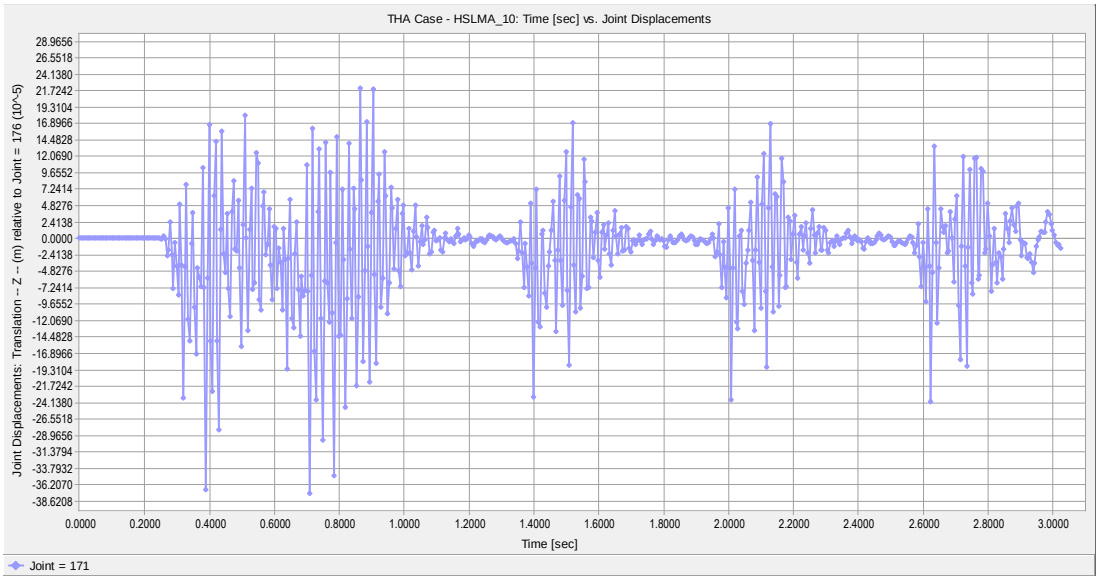

Figure A.89 Deck Twist vs. Time graph of the bridge having 8.75 m span length, 0.75 m girder height, 700 MPa ballast stiffness for 44.13 m/s vehicle speed.

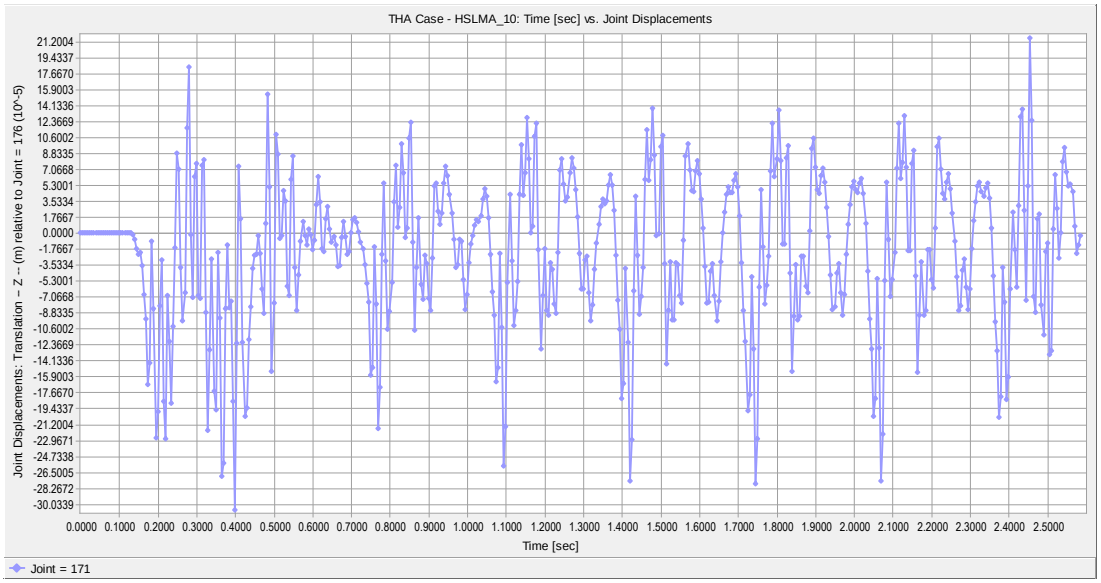

Figure A.90 Deck Twist vs. Time graph of the bridge having 8.75 m span length, 0.75 m girder height, 700 MPa ballast stiffness for 83 m/s vehicle speed.

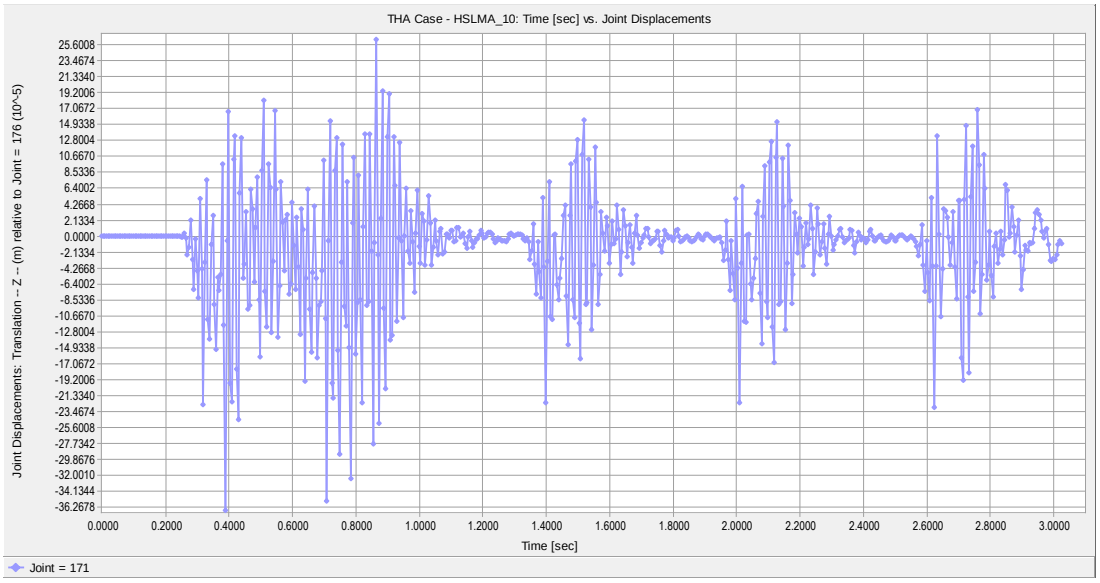

Figure A.91 Deck Twist vs. Time graph of the bridge having 8.75 m span length, 0.90 m girder height, 700 MPa ballast stiffness for 44.13 m/s vehicle speed.

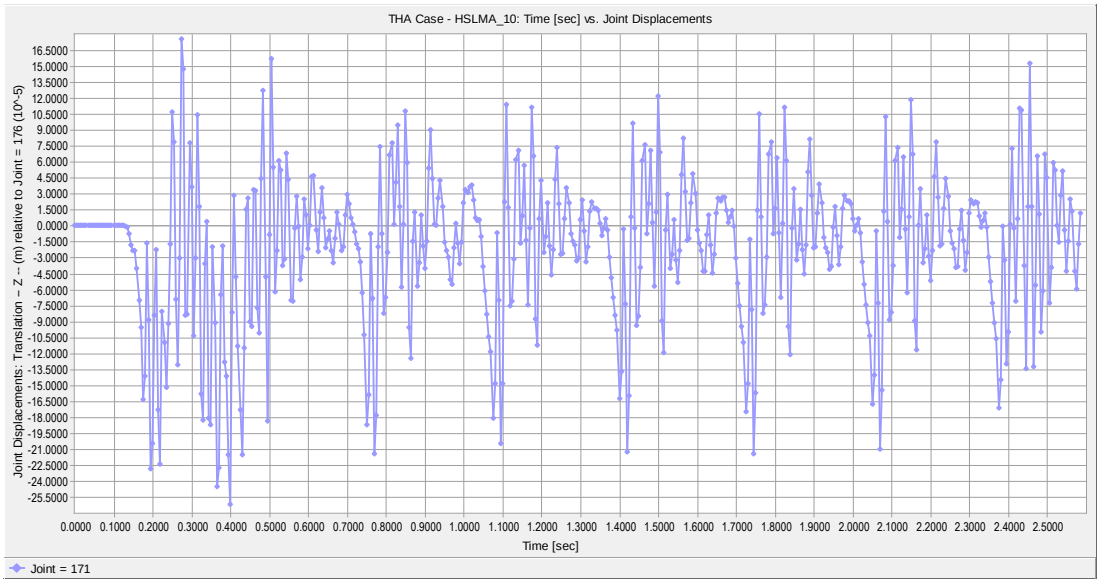

Figure A.92 Deck Twist vs. Time graph of the bridge having 8.75 m span length, 0.90 m girder height, 700 MPa ballast stiffness for 83 m/s vehicle speed.

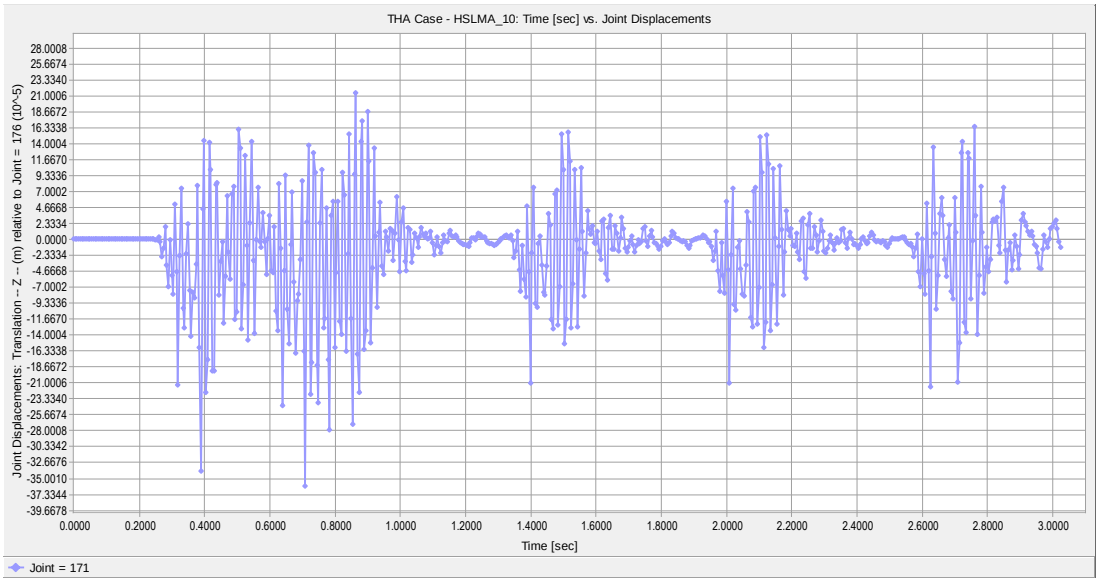

Figure A.93 Deck Twist vs. Time graph of the bridge having 8.75 m span length, 1.10 m girder height, 700 MPa ballast stiffness for 44.13 m/s vehicle speed.

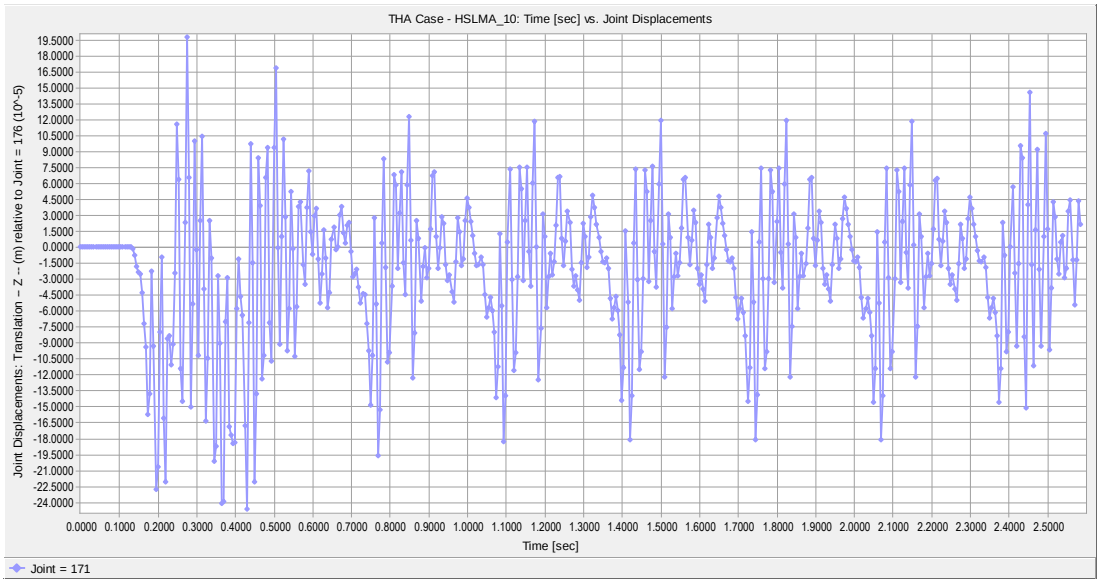

Figure A.94 Deck Twist vs. Time graph of the bridge having 8.75 m span length, 1.10 m girder height, 700 MPa ballast stiffness for 83 m/s vehicle speed.

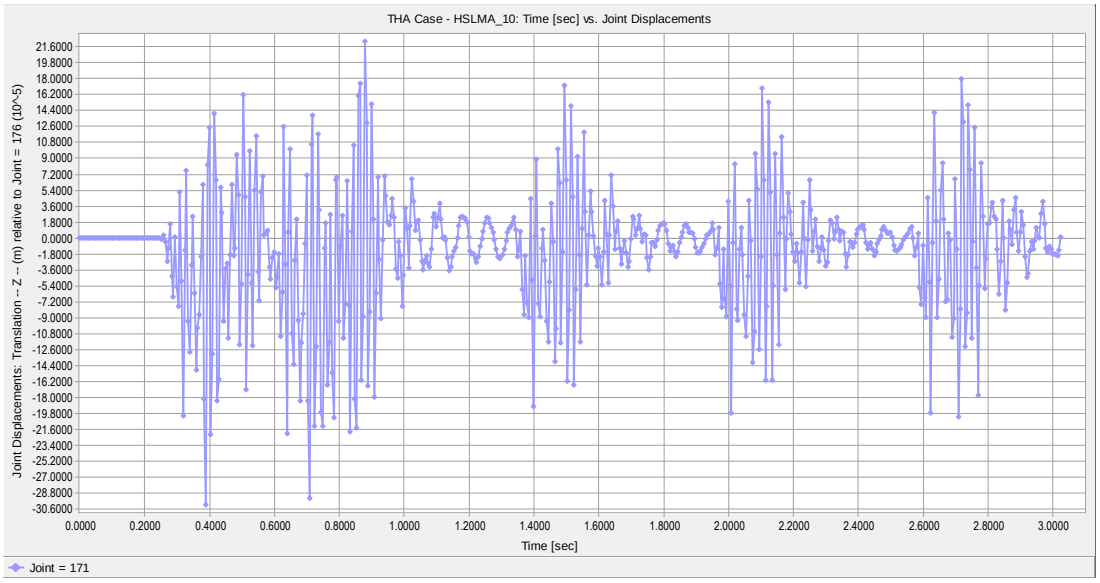

Figure A.95 Deck Twist vs. Time graph of the bridge having 8.75 m span length, 1.30 m girder height, 700 MPa ballast stiffness for 44.13 m/s vehicle speed.

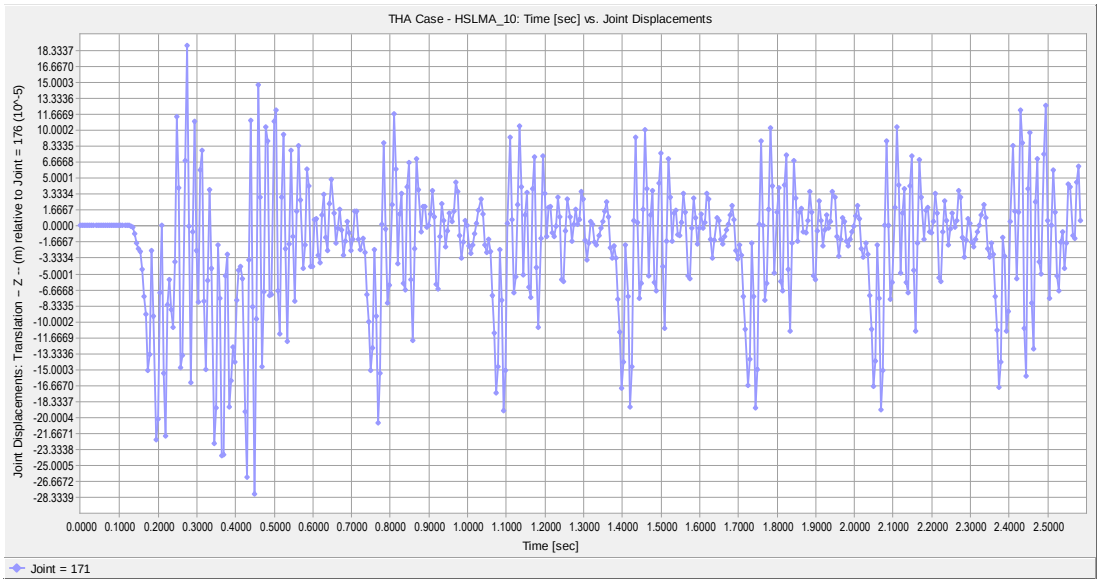

Figure A.96 Deck Twist vs. Time graph of the bridge having 8.75 m span length, 1.30 m girder height, 700 MPa ballast stiffness for 83 m/s vehicle speed.

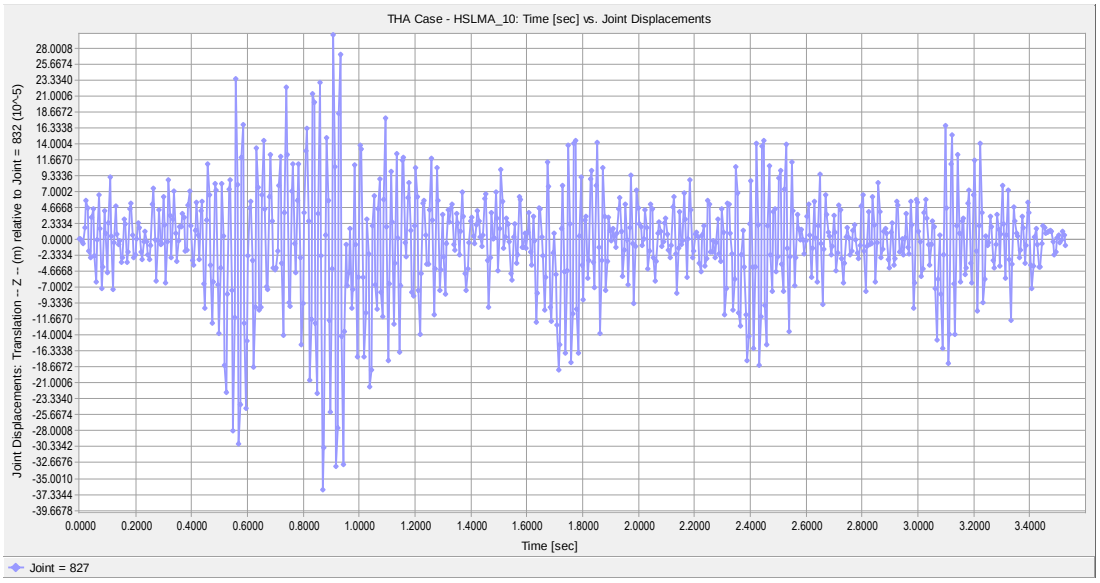

Figure A.97 Deck Twist vs. Time graph of the bridge having 24.5 m span length, 0.75 m girder height, 300 MPa ballast stiffness for 40 m/s vehicle speed.

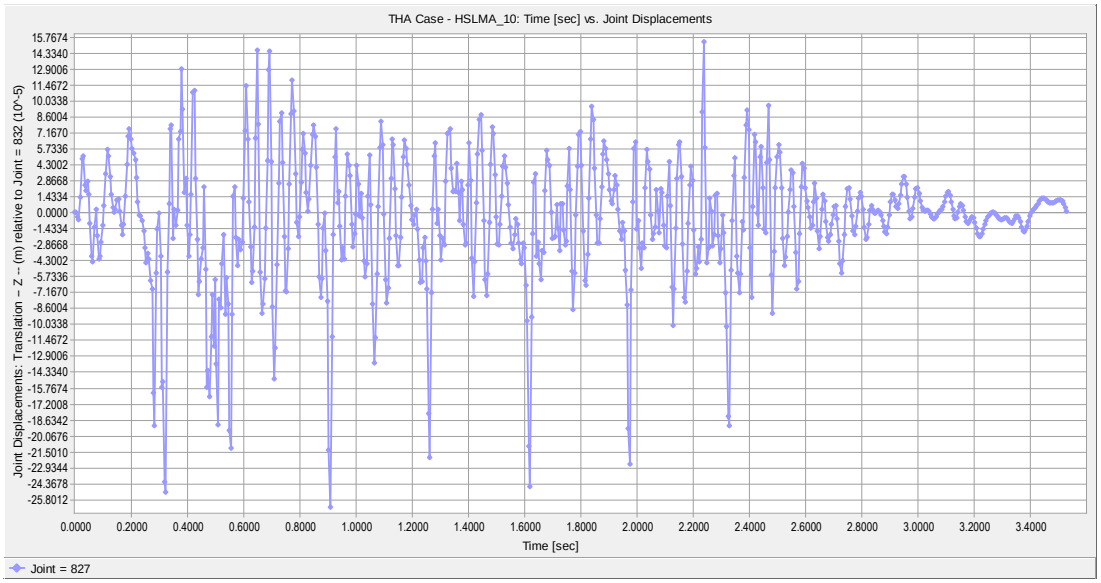

Figure A.98 Deck Twist vs. Time graph of the bridge having 24.5 m span length, 0.75 m girder height, 300 MPa ballast stiffness for 76.08 m/s vehicle speed.

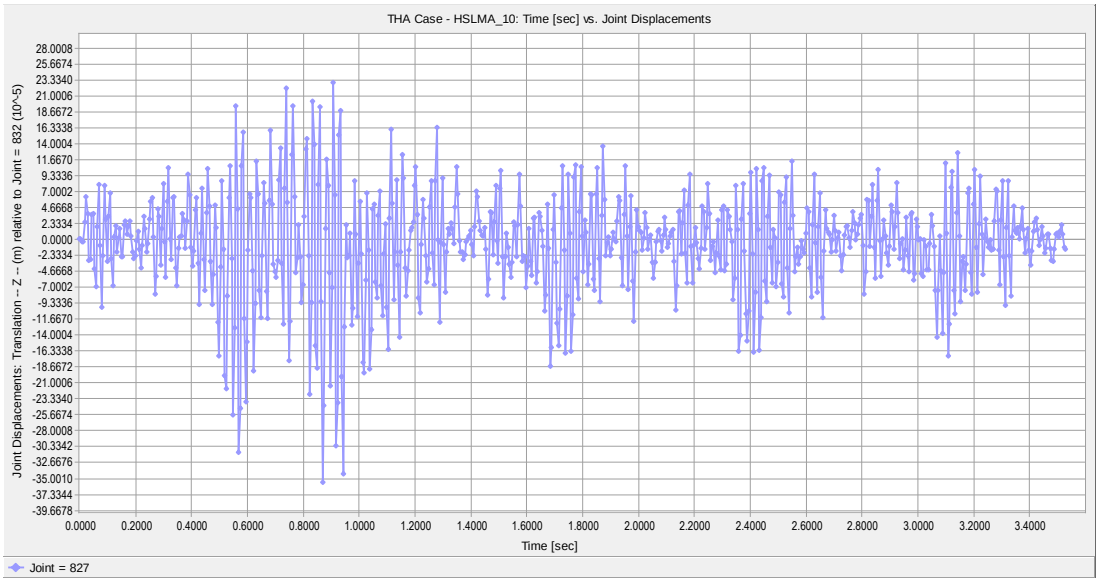

Figure A.99 Deck Twist vs. Time graph of the bridge having 24.5 m span length, 0.90 m girder height, 300 MPa ballast stiffness for 40 m/s vehicle speed.

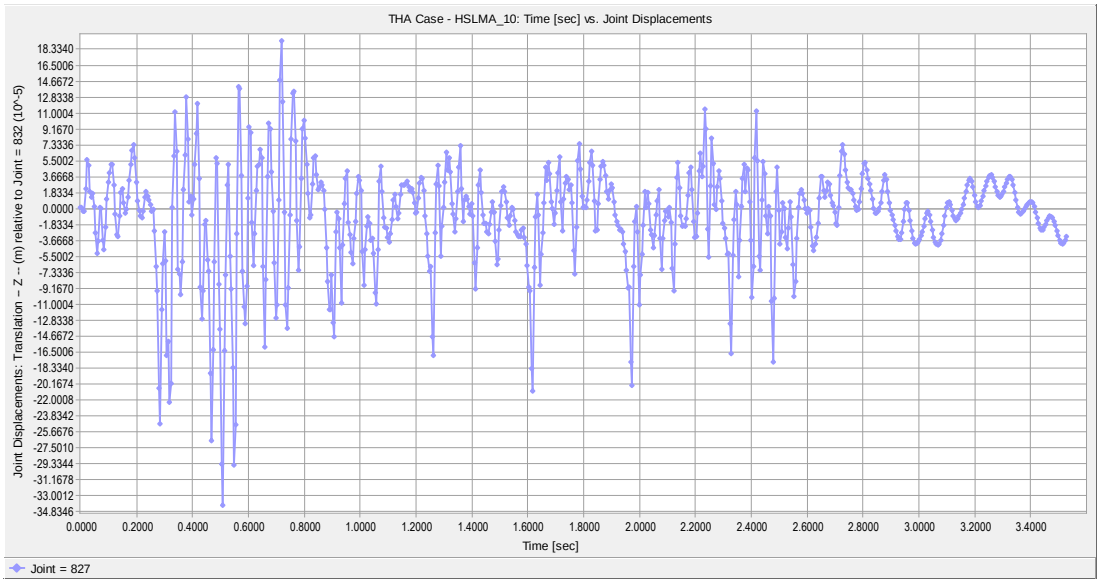

Figure A.100 Deck Twist vs. Time graph of the bridge having 24.5 m span length, 0.90 m girder height, 300 MPa ballast stiffness for 76.08 m/s vehicle speed.

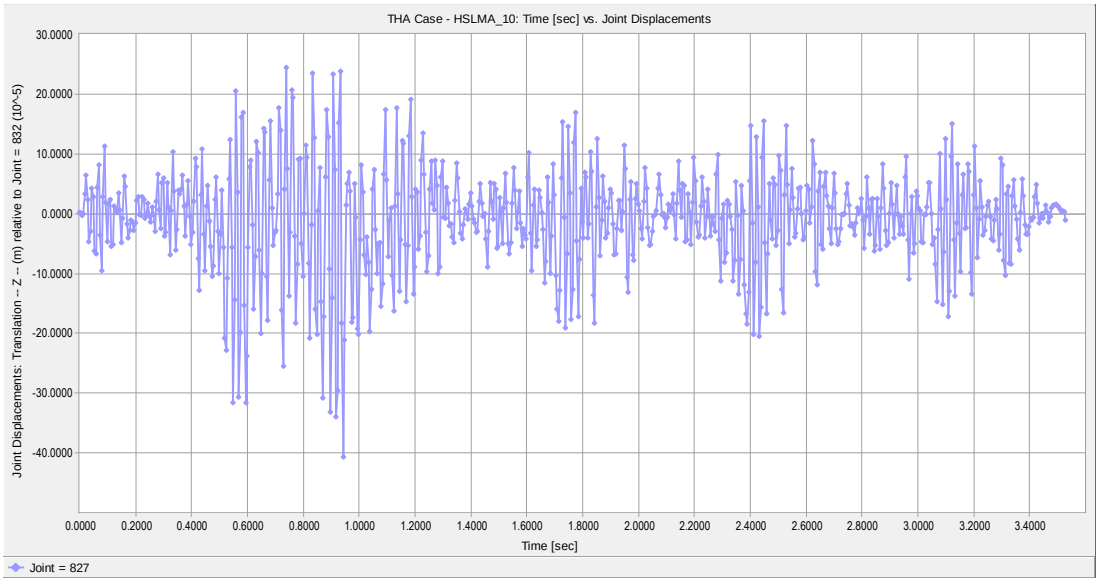

Figure A.101 Deck Twist vs. Time graph of the bridge having 24.5 m span length, 1.10 m girder height, 300 MPa ballast stiffness for 40 m/s vehicle speed.

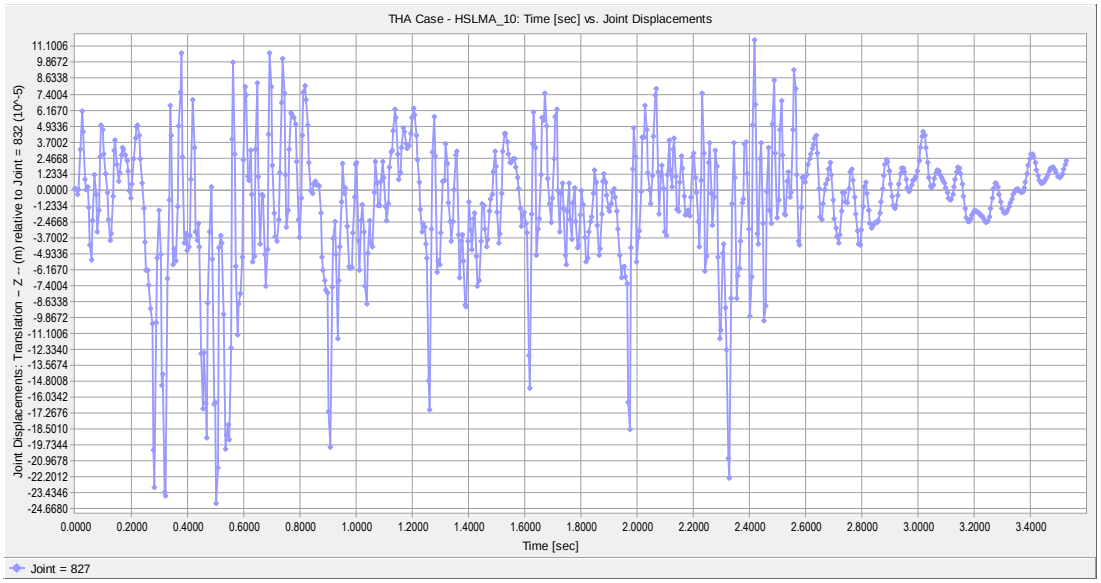

Figure A.102 Deck Twist vs. Time graph of the bridge having 24.5 m span length, 1.10 m girder height, 300 MPa ballast stiffness for 76.08 m/s vehicle speed.

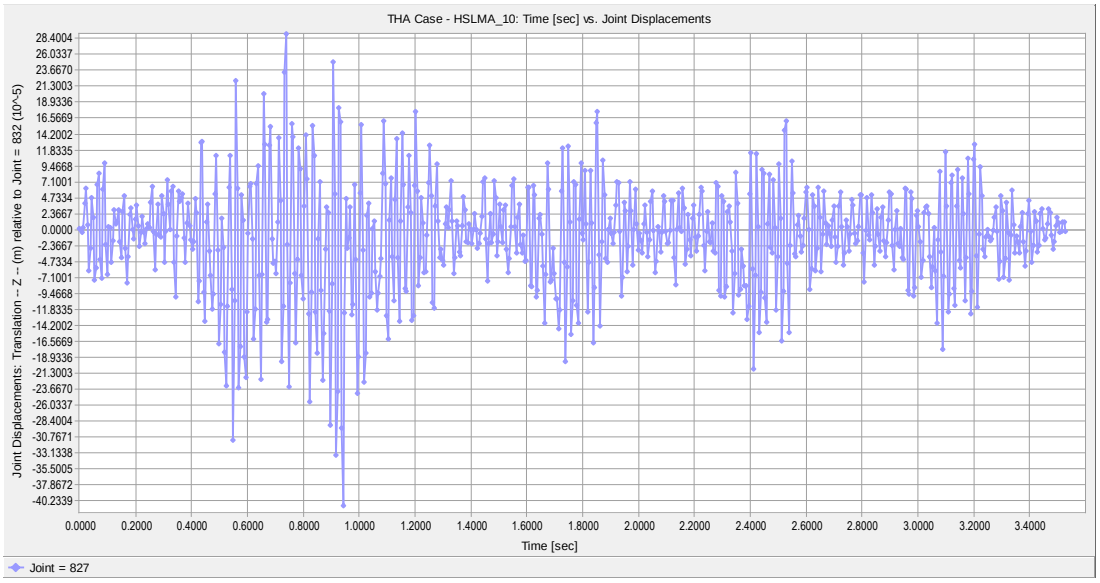

Figure A.103 Deck Twist vs. Time graph of the bridge having 24.5 m span length, 1.30 m girder height, 300 MPa ballast stiffness for 40 m/s vehicle speed.

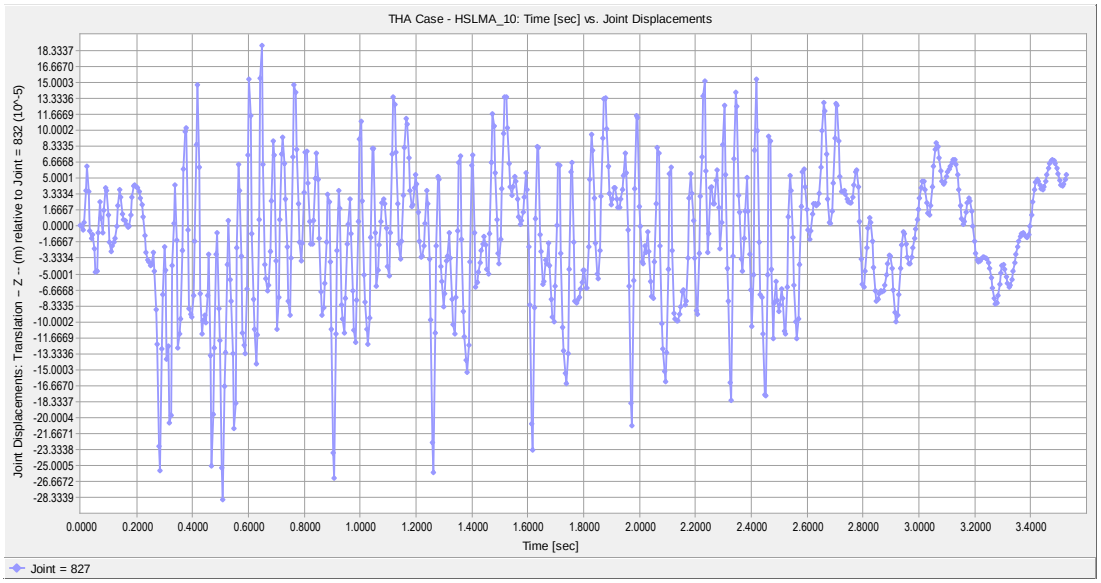

Figure A.104 Deck Twist vs. Time graph of the bridge having 24.5 m span length, 1.30 m girder height, 300 MPa ballast stiffness for 76.08 m/s vehicle speed.

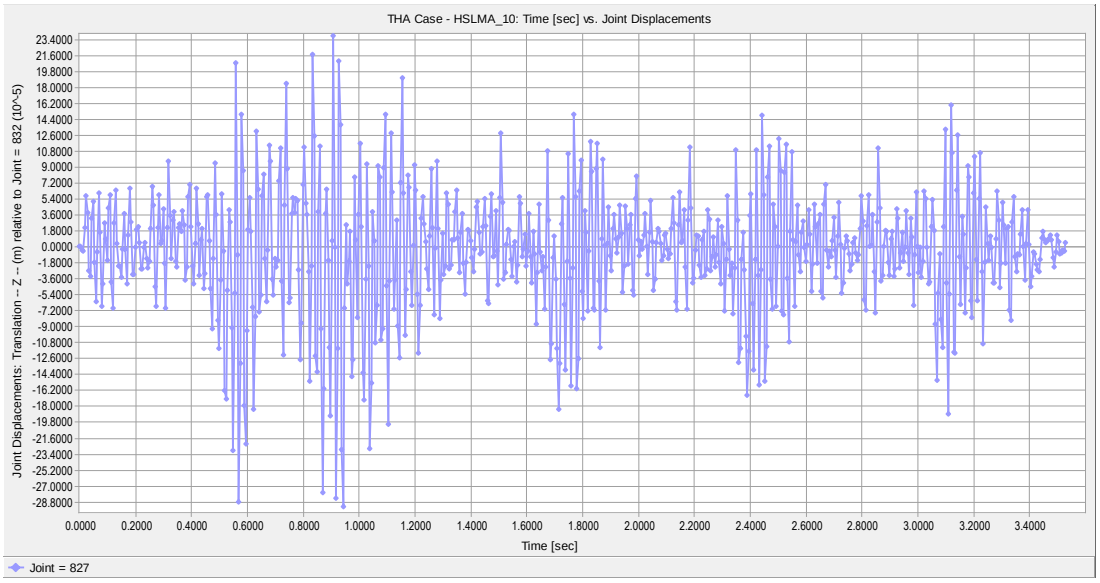

Figure A.105 Deck Twist vs. Time graph of the bridge having 24.5 m span length, 0.75 m girder height, 700 MPa ballast stiffness for 40 m/s vehicle speed.

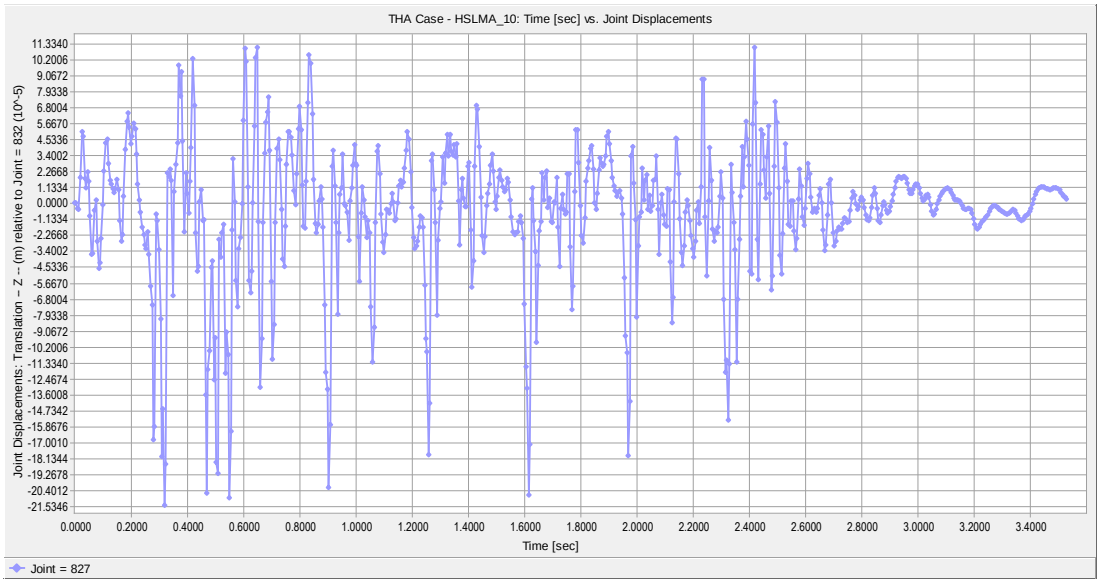

Figure A.106 Deck Twist vs. Time graph of the bridge having 24.5 m span length, 0.75 m girder height, 700 MPa ballast stiffness for 76.08 m/s vehicle speed.

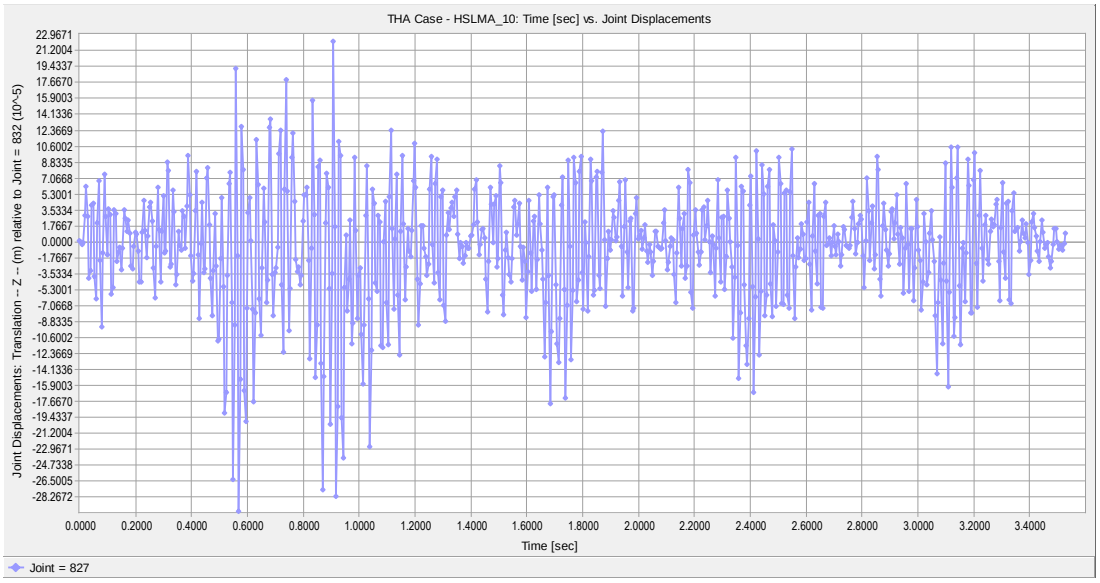

Figure A.107 Deck Twist vs. Time graph of the bridge having 24.5 m span length, 0.90 m girder height, 700 MPa ballast stiffness for 40 m/s vehicle speed.

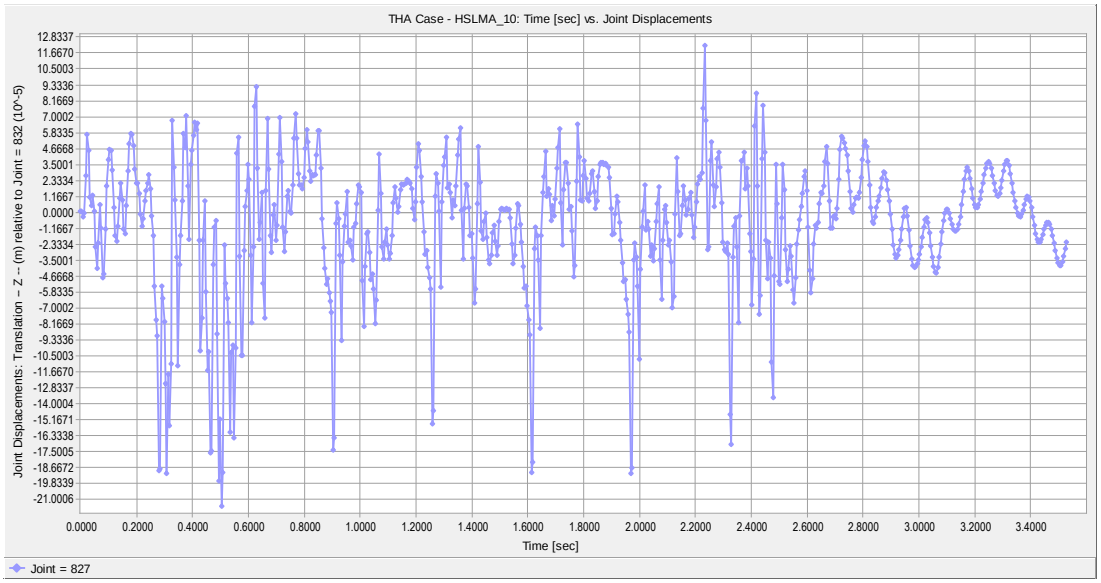

Figure A.108 Deck Twist vs. Time graph of the bridge having 24.5 m span length, 0.90 m girder height, 700 MPa ballast stiffness for 76.08 m/s vehicle speed.

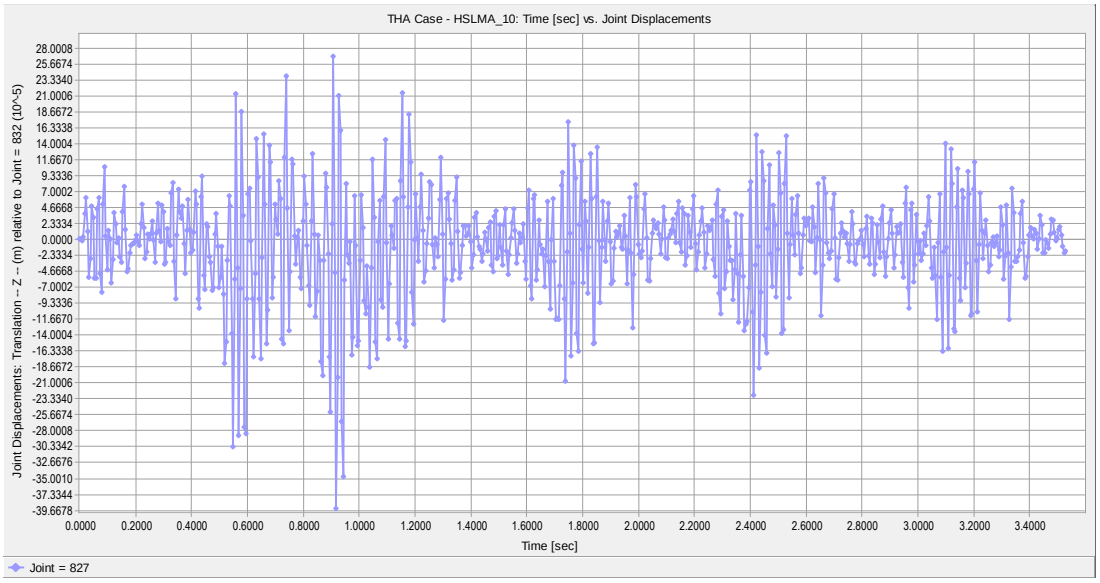

Figure A.109 Deck Twist vs. Time graph of the bridge having 24.5 m span length, 1.10 m girder height, 700 MPa ballast stiffness for 40 m/s vehicle speed.

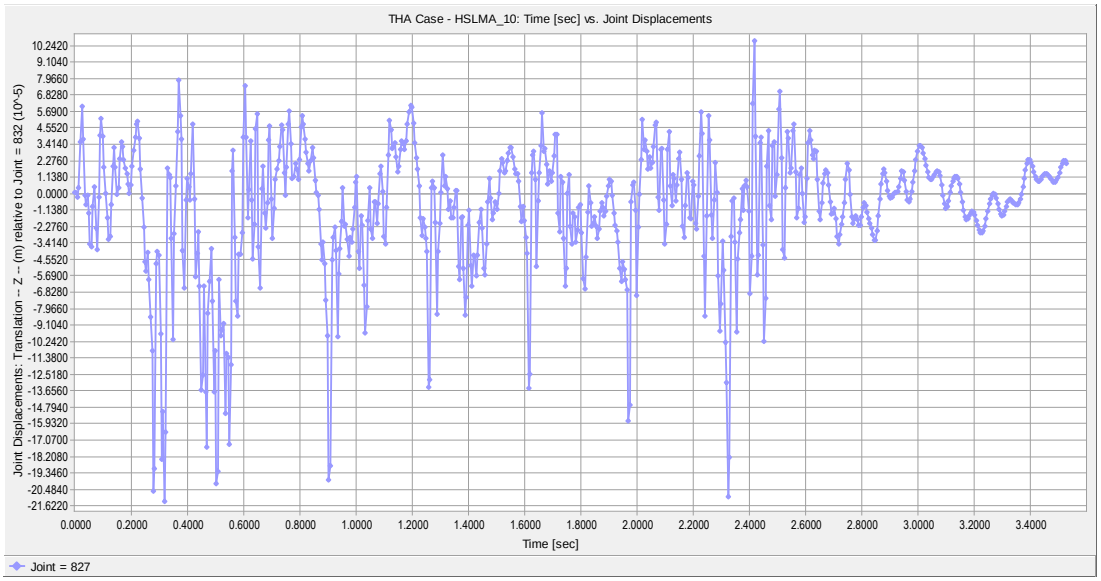

Figure A.110 Deck Twist vs. Time graph of the bridge having 24.5 m span length, 1.10 m girder height, 700 MPa ballast stiffness for 76.08 m/s vehicle speed.

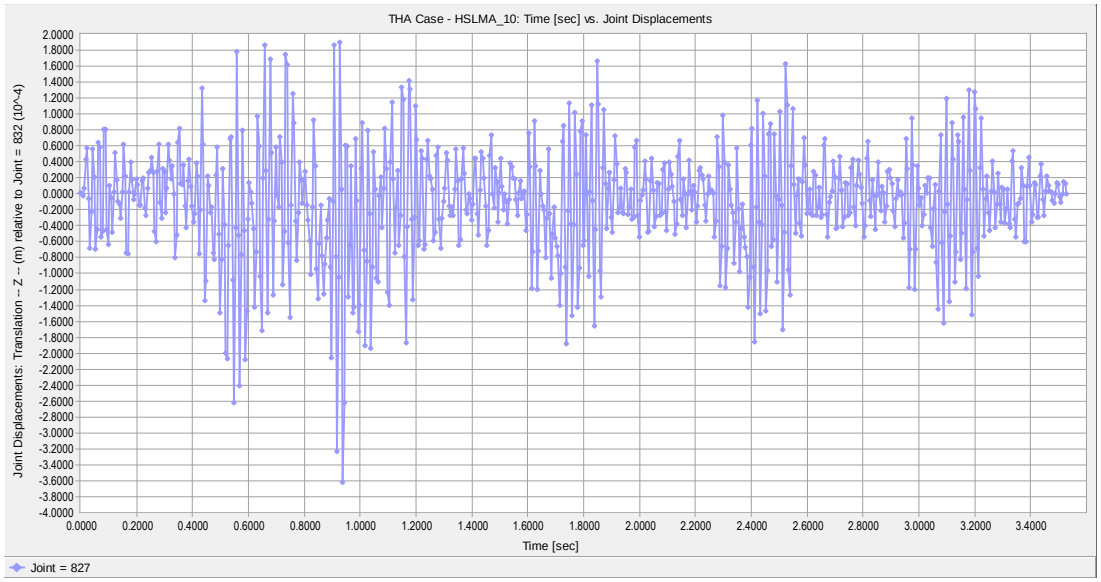

Figure A.111 Deck Twist vs. Time graph of the bridge having 24.5 m span length, 1.30 m girder height, 700 MPa ballast stiffness for 40 m/s vehicle speed.

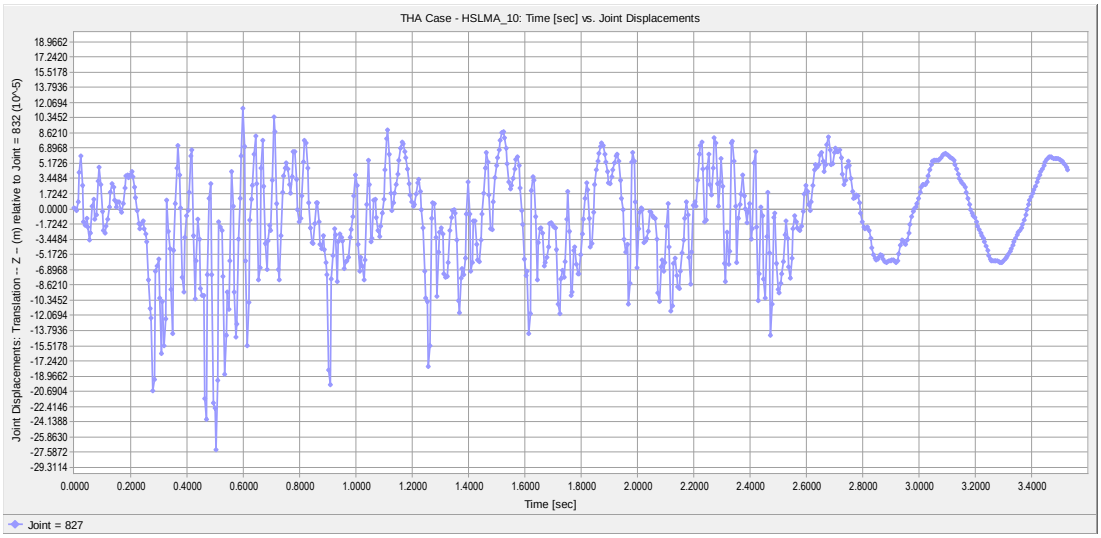

Figure A.112 Deck Twist vs. Time graph of the bridge having 24.5 m span length, 1.30 m girder height, 700 MPa ballast stiffness for 76.08 m/s vehicle speed.

APPENDIX B

COMPOSITE SECTION SELECTED CALCULATIONS & CHECKS

B.1. Calculations for Bridge Having 8.75 m Span Length, 0.75 m Girder Height and 350 MPa Ballast Stiffness

Material Properties :

Concrete	:	C 30	γc =	24.0	kN/m^3	fc =	30	MPa	Ec =	24,837 MPa
Steel	:	SJ235	γs =	78.5	kN/m^3	fy =	244	MPa	Es =	200,000 MPa
Ballast	:		γb =	19.2	kN/m^3	Moduler Ratio			n =	8

Geometric Properties :

Lenght of bridge	L =	8.75	m
Effective width	b =	1.4	m
Thickness of slab	ts =	0.25	m
Height of girder	h =	0.75	m
Width of flange	bf =	0.32	m
Thickness of flange	tf =	0.035	m
Thickness of web	tw =	0.012	m

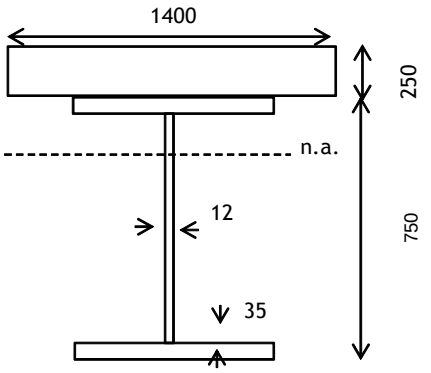

Check :	FLB :	bf/(2tf) =	4.57	≤	0.38$\sqrt{E/Fy}$ =	10.88		O.K.
	WLB :	hw/tw =	56.67	≤	3.76$\sqrt{E/Fy}$ =	107.65		

Section area	A =	0.0306	+	0.3500	=	0.38	m2		
Section weight	q =	10.80	kN/m	Moment of Inertia girder		I =	0.00318	m4	

for composite section :

Effective width of concrete	b_e = b / n	=	0.17	m
Center of gravity of composite section	n.a. = *(from base)*	=	0.67	m
Momentof inertia of composite section	I =	=	0.00789	m4
Section modulus wrt. girder base	S_b =	=	0.01180	m3
Section modulus wrt. girder top	S_t =	=	0.02381	m3

Frequencies :

Deflection at mid span due to permanent actions δ_0 = = 3.5 mm

Check : (δ_0 = 3.5 mm ≤ δ_a = L / 640 = 13.7 mm) **O.K.**

First natural frequency n0 = $\frac{17.75}{\sqrt{\delta_0}}$ = 9.488 Hz

Limiting values $n_0 = 80/L$ for $4\text{m} \le L \le 20\text{m}$; $n_0 = 23{,}58L^{-0{,}592}$ for $20\text{m} < L \le 100\text{m}$ n0 = 9.143 ≤ n0 ≤ n0 = $94{,}76L^{-0{,}748}$ = 18.707

Unloaded first natural frequency	n0 =	=	12.5	Hz
Loaded first natural frequency	f1 =	=	9.55	Hz
Loaded second natural frequency	f2 =	=	12.82	Hz

Dynamic Factors :

EUROCODE :

Cross Girder Spacing		w_g =	=	1.75	m
Determinant Length	*(table 6.2)*	Lφ = 2 w_g	=	3.5	m
Permitted velocity		v =	=	83	m/s
$\alpha = \frac{v}{22}$ if $v \le 22$ m/s; $\alpha = 1$ if $v > 22$ m/s		α =	=	1	

$$\varphi'' = \frac{\alpha}{100}\left[56e^{-\left(\frac{L_\phi}{10}\right)^2} + 50\left(\frac{L_\phi n_0}{80} - 1\right)e^{-\left(\frac{L_\phi}{20}\right)^2}\right]$$ = = **54%** > 0

AREMA :

For L < 24.4 m % $= 40 - \frac{3x(L*3.28)^2}{1600}$

For L ≥ 24.4 m % $= 16 + \frac{600}{(L*3.28) - 30}$

= 38.46 %

For ballasted deck bridge 90% of impact should be taken : = 34.61 %

Impact load due to rocking efffect : = 20 %

Total Dynamic effect, φ = = **55%**

Damping Coefficients :

EUROCODE **Table 6.6 - Values of damping to be assumed for design purposes**

Bridge Type	ζ Lower limit of percentage of critical damping [%]	
	Span L < 20m	Span $L \geq$ 20m
Steel and composite	$\zeta = 0,5 + 0,125\ (20 - L)$	$\zeta = 0,5$
Prestressed concrete	$\zeta = 1,0 + 0,07\ (20 - L)$	$\zeta = 1,0$
Filler beam and reinforced concrete	$\zeta = 1,5 + 0,07\ (20 - L)$	$\zeta = 1,5$

Lower limit of percentage of critical damping for composite bridge type, ζ = 1.91 %

For spans less than 30 m dynamic vehicle/bridge mass interaction effects tend to reduce the peak response at resonance.

$$\Delta\zeta = \frac{0,0187L - 0,00064L^2}{1 - 0,0441L - 0,0044L^2 + 0,000255L^3}[\%]$$ *(Eqn. 6.13)* Δ ζ = 0.26 %

Total critical damping for composite bridge type ζ = ζ + Δ ζ = 2.16 %

RAYLEIGH DAMPING COEFFICIENTS

Loaded first natural frequency f1 = 9.55 Hz w1 = f1 x 2 π = 60.00

Loaded second natural frequency f2 = 12.82 Hz w2 = f2 x 2 π = 80.55

Mass proportional coefficient, $a_0 = \zeta \frac{2\omega_1\omega_2}{\omega_1 + \omega_2}$ = 1.487

Stiffness proportional coefficient, $a_1 = \zeta \frac{2}{\omega_1 + \omega_2}$ = 3.08E-04

Design Speeds :

For simply supported bridges that may be modelled as a line beam the Resonant Speeds may be estimated using Equation 6.9

40 m/s ≤ $v_i = n_0 \lambda_i$ ≤ Max. Design speed = 83 m/s

Unloaded first natural frequency n0 = = 12.50 Hz

Principal wavelength of frequency of excitation $\lambda_i = \frac{d}{i}$, i = 1 , 2 , 3 , 4

Regular spacing of groups of axles d = = 11 m

Resonant Speeds V_1 = 137.50 m/s , V_2 = 68.75 m/s , V_3 = 45.83 m/s , V_4 = 34.38 m/s

Design Speeds: *taken from modal frequency picks*

V_1 = 40.00 m/s V_2 = 83.00 m/s V_3 = 68.75 m/s V_4 = 28.65 m/s V_5 = 44.13 m/s

Reactions : Notation : 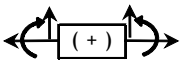

	Eurocode Sta.Analy	Arema Sta.Analy	V1	V2	V3	V4
Axial Force of girder, P_g (kN):	248.58	249.88	123.27	121.43	124.69	157.99
Moment of girder, M_g (kN.m):	237.95	219.18	144.48	158.42	162.69	229.43
Axial Force of slab, P_s (kN):	93.55	94.09	249.25	236.78	261.81	335.07
Moment of slab, M_s (kN.m):	-33.17	-33.35	15.16	15.52	8.87	14.96

Moment of composite section; M_{comp} = P_g x b + M_g + P_s x a + M_s

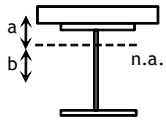

M_{comp} (kN.m):	297.06	278.61	247.27	258.46	262.20	359.94

Long term period section stress; Compression in top extreme fibers due to bending, δ_{ct} = M_{comp} / S_t

Tesion in bottom extreme fibers due to bending, δ_{tb} = M_{comp} / S_b

δ_{ct} = (MPa):	12.475	11.700	10.384	10.854	11.011	15.116
δ_{tb} = (MPa):	25.167	23.603	20.948	21.896	22.213	30.493

Check : δ_a = 0.55 fy ≥	O.K.	O.K.	O.K.	O.K.	O.K.	O.K.
used flexural capacity :	19%	18%	16%	16%	17%	23%

Max. Joint acceleration, a_m (m/s²):	---	---	31.24	46.18	28.06	28.1

B.2. Calculations for Bridge Having 24.5 m Span Length, 0.75 m Girder Height and 350 MPa Ballast Stiffness

Material Properties :

Concrete	:	C 30	γ_c =	24.0	kN/m³	fc =	30	MPa	Ec =	24,837 MPa
Steel	:	SJ235	γ_s =	78.5	kN/m³	fy =	244	MPa	Es =	200,000 MPa
Ballast	:		γ_b =	19.2	kN/m³	Moduler Ratio			n =	8

Geometric Properties :

Lenght of bridge	L =	24.5	m
Effective width	b =	1.4	m
Thickness of slab	ts =	0.25	m
Height of girder	h =	0.75	m
Width of flange	bf =	0.32	m
Thickness of flange	tf =	0.035	m
Thickness of web	tw =	0.012	m

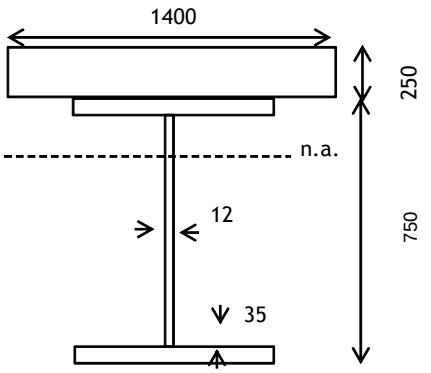

Check :								
FLB	:	bf/(2tf) =	4.57	≤	$0.38\sqrt{E/Fy}$ =	10.88	O.K.
WLB	:	hw/tw =	56.67	≤	$3.76\sqrt{E/Fy}$ =	107.65	

Section area A = 0.0306 + 0.3500 = 0.38 m2

Section weight q = 10.80 kN/m Moment of Inertia girder I = 0.00318 m4

for composite section :

Effective width of concrete	b_e = b / n	=	0.17 m
Center of gravity of composite section	n.a. = *(from base)*	=	0.67 m
Momentof inertia of composite section	I =	=	0.00789 m4
Section modulus wrt. girder base	S_b =	=	0.01180 m3
Section modulus wrt. girder top	S_t =	=	0.02381 m3

Frequencies :

Deflection at mid span due to permanent actions δ_0 = = 17 mm

Check : (δ_0 = 17.0 mm ≤ δ_a = L / 640 = 38.3 mm) **O.K.**

First natural frequency n0 = $\frac{17,75}{\sqrt{\delta_0}}$ = 4.305 Hz

Limiting values $n_0 = 80/L$ for $4m \le L \le 20m$; $n_0 = 23,58L^{-0,592}$ for $20m < L \le 100m$ n0 = 3.549 ≤ n0 ≤ n0 = $94,76L^{-0,748}$ = 8.660

Unloaded first natural frequency n0 = = 2.01 Hz

Loaded first natural frequency f1 = = 1.82 Hz

Loaded second natural frequency f2 = = 3.84 Hz

Dynamic Factors :

EUROCODE :

Cross Girder Spacing		w_g =	= 1.75 m
Determinant Length	*(table 6.2)*	Lφ = 2 w_g	= 3.5 m
Permitted velocity		v =	= 83 m/s

$$\alpha = \frac{v}{22} \quad \text{if } v \le 22 \text{ m/s}$$
$$\alpha = 1 \quad \text{if } v > 22 \text{ m/s}$$

α = = 1

$$\varphi'' = \frac{\alpha}{100}\left[56e^{-\left(\frac{L_\phi}{10}\right)^2} + 50\left(\frac{L_\phi n_0}{80} - 1\right)e^{-\left(\frac{L_\phi}{20}\right)^2}\right]$$

= = 31% > 0

AREMA :

For L < 24.4 m % $= 40 - \frac{3x(L*3.28)^2}{1600}$

For L ≥ 24.4 m % $= 16 + \frac{600}{(L*3.28) - 30}$

= 27.91 %

For ballasted deck bridge 90% of impact should be taken : = 25.12 %

Impact load due to rocking efffect : = 20 %

Total Dynamic effect, φ = = 45%

Damping Coefficients :

EUROCODE

Table 6.6 - Values of damping to be assumed for design purposes

Bridge Type	ζ Lower limit of percentage of critical damping [%]	
	Span L < 20m	Span $L \ge 20$m
Steel and composite	$\zeta = 0{,}5 + 0{,}125\ (20 - L)$	$\zeta = 0{,}5$
Prestressed concrete	$\zeta = 1{,}0 + 0{,}07\ (20 - L)$	$\zeta = 1{,}0$
Filler beam and reinforced concrete	$\zeta = 1{,}5 + 0{,}07\ (20 - L)$	$\zeta = 1{,}5$

Lower limit of percentage of critical damping for composite bridge type, ζ = 0.50 %

For spans less than 30 m dynamic vehicle/bridge mass interaction effects tend to reduce the peak response at resonance.

$$\Delta\zeta = \frac{0{,}0187L - 0{,}00064L^2}{1 - 0{,}0441L - 0{,}0044L^2 + 0{,}000255L^3}[\%] \quad \textit{(Eqn. 6.13)}$$

Δ ζ = 0.07 %

Total critical damping for composite bridge type ζ = ζ + Δ ζ = 0.57 %

RAYLEIGH DAMPING COEFFICIENTS

Loaded first natural frequency f1 = 1.82 Hz w1 = f1 x 2 π = 11.44

Loaded second natural frequency f2 = 3.84 Hz w2 = f2 x 2 π = 24.13

Mass proportional coefficient, $a_0 = \zeta \frac{2\omega_1\omega_2}{\omega_1+\omega_2}$ = 0.089

Stiffness proportional coefficient, $a_1 = \zeta \frac{2}{\omega_1+\omega_2}$ = 3.22E-04

Design Speeds :

For simply supported bridges that may be modelled as a line beam the Resonant Speeds may be estimated using Equation 6.9

40 m/s ≤ $v_i = n_0\lambda_i$ ≤ Max. Design speed = 83 m/s

Unloaded first natural frequency n0 = = 2.01 Hz

Principal wavelength of frequency of excitation $\lambda_i = \frac{d}{i}$, i = 1 , 2 , 3 , 4

Regular spacing of groups of axles d = = 27 m

Resonant Speeds V_1 = 54.27 m/s , V_2 = 27.14 m/s , V_3 = 18.09 m/s , V_4 = 13.57 m/s

Design Speeds: *taken from modal frequency picks*

V_1 = 40.00 m/s V_2 = 83.00 m/s V_3 = 54.27 m/s V_4 = 51.48 m/s V_5 = 76.08 m/s

Reactions : Notation : 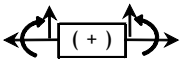

		Eurocode Sta.Analy	Arema Sta.Analy	V1	V2	V3	V4
Axial Force of girder,	P_g (kN):	688.45	726.32	591.28	727.17	789.51	870.54
Moment of girder,	M_g (kN.m):	650.73	688.98	496.74	765.74	820.50	952.31
Axial Force of slab,	P_s (kN):	2625.09	2786.32	1799.02	2235.81	2397.27	2568.58
Moment of slab,	M_s (kN.m):	4.23	4.36	32.15	22.56	21.40	36.38

Moment of composite section; $M_{comp} = P_g \times b + M_g + P_s \times a + M_s$ 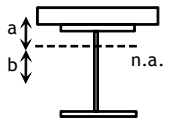

M_{comp} (kN.m):		1398.94	1481.72	1073.83	1463.30	1568.53	1774.47

Long term period section stress; Compression in top extreme fibers due to bending, $\delta_{ct} = M_{comp} / S_t$

Tesion in bottom extreme fibers due to bending, $\delta_{tb} = M_{comp} / S_b$

δ_{ct} = (MPa):	58.749	62.225	45.096	61.452	65.871	74.519
δ_{tb} = (MPa):	118.515	125.528	90.973	123.967	132.882	150.329

Check : $\delta_a = 0.55\ fy \geq$	**O.K.**	**O.K.**	**O.K.**	**O.K.**	**O.K.**	**Not O.K.**
used flexural capacity :	88%	94%	68%	92%	99%	112%

Max.Joint acceleration, a_m (m/s^2):	---	---	37.82	31.39	34.21	37.07

APPENDIX C

CORRELATION OF PASSENGER COMFORT PARAMETERS & COMPOSITE SPAN FLEXURAL RIGITY FOR CONSTANT VEHICLE SPEEDS

C.1. Joint Acceleration vs. Span Flexural Rigidity Graphs

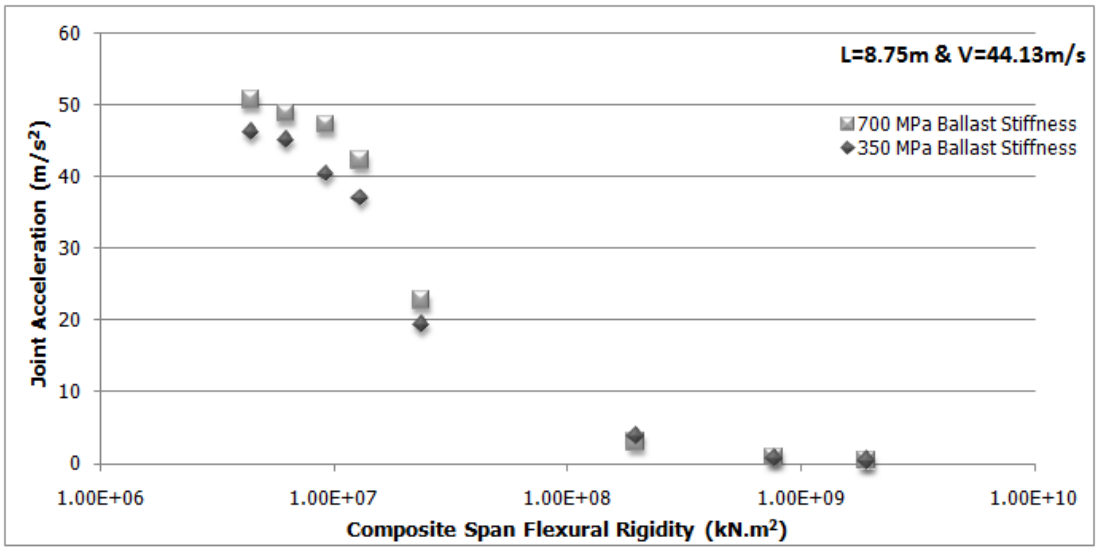

Figure C.1 Joint Acceleration vs. Span Flexural Rigidity graph of the bridge having 8.75 m span length for 44.13 m/s vehicle speed.

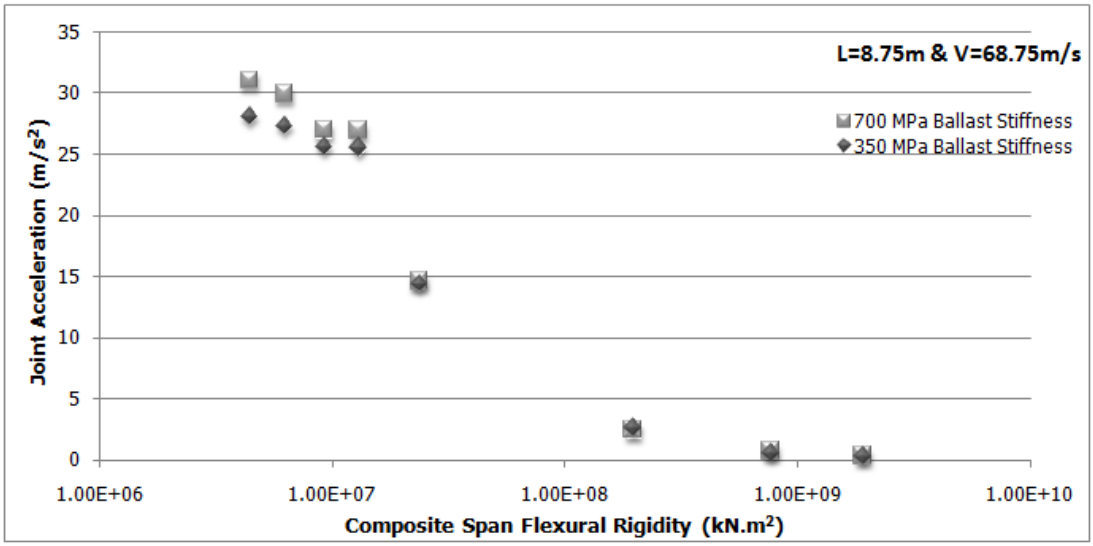

Figure C.2 Joint Acceleration vs. Span Flexural Rigidity graph of the bridge having 8.75 m span length for 68.75 m/s vehicle speed.

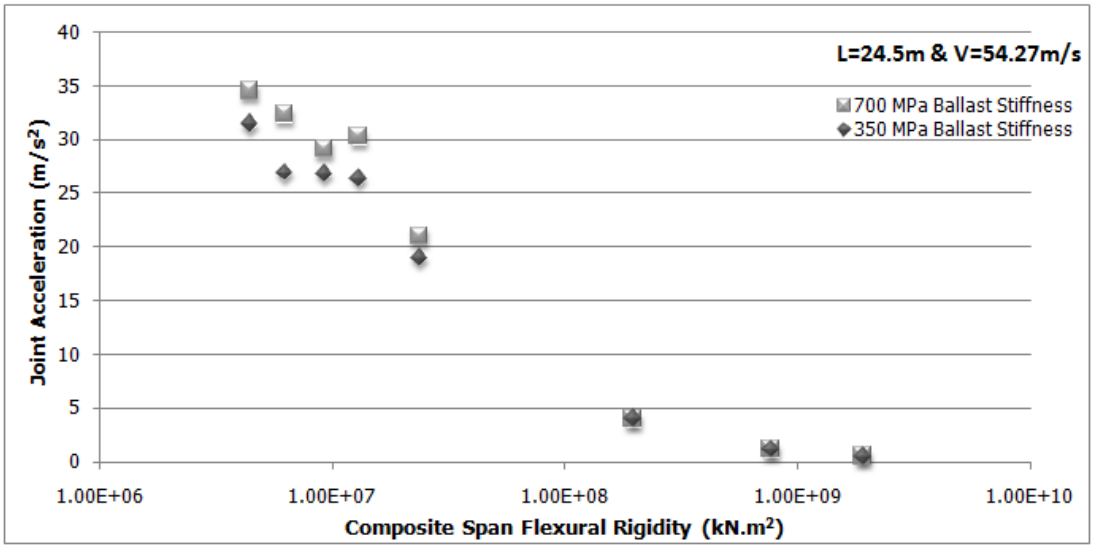

Figure C.3 Joint Acceleration vs. Span Flexural Rigidity graph of the bridge having 24.5 m span length for 54.27 m/s vehicle speed.

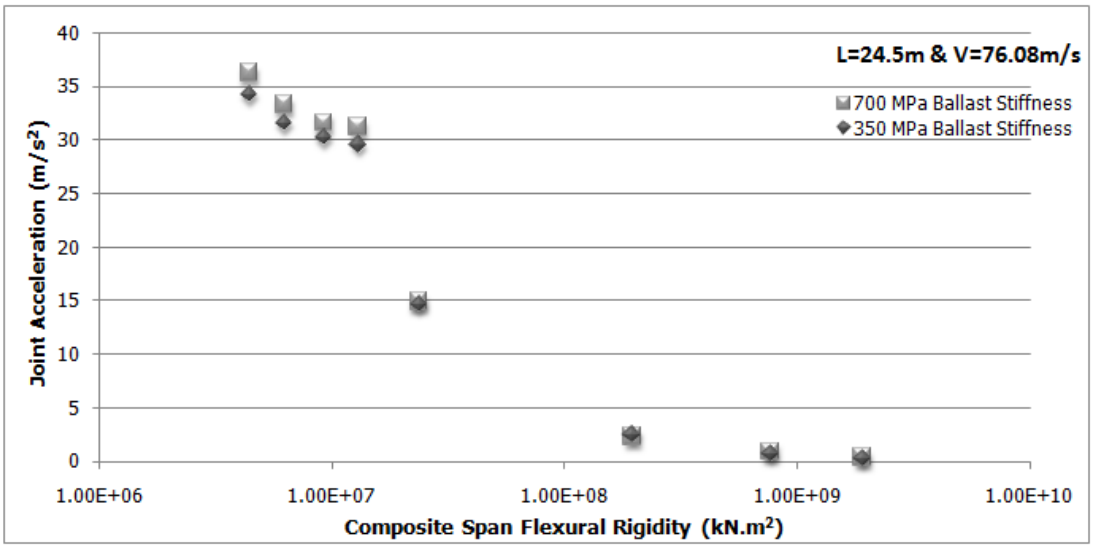

Figure C.4 Joint Acceleration vs. Span Flexural Rigidity graph of the bridge having 24.5 m span length for 76.08 m/s vehicle speed.

C.2 Joint Displacement vs. Span Flexural Rigidity Graphs

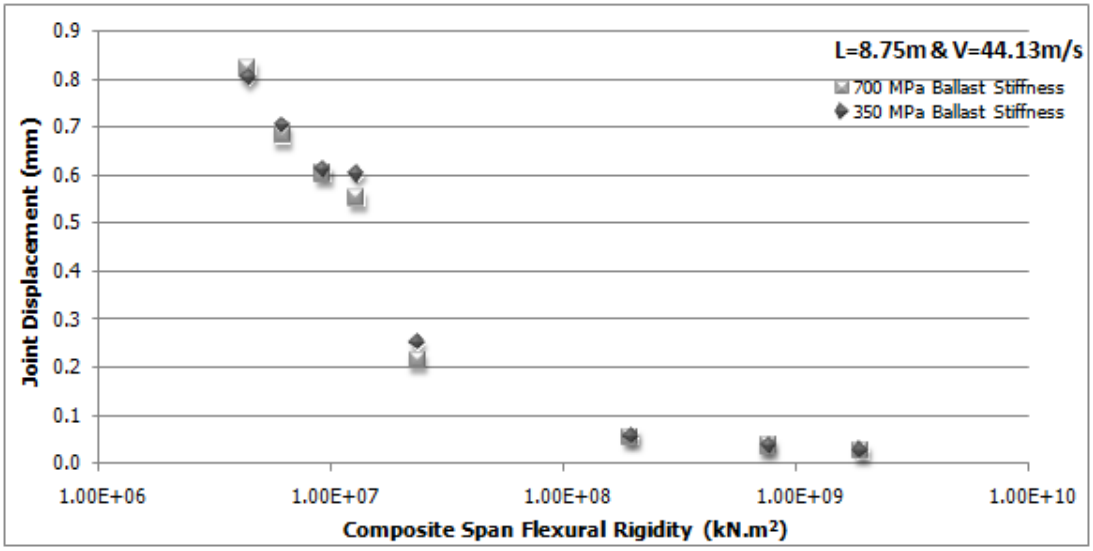

Figure C.5 Joint Displacement vs. Span Flexural Rigidity graph of the bridge having 8.75 m span length for 44.13 m/s vehicle speed.

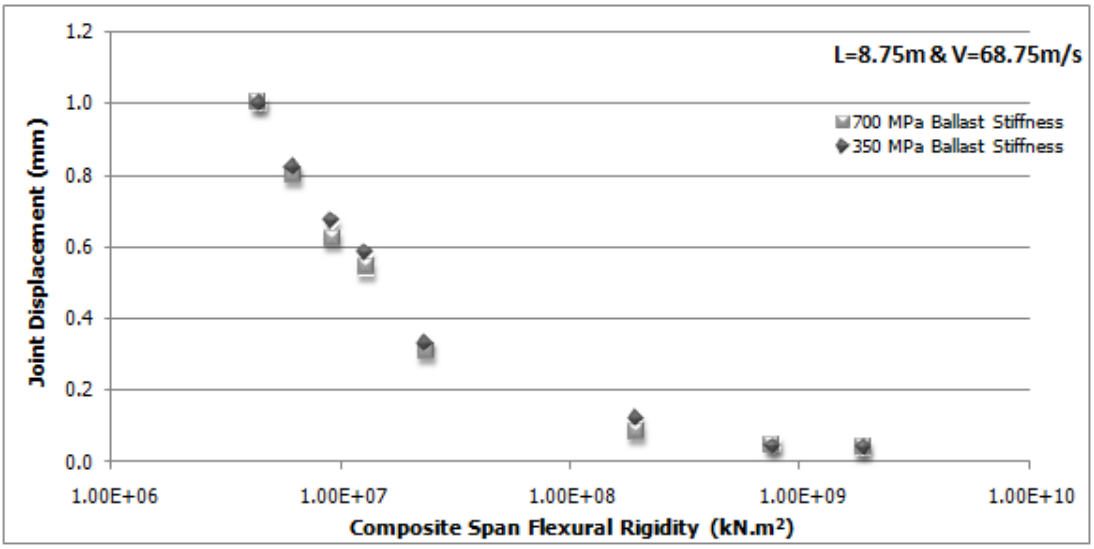

Figure C.6 Joint Displacement vs. Span Flexural Rigidity graph of the bridge having 8.75 m span length for 68.75 m/s vehicle speed.

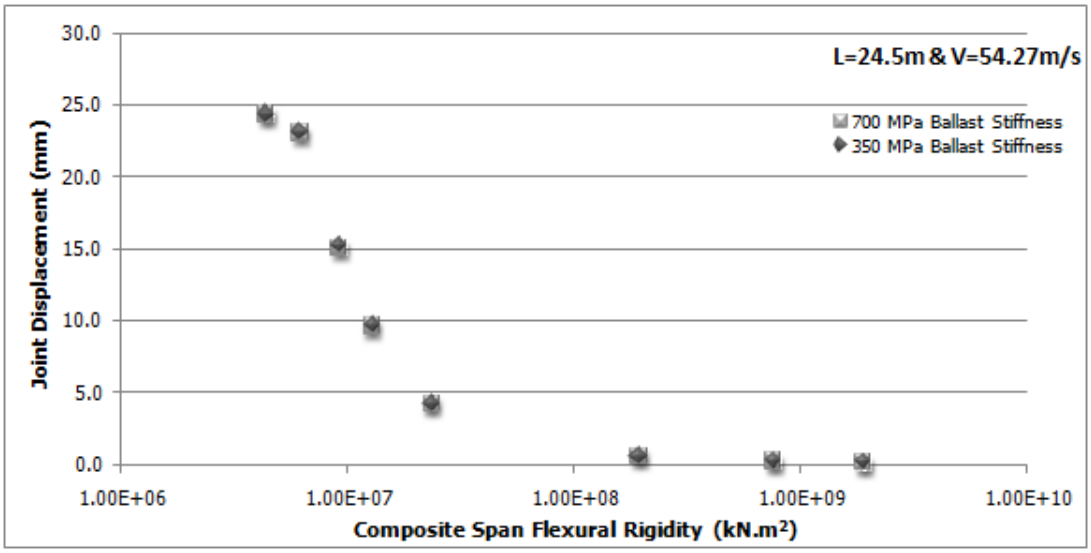

Figure C.7 Joint Displacement vs. Span Flexural Rigidity graph of the bridge having 24.5 m span length for 54.27 m/s vehicle speed.

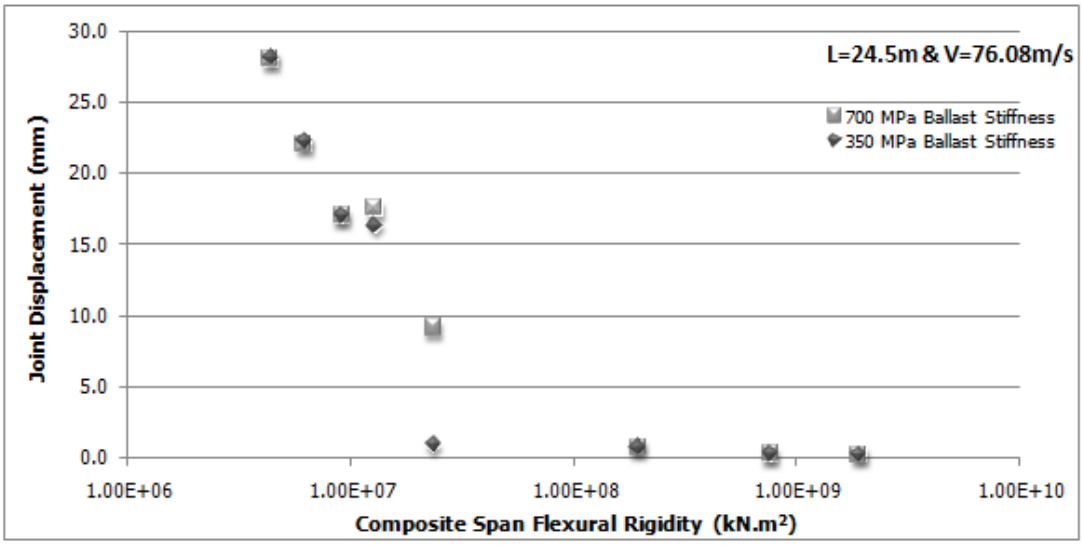

Figure C.8 Joint Displacement vs. Span Flexural Rigidity graph of the bridge having 24.5 m span length for 76.08 m/s vehicle speed.

C.3 Deck Twist vs. Span Flexural Rigidity Graphs

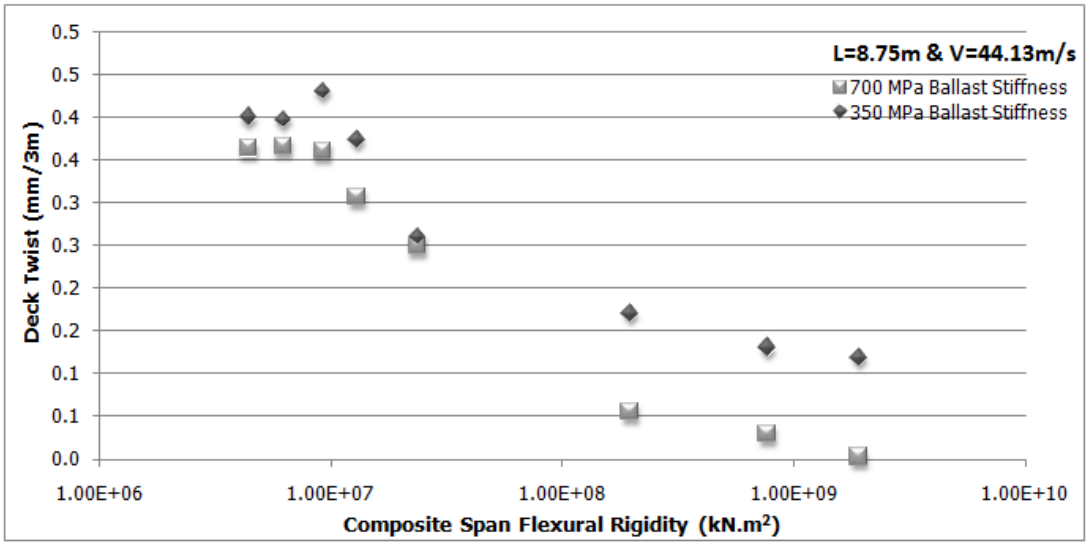

Figure C.9 Deck Twist vs. Span Flexural Rigidity graph of the bridge having 8.75 m span length for 44.13 m/s vehicle speed.

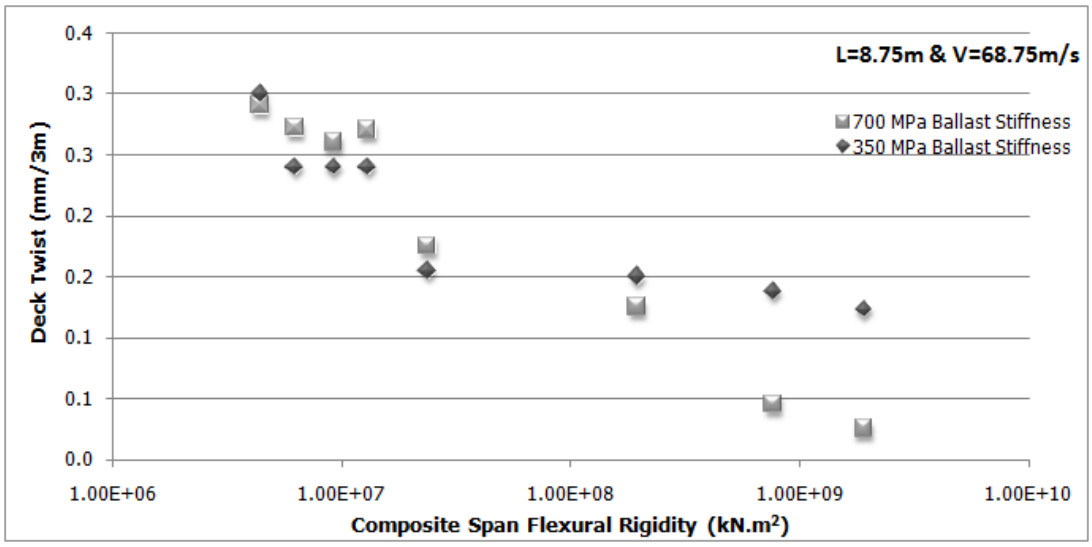

Figure C.10 Deck Twist vs. Span Flexural Rigidity graph of the bridge having 8.75 m span length for 68.75 m/s vehicle speed.

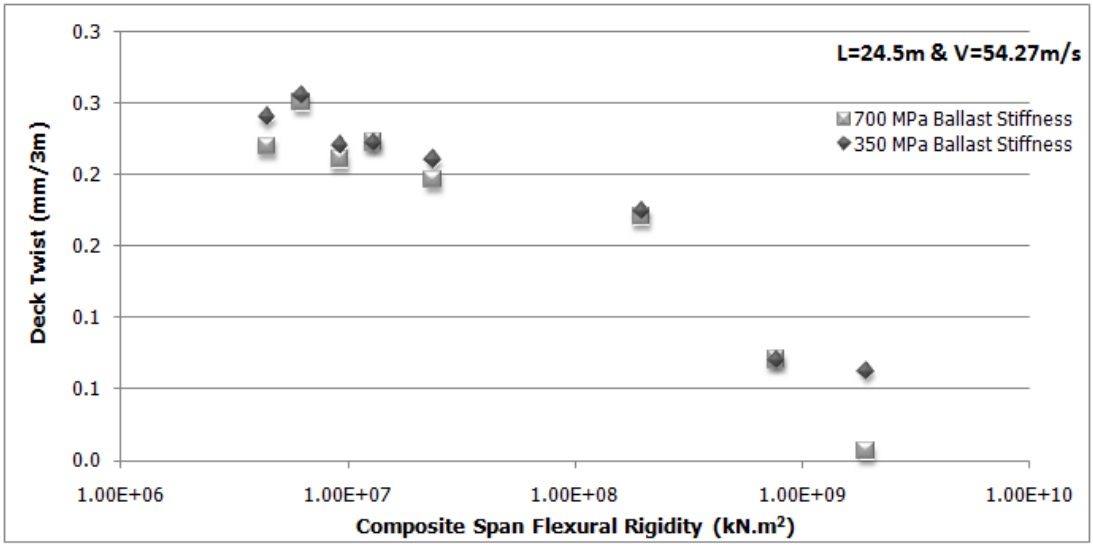

Figure C.11 Deck Twist vs. Span Flexural Rigidity graph of the bridge having 24.5 m span length for 54.27 m/s vehicle speed.

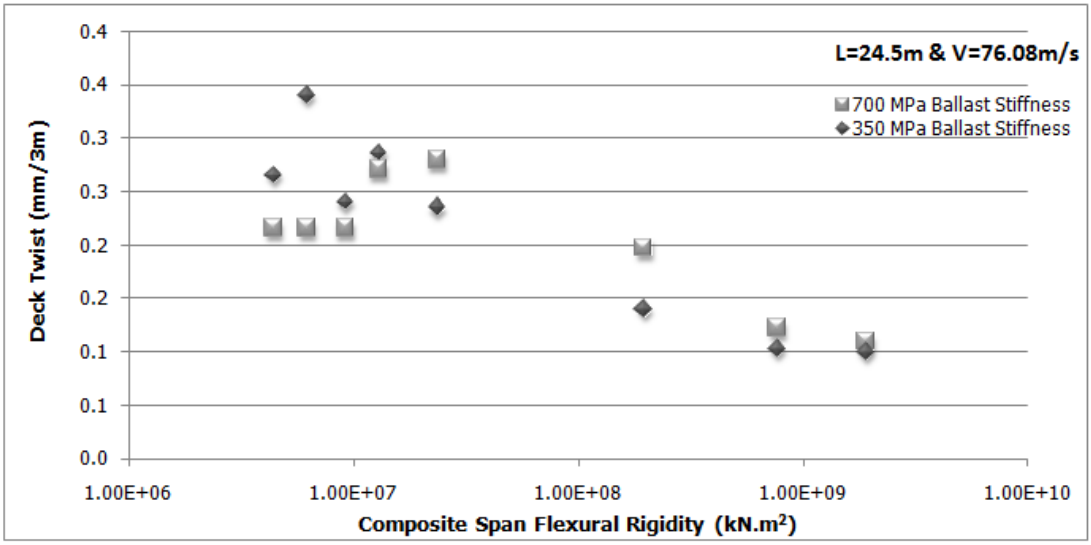

Figure C.12 Deck Twist vs. Span Flexural Rigidity graph of the bridge having 24.5 m span length for 76.08 m/s vehicle speed.

APPENDIX D

MODAL DISPLACEMENT COMPARISONS

D.1. Vertical Modal Displacements for Selected Frequencies

Table D.1 Vertical Modal Displacements of Selected Frequencies and Frequencies cause Peak Modal Displacement in Range of Design Speed Frequencies for Bridge having 8.75 m Span Length and 40 m/s Design Speed

Span Flexural Stiffness, EI/L ($kN.m^2/m$)	**V_{min} = 40.00 m/s , $n_{selected}$ = 13.33 Hz**				
	n_{close} (Hz)	**u_{close}** (10^{-3})	**n^r_{peak}** (Hz)	**u^r_{peak}** (10^{-3})	**$\frac{u_{close}}{u^r_{peak}}$**
505,322	12.82	0.12	18.64	6.97	0.02
713,689	12.83	11.70	15.53	4.40	2.66
1,058,281	12.84	10.20	16.64	2.29	4.45
1,483,568	12.93	106.30	17.70	0.90	118.11
2,714,390	12.76	1.23	15.59	84.61	0.01
22,388,361	13.01	0.21	25.42	23.22	0.01
87,801,583	13.88	19.15	24.51	2.62	7.31
218,619,493	13.46	0.00	24.91	1.36	0.00

Table D.2 Vertical Modal Displacements for Selected Frequencies and Frequencies cause Peak Modal Displacement in Range of Design Speed Frequencies for Bridge having 8.75 m Span Length and 44.13 m/s Design Speed

Span Flexural Stiffness, EI/L ($kN.m^2/m$)	**V_{min} = 44.13 m/s , $n_{selected}$ = 14.71 Hz**				
	n_{close} (Hz)	**u_{close}** (10^{-3})	**n^r_{peak}** (Hz)	**u^r_{peak}** (10^{-3})	**$\frac{u_{close}}{u^r_{peak}}$**
505,322	14.71	6.98	18.64	6.97	1.00
713,689	15.53	4.40	15.53	4.40	1.00
1,058,281	16.64	2.29	16.64	2.29	1.00
1,483,568	12.93	106.30	17.70	0.90	118.11
2,714,390	15.59	11.11	15.59	84.61	0.13
22,388,361	17.39	37.34	25.42	23.22	1.61
87,801,583	13.88	19.15	24.51	2.62	7.31
218,619,493	14.76	0.00	24.91	1.36	0.00

Table D.3 Vertical Modal Displacements for Selected Frequencies and Frequencies cause Peak Modal Displacement in Range of Design Speed Frequencies for Bridge having 8.75 m Span Length and 68.75 m/s Design Speed

Span Flexural Stiffness, EI/L ($kN.m^2/m$)	**V_{min} = 68.75 m/s , $n_{selected}$ = 22.97 Hz**				
	n_{close} (Hz)	**u_{close}** (10^{-3})	**n^r_{peak}** (Hz)	**u^r_{peak}** (10^{-3})	**$\frac{u_{close}}{u^r_{peak}}$**
505,322	22.39	0.00	18.64	6.97	0.00
713,689	22.39	0.00	15.53	4.40	0.00
1,058,281	22.39	0.02	16.64	2.29	0.01
1,483,568	22.39	0.00	17.70	0.90	0.00
2,714,390	22.39	0.02	15.59	84.61	0.00
22,388,361	22.39	0.04	25.42	23.22	0.00
87,801,583	22.39	0.00	24.51	2.62	0.00
218,619,493	22.39	0.00	24.91	1.36	0.00

Table D.4 Vertical Modal Displacements for Selected Frequencies and Frequencies cause Peak Modal Displacement in Range of Design Speed Frequencies for Bridge having 8.75 m Span Length and 83.3 m/s Design Speed

Span Flexural Stiffness, EI/L ($kN.m^2/m$)	**V_{min} = 83.33 m/s , $n_{selected}$ = 27.77 Hz**				
	n_{close} (Hz)	**u_{close}** (10^{-3})	**n^r_{peak}** (Hz)	**u^r_{peak}** (10^{-3})	**$\frac{u_{close}}{u^r_{peak}}$**
505,322	28.41	0.01	18.64	6.97	0.00
713,689	28.70	0.00	15.53	4.40	0.00
1,058,281	29.17	0.00	16.64	2.29	0.00
1,483,568	29.78	0.00	17.70	0.90	0.00
2,714,390	28.67	0.00	15.59	84.61	0.00
22,388,361	28.22	41.60	25.42	23.22	1.79
87,801,583	27.62	16.97	24.51	2.62	6.48
218,619,493	26.13	0.20	24.91	1.36	0.14

Table D.5 Vertical Modal Displacements of Selected Frequencies and Frequencies cause Peak Modal Displacement in Range of Design Speed Frequencies for Bridge having 24.5 m Span Length and 40 m/s Design Speed

Span Flexural Stiffness, EI/L ($kN.m^2/m$)	**V_{min} = 40.00 m/s , $n_{selected}$ = 13.33 Hz**				
	n_{close} (Hz)	**u_{close}** (10^{-3})	**n^r_{peak}** (Hz)	**u^r_{peak}** (10^{-3})	**$\frac{u_{close}}{u^r_{peak}}$**
180,472	12.30	58.22	20.56	7.34	7.93
254,889	13.72	59.00	27.37	21.10	2.80
377,958	12.13	13.80	22.39	30.91	0.45
529,846	16.39	2.93	26.51	14.25	0.21
969,425	13.33	0.10	16.15	49.26	0.00
7,995,843	13.63	43.57	25.37	17.73	2.46
31,357,708	13.08	11.31	21.49	15.08	0.75
78,078,390	12.56	0.01	21.44	9.13	0.00

Table D.6 Vertical Modal Displacements for Selected Frequencies and Frequencies cause Peak Modal Displacement in Range of Design Speed Frequencies for Bridge having 24.5 m Span Length and 54.27 m/s Design Speed

Span Flexural Stiffness, EI/L ($kN.m^2/m$)	**V_{min} = 54.27 m/s , $n_{selected}$ = 18.09 Hz**				
	n_{close} (Hz)	**u_{close}** (10^{-3})	**n^r_{peak}** (Hz)	**u^r_{peak}** (10^{-3})	**$\frac{u_{close}}{u^r_{peak}}$**
180,472	17.16	0.60	20.56	7.34	0.08
254,889	18.43	0.10	27.37	21.10	0.00
377,958	20.11	0.08	22.39	30.91	0.00
529,846	16.97	0.30	26.51	14.25	0.02
969,425	16.15	0.54	16.15	49.26	0.01
7,995,843	18.26	0.00	25.37	17.73	0.00
31,357,708	18.59	11.41	21.49	15.08	0.76
78,078,390	17.81	0.12	21.44	9.13	0.01

Table D.7 Vertical Modal Displacements for Selected Frequencies and Frequencies cause Peak Modal Displacement in Range of Design Speed Frequencies for Bridge having 24.5 m Span Length and 76.07 m/s Design Speed

Span Flexural Stiffness, EI/L ($kN.m^2/m$)	**V_{min} = 76.07 m/s , $n_{selected}$ = 25.36 Hz**				
	n_{close} (Hz)	**u_{close}** (10^{-3})	**n^r_{peak}** (Hz)	**u^r_{peak}** (10^{-3})	**$\frac{u_{close}}{u^r_{peak}}$**
180,472	25.36	3.75	20.56	7.34	0.51
254,889	25.36	0.00	27.37	21.10	0.00
377,958	25.36	0.05	22.39	30.91	0.00
529,846	25.36	0.00	26.51	14.25	0.00
969,425	25.35	0.00	16.15	49.26	0.00
7,995,843	24.30	0.12	25.37	17.73	0.01
31,357,708	25.45	2.70	21.49	15.08	0.18
78,078,390	25.37	0.01	21.44	9.13	0.00

Table D.8 Vertical Modal Displacements for Selected Frequencies and Frequencies cause Peak Modal Displacement in Range of Design Speed Frequencies for Bridge having 24.5 m Span Length and 83.3 m/s Design Speed

Span Flexural Stiffness, EI/L ($kN.m^2/m$)	**V_{min} = 83.33 m/s , $n_{selected}$ = 27.77 Hz**				
	n_{close} (Hz)	**u_{close}** (10^{-3})	**n^r_{peak}** (Hz)	**u^r_{peak}** (10^{-3})	**$\frac{u_{close}}{u^r_{peak}}$**
180,472	27.10	0.20	20.56	7.34	0.03
254,889	27.73	2.11	27.37	21.10	0.10
377,958	27.75	0.13	22.39	30.91	0.00
529,846	26.54	0.70	26.51	14.25	0.05
969,425	27.93	0.44	16.15	49.26	0.01
7,995,843	27.04	0.06	25.37	17.73	0.00
31,357,708	27.25	1.47	21.49	15.08	0.10
78,078,390	27.78	0.00	21.44	9.13	0.00